LOW FIRING TEMPERATURE THICK-FILM PIEZORESISTIVE COMPOSITES - PROPERTIES AND CONDUCTION MECHANISM

THÈSE N^{O} 3290 (2005)

PRÉSENTÉE À LA FACULTÉ SCIENCES ET TECHNIQUES DE L'INGÉNIEUR

Institut de production microtechnique

SECTION DE MICROTECHNIQUE

ÉCOLE POLYTECHNIQUE FÉDÉRALE DE LAUSANNE

POUR L'OBTENTION DU GRADE DE DOCTEUR ÈS SCIENCES

PAR

Sonia VIONNET MENOT

DEA en chimie-physique des interfaces, Université de Franche-Comté, Besançon, France
et de nationalité française

acceptée sur proposition du jury:

Prof. P. Ryser, directeur de thèse
Prof. C. Ballif, rapporteur
Prof. H. Hofmann, rapporteur
Dr M. Hrovat, rapporteur

Lausanne, EPFL
2005

A mon Papa ...

Abstract

Thick-film technology has found applications on miniaturised hybrid circuits in various fields (automotive electronics, televisions, ...). This technology is also now widely used for the fabrication of force and pressure sensors that use the piezoresistive properties of thick-film resistors.
The goal of this work has been generated by the fact that usual piezoresistive pastes / inks were optimised for applications on alumina, which is the standard substrate for thick-film technology, but ill suited for more flexible substrates such as aluminium, steel or Ti alloys. We were limited by the process conditions of the commercial pastes, in particular the too high firing process that does not allow the use of substrates with melting temperature < 850°C. This technological lack leads to manufacture a new generation of piezoresistive pastes with low firing temperatures (T_f: 500 ... 700°C). In parallel, we aim to optimise the electrical properties (resistance *R*, temperature coefficient of resistance TCR and gauge factor GF values) by highlighting the link with the structural evolution during the firing process and the obtained properties, and by understanding the conduction process in such percolative systems.

Study of usual commercial piezoresistive pastes allowed us to determine that such piezoresistive pastes are composed of a percolating network of nanoconductive RuO_2 grains embedded in a lead borosilicate glassy matrix. Evolution during the firing process was emphasised and showed the importance of controlling the firing parameters to assure the best properties for the final thick-film. Commercial pastes are characterised by a TCR value close to 0 ppm/°C, a reasonable sheet resistance value (R ~ 10 KOhms) and a gauge factor comprise between 10-12, that can be influenced by structural and process parameters. Indeed, complementary studies on sensitivity and stability were realised, because of limited available information in literature concerning the effect of firing schedule, particularly of quenching, and have shown that these properties are very dependent on the conditions of firing, although the main commercial pastes showed a moderate stability. In fact, this study showed that a compromise should be found between the different properties (for instance, high GF pastes presents a poor stability), and emphasises the fact that they should be optimised.

A manufacturing process has been developed, process never well described in the literature, leading to the realisation of different lead borosilicate glasses. It has resulted in the ability to realise three series of model piezoresistive pastes with different ranges of firing temperatures corresponding to high (700°C), low (600°C) and very low (500°C) firing temperatures. The control of several parameters (glass composition, conductive phase concentration, grain size, firing temperature...) allowed us to direct precisely our research to elucidate the principle of conduction in such percolative systems and the reactions occurring between the elements and their influence on the electrical properties.

Structural and electrical properties were studied by varying diverse parameters such as conductive grain size, concentration and firing temperature, and a coherence was found between the electrical behaviour (conduction process) and its relation to the complex nanostructure. In other words, this key chapter presents the results and their interpretation by a model of conduction based on a nonuniversal tunnelling percolation theory and based on a previously unpublished hypothesis. Indeed, it was demonstrated that the piezoresistive response of the pastes changed dramatically depending on whether the composites were universal or not. For the composites with critical exponent t ~ 2, the piezoresistive factor Γ showed no dependence upon the RuO_2 volume fraction x, whereas the nonuniversal composites displayed a logarithmic divergence of Γ near the percolation threshold. We have interpreted the piezoresistivity results

as being due to a strain dependence of the critical exponent when this was nonuniversal. We have brought forth a microscopic formulation to the phenomenological level proposed by Balberg, and we can now assert that thick-film resistors (TFR) are mainly nonuniversal compounds showing transport exponent *t* larger than the universal limit *t* = 2.0. This exponent *t* depends on strain and leads to a logarithmic divergence of the gauge factor. The possibility of influencing *t* by external means (e. g. strain) has never been studied so far. We have proposed a new way to investigate percolative systems by studying the behaviour of piezoresistive pastes.

After having elucidated the conduction mechanism in such piezoresistive pastes, we studied the influence of different parameters (T_f, grain size, concentration, dwell time) on the main electrical properties (*R*, TCR and GF). Structural analysis gave a possible interpretation of the results. RuO_2 parameters have direct effects on the *R*, TCR and GF values. T_f acts on microstructure provoking interactions between the bulk components and the substrate (in case of high T_f), and consequently leading to a modification of the electrical properties.
The same complementary studies as commercial pastes on stability showed a combined influence of the cooling rate and the temperature dwell-time on *R* and TCR values. The results are in coherence with commercial pastes. The evolution of the values can be explained by diffusion phenomenon and local microscopic strains due to important cooling rates.

The evolution of *R* upon annealing 250°C was found to depend strongly on the cooling rate for commercial and model pastes, but this observed trend tends to saturate. These new series of low firing temperature were shown to be not as stable as the «best» commercial pastes, but their variations are much similar to «medium» commercial one's. At 250°C, possible evolution mechanisms could involve Ru in glass (dissolved or in clusters), or mechanical relaxation that can be extrinsic (macroscopic thermal mismatch between resistor and substrate) or intrinsic (local thermal mismatch between glass and conductive phase), and which can later relax during annealing.

During this analysis, technological problems have been emphasised and a section was dedicated to resolve the problem of the unsuitability of the substrate to the very low firing temperature system, which showed local strain that induced cracks and leading to electrical instability. Moreover, it was shown that these new pastes could be optimised by additives or used on more adapted substrates.

However, these obtained series offers a large range of TCR and *R* values for different low T_f and it would be useful for technological goals. The best proof of the success of our study was the realisation of sensor prototypes based on different substrates such as steel, aluminium and even glass.

This work has allowed to realise a detailed study of piezoresistive pastes and to complete previous research in this field concerning the influence of firing parameters (quenching) and annealing studies.
From a scientific point of view, this first step allowed to show that nanostructure, conduction mechanism and electrical properties are intimately linked. By choosing adequate and relevant compositions, structure and firing, we proposed a new way to unveil the conduction process that has not been yet elucidated. From a technical point of view, their stability could be enhanced with a higher GF or adapted TCR. However, they present a large range of applications because of their different T_f and their different TCRs. Thanks to this particularity, these pastes could be used on different substrates, and we could expect a larger technological impact by optimising our piezoresistive pastes by additives to better control their properties.

Version Abrégée

La technologie des couches épaisses est couramment utilisée pour la réalisation de circuits hybrides miniatures touchant divers domaines (électronique de voitures, télévisions, ...). Cette technologie a ainsi trouvé des applications dans la réalisation de capteurs de force et de pression qui utilisent les propriétés piézorésistives des résistances en couches épaisses. L'origine de ce travail de thèse est basée sur le fait que les encres / pâtes piézorésistives commerciales usuellement utilisées sont optimisées pour des substrats en alumine, mais mal adaptées à des substrats aux propriétés mécaniques plus intéressantes (comme l'aluminium ou l'acier, plus flexibles). L'utilisation de pâtes commerciales nous contraint à des procédés de mise en oeuvre nécessitant de hautes températures de cuisson (T_f: 850°C), ce qui interdit toute possibilité d'utiliser des substrats se dégradant dans ces conditions, tels que les alliages d'aluminium et de titane, ainsi que la plupart des aciers. Ce manquement technologique nous a donc amené à mettre au point une nouvelle génération de pâtes piézorésistives ayant de basses températures de mise en oeuvre (500...700°C). Dans un même temps, nous nous sommes intéressés à optimiser leur propriétés électriques (valeurs de resistance *R*, de coefficient en température de la résistance TCR, de facteur de jauge GF) d'une part en mettant en relation l'évolution structurale durant la cuisson et les propriétés obtenues et d'autre part en expliquant le procédé de conduction dans de tels systèmes percolatifs.

L'étude de pâtes commerciales courantes nous a permis de mettre en évidence un réseau percolatif de nanoparticules de RuO_2 dispersées dans une matrice de verre de type borosilicate de plomb. L'évolution de ces pâtes pendant la cuisson a montré l'importance de contrôler les paramètres de cuisson qui assurent des propriétés optimales pour de tels films. Les pâtes commerciales «optimales» sont caractérisées par une valeur de TCR proche de 0 ppm/°C, une valeur de résistance raisonnable ($R \sim 10$ kOhms) et un facteur de jauge compris entre 10 et 12. Ces propriétés peuvent être influencées par des paramètres de mise en oeuvre mais aussi structuraux. En effet, des études complémentaires dédiées à la sensibilité et à la stabilité, vu le manque de données concernant l'influence des conditions de cuisson, en particulier de la trempe, ont permis de démontrer une forte dépendance de ces propriétés sur les conditions de cuisson, malgré la relative stabilité observée pour la majeure partie des pâtes commerciales. En fait, un compromis est généralement fait entre les différentes propriétés (par exemple, les pâtes à haut GF présentent une stabilité amoindrie), et souligne la nécessité d'une optimisation.

Un procédé de fabrication a été mis au point - procédé toujours trop brièvement décrit dans la littérature - et a permis de réaliser trois séries de pâtes piézorésistives modèles basées sur différents verres au borosilicate de plomb afin d'obtenir différentes températures de cuisson: une haute (700°C), basse (600°C) et très basse (500°C) température de cuisson. Le contrôle de plusieurs paramètres (tels que la composition du verre, la concentration en phase conductrice, la granulométrie ou encore la température de cuisson) nous a permis d'orienter précisément nos recherches afin de mettre en évidence le principe de conduction dans de tels systèmes percolatifs et les réactions entre les différents composants ainsi que leur influence sur les propriétés électriques.

Les propriétés structurales et électriques ont donc été étudiées en fonction de différents paramètres tels que la granulométrie du RuO_2, sa concentration et la température de cuisson. Ainsi, les propriétés électriques (liées au procédé de conduction) et ces nanostructures complexes ont été corrélées. En d'autres termes, ce chapitre clef présente une interprétation des résultats par un modèle de conduction fondé sur la théorie de percolation basée sur un transport par effet tunnel non universel, qui s'appuie sur une hypothèse originale et auparavant non

publiée. En effet, la réponse piézorésistive de ces pâtes dépend de l'universalité ou non du transport, déterminé par la valeur de l'exposant critique *t*. Un exposant égal à 2 dénote un transport universel entre les nanoparticules ce qui est traduit par un facteur piézorésistif indépendant de la concentration volumique de RuO_2. Par contre, dans le cas d'un transport non universel (t>2), le facteur piézorésistif présente une divergence logarithmique près du seuil de percolation. En montrant que dans ce cas, *t* est dépendant de la contrainte appliquée, nous avons apporté une formulation microscopique au phénomène mentionné par Balberg. La possibilité d'influencer *t* par une contrainte externe n'a jamais été proposée auparavant. Nous avons donc ouvert une nouvelle voie pour l'étude de tels systèmes percolatifs.

Après avoir élucidé le mécanisme de conduction, l'influence de différents paramètres (T_f, granulométrie, concentration, temps de cuisson) sur les propriétés électriques a été étudiée à la lumière d'analyses structurales. Les paramètres liés à la phase conductrice ont des effets directes sur les valeurs de *R*, TCR et GF. T_f agit plutôt sur la microstructure en favorisant les interactions soit entre les composants de la pâte ou soit avec le substrat (en cas de haute température), et mène donc à une modification des propriétés électriques. Comme pour les pâtes commerciales, les études similaires de stabilité ont été menées et ont montré une influence conjuguée de la vitesse de refroidissement et du temps de cuisson sur les valeurs de *R* et TCR. Ces résultats sont en accord avec ceux des pâtes commerciales. L'évolution de ces valeurs peut être expliquée par des phénomènes de diffusion ou des contraintes microscopiques locales dues à un rapide refroidissement. A l'opposé, des refroidissements plus lents tendent à homogénéiser la microstructure des résistances.

L'évolution de *R* durant le recuit à 250°C montre une forte dépendance des pâtes (commerciales ou modèles) sur la vitesse de refroidissement. Mais, dans chaque cas, l'évolution observée tend à se stabiliser. Evidement, ces nouvelles pâtes ne s'avèrent pas être aussi stable que les pâtes commerciales les plus prometteuses mais leur stabilité est comparable à d'autres moins optimisées. A 250°C, le ruthénium dissout dans le verre pendant la cuisson peut influencer la stabilité, d'autre part, cette haute température de recuit peut favoriser la relaxation de contraintes mécaniques extrinsèques (dues à des différences de contraintes entre le substrat et la résistance) ou intrinsèques (contraintes entre les particules conductrices et le verre).

Une partie de cette étude a été dédiée à résoudre des problèmes technologiques concernant la non adéquation du substrat avec les pâtes à très basses températures de cuisson, engendrant des fissures, cause d'instabilité électrique. Il s'avère donc que ce type de pâte doit encore être optimisé par des additifs ou utilisé sur un substrat adapté.

Malgré cela, les séries obtenues offrent une large gamme de valeurs de TCR et *R* pour de relativement basses températures de cuisson, ouvrant ainsi sur des applications technologiques prometteuses. Une des meilleurs preuves du succès de cette étude est la réalisation de capteurs prototypes basés sur différents substrats tels que l'acier, l'aluminium ou même le verre.

Ce travail a donc permis de réaliser une étude détaillée de pâtes piézorésistives et de compléter de précédentes recherches dans le domaine, concernant l'influence des paramètres de cuisson et du recuit. D'un point de vue scientifique, il a été démontré que nanostructure, mécanisme de conduction et propriétés électriques sont intimement liés. Grâce à la sélection adéquate de différents paramètres, nous avons proposé une nouvelle voie pour élucider le mécanisme de conduction. D'un point de vue technologique, bien que ces nouvelles pâtes nécessitent d'être optimisées pour augmenter leur GF ou adapter leur TCR, elles offrent un large éventail de possibilités prometteuses, et le contrôle futur de leurs propriétés par l'ajout d'additifs prédit un plus grand impact technologique.

Table of contents

Remerciements

Je dédie cette page à toutes les personnes qui ont contribué de près ou de loin à la réalisation de ce travail. Je tiens à remercier plus particulièrement:

Le **Prof. Peter Ryser**, mon directeur de thèse, qui m'a accueillie au sein de son Laboratoire de Production Microtechnique et sans qui je n'aurais pu mener à bien mon projet.

Le **Prof. Heinrich Hofmann** pour m'avoir donné l'accès libre aux appareils de caractérisation au sein de son laboratoire de technologie des poudres, et pour ses conseils.

Le **Dr Thomas Maeder** pour son aide tout au long de ma thèse, pour sa mine d'idées (parfois saugrenues), pour nos discussions constructives et pour le temps qu'il m'a consacré pour la correction de ma thèse.

Le **Dr Claudio Grimaldi** sans qui les parties relatives à la physique et à la théorie n'auraient pas pu aussi bien aboutir. Merci aussi pour ton aide pour les (très ennuyeuses) mesures électriques et pour la rédaction de nos articles.

Toutes les personnes du «niveau 0», **Giancarlo Corradini** pour ses conseils et son aide technique, **Matthias Garcin** pour les centaines d'échantillons qu'il m'a sérigraphiés (sans «broncher»), **Timothée Haller**, notre apprenti, pour son aide ponctuelle pour les (ennuyeuses) mesures électriques, **Igor Saglini** pour son assistance pour la mise au point des systèmes de mesures, et enfin, **Caroline Jacq** pour nos discussions professionnelles (ou non...).

Le **Dr Raymond Houriet** (laboratoire de technologie des poudres) pour sa gentillesse et pour son aide au début de ce travail.

L'équipe du Centre Interdépartemental de Microscopie Electronique - CIME - Lausanne, en particulier **Danièle Laub** et le **Prof. Philippe Buffat** pour les observations au TEM, mais aussi **Brian Senior** pour les analyses et conseils pour les observations SEM.

L'équipe du laboratoire de céramique, en particulier le **Dr Marlyse Demartin-Maeder** pour ses conseils et son aide pour les mesures dilatométriques et les broyages, et le **Dr Sandrine Gentil** pour avoir eu la gentillesse de me donner l'accès à ses fours.

Mon ancien collègue de bureau (même s'il a quitté le navire avant la fin...), **Sylvain Menot**, qui a été (malgré lui) mon spécialiste informatique attitré (et aussi parce que je le lui avais promis...).

La Direction du programme **TOP NANO 21** pour son soutien financier pour le projet NAMESA, n°5557.2.

Mes parents pour m'avoir offert l'opportunité de suivre des études malgré les sacrifices que cela représentait.

Enfin, je ne saurais oublier **Sébastien Menot,** mon ancien voisin de bureau, devenu maintenant mon mari, qui m'a encouragé dès le début de ma thèse. Merci pour ton soutien sans limite, pour ta patience et ton amour, et merci d'avoir cru en moi!. Merci encore pour tous nos instants de bonheur passés et à venir.

Introduction

a remote oil level measurement system
a scale
a tension sensor to secure the rigidity of cable on building sites
a wireless power sensor for bikers.

Do you know what the common originality of these usual products is?

Apart from the fact that they are common, robust and mass-produced, these consumer-products are based on a same high-tech process: THICK-FILM TECHNOLOGY.

Hybrid thick-film technology is employed for manufacturing electronics (essentially), ensuring excellent stability, robustness, and a very long operating life [1]. The low-cost design integrates batch production and automated assembly, ensuring an excellent performance-to-cost ratio. They have found applications in various areas such as televisions and mobile phones [2].

A thick-film circuit is characterised by a superposition of special inks (or pastes), deposited and fired onto an insulating substrate. One of the key factors which distinguishes a thick-film circuit from a printed circuit board is the method of film deposition: the screen-printing [3,4]. This method, closely inspired from traditional silk screen printing, allows a high-definition design of the circuits. Moreover, the superposed multi-layers enable a high component packing density: passive components (resistors,..) are deposited by screen-printing, whereas active devices (transistors, diodes...) are usually soldered onto the thick-film conductor pads.

Although diverse sensors are based on thick-film technology (gas, thermal sensors, or mechanical sensors...), we will take an interest on all the applications where the strain gauge principle is used. The knowledge of this principle allows not only to measure pressure but also includes vibration, displacement, force and temperature measurement.

As we will see later, the main measuring principle depends on piezoresistivity which is characterised by the response of electrical resistance to mechanical strain [5]. Over a given

range of strains, it is linear, and the ratio between the relative variation of electrical resistance and strain is called the gauge factor. Although all conductive materials exhibit a piezoresistive gauge factor, this property is enhanced by the special conduction mechanism through the complex nanostructure of the thick-film resistor material. Indeed, this kind of paste is composed by conductive nanoparticles randomly dispersed through an insulating matrix. The electrical transport and the piezoresistive response will be influenced by the distance between these nanoconductive particles, their arrangement within the insulating matrix and the material properties of both phases.
This complex behaviour has not been studied much although understanding it is essential for progress in controlling the properties of sensors. The comprehension of the behaviour of thick-film resistors is a key of success in a lot of practical applications.

The aim of this work is to understand the firing behaviour and the evolution of the current piezoresistive pastes and to modify them to improve their properties. Indeed, the materials for these commercial thick-film sensor applications have not especially been developed for strain sensors and hence don't possess the optimal sensing properties.
Until now, commercial piezoresistive pastes were screen-printed on alumina (Al_2O_3) substrate - an insulating stable material. But, although alumina is considered as a standard for thick-film technology [6], this material is not optimal for piezoresistive sensing applications, as its elastic modulus is high and its strength rather low. Additionally, alumina is brittle and therefore ill suited to the mechanically harsh environments found in industrial applications. Zirconia and zirconia thoughened alumina (ZTA) have the advantage of being sturdier than alumina, but with the same abovementioned inconvenients of the ceramics (brittle, ...). Aluminium or aluminium alloys offer better advantages in applications such as high power electronics or high-range load cells, due to their excellent thermal dissipation, mechanical sturdiness, and easy packaging. However, the high temperatures associated with processing of commercial thick-film resistors (850°C) are not compatible with aluminium owing to its low melting point: an appropriate low-temperature thick-film paste is therefore necessary. For piezoresistive sensors, steel and titanium alloys are also good substrates, but their temperature / stability is also limited by oxidation and degradation of mechanical properties.
We therefore endeavour to investigate novel low-temperature thick-film resistors and present the results of the electrical properties of such a system compared to commercially available ones.

From the above considerations, the main desirable properties of these piezoresistive pastes are:
- good stability
- high gauge factor
- moderate resistivity
- small temperature dependence
- low process temperature, in the 500-650°C range.

In order to reach the abovementioned technical goals, it is necessary to understand the mechanisms responsible for these properties. Therefore, this project presents two inter-connected levels of approach :

- a scientific goal: to obtain a better understanding of the evolution of the properties. To this end, the gauge factor and the resistance values will be particularly studied and a coherence between the electrical transport (conduction process) and its relation to the complex nanostructure will

be found. In other words, we would like to realise a model of the physical phenomenon that corresponds to the tunnelling effect between the conductive particles and its response to mechanical strain. This part, based on physical studies, will allow us to better understand the evolution of electrical properties and consequently to enhance piezoresistive pastes.
On the other hand, these properties are also influenced by processing steps such as firing conditions. By this way, we will take an interest particularly to the understanding of chemical reactions by studying phase and structure transformations during the sintering and firing process.

- a technological goal: to improve and optimise the current piezoresistive pastes so that they can be adapted to others applications (screen-printing on steel or aluminium alloy substrates). In order to reach this aim, we should study this chemical phenomenon, which corresponds to the reaction between the elements (exchange of atoms) during the elaboration process. The influence of different parameters like the change of conductive grain size, or of the glass composition will be studied. This chapter rests principally on chemical and material knowledge. The resulting electrical properties will be examined and correlated to the structural modifications.

Current commercial piezoresistive pastes will be considered as reference for our work, although we will try to enhance and optimise them by structural and electrical studies. The obtained results of such an analysis, based on a model of conduction mechanism, will allow us to direct our studies to a new generation of low temperature piezoresistive pastes.

References - Introduction:

1. White NM, Turner JD, *Thick-film sensors: past, present and future*, Meas. Sci. Technol., 1997, **8**, 1-20.
2. Prudenziati M, *Handbook of sensors and actuators 1*, 1994(elsevier), 189-206.
3. Vest RW, *Materials aspects of thick-film technology-chap8*, 444-49.
4. Haussonne JM, *Céramiques pour l'électronique et l'électrotechnique*, Presses polytechniques et universitaires romandes, 2002, 88-91.
5. Morten B, Prudenziati M, *Thick-film sensors*, Piezoresistive thick-film sensors, 1994, 189-208.
6. White NM, *A study of the piezoresistive effect in thick-film resistors and its application to load transduction*, Doctoral thesis, university of Southampton, Faculty of engineering and applied science, 1988.

CHAPTER I:

Thick-film resistor technology: overview

The properties of thick-film resistive pastes cover a vast range of research. The production and the control of properties of these complex systems, whose industrial manufacturing remains confidential, necessitate the mastery of various fields, such as the knowledge of microstructure analysis, electrical measurements, mechanical behaviour and physical modelling.
Thick film resistors consist of a percolating network of conducting oxide nanoparticles dispersed in an insulating glassy matrix. The nature and the relative concentrations of the metallic and the glassy phases as well as the fabrication procedures are key ingredients governing the thick-film resistors electrical and piezoresistive properties. The tailoring of these factors and the knowledge of their effects on thick-film resistors properties are therefore of primary importance in the production of reliable thick-film sensor devices.
Thick-film resistors are characterised by their structural and electrical properties that are dependant on firing conditions and composition. Moreover, their properties are governed by a specific conduction mechanism. This complex conduction process can be presented as an electrical conduction by percolation coexisting with electron tunnelling. Resistive properties are dominated by quantum tunnelling across insulating layers separating adjacent conducting grains.
Our aim is not only to study the structural and electrical behaviours but to define a conduction model by using the obtained results. The combination of these observations will contribute to the understanding of the behaviour of piezoresistive pastes and to plan other technological applications (realisation of more sensitive sensors).

Our work rests on the variation of different parameters: conductive phase concentration, conductive grain size, glass composition and firing schedules.

I . 1 . Advantage and use - Example of sensors

Miniaturisation, reliability, performance and low-cost production are the main key words in the electronic components research field. Although this technology can be followed back to the 1950s, it answers to the present industrial needs. The moderate required investment and the high degree of automatisation of thick-film technology allow a high output [1].
This new kind of process was envisaged for the replacement for the printed circuit board development and gave rise to hybrid technology.

Nowadays, the steps of realisation of a hybrid circuit have not changed [1, 2]:
- the deposition of conductive, resistive and dielectric pastes on a substrate by screen-printing,
- the firing of the different films,
- the addition of active and passive component by wire-bonding, gluing and /or soldering.

Thick-film hybrid circuits have found application in areas such as televisions, calculators, telephones, automotive electronics... This technology is also widely used for the fabrication of chemical and gas sensors and many commercial devices exist.
Different types of sensors are based on thick-film technology [3, 4]. The main categories are:
- thermal sensors: surface temperature sensors or heat flow sensors,
- sensors for mechanical quantities: piezoresistive, piezoelectric or capacitive sensors,
- sensors for chemical quantities: gas sensors or biosensors,
- sensors for radiation: photoconducting sensors or solar cells.
Of course, this list is not exhaustive, as the field of application is vast.

In this work, we will take an interest to mechanical sensors and particularly to piezoresistive sensors. This kind of sensor is based on an elastic structure and a sensing material exhibiting a change in bulk resistivity when it is subjected to deformation by an applied force. The two main classes of piezoresistive sensors are force or acceleration sensors (based in our case on cantilever beam-type) and pressure sensors (based on membrane-type structures). Two examples of sensors corresponding to each mentioned class are shown in figure 1.

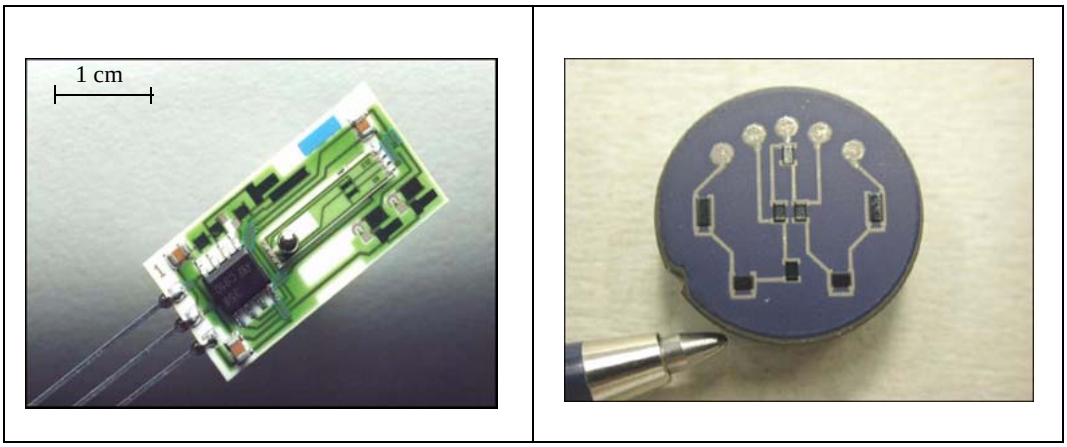

Figure 1: A force sensor (left) - A pressure membrane (right) from our lab

I . 2 . Process

To realise a simple sensor based on thick-film technology, four basic elements are necessary:
- an appropriate set of pastes (or inks),
- an appropriate substrate,
- a screen-printing machine,
- two ovens.

• the paste:

There are three main kinds of pastes with specific properties: conductor, dielectric and resistive [51].
- The first is used directly on the substrate for interconnections between the different components.
- The second acts as an insulating material (for example if the substrate is conductive or could react with the conductor) but can be used as hermetic sealing.
- The third paste plays a relevant role in sensor as it makes it operational. It converts the applied strain on the sensor into an electrical signal.

• the substrate:

It is generally an inert element. But for strain sensors, it must be robust and flexible. Aluminium oxide is the standard substrate used for thick-film technology, but is not ideal for piezoresistive sensing due to its brittleness, moderate strength and high elastic modulus. To make up for this disadvantage, metallic substrates (steel, aluminium) are proposed [5, 6]. They are not often used as they are not compatible with the high firing temperatures of the pastes [6].

• the screen-printing machine:

One of the most distinguishing aspects of the thick-film process is the method used for deposition of the films. Screen-printing, traditionally recognised as art, has had to be modernised and transformed into a more precise tool for thick-film technology. But the technique remains very similar to graphic art reproduction.
This method permits to deposit a paste with a precise layout.
For this, a screen is first stretched to the proper tension and attached to a frame. An UV-sensitive emulsion is then applied to the screen, exposed through a positive or negative of the desired pattern produced using the appropriate design rules, and then developed to remove the emulsion in the pattern regions [7].
The screens used in thick-film technology are made with stainless steel wire, which deforms less than alternative materials such as polyester or nylon, and therefore allows more precise printing.

The pattern screen is then fixed to the printer, ink is placed on top of the screen, and a print cycle is initiated, as shown in figure 2.

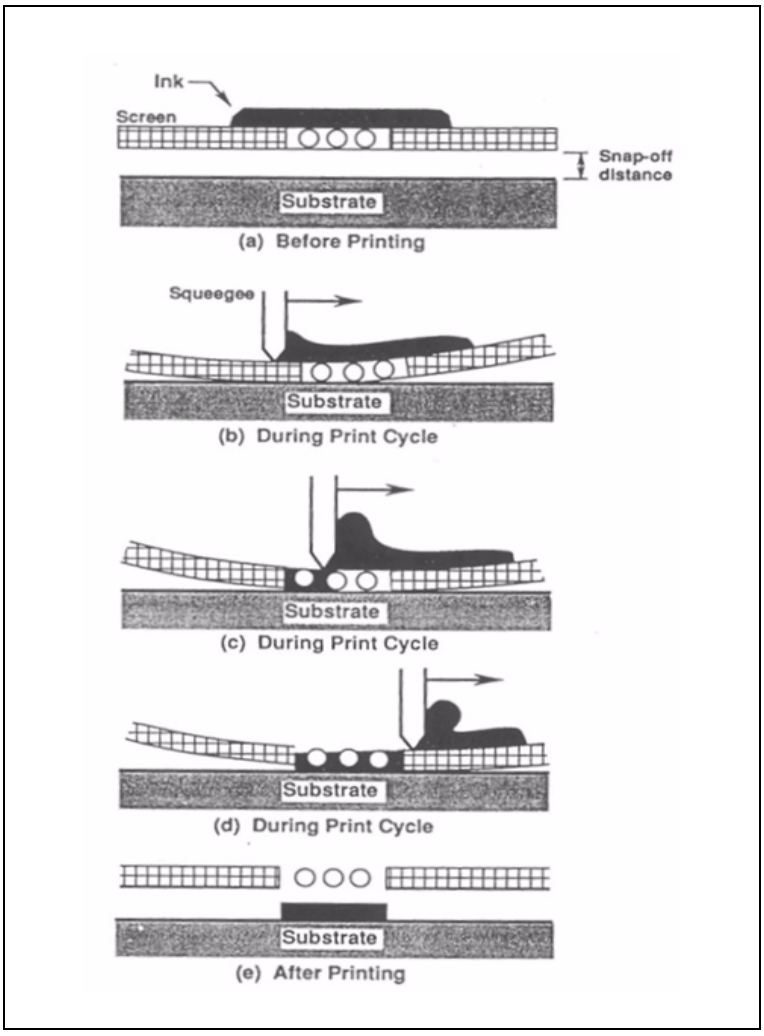

Figure 2: Screen-printing process

The ink is forced through the openings in the screen by a flexible rubber squeegee which depresses the screen to contact the substrate as it traverses the pattern. Directly behind the squeegee the screen peels away from the substrate and leaves behind a deposit of ink, having the required pattern, on the substrate surface.

After a time of relaxation in order to allow levelling of the paste surface, usual measured thickness can range from 20 to 100 µm. In fact, the thickness depends on several parameters such as the opening mesh area of the screen, the rate of the squeegee, the tension of the screen, the viscosity of the paste...[8].

- **the ovens:**

They play two consecutive roles, as they allow:

- Drying: the evaporation of solvents used to adjust the required viscosity of the paste (this step can be carried out in the same furnace as the firing step or more often in a drying oven).
- Firing: the densification and the reaction of the different components.
  We will see later that the properties of the screen-printed paste are very dependent on the firing cycle.

Figure 3 depicts a typical firing profile for a piezoresistive paste.

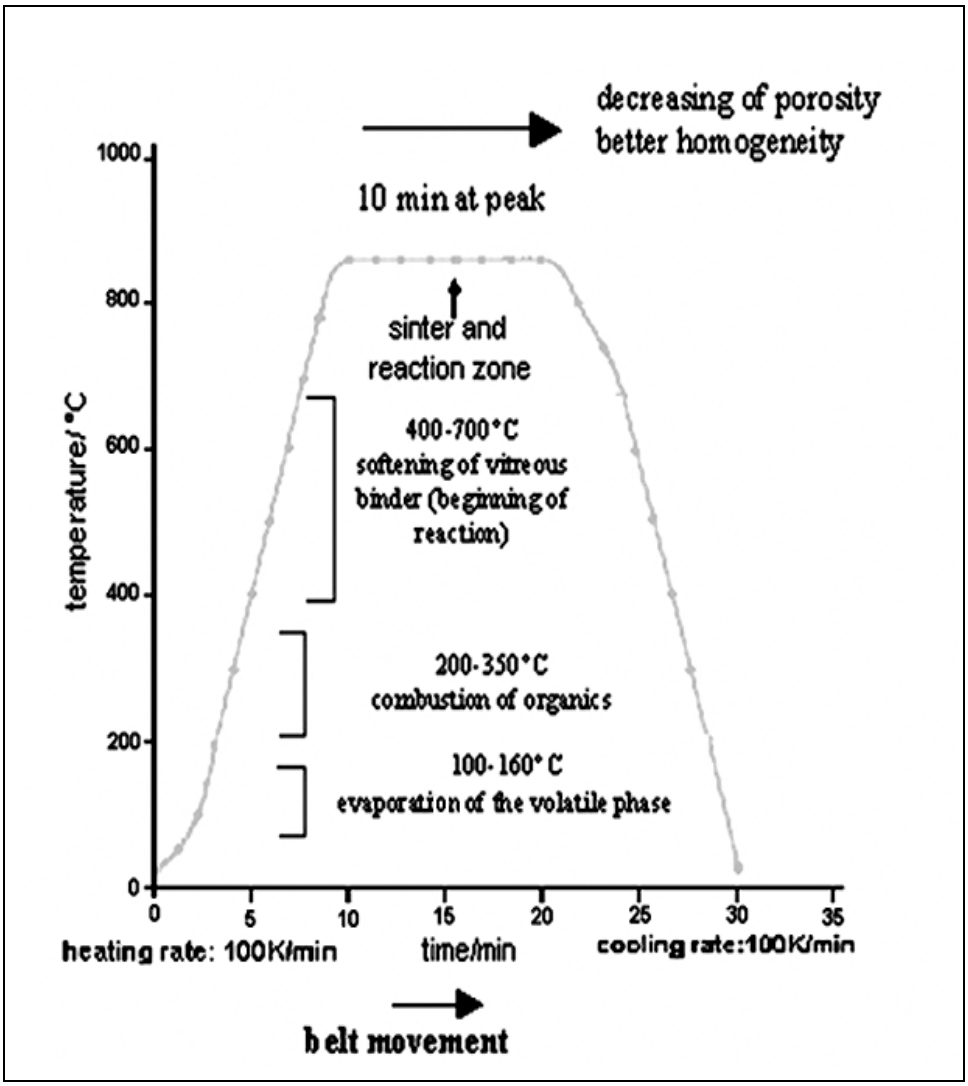

Figure 3: Typical firing schedule for a piezoresistive paste

The firing schedule is controlled in a belt furnace, in which different steps are programmed under dried air:

- the heating step:
The temperature slowly ramps up towards the peak firing temperature (typically 850°C). Below 150°C (drying process), the volatile organic phase is evaporated. Between 150 and 350°C, the remaining organics (polymer binder) are removed. After the first drying step (150°C), the screen-printed film can be manipulated for other printing or drying steps, for instance. Indeed, the remaining binder gives the dried film moderate mechanical stability: this is a non negligible advantage of this printing technique.
When the temperature reaches 400-700°C, the glass frit softens and promotes sintering and reactions between the components of the ink and with the substrate. (Notice that some conductor films such as Ag and Au-rich compositions can sinter in the 700-900°C range without a glass frit.)

- the high temperature dwell:
The temperature remains constant for about 10 minutes (typical). During this time, the active material sinters and various reactions may take place.

- the cooling stage:
The temperature decreases at 100°C/min. The solidification of the glass stops the reactions.

After this schedule, the material, with a typical final film thickness of about 10 microns, has acquired the adequate electrical properties.

After firing, discrete components can be mounted, and the value of piezoresistive pastes can be adjusted by laser-trimming [9].

I . 3 . Properties of piezoresistive pastes

The aim of this work is to study piezoresistive pastes.
These inks should be qualified at different steps of the fabrication of a sensor. By this way, the whole process may be adequately controlled:
- before screen-printing and firing: the unfired state of the paste will be called the "raw state".
- after firing: at this moment, the paste ideally does not undergo any more material modifications.

Whereas the raw state is essentially qualified by physico-chemical properties, the fired one is based on electrical properties.

I . 3 . 1 . Material properties (before screen-printing)

This phase is important as it fixes the properties after firing.
Different parameters should be controlled but all depend on the composition.

This basic and unavoidable part has been studied by different ways on commercial pastes. Diverse, but complementary techniques of analysis are used to determine the large amount of components disposed in a complex arrangement. The used analytical techniques remain more or less the same:
Scanning electron microscopy (SEM) observations are performed to detect phase morphology and particle size [10-12]. For more details, Transmission electron microscopy (TEM) is used to go further into the examination of the crystallinity, phase morphology and phase identification [13, 14]. In addition, x-ray energy dispersive spectroscopy (XR-EDS) is required for elemental composition determination, and X-ray diffraction (XRD) for crystalline phase identification [10, 11, 13, 14].

From these different results, it has been established that current piezoresistive inks consist basically of a mix of two powders: a fine-grained (20-100 nm) conductive phase (RuO_2 or ruthenate) and a lead borosilicate glass frit (1-3µm) [15]. A temporary organic vehicle (solvent and binder) is added in order to allow screen-printing and to allow manipulation of the printed substrate after the drying process if several layers are to be co-fired. Some other oxides are also added as minor additives to modify the temperature coefficient of resistance (TCR) [16-20] or the temperature coefficient of expansion (TCE) of the glass phase [21].

The following figure (figure 4) represents a typical piezoresistive paste composition:

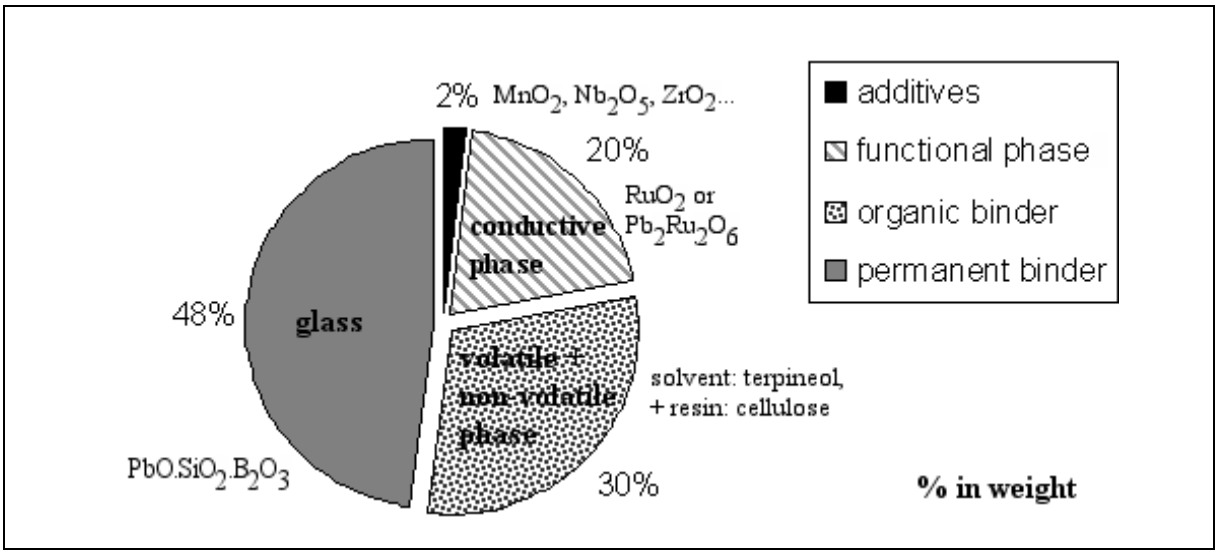

Figure 4: General composition of piezoresistive pastes

As shown in this pie-chart, inks are composed of four complementary parts:
- a glassy matrix ($PbO\text{-}SiO_2\text{-}B_2O_3$),
- a conductive phase (RuO_2 or ruthenate),
- an organic phase (solvent + polymer + dispersant + plasticizer): the vehicle,
- different additives.

Each part contributes to one specific parameter.

- **The glass**

A micrometer grain size glass frit is used.
The composition of this glassy matrix defines the firing temperature range of the paste. In thick-film resistors, densification occurs by liquid-phase sintering. The glass of the piezoresistive paste melts and surrounds the conductive nano-grains.
In order to optimise reliability, the temperature coefficient of expansion (TCE) of the glass should be close to that of the substrate, preferentially slightly lower in order to impart a moderate compressive strain.

These above conditions are met by the series of lead-borosilicate glasses ($PbO\text{-}SiO_2\text{-}B_2O_3$). Lead oxide (PbO) decreases the fusion temperature of the glass and lowers the dependence of viscosity on temperature, quartz (SiO_2) and boron oxide (B_2O_3) are considered as common network formers. Moreover, B_2O_3 is used to decrease the softening temperature of the glass that is increased by the presence of SiO_2. The variations between the concentration of these three components allow to adjust the film TCE to that of the used substrate. A high PbO concentration favours the stabilisation of ruthenate based phases instead of the oxide form of ruthenium [22, 23]. Depending on whether RuO_2 or ruthenates ($Pb_2Ru_2O_6$) are produced, the value of resistivity is not the same... [24, 25].

• The conductive phase

It is the other main element of a piezoresistive paste and it determines the electrical properties of the inks by its morphology and concentration. The grain-size, the specific surface area and the morphology of the powders represent some important parameters.

The used conductive powders are generally nanometer size, spherical and well-crystallised metallic oxide powders. In our case, the composition is based on ruthenium oxides (RuO_2 or $Pb_2Ru_2O_6$) because of their stability. Note that the stoechiometric composition of the lead ruthenate is not trivial as a deficiency in oxygen has been observed leading to a $Pb_2Ru_2O_{6+y}$ composition. The studies of Goodenough and Muller on properties of oxygen deficient pyrochlores have shown that *y* corresponds in general to 0 [26,27].

The concentration of RuO_2 and the grain size will determine, among other properties, the resistivity value [28-30].

• The organic phase (the vehicle)

It guarantees the rheological properties for optimum screen-printing, suitable homogenisation, and its two-step removal allows handling after the drying process due to the cohesion imparted by the binder.

Few details are given in the literature concerning the organic binder composition, although the quality of the resulting film depends on its nature and properties. However, Prudenziati et al. give some details about the common organic vehicles by taking an interest in the rheological properties [31]. In addition, Baudry et al. present some measurement principles and results with some inks [32].

The vehicle is mainly composed of a volatile phase (solvent: terpineol) and a non-volatile phase (polymer: ethyl-cellulose) [31] - additionally, small quantities of dispersants and plasticizers improve the homogeneity and the printability of the paste. The combination of these elements will allow to master the viscosity of the paste.

Indeed, optimum screen-printing requires a pseudoplastic or thyxotropic behaviour of the paste [32]. This function is complex, and there are conflicting requirements for the ink viscosity when it is subjected to the various printing stages: without mechanical stress, the viscosity of the paste should be high in order to avoid flowing on the screen. But when the ink is being forced through the screen by the squeegee (application of a shear stress), a low viscosity is needed. After printing, the film must retain its printed geometry and not run, and therefore recover a high viscosity. Contrary to Newtonian fluids, the viscosity of thick-film pastes is modified by an applied pressure.

Figure 5 shows the variation of the viscosity of a thick-film paste at different stages during the printing cycle [7].

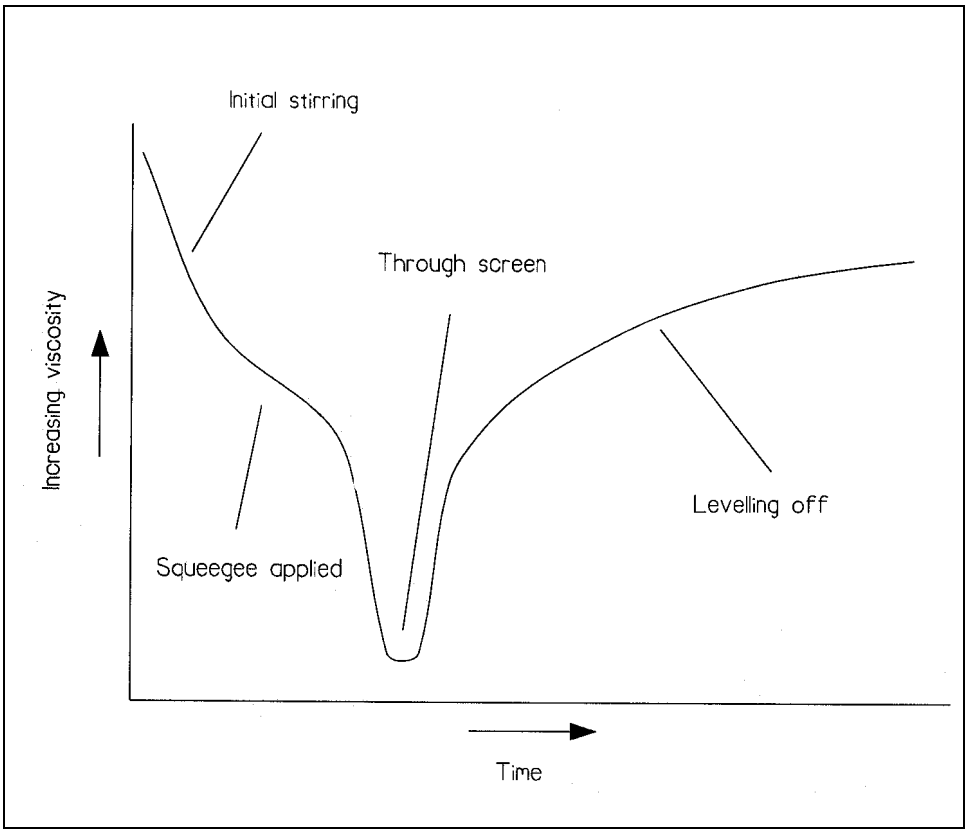

Figure 5: Variation of viscosity of a paste during the screen-printing cycle

After the screen-printing process, the organic vehicle is removed during the firing cycle. The volatile part is evaporated below 150°C, whereas the non-volatile phase (polymer), which assures cohesion of the film when the solvent (terpineol) is evaporated, is burnt out between 300 and 400°C.

- **The additives**

They are used to modify some properties. They are generally added to the glass as oxide powders. Different series of additives are used [33] for various purposes:

- modification of TCR: whereas TiO_2, CdO, MnO_2 are negative TCR drivers, copper oxides or precious metals shift the TCR in the positive direction.

- modification of resistance value: an increase of the conductive phase concentration contributes to a decrease of resistivity and an increase of TCR. In most cases, negative / positive TCR drivers increase / decrease resistivity.

- modification of piezoresistive properties: the gauge factor increases by decrease of conductive phase fraction [35-36], and small surface area of conductive phase leads to resistors of relatively high GF [34, 35].

I . 3 . 2 . Electrical properties (after firing process), structural evolution and conduction mechanism

After the firing process, the material structure, which defines the electrical properties, is stabilised, and the electrical properties thus defined. These properties depend on the firing conditions. For instance, it has been shown that high firing temperatures and times favour kinetics of reaction between conductive and insulating grains [37]. This can lead to a modification of the phases, such as dissolution of the conductive phase in the glass, that causes a variation of the resistance.
It is evident that structural evolution and electrical properties are intimately linked.

I . 3 . 2 . 1 . Electrical properties

The electrical properties characterising a piezoresistive paste are:
- the resistance value (R)
- the gauge factor value (GF)
- the temperature coefficient of resistance value (TCR)

• Resistance value

This value (R) can be expressed with the Ohm's law:

$$R = \rho \cdot \frac{l}{b \cdot h} \quad \text{(ohms)}$$

ρ: resistivity (ohm/m)
l: length of the resistor (m)
h: thickness (m)
b: width (m)

In thick-film technology, the sheet resistance (R_S) is more commonly used, and corresponds to the resistance of a square (length = width). Hence, the sheet-resistance of any thick film can expressed as following:

$$R_S = \frac{R}{N_s} \text{ , where } N_S = \frac{l}{b}$$

N_s: number of squares along the path of the current flow

A large range of values can be obtained as it depends on the concentration of the conductive phase. But, the usual values are comprised between 0.1 and 100 kΩ/square.

• Gauge factor value - Piezoresistive factor

The change of resistance of a resistor under an applied stress is partly due to deformation, i.e. the changes in the dimensions of the resistor, and partly due to alterations in the specific resistivity as a result of microstructural changes [38]. The gauge factor (GF) of a resistor is defined as the ratio of the relative change in resistance ($\Delta R/R$) and the strain ($\varepsilon = \Delta l/l$):

$$GF = \frac{(\Delta R)/R}{(\Delta l)/l} = \frac{(\Delta R)/R}{\varepsilon} \qquad (1)$$

We are interested in separating the true piezoresistive effect from effects due to geometric change and boundary conditions. This expression can therefore be decomposed into a piezoresistive and a geometric term.
Taking the *R* value of a parallelepipedic resistor (figure 6) of an isotropic material, we should consider two cases: the longitudinal case (L), where the current flows along *l* (the current is parallel to the applied strain), and the transverse case (T), where the current flows along *b* (the current is perpendicular to the strain).

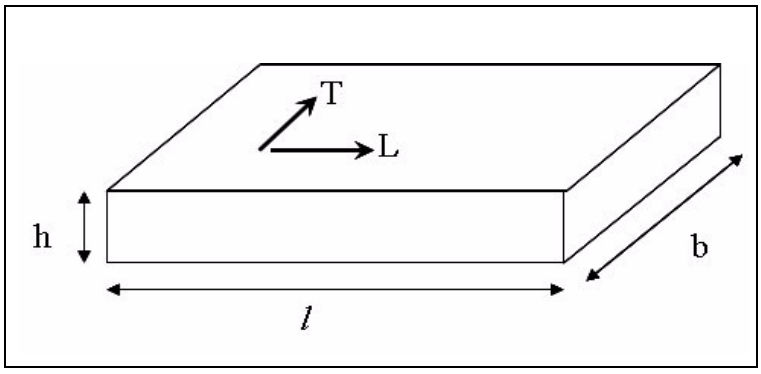

Figure 6: Representation of the parameters for a parallelipipedic resistor (we define *l* as the direction of the applied strain)

Case L:

$R_L = \rho \cdot \frac{l}{h \cdot b}$, taking into account that $\Delta \ln(xy) = \frac{\Delta x}{x} + \frac{\Delta y}{y}$ (with x and y: variable)

then $\frac{\Delta R_L}{R_L} = \frac{\Delta \rho_L}{\rho} + \frac{\Delta l}{l} - \frac{\Delta h}{h} - \frac{\Delta b}{b}$

In fact, $\frac{\Delta \rho_L}{\rho}$ reflects the piezoresistive response, whereas $\frac{\Delta l}{l} - \frac{\Delta h}{h} - \frac{\Delta b}{b}$ corresponds to the geometric variation.

The same reasoning is realised for the case T:

$R_T = \rho \cdot \frac{b}{h \cdot l}$, then $\frac{\Delta R_T}{R_T} = \frac{\Delta \rho_T}{\rho} + \frac{\Delta b}{b} - \frac{\Delta h}{h} - \frac{\Delta l}{l}$

In fact, $\frac{\Delta \rho_T}{\rho}$ reflects the piezoresistive response, whereas $\frac{\Delta b}{b} - \frac{\Delta h}{h} - \frac{\Delta l}{l}$ corresponds to the geometric variation.

The geometric contribution is relatively low, as for longitudinal and transverse strain (if we define a coordinate system specific to the geometry of the beam):

$$\frac{\Delta l}{l} = \varepsilon \; ; \; \frac{\Delta b}{b} = 0 \; ; \; \frac{\Delta h}{h} = -\varepsilon \cdot \frac{\nu}{1-\nu} , \qquad (2)$$

with ν: Poisson's coefficient of the resistor ~ 0.3

We obtain then from Eq.1, 2, the corresponding longitudinal and transverse gauge factor (GF_L and GF_T):

$$GF_L = \frac{\Delta R_L}{R_L} \cdot \frac{1}{\varepsilon} = \frac{\Delta \rho_L}{\rho \cdot \varepsilon} + 1 + \frac{\nu}{1-\nu} \quad \text{and} \quad GF_T = \frac{\Delta R_T}{R_T} \cdot \frac{1}{\varepsilon} = \frac{\Delta \rho_T}{\rho \cdot \varepsilon} - 1 + \frac{\nu}{1-\nu}$$

with the first term corresponding to the piezoresistive contribution and the second one reflecting the geometric contribution.

Then, the longitudinal and transverse piezoresistive factors (respectively Γ_L and Γ_T) can be expressed as:

$$\Gamma_L = \frac{\Delta \rho_L}{\rho \cdot \varepsilon} \text{ and } \Gamma_T = \frac{\Delta \rho_T}{\rho \cdot \varepsilon}.$$

From this, the isotropic (or hydrostatic) piezoresistive factor Γ defined as the resistivity change is induced by an isotropic strain field, is:

$$\Gamma = \frac{\Delta \rho}{\rho \cdot \varepsilon} = \Gamma_L + 2\Gamma_T,$$

which is a useful relation when the experimental set up does not permit to apply an isotropic strain field. Moreover, this piezoresistive factor Γ will be used for the interpretation of conduction models (in chapter IV).

The GF values of thick-film resistors lie mostly between 3 and 35 [39-41]. The observed high GF values are due to microstructural changes that alter the specific conductivity. For a 10kOhms/square resistance, a gauge factor value = 12 is usual.
This value is however strongly dependent on materials and microstructural parameters, such as the nature and grain size of the conductive phase, the interactions with the substrate, the firing temperature...

- **Temperature coefficient of resistance value (TCR)**

$$TCR = \frac{R_T - R_{25}}{R_{25}(T-25)} \times 10^6 \quad \text{(ppm/°C)}$$

R_{25}: resistance of the material at 25°C (ohms)
R_T: resistance of the material at T temperature (ohms)
T: temperature of the measurement of R_T

The temperature dependence of R may be significantly nonlinear, which is characterised in practice, by two TCRs: the hot TCR (HTCR) where T can vary from 80 to 125°C and the cold TCR (CTCR) where T varies from 0 to -40°C: these temperatures are not standard and depend on the application of the thick-film resistor.

Unless it is intended for temperature measurements, a good thick-film resistor should have both hot and cold TCR absolute values of less than 100 ppm/°C, but it can go from 50 to 200ppm/°C [42] for our applications.

I . 3 . 2 . 2 . Structural evolution

• Correlation between electrical properties and structure

Several studies have been investigated concerning the influence of some selected parameters on the electrical properties.

Hrovat et al. show that the gauge factor depends on the conductive grain size. The value is low for homogeneous material with many small grains and short distances between them [14]. Likewise, Prudenziati et al. concluded that a very high gauge factor can be obtained by using large-sized RuO_2 grains [28, 34].

Moreover, the gauge factor increases with increasing resistivity [39, 42]. In other words, if the mixing ratio of RuO_2 to glass is kept constant, the larger the RuO_2 particle-sizes, the higher the resistances [43]. It comes from the fact that the specific surface area is decreasing and that the conduction channels are reduced.

However, the parameter having the greatest influence on the specific resistivity of the resistor is the ratio between conductive and glass phases.

On the opposite, Canali et al. find no evidence of correlation between gauge factors and grain size of the conductive phase [35], as similar GF is reported in resistors with very different grain sizes. Moreover, very different GF values are obtained with comparable grain sizes. In the same article, it is explained that there is no specific relation between gauge factors and temperature coefficient of resistance (TCR), as resistors with different GF values have similar TCR's. Strain sensitivity is dominated by the nature of the conductive phase and not affected by the glass composition and additives present in the glassy matrix, while, on the contrary, these latter features (glass composition and additives) strongly affect the temperature dependence of thick-film resistance.

• Material aspect

Upon firing, the organic material is first burnt out, followed by densification of the material to give a nanoscale composite consisting of chains of conductive islands in an insulating matrix.

Apart from the knowledge of composition, it is essential to understand the possible reactions between the particles that occur during the firing process. Some authors have detected the apparition of new phases. The constituents of the materials react with each other (conductive oxides, glass phase and additives). Dissolution / reprecipitation of the conductive phase have been observed [22,24,44-46]. Also, the conductive phase may exchange lead oxide with the glass matrix, leading to decomposition of ruthenate into RuO_2 or the reverse reaction depending on the glass composition and firing temperature [22,24,44]. Reaction of the glass with the alumina substrate has also been observed [23,47-49].

The usual firing and cooling times (each ca.10 min) are presumably not sufficient for the material to reach equilibrium [21], as increasing firing time, and temperature [22] or refiring several times lead to significant changes in structure, chemistry and electrical properties [50-52].

The increase of the firing time leads to the components of the inks to reach equilibrium. Hrovat measured a decrease of sheet resistance, whereas absolute TCR values of resistors tend to increase significantly [15, 21]. For a given paste composition (glass and conductive phase), the increase of the firing temperature gives quite different properties due to changes in microstructure and composition promoted in resistors by thermal treatment, including chemical exchange (PbO) between the glass and the conductive phase. For instance, sheet-resistance and gauge factor depends on the firing temperature [53]. It is interesting to note that piezoresistance

appears to be one of the properties most sensitive to the evolution of microstructure and composition of thick-film resistors.
Whereas some observations are contradictory (grain size influence on the gauge factor value), some other are convergent. It would be interesting to study this aspect.

I . 3 . 2 . 3 . The conduction mechanism

In addition to the technological aspects, thick-film piezoresistors have very interesting properties concerning the interplay between percolation processes, tunnelling, and microstructure, rarely encountered in other disordered conductor-insulator composites. For example, close to the percolation threshold, transport properties of thick-film resistors cannot be easily understood within standard percolation theory [54-60]. Even more striking is the divergence of the piezoresistive response at the percolation threshold reported some years ago [36-61]: The conductivity is shown to vanish near a critical concentration of conductive phase, where piezoresistive properties diverge [36]. The behaviour of the resistors in this region is interesting.
Tunnelling processes are at the origin of the high sensitivity of the thick film resistors to applied strains. The conduction is dependent on the glass layer between conductive particles. In the case of piezoresistive pastes whose resistance changes with an applied strain, the strain creates a distortion inside the material, which moves the particles away from or closer to each other. This perturbation can modify the electrical response that is dependent on the concentration of the conductive grains.

The interpretation of the measured results led us to propose a conduction mechanism based on the tunnelling-percolation model proposed by Balberg. This model of transport non-universality is based on an inverted random-void model in which current flows through tunnelling process between conducting spheres immersed in an insulating medium [62, 63]. This model can be applied to composites where intergrain tunnelling is the main microscopic mechanism of transport.

According to the classical theory of transport in percolating systems, the resistance R of a metal-insulator composite with metallic volume concentration x follows a power-law behaviour of the form [55]:

$$R \cong R_0 \cdot (x - x_c)^{-t}$$

R_0 : prefactor
x_c: percolation critical concentration (threshold)
t: transport critical exponent

Random resistor network theories predict that R_0 and x_c depend on the microscopic details of the composite, such as the arrangement of the conducting phase within the sample and the elemental resistances connecting two neighbouring sites. The transport exponent t is assumed to be universal and to be constant for a fixed dimensionality. But deviations from universality have been reported with RuO_2, among other systems. Contrary to a vast class of material which display the same constant t value, the transport is supposed to be affected by microscopic properties. The aim is to investigate further the universality breakdown of thick film resistors and its microscopic origin.

I . 4 . Programme of this thesis

In this thesis, the initial study of some commercial pastes is considered as reference. A second part is devoted to the synthesis and study of new model piezoresistive pastes to understand and enhance the structural and electrical properties, and to answer technological needs.

In this previous chapter, an overview of usual piezoresistive pastes is presented: process, required properties and applications. We highlight that, whereas some aspects are well studied (composition..), some others stay less examined (conduction mechanisms...).
The general aim of this thesis is, on one hand, to develop and to optimise piezoresistive pastes by studying their electrical and structural properties depending on process parameters and conduction mechanism. On the other hand we pay attention to the conduction process, that is to say, to physical phenomena that govern piezoresistive properties. The understanding of conduction mechanism will be helpful for the optimisation of piezoresistive pastes.
We will try to find a coherence between the structure evolution, the electrical response, the variation of parameters and the conduction mechanism.

Chapter 2 is devoted to the study of commercial pastes. The obtained results of structural analysis, composition, electrical properties are considered as a reference for our further work. Moreover, the stability of these inks is tested by changing the firing process. These aspects, which have been little studied previously, allow us to emphasise the interactions between the different components.
According to these observations, we propose to study, on one hand, the influence of the firing schedule (temperature and time) on the properties and stability of several thick-film resistors compositions. On the other hand, we will emphasise the role of the cooling rate (quenching or not) on the same properties. Until now, all the structural analysis and studies of electrical properties presented in the literature have been realised after the firing cycle [10, 13, 14]. By quenching, the elements don't have time to reach equilibrium during cooling. By this way, we expect to "freeze" the microstructure at the end of the high-temperature dwell. The observations will help us to understand the mechanisms occurring during this high-temperature dwell. After that, a prolonged annealing may highlight a structural evolution towards an equilibrium state.
At the end of this chapter, it will appear that the studied current commercial pastes could be optimised. For instance, their stability as a function of the firing process could be enhanced. Moreover, these kind of pastes cannot be used with temperature sensitive substrates because of their high firing temperature.

Based on these results, chapter 3 is focused on the development of new piezoresistive pastes.
After having understood the role of each process and composition parameter (firing steps, phase composition of the paste), three series of pastes are realised following different parameters (glass composition, concentration and grain size of the conductive phase). A detailed manufacturing process is established - aspect that has never been fully described in the literature. Judicious parameters are chosen following two inter-correlated original approaches:
- a technological goal: to enhance the properties and to adapt the paste on other applications (steel substrates instead of alumina substrates),
- a theoretical aim: to understand the conduction mechanism by analysing the complex nanostructure and the electrical results and to validate a model by a new approach. The conduction mechanism will allow us to understand and optimise electrical properties in piezoresistive pastes.

In order to study the physico-chemical evolution and to propose technological solutions (more flexible substrate to enhance the piezoresistive response), we choose uncommon but judicious glass compositions: the choice is representative of a range of temperature based on the phase diagram of lead-borosilicate glass [64-66]. In spite of the low melting temperature, we expect to highlight phase transitions. Indeed, from Adachi's studies, the stable conductive phase (RuO_2 or lead ruthenate) depends on the glass composition [22], and overfiring studies will be carried out to experimentally verify the stability of the phases.
Different works have been realised on standard glass compositions but less with those for low temperatures. Of course, low firing temperatures don't promote the kinetics of chemical reactions. It will therefore allow us to study separately the physical phenomenon of conduction from the chemical reactions. And from the point of view of technology, low firing temperatures allow use of other more flexible substrates (aluminium or steel) that don't tolerate high firing temperatures (850°C).

Chapter 4 - the key chapter - presents the results and their interpretation by a model of conduction based on a yet unpublished hypothesis. In order to be coherent with the study of commercial pastes in chapter 2 and to propose some interpretations of non-explained results, the stability is evaluated with nearly the same experiments (variation of the firing conditions).
We present our research on RuO_2-based thick-film resistors prepared with several volume fraction values x of RuO_2 with two different mean grain sizes, for both low- and high-temperature glasses. We have studied the effects of the percolation transition to the insulating state on the resistivity and the piezoresistivity response.
We present our contribution to the understanding of the origin of transport nonuniversality by attacking the problem from a different point of view. In contrast with the mean-field hypothesis [67], the random-void model [68, 69], and its extension [70], the tunnelling-percolation model of Balberg predicts that the critical exponent t, which governs universal or non-universal behaviour, acquires an explicit dependence upon a microscopic variable (the mean-tunnelling distance a), which could be altered by a suitable external perturbation. So, if transport nonuniversality is driven by tunnelling, it would be possible to change the value of the transport critical exponent t by applying a pressure or a strain to the composite. The possibility of influencing t by external means (e. g. strain) has never been studied previously. Thus, we propose a new way to investigate percolative systems thanks to the study of various series of RuO_2-based thick-film resistors which display universal [71] and non-universal transport [36,61,62,67-72] behaviours.

At the end of this chapter, the best new piezoresistive pastes are selected for the development of a complete system in a sensor. The application of this new generation of pastes is described in chapter 5.

Chapter 6 can be considered as an outlook as different optimisations are proposed to resolve some persisting problems; troubles that remain unavoidable in the case of the development of new generation of products. Although a new generation of low firing temperature pastes have been proposed and successfully tested in this work, their behaviour could be optimised. For instance, their TCR can be controlled by the addition of metal oxides. Moreover, in order to use environmentally friendly materials, it would be interesting to use a lead-free glass what implies important modifications of the present system. Concerning the conduction mechanism, our hypothesis based on the dependence of the critical exponent t on microscopic properties in non-universal systems has been validated, but the studies of such conduction mechanisms could be investigated further by the evaluation of «extreme systems», where the glassy matrix would be

replaced by a polymer - we would obtained a soft system (polymer) in which hard small particles would be dispersed.

To summarise, this work is relevant and innovating as it combines physical, chemical and material phenomena and it is based on a new generation of low temperature inks, using standard inks as reference. In order to validate our work, a complete system will be presented for application of sensors on metal substrates.

References - Chapter I:

1. Funk W, *Thick-film technology*, Acta Electronica, 1978, **21**(4), 251-55.
2. Larry JR, Rosenberg RM, Uhler RO, *Thick-film technology: An introduction to the materials*, IEEE Transactions on components, hybrids, and technology, 1980, **CHMT-3** (2), 211-25.
3. Prudenziati M, *Handbook of sensors and actuators*, elsevier, 1994, **1**, 127-379.
4. White NM, Turner JD, *Thick-film sensors: past, present and future*, Meas. sci. technol., 1997, **8**, 1-20.
5. Prudenziati M, *Handbook of sensors and actuators*, elsevier, 1994, **1**, 59-63, 198-205.
6. Coleman M, *Thick-film materials for hybrids*, The Radio and Electronic Engineer, 1981, **52**, 227-34.
7. Prudenziati M, *Handbook of sensors and actuators*, elsevier, 1994, **1**, 1-13.
8. Haussonne JM, *Céramiques pour l'électronique et l'électrotechnique*, Presses polytechiques et universitaires romandes, 2002, 88-92.
9. Prudenziati M, *Handbook of sensors and actuators*, elsevier, 1994, **1**, 20-4.
10. Morten B, Masoero A, Prudenziati M, Manfredini T, *Evolution of ruthenate-based thick-film cermet resistors*, journal Phys. D: Appl. Phys., 1994, **27**, 2227-35.
11. Meneghini C, Mobilio S, Pivetti F, Selmi I, Prudenziati M, Morten B, *RuO_2-based thick-film resistors studied by extended x-ray abosrption spectroscopy*, Journal of applied physics, 1999, **86**(7), 3590-93.
12. Vest RW, *Materials science of thick film technology*, Ceramic Bulletin, 1986, **65**(4), 631-36.
13. Nordstrom TV, Hills CR, *Transmision electron microscopy studies of the microstructure of thick-film resistors*, International journal of hybrid microelectronics, 1980, **3**, 14-19.
14. Hrovat M, Drazic G, Holc J, Belavic D, *Correlation between microstructure and gauge factors of thick-film resistors*, Journal of materials science letters, 1995, **14**, 1048-51.
15. Hrovat M, Samardzija Z, Holc J, Belavic D, *Microstructural, XRD and electrical characterization of some thick film resistors*, Journal of materials science: materials in electronics, 2000, **11**, 199-208.
16. Hamer DW, Biggers JV, *Thick film hybrid microcircuits technology, Wiley, New-York*, 1972.
17. Inokuma T, Taketa Y, Haradome M, *Strange temperature characteristics of RuO2-based thick-film resistors*, Electrocomp. Sci. Technolo., 1982, **9**, 205-7.
18. Kuzel R, Broukal J, Kindl D, *X-ray and microscopic investigatoins of resistors containing CdO and RuO_2*, IEEE Trans. CHMT, 1981, **4**, 245-9.
19. Casale MEA, Iles GS, Collier ON, *Improvements in or relating to resistor composition*, British Pat. 1 210 493, 1967.
20. Iles GS, *Ruthenium resistor glazes for thick films circuit.*, Radio and electron. eng., 1968, 299-304.

21. Hrovat M, Holc J, Samardzija Z, Belavic D, *The influence of firing temperature on gauge factors and the electrical and microstructural characteristics of of thick film resistors*, J. of materials science letters, 2001, **20**(8), 701-05.

22. Adachi K, Kuno H, *Decomposition of ruthenium oxides in lead borosilicate glass*, J. Am. ceram. Soc., 1997, **80**(5), 1055-64.

23. Palanisamy P, Sarma DHR, Vest RW, *Solubility of ruthenium dioxide in lead borosilicate glasses*, J. Am. ceram. Soc., 1989, **72**(9), 1755-56.

24. Hrovat M, Samardzija M, Belavic D, Holc J, *Microstructural and electrical characteristics of some "overfired" thick-film resistor*, Journal of materials science letters, 2001, **20**(4), 347-51.

25. Pierce JW, Kuty DW, Larry JR, *The chemistry and stability of ruthenium-based resistors*, Solid state technology, 1982, oct., 85-93.

26. Longo JM, Raccah PM, Goodenough JB, *$Pb_2M_2O_{7-x}$ (M= Ru, Ir, Re) - Preparation and properties of oxygen deficient pyrochlores*, Mat. Res. Bull., 1969, **4**, 191-202.

27. Muller O, White WB, Roy R, J. Inorg. Nucl. Chem., 1964, **26**, 2075-86.

28. Tamborin M, Piccinini S, Prudenziati M, Morten B, *Piezoresistive properties of RuO_2-based thick-film resistors: the effect of RuO_2 grain size.*, Sensors and actuators A, 1997, **58**, 159-64.

29. Yamaguchi T, Iiuka K, *Mirostructure development in RuO_2-glass thick-film resistors and its effect on the electrical resistivity*, J. am. ceram. soc., 1990, **73** (7), 1953-57.

30. Abe O, Taketa Y, Haradome M, *The effect of various factors on the resistance and TCR of RuO_2 thick-film resistors -- Relation between the electrical properties and particle size of constituents, physical properties of glass and firing temperature*, Electrical engineering in Japan, 1989, **109** (3), 12-18.

31. Prudenziati M, *handbook of sensors and actuators1*, 1994, **1**, 113-16.

32. Baudry H, Franconville F, *Encres sérigraphiables pour haute définition. Rhéologie et impression.*, Acta electronica, 1978, **21**(4), 283-95.

33. Inokuma T, Taketa Y, *Control of electrical properties of RuO_2 thick film resistors*, Active and passive elec. comp., 1987, **12**, 155-60.

34. Prudenziati M, Morten B, Cilloni F, Ruffi G, *Very high strain sensitivity in thick-film resistors: real and false super gauge factors.*, sensors an actuators, 1989, **19**, 401-14.

35. Canali C, Malavasi D, Morten B, Prudenziati M, Taroni A, *Piezoresistive effects in thick-film resistors*, J. applied phys., 1980, **51**(6), 3282-88.

36. Carcia PF, Suna A, Childers WD, *Electrical conduction and strain sensitivity in RuO_2 thick-film resistors.*, J. Apl. Phys., 1983, **54**, 6002-8.

37. Pike GE, Seager GH, *Electrical properties and conduction mechanisms of Ru-based thick-film (cermet) resistors*, J. appl. phys., 1977, **48**, 5152-69.

38. Hoffman K, *An introduction to measurements using strain gauges*, Hottinger Baldwin Messtechnik GmbH, Darmstadt, 1989.

39. Hrovat M, Belavic D, Samardzija Z, Holc J, *A characterisation of thick film resistors for strain gauge applications,* Journal of materials science, 2001, **36** (11), 2679-89.

40. Canali C, Malavasi D, Morten B, Prudenziati M, Taroni A, *Piezoresistive effects in thick-film resistors,* J. appl. phys, 1980, **51**, 3282-88.

41. Prudenziati M, Morten B, Cilloni F, Ruffi G, *Very high strain sensitivity in thick-film resistor: real and false super gauge factors*, Sensors and actuators, 1989, **19**, 401-14.

42. Hrovat M, Holc J, Belavic D, Soba S, *An evaluation of some commercial thick-film resistor materials for strain gauges.*, Journal of materials science letters, 1994, **13**, 992-95.

43. Inokuma T, Taketa Y, Haradome M, *Conductive and insulative particle size effects on the electrical properties of RuO_2 thick-film resistors.*, IEEE Transactions on components, hybrids and manufacturing technology, 1985, **CHMT-8**(3), 372-3.

44. Bube KR, *The effect of prolonged elevated temperature exposure on thick-film resistors,* Proceedings of international microelectronics sympsium (Washington, DC). International society for hybrid microelectronics, 1972, 2A6-1-2A6-13.

45. Morten B, Prudenziati M, Sacchi M, Sirotti F, *Phase transitions in Ru based thick-film (cermet) resistors,* J. Appl. Phys., 1988, **63**, 2267-71.

46. Adachi K, Kuno H, *Effect of glass composition on the electrical properties of thick-film resistors,* J.Am.Ceram.Soc., 2000, **83**(10), 2441-48.

47. Cattaneo A, Marelli M, Prudenziati M, *Effects of refiring processes on electrical and structural properties of thick-film resistors*, Proceedings of the European hybrid microelectronics conference, 1979, **2**, 241-53.

48. Moriwaki H, Suzuki A, Watanabe Y, Ishiwata M, Kamata T, Adachi K, *Interactions between thick-film resistors and alumina substrate.*, proceedings of Japan international electronic materials technology symposium, IEEE, Tokyo, 1993, 46-49.

49. Hoffman LC, *An overview of thick-film hybrid materials,* Am. Ceram. Soc. Bull., 1984, **63**, 572-76.

50. Hrovat M, Belavic D, Samardzija Z, Holc J, *The development of microstructural and electrical characteristics in some thick-film resistors during firing*, J. of materials science letters, 2002, **37**, 2331-39.

51. Lee J, Vest RW, *Firing studies with a model thick film resistor system,* IEEE Transactions on components, hybrids, and manufacturing technology, 1983, **CHMT-6**(4), 430-35.

52. Hrovat M, Belavic D, Samardzija Z, Holc J, *The development of thick film resistor properties during firing*, Conf. proceedings. MIDEM, Soc. microelectron. components and mater, Dunajaska, Slovenia, 1999, 169-74.

53. Prudenziati M, Tankiewicz S, Morten B, Piccinini S, Golonka L, *Piezoresistive effects in thick-film piezoresistors: the effect of the conductive phase,* Proceedings of international spring seminar on electronic technology- ISSE'97- Poland, 1997, 76-81.

54. Nan CW, *Physics in inhomogeneous inorganic materials.*, Prog. Mater. Sci., 1993, **37**, 1-116.

55. Kirkpatrick S, *Percolation and conduction,* Rev. Mod. Phys., 1973, **45**, 574-88.

56. Webman I, Jortner J, Cohen MH, *Numerical simulation of electrical conductivity in microscopically inhomogeneous materials*, Phys. Rev. B, 1975, **11**, 2885-92.

57. De Gennes PG, *La percolation, un principe unificateur*, La recherche, 1976, **7**, 919-27.

58. Malliaris A, Turner DT, *Influence of particle size on the electrical resistivity of compacted mixtures of polymeric and metallic powders*, J. appl. phys., 1971, **42**, 614-8.

59. Ottavi H, Clerc J, Giraud G, Roussenq J, Guyon E, Mitescu CD, *Electrical conductivity of a mixture of conducting and insulating spheres: an application of some percolation concepts*, J. phys.C, 1978, **11**, 1311-29.

60. Seager GH, Pike GE, *Percolation and conductivity: a computer study. II*, Phys. rev. B,1974, **10**, 1435-46.

61. Nicoloso N, LeCorre-Frisch A, Maier J, Brook RJ, *Conduction mechanisms in RuO_2-glass composites*, Solid state ionics, 1995, **75**, 211-16.

62. Balberg I, *Tunneling and nonuniversal conductivity in composite materials*, Phys . Rev. Lett., 1987, **59**, 1305-8.

63. Forlani F, Prudenziati M, *Electrical conduction by percolation in thick film resistors*, Electrocomponent science and technology, 1976, **3**, 77-83.

64. Johnson DW, Hummel FA, *Phase equilibria and liquid immiscibility in the system PbO-B_2O_3-SiO_2*, Journal of the american ceramic society, 1968, **51**(4), 196-201.

65. Geller RF, Bunting EN, *The system PbO-B_2O_3-SiO_2*, Journal Res. Natl. Bur. Std, 1939, **23**(8), 275-83.

66. Trubnikov IL, *Thermal expansion, vitrification temperature,and corrosion behavior of lead-borosilicate glasses.*, Refractories and inductrial ceramics, 2000, **41**(5-6), 169-71.

67. Heaney MB, *Measurement and interpretation of nonuniversal critical experiments in disordered conductor-insulator composites*, Phys. Rev. B, 1995, **52**, 12477-80.

68. Halperin BI, Feng S, Sen PN, *Differences between lattice and continuum percolation transport exponents*, Phys. Rev. Lett., 1985, **54**, 2391-4.

69. Halperin BI, Feng S, Sen PN, *Transport properties of continuum systems near the percolation threshold*, Phys.Rev. B, 1987, **35**, 197-214.

70. Balberg I, *Limits on the continuum-percolation transport exponents*, Phys. Rev. B, 1998, **57**, 13351-4.

71. Clerc JP, Podolskiy VA, Sarychev AK, *Precise determination of the conductivity exponent of 3D percolation using exact numerical renormalization*, Eur.Phys.Journal B., 2000, **15**, 507-16.

72. Kusy A, *Classical percolation threshold and resistance versus temperature behaviour of RuO_2-glass films*, Physica B, 1997, **240**, 226-41.

CHAPTER II:

Study of commercial piezoresistive pastes

Before optimising and realising new piezoresistive pastes, it is unavoidable to study current commercial inks. In this chapter, we aim to understand firstly the composition / structure of current pastes.
After having selected three representative thick-film resistor compositions used in force and pressure sensors, we'll take an interest to their electrical properties. By this way, the dependence of the materials' microstructure and properties (sheet resistance and its temperature coefficient, gage factor) is studied as a function of firing temperature and time, and cooling rate (furnace or quench).
Then, the stability of the properties is assessed by annealing at intermediate temperatures (100 and 250 °C).
Microscopic and structural analysis are carried out to highlight some possible evolution mechanisms of the resistor materials. The obtained results should be considered as references and will contribute to the fabrication of new optimised piezoresistive pastes.

II . 1 . Composition and microstructure analysis

One of the most common pastes is a Du Pont paste (DP 2041), a standard composition widely used in piezoresistive sensors. This paste, considered as stable, is characterised by a nominal sheet resistance value of 10 kΩ / square.
But its composition remains unclear and complex because of the multitude of components added to realise this paste. A first step is to understand the composition and the structure of this kind of system.

Before beginning analysis, it's necessary to itemise the known parameters. Indeed, we know that the mineral content of piezoresistive pastes is composed of 2 kinds of grains with different sizes:
- glass grains, an usually micrometer lead borosilicate glass

- smaller (nanometer) conductive particles: ruthenium dioxide (RuO_2), lead ruthenates ($Pb_2Ru_2O_6$) or bismuth ruthenates ($Bi_2Ru_2O_7$).

In addition, several additives (oxides) are in most cases adjoined to the glass to control the electrical properties.
The organic vehicle is used to allow the mixture to be screen-printed with an appropriate rheology. This vehicle consists mainly of two phases:
- a volatile solvent
- a non-volatile binder (polymer).

The solvent first evaporates below 150°C in the drying step. Then, during the firing process, the resin is burned out between 300-400°C. Above 600°C, the glass melts and reactions occur between the glassy matrix and the conductive phase.

From these previous observations, it would be judicious to study the composition and the structure of the pastes before and after firing.

II . 1 . 1 . Analytical processes

The following diagram sums up the different kinds of the used techniques (figure 1)

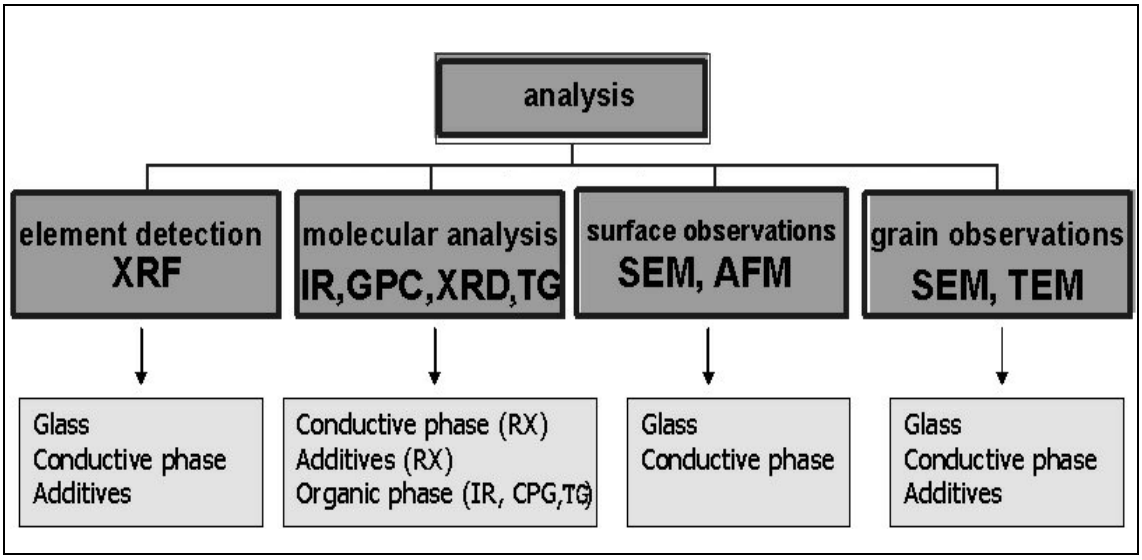

Figure 1: Analysis methods used to study commercial piezoresistive paste composition

Definitions of the different techniques of analysis:

- **XRF: X-Ray Fluorescence spectroscopy**

This non-destructive method allows a global identification of the elements. As no preparation of the sample is necessary, this technique is easy to apply.

Principle of detection:
An X-ray beam (X photons) is projected on the sample. Its elements absorb the energy and release it in the form of fluorescence: an electron of the atom absorbs the energy of the incident photon, which provokes an excitation of the electron that after a relaxation time comes back to its stable level by the emission of a X-photon. The emission of the radiations depends on the

transitions of the electrons between the different electronic layers of the atoms, which are characteristic of each element.
A detector traduces these different emissions by qualitative and semi-quantitative peaks corresponding to each element. (this method doesn't allow to quantify precisely an element but permits to determine whether a component is in high concentration or in trace amounts).

- **IR: Infra-Red spectroscopy**

Infrared spectroscopy is one type of vibration spectroscopy, which, as you might have guessed, is a spectroscopic technique where molecular vibrations are analysed. The most useful I.R. region lies at wavenumbers between 4000 - 670cm^{-1}.

Principle of detection:
An object, which resonates at a certain frequency can absorb excitation having the same frequency. This principle is associated to this method by considering each molecule as a simple harmonic oscillator system. When the emission light is absorbed, the little oscillators in the molecule will continue to vibrate at the same frequency, but since they have absorbed the energy of the light, they will have a larger amplitude of vibration.
The remaining light which is not absorbed by any of the oscillators in the molecule is transmitted through the sample to a detector, and a computer will analyse the transmitted light and determine what frequencies were absorbed.

IR spectroscopy is a simple analytical technique. The material to be analysed should only put in some form that can be insert into the infrared spectrometer. This is usually accomplished by casting a film on a sodium chloride (rock salt) plate, or by mixing the material with potassium bromide, KBr, and making a pellet out of it. These salts are used because they are invisible to IR light.

- **GPC: Gaseous Phase Chromatography**

Gaseous Phase Chromatography is used to separate and analyse the volatile components of a mixture.
Chromatographic separation involves the use of a stationary phase and a mobile phase. Components of a mixture carried in the mobile phase are differentially attracted to the stationary phase and thus move through the stationary phase at different rates.

A small amount of the sample to be analysed is vaporised through an injector into the head of the chromatographic column. A carrier gas, such as helium, flows through the injector and pushes the gaseous components of the sample through the Gas Chromatographic (GC) column. It is within the column (coated or filled with the stationary phase) that separation of the components takes place. Molecules alternate between the carrier gas (the mobile phase) and the high boiling liquid or solid phase (the stationary phase) within the GC column.
After components of the mixture move through the GC column, they reach a detector. Ideally, components of the mixture will reach the detector at varying times due to differences in the partitioning between the mobile and stationary phases. The detector sends a signal to the chart recorder which results in a peak on the chart paper. The area of the peak is proportional to the number of molecules generating the signal.

- **XRD: X-Ray Diffraction**

The principle of X-ray diffraction is used to detect crystalline phases.

X Radiations have the property to penetrate a material and to be diffracted in preferential directions by the atoms situated in a reticular plane (according to the Bragg's law): the degree of diffraction depends on the energy of the incidental radiation and the atomic distribution (more or less crystalline structure). The spectrum of diffraction constitutes the signature structural feature of the analysed crystalline substances. Measurements are taken with an apparatus consisted of a X-ray generating tube and a detector arranged on a goniometer. The technique is mainly used for substances of crystalline structure, especially mineral ones. The diffraction spectra can be obtained directly starting from a solid fragment, or small quantities of powder (powder spectrum).

X-rays, like all electromagnetic waves, cause a displacement of the electronic cloud compared to the core in the atoms; these induced oscillation cause a re-emission of electromagnetic waves of the same frequency; this phenomenon is called Rayleigh diffusion. The wavelength of X-rays is of about equal to the size of the interatomic distances (a few angströms). According to the arrangement of atoms, some directions of space will be favoured and the flow of photons X will more intense: these variations according to directions form the phenomenon of X-rays diffraction.

No specific preparation of the sample is necessary: the sample can be a powder, or a polycrystalline solid.

- **TG: Thermogravimetry**

This technique involves monitoring the weight variation of the sample in a chosen atmosphere (usually nitrogen or air) as a function of temperature. The loss or the gain of mass is measured by a scale. The usefulness of TG for analysing complex systems is greatly enhanced by the introduction of the ability to record simultaneously the first derivative of the variation of weight. This is sometimes referred to as derivative thermogravimetric analysis (DTA).
In order to perform this technique, TG is often coupled with Differential Scanning Calorimetry (DSC). This method allows to measure the exchange of heat flux (measurement of enthalpy). Phase transformations (solidification, fusion..) are detected by exo- or endothermic peaks or by changes of slope (for second-order phase transitions, such as the glass transition).

- **SEM: Scanning Electron Microscopy**

This method allows to observe surfaces with a resolution down to 10nm. It is usually coupled with a system of Energy Dispersive Spectroscopy EDS for qualification and quantification.

Electronic microscopy rests on the same principle as optical microscopy, with the difference that the incidental ray consists on an electron beam, scanning the surface of a sample, instead of a visible ray of light. SEM allows to obtain a highly magnified image (X 100 000 or more) of the sample, revealing details (like "the depth effect") impossible to detect differently and of minute size.
This technique of analysis is employed for the study of metals, minerals, and other materials.
One drawback is the charging of insulating surface by the incident electrons. In this case, one must reduce the beam intensity and / or deposit a conductive thin film (carbon or gold) on the sample.

In order to perform this kind of analysis, elements can be detected with an EDS system installed on the SEM. The electron beam sent on the sample generates x-rays of fluorescence that are collected and detected.

• TEM: Transmission Electron Microscopy

TEM is a more powerful microscope than SEM. This technique allows the determination of:
- the morphology of a sample: the size, shape and arrangement of the particles which make up the specimen as well as their relationship to each other on the scale of atomic diameters.
- crystallographic information: the arrangement of atoms in the specimen and their degree of order, detection of atomic-scale defects in areas a few nanometers in diameter.
- the composition (if so equipped): the elements and compounds whose the sample is composed of and their relative ratios, in areas a few nanometers in diameter.

The transmission microscope is close in its principle to the optical microscope. The electronic beam (produced, for instance, by heating a tungsten filament) crosses the sample and loses in the passing a certain number of electrons.
A TEM works much like a slide projector. A projector shines a beam of light through (transmits) the slide, as the light passes through it is affected by the structures and objects on the slide. These effects result in only certain parts of the light beam being transmitted through certain parts of the slide. This transmitted beam is then projected onto the viewing screen, forming an enlarged image of the slide (up to 1 000 000 X!).

• AFM: Atomic Force Microscopy

The AFM utilises a sharp probe moving over the surface of a sample in a raster scan (resolution: a few angströms). In the case of the AFM, the probe is a tip on the end of a cantilever which bends in response to the force between the tip and the sample. It corresponds to the interaction forces between atoms of the sample and the tip.
The changes in the bending of the cantilever are measured, usually by monitoring the reflection of a laser beam on the cantilever surface.
The movement of the tip or sample is performed by an extremely precise positioning device made from piezo-electric ceramics, most often in the form of a tube scanner. The scanner is capable of sub-angström resolution in x-, y- and z-directions.
It produces a topographical map of the scanned region with a 0.2 nm resolution.

After describing these techniques, we present the most significant results in the following sections.

II . 1 . 2 . Element detection

XRF (Kevex Omicron X-ray fluorescence micro-spectrometer) is realised on dried paste. As we can observe on the spectrum below (figure 2), different elements (L-ray) are detected:
- major elements: lead, ruthenium.
- minor elements: zinc, niobium, zirconium.

Notice that silicon and barium are not detected as they are only perceptible for energy > 25keV. In the opposite, boron is not detected as its energy is too low.

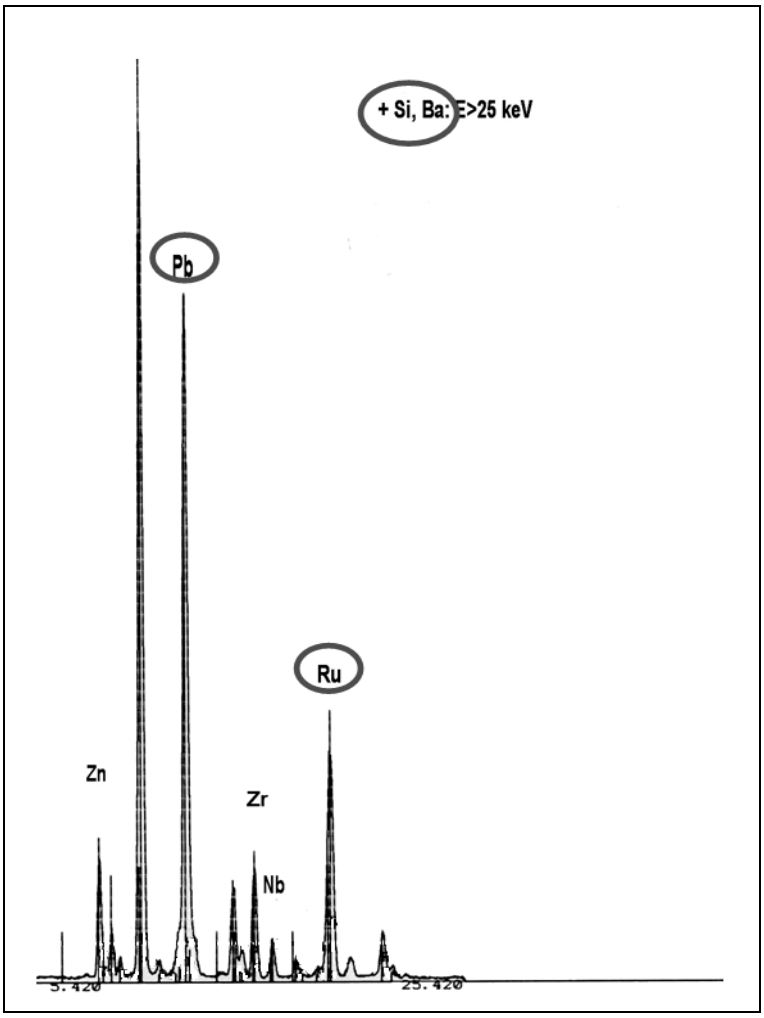

Figure 2: XRF detection: element detection for the DP2041 paste

From this first analysis, we can conclude that as no bismuth was detected, the conductive phase can only be composed of ruthenium dioxide or lead ruthenate: bismuth ruthenate can be eliminated.
Minor elements are attributed to additives under oxide form.

Knowing the element composition, we can carry out the molecular analysis.

II . 1 . 3 . Molecular analysis

- **Conductive phase**

XRD enable to detect crystalline phases: conductive phases and additives. Of course, the glassy matrix is not detected as it is amorphous.
The following XRD spectrum (figure 3), realised with a Kristalloflex 805 Siemens apparatus, corresponds to a dried paste screen-printed on an alumina substrate. This method allows us to determine the initial phases before the firing.

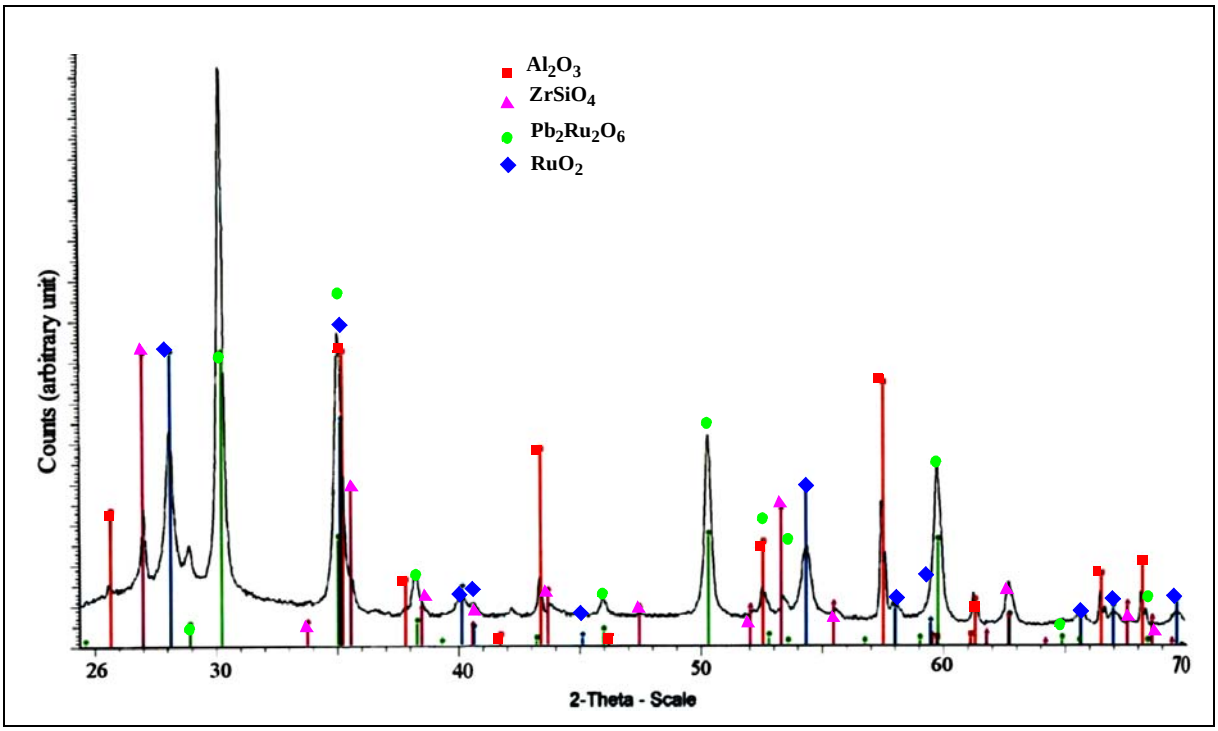

Figure 3: XRD spectrum of DP2041 (dry): determination of cristalline phases

Different crystalline phases are detected:
- RuO_2 and $Pb_2Ru_2O_6$: corresponding to the conductive grains
- Al_2O_3: belonging to the substrate (the thickness of the paste is not sufficient to absorb the beam). If the used alumina substrate is replaced by an other material (such as glass), these alumina peaks disappear.
- $ZrSiO_4$: crystalline additive (or by-product of the milling process).

From these results, we can assert that the DP 2041 paste is composed of a mixture of two kinds of conductive phases: RuO_2 and $Pb_2Ru_2O_6$.

- **Organic phase**

The molecular composition the organic phase can be determined.

The composition of the volatile part is obtained by GPC coupled with mass spectroscopy (Hewlett-Packard HP 5890/5971 GCMS apparatus) system analysis (figure 4).

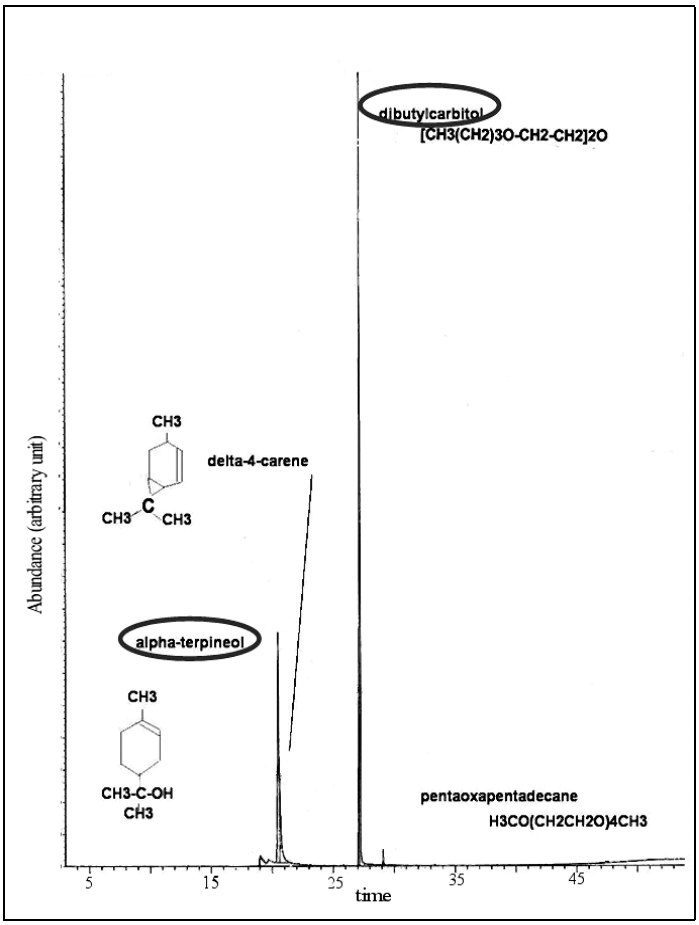

Figure 4: GPC detection: identification of the volatile phase

The spectrum reveals the presence of two major elements: terpineol and dibutyl carbitol. They are used to adjust the viscosity by dissolving the resin.

Concerning the analysis of the resin (non volatile binder), IR analysis (figure 5) indicates that our hypothesis on the presence of cellulose can be validated... but notice that this following result is only indicative and can not be considered as a rigorous scientific result: this was only a test to validate our hypothesis founded on literature [1, 2].

To confirm our hypothesis, we compare the IR spectrum (Nicolet 510 FT-IR spectrometer) of a «real» paste (DP 2041) with a «simulated» system. To realise this system we associate the main components detectable by IR spectroscopy: glass + volatile phase (terpineol + dibutyl carbitol) + ethyl cellulose (with arbitrary proportions).
Notice that we take an interest to peaks at low wavenumbers (> 2000 cm^{-1}), as they better represent the characteristic molecular «fingerprint» of each component.

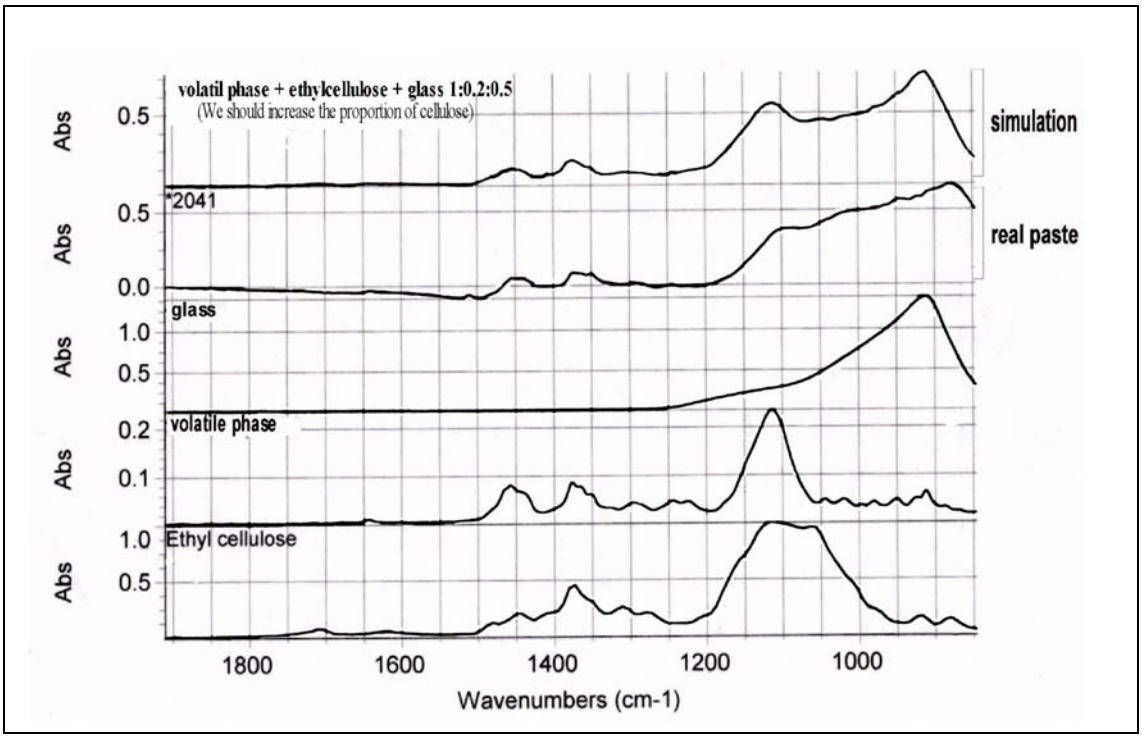

Figure 5: IR spectra: identification of the organic phase (test: no scientific value!)

The simulation spectrum looks like to the one of the commercial paste (called «real paste»):
- around 1400 cm^{-1}, we observe 2 peaks corresponding to the vibration of deformation (scissoring) of H atoms in CH_2 groups of terpineol.
- between 1200 and 1000 cm^{-1}, we detect M-O and C-O oscillations corresponding to terpineol but ethyl cellulose too.
- below 1000 cm^{-1}, oscillations of the glass appear.

Some persistent dissimilitudes between the two spectra could be attributed to the presence of other additives in the commercial paste, to the different composition of the used glass and to a difference of proportions between the components (for instance, the concentration of cellulose could be increased).

From this last analysis, it is reasonable to suppose that the organic phase is composed of terpineol (+dibutyl carbitol) and ethyl cellulose. Note that this proposition will be validated by latter rheological studies (see chapter III).

II . 1 . 4 . Structural observations

Structural observations (surface and bulk) contributes to the detection of the different phases and the observation of their behaviour and interactions during firing.
We intend to observe the paste before, during and after the firing process. But, all these observations don't tolerate the presence of organics, as their evaporating vapours can damage the devices. This is why, in a first step, it is useful to observe the behaviour of organics in order to determine the drying conditions of the samples before analysis.

The TG/DTA (Mettler DSC25 apparatus) diagram (figure 6) shows that practically all organics are evaporated below 300°C. No loss of mass is detected after 300°C.

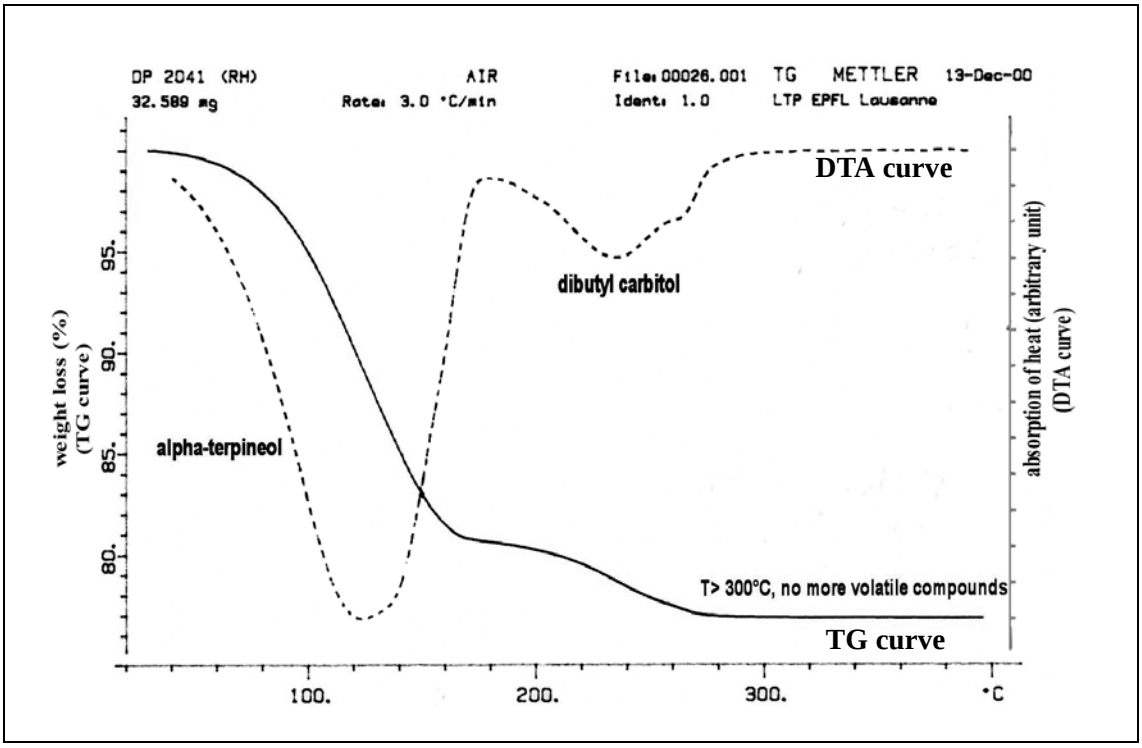

Figure 6: TG (full line) /DTA (dotted line) diagram: volatile phase quantification

First, terpineol evaporates up to ca. 160°C. Dibutyl carbitol then decomposes in two steps, ending at ca. 300°C. Note that the proportion of the resin (binder) is so small that its corresponding loss of mass is not detected.

The following experiments are realised on DP 2041 paste dried at 300°C and fired at 850°C.
Firing constitutes a key step in the process of thick-film resistors. The change of morphology is associated to the occurring reactions between the components. The obtained result corresponds to a stabilisation of the electrical properties.
The behaviour (change of morphology) is well represented by SEM micrographies (Philips XL30-FEG) for different temperatures during firing (figure 7).

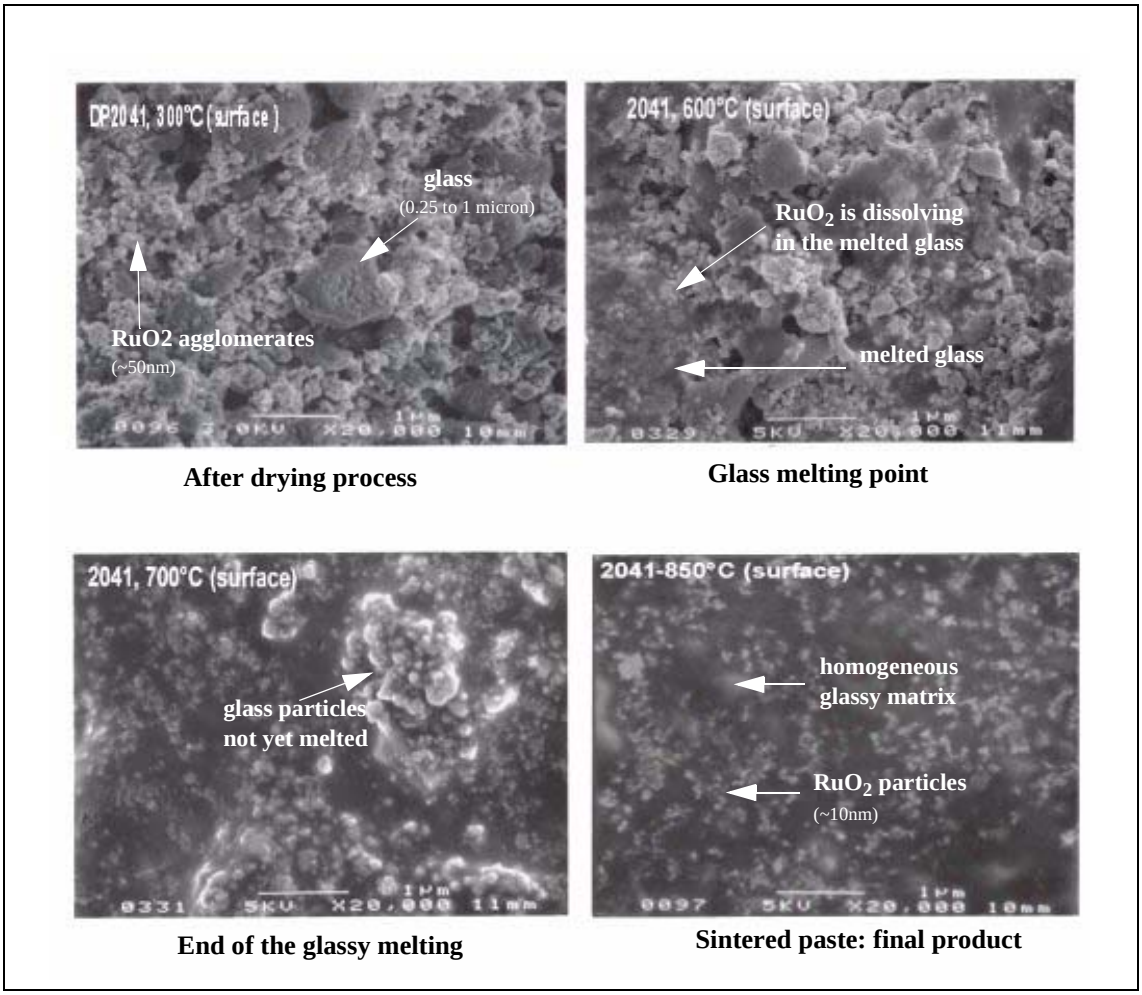

Figure 7: SEM observation of the evolution of the morphology of DP2041 during the firing

SEM micrographies show an inhomogeneous medium. Before the firing process (300°C), the paste is composed by two kinds of grain with different sizes:
- glass particles (0.25-1 µm)
- agglomerated conductive grains (~50 nm).

By increasing temperature, the glass begins to melt (near 600°C) and gradually surrounds RuO_2 particles. At the end of firing (850°C), the final product is a sintered film consisting in a homogeneous glassy matrix in which conductive grains are dispersed and de-agglomerated.

Notice that the nature of each above-mentioned particle was determined by EDS analysis (figure 8).

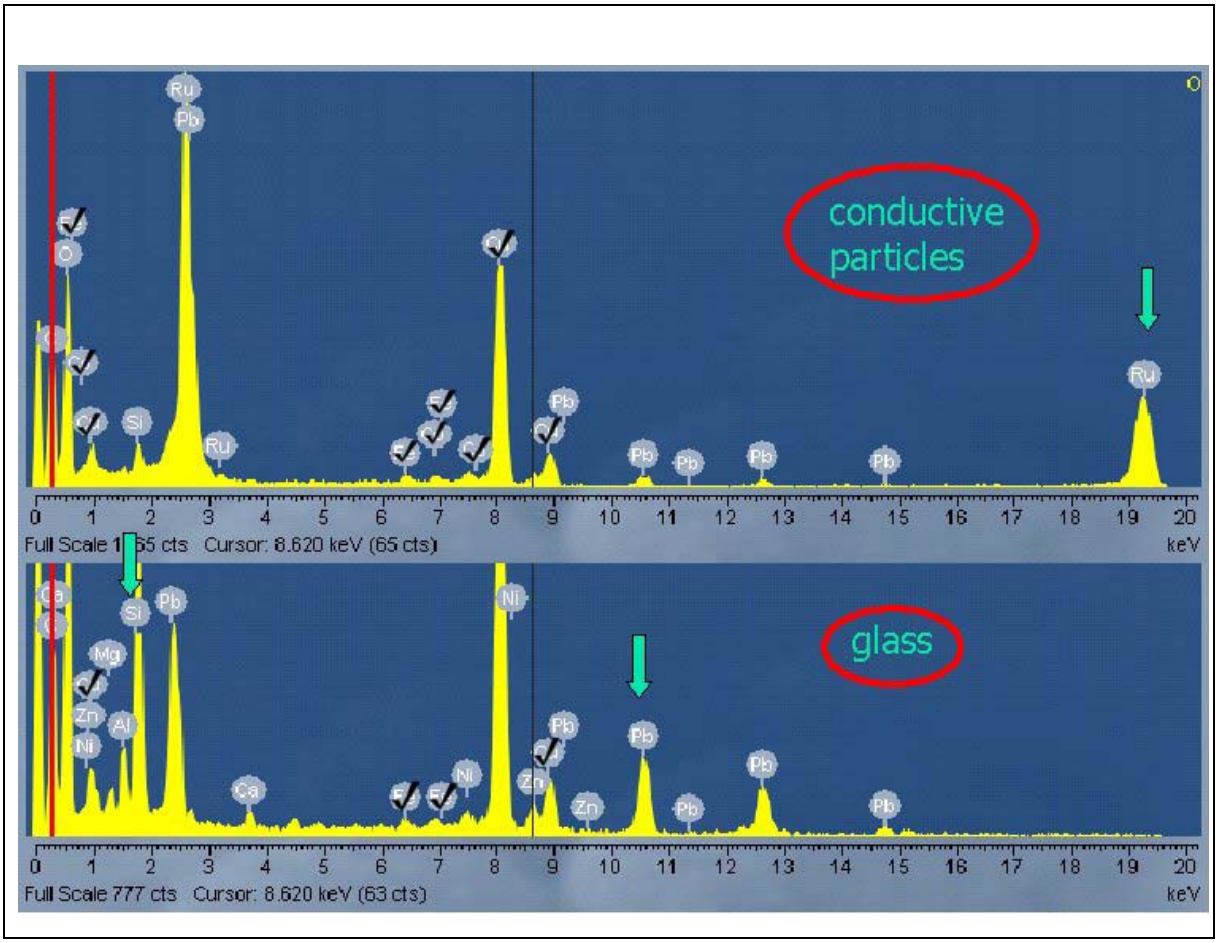

Figure 8: EDS analysis: element detection of particles observed for DP2041 paste

The crossed out elements originate from the microscope and the sample-holder.

The conductive particles are essentially composed of ruthenium oxide. The small amount of detected lead shows that ruthenate phase is certainly not the major conductive phase. The nature of the conductive phase is principally based on RuO_2 with few ruthenate particles.
The glass spectrum is characterised by a majority of lead element. It also contains silicon and aluminium. But it's evident that no ruthenium is detected.
Moreover, it is interesting to note that the additives are essentially present in the glass (Ca, Mg, Zn).

Evolution during the firing process can be illustrated by the following AFM (Digital instruments- Nanoscope IIIa) study (figure 9).

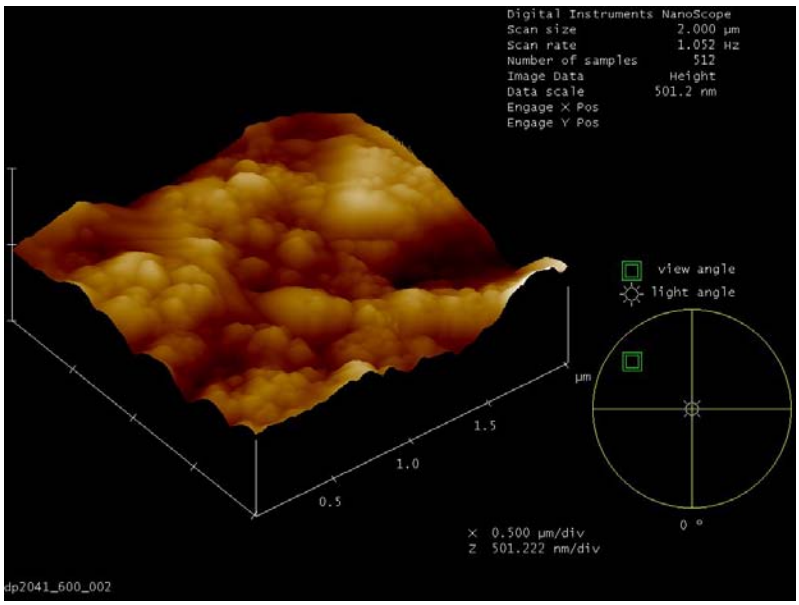

Surface observation of a DP2041 sample fired at 600°C (melted glass)

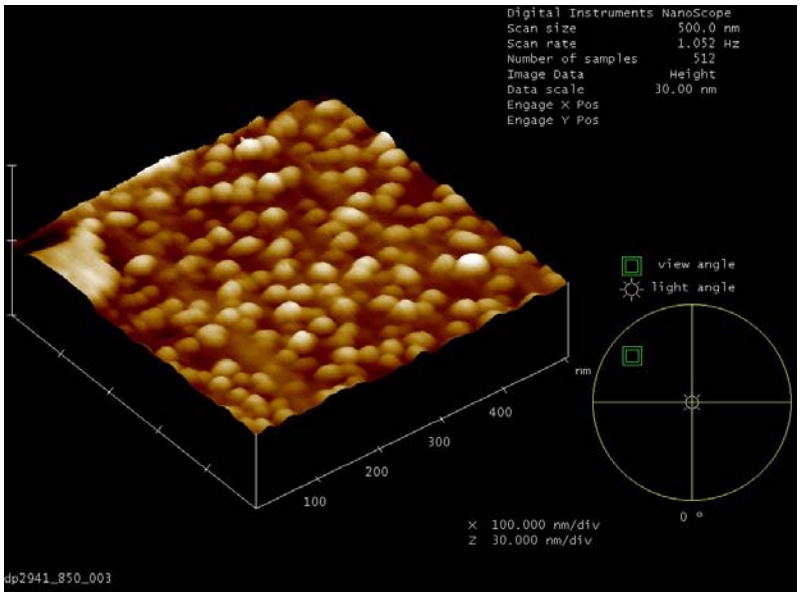

Surface observation of a DP2041 sample fired at 850°C (dispersion of RuO_2 in the glass)

Figure 9: AFM observation: particle organisation

Pictures show an important change of morphology according to the temperature. At 600°C, the glass is melting and no structure is apparent. However, at 850°C, we discern a nano-particle network, which favours specific properties of conduction (tunnelling) described in the next chapter.

It is unavoidable that chemical reactions occur during firing. These phenomena depend from the local distribution of the elements. So, after some surface studies, bulk observations are carried out.
TEM (Philips EM 430) permits to access to these kinds of details, and the associated mapping studies give idea of distribution of elements.
Figure 10 is a representation of the bulk (thinned by ionic bombardment) of a fired screen-printed resistor. (the substrate isn't visible).

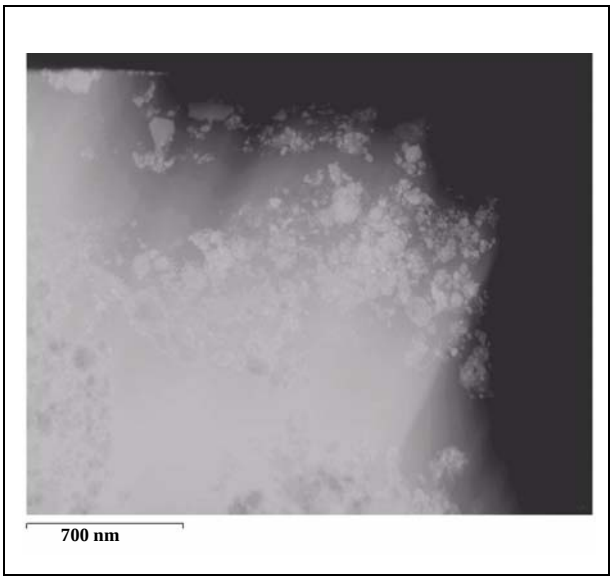

Figure 10: TEM dispersion bulk analysis on a DP2041 sample fired at 850°C

We remark an inhomogeneous system with small grains in an continuous matrix.
Mapping micrographies allow to locate some components. In the following picture (figure 11), we mainly study the repartition of major elements (Ru, Pb, Si) and some additives (Ca, Zr), which are present in different kinds of grains.

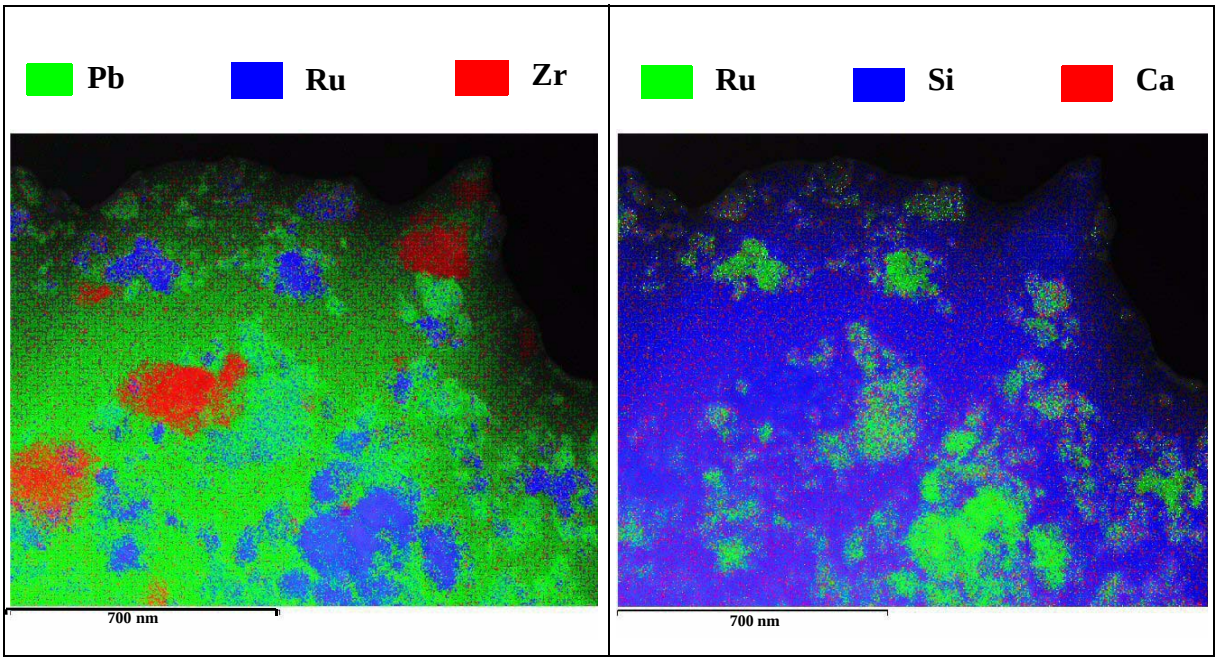

Figure 11: Mapping representation of the spacial distribution of elements from fig.10

We distinguish several well-defined zones, in particular ruthenium regions localised in a lead-rich area. This corresponds to the conductive grains (agglomerates) dispersed in the glass. The second map validates the idea that most of the lead is located in the glassy matrix, as silicon is observed in the same region as lead. Indeed, these two elements are associated to form the glassy matrix.
Note that boron element (contained in the glass) cannot be detected by this kind of method because of its too low energy of excitation.

Concerning additives, different distributions are highlighted. Zirconia seems very localised (like ruthenium), whereas calcium is dispersed. It certainly comes from the process: calcium is added directly to the glass, while zirconia is added in the paste as a crystalline component ($ZrSiO_4$) as detected by previous X-ray analysis.

EDS micro-analysis give access to more details (figure 12):

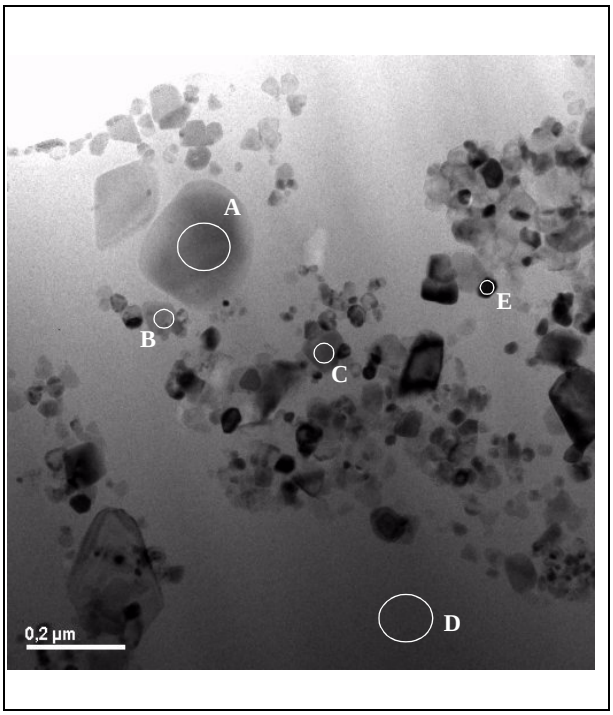

Figure 12: TEM microanalysis: local composition in a DP2041 sample fired at 850°C

The analysis of the granular phase shows a great disparity of composition and of particle size. Here is a detail of the selected areas:
zone A: Nb, Pb, Ca, Al
zone B: Ru, Pb, Si, Al
zone C: Zr, Pb, Mg, Al, Si
zone D: Pb, Zn, Ba, Si, Mg, Ca, Al
zone E: Ru, Pb, Si, Al
(B can not be detected!)

The systematic detection of lead in each element is due to the fact that all particles are embedded in the lead glass. Zone D shows that the homogeneous area corresponds to the glassy matrix. We can find a relation between the size and the composition of the particles. The smallest (B, E) correspond to conductive grains, whereas the intermediate and largest (C, A) can be

considered as additives that have been added during the process or that have been formed during the firing.

II . 1 . 5 . Outlook

These preliminary series of analysis constitute a first step in the understanding of composition and behaviour in piezoresistive pastes (particularly, DP 2041 paste):
Nanograin size RuO_2 or lead ruthenates are initially mixed with an organic binder (terpineol + ethylcellulose) and some micrometer glass grain (lead borosilicate glass). During the firing, organics are burnt out. Then occurs the sintering process, and the melting glass surrounds the conductive grains. The final product is composed of nanoparticles dispersed in a homogeneous glassy matrix. To control the properties, additives under oxide form can be added directly in the glass or as a separated phase.

Obviously, transformations occur during the firing. Indeed, physical modifications have been highlighted by SEM and AFM analysis. The result is a new organisation of the particle network, resulting in a change and a stabilisation of the required electrical properties. These physical transformations associated to a modification of properties are certainly associated to chemical modifications.
Considering literature [3-5] and the precedent results, we can propose some hypothesis: It rests on a possible exchange of atoms during the firing (figure 13). Lead of glass could be transferred to RuO_2 conductive grains to generate a new ruthenate phase (or vice versa). On the contrary, ruthenium atoms are expected to be dissolved partially and locally in the glassy matrix. this chemical changes will cause a modification of the conductivity and then of the properties, resulting in a supposed tunnelling conduction.

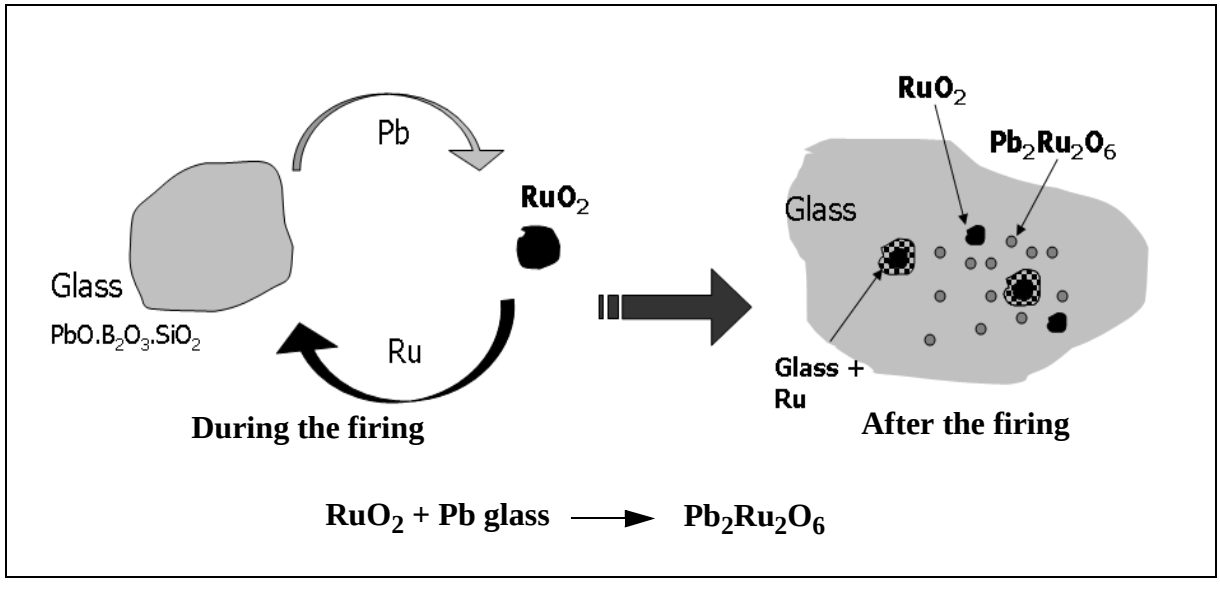

Figure 13: Hypothesis of exchange mecanism during the firing

This first part (general composition of DP 2041) can be considered as the beginning in the understanding of complex phenomena that we expect to clarify in the following chapter. Indeed, we will try to emphasize the events occurring during the firing, and particularly the exchange hypothesis by showing the formation of new phases.

Notice that for standard conditions (850C, 15min), no significant transformations were observed with X-ray analysis of DP 2041 at 300 and 850°C (figure 14).

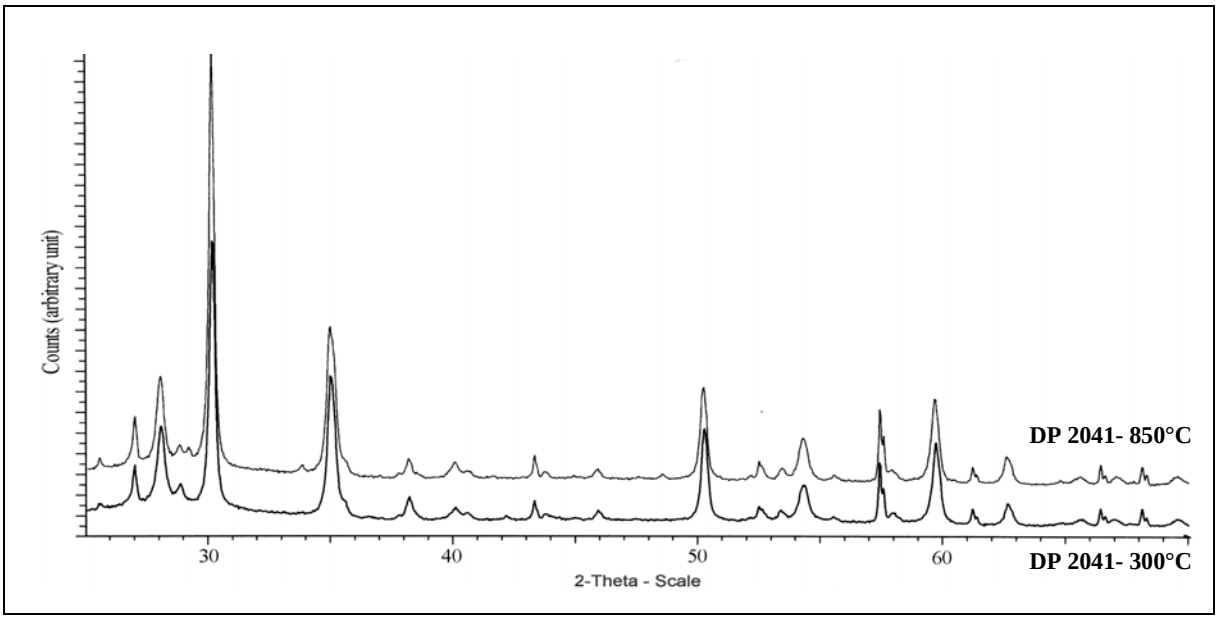

Figure 14: Phase evolution vs. firing temperature (300-850°C) for DP2041 sample

A possible atom exchange forming a new phase was not detected, as the initial conducting phase already includes a mixture of RuO_2 and lead ruthenate phase. In order to emphasise this phenomenon, it would be judicious to change the firing conditions and to choose other piezoresistive pastes characterised by a single conductive phase. That is the purpose of the following chapter.

II . 2 . Study of properties

II . 2 . 1 . Choice of selected pastes

All the selected commercial pastes are similar, as they share the same nature of glass (a lead borosilicate glass) and conductive phase based on ruthenium.
Besides the fact that the glass composition differs concerning the concentration of the elements as the firing temperature is not the same for the three pastes, the main difference comes from the conductive composition and the grain size. These dissimilitudes have probably repercussions on the structure after firing and then will influence electrical properties.

In this work, 3 compositions with R_s = 10 kOhms / sq nominal sheet resistance are evaluated:
1) Du Pont (DP) 2041: a standard, considered as stable, composition widely used in piezoresistive sensors,
2) Electro Science Laboratories (ESL) 3414: specifically formulated to have high gauge factor (GF) values,
3) ESL 3114: a low-firing (625 vs. 850°C for DP 2041 & ESL 3414) composition for applications on enamelled steel substrates.

These compositions exhibit different conductive phases: RuO_2 only in ESL 3114, ruthenate ($Bi_2Ru_2O_7$) only in ESL 3414, and a mixture of RuO_2 and ruthenate (presumably $Pb_2Ru_2O_6$) in DP 2041.

II . 2 . 2 . Experiments - sample description

All the substrates are 96% pure alumina (Kyocera, Japan, A-476), the standard thick-film substrate material. In order to minimise termination effects due to diffusion, gold (ESL 8837) is chosen as termination material. A single layout (figure 15) is used to provide samples for all measurements: structural and microscopic investigations (10 x 10 mm^2 squares) (part A), R_S and TCR (1.5 mm wide resistors of several lengths) (part B), and longitudinal and transverse GF (Wheatstone bridge on cantilever beam), 1 x 1 mm^2 resistors (part C).

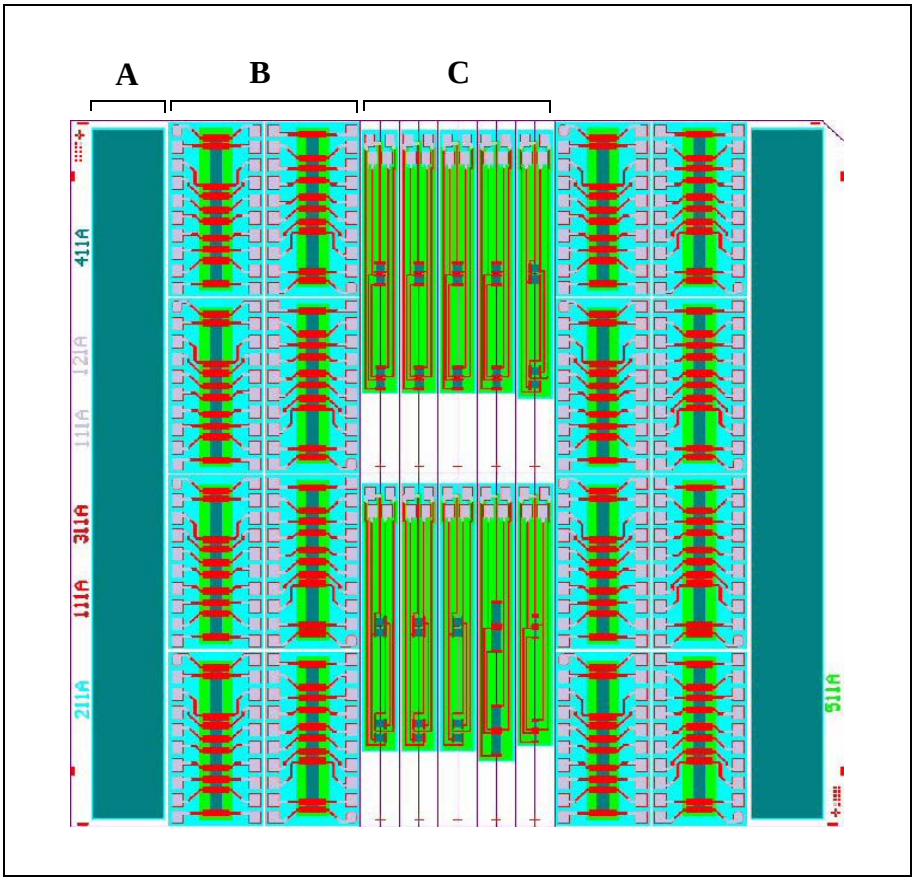

Figure 15: Layout design of a substrate

- **measurements**

R_S and TCR are measured as a function of resistor length between room temperature (*RT* = 23…26°C) and 100°C. R_S is always given at 25°C by correcting the *RT* value with the measured TCR. The mean resistivity is determined from 1.5 mm wide resistors with 8 different lengths ranging from 0.3 mm up to 5 mm and thickness of about 10 µm.

GF is determined at *RT* by applying weights at the end of the test cantilevers, with test elastic strains of ca. 200 ppm (figure 16).

To measure the piezoresistive response, the pastes are screen printed in a Wheatstone bridge geometry on 96% Al_2O_3 cantilever bars 50.8 mm long, b=5.08 mm wide, h=0.63 mm thick, and with an effective Young modulus of E^* = 333 GPa. The cantilever is clamped at one end, whereas on the opposite end a known force F is applied at a distance d= 27.8 mm from the farthest resistor. In this way, we can deduce the surface strain $\varepsilon = 6\,F\,d\,/\,(E^*\,b\,h^2)$ along the main cantilever axis, which is transferred to the TFR.
We speak about effective Young modulus as its value is a little higher than the modulus mentioned in the literature (E ~ 315 GPa). This increase is due to the geometry of the beam. Indeed, b being much larger than h, the plane strain model (ε ~ 0 in the plane of the beam, perpendicularly to the beam axis) is appropriate.
In this case:

$$E^* = \frac{E}{1-\nu^2}$$

ν : Poisson's coefficient of the material (0.23 for alumina).

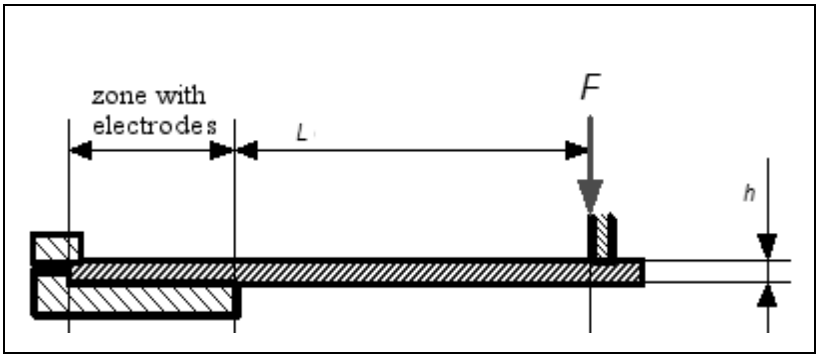

Figure 16: Strain beam mounting for GF evaluation

Typically, four resistors connected in a Wheatstone bridge are used to measure the GF value. For better sensitivity (i.e. a greater change in the balance of the Wheatstone bridge), two resistors are normally under tension (an increase of resistance) and two under compression (a decrease of resistance). In our case, we chose to screen-print the four resistors on the same side of the beam (you can see on figure 15 that the resistors are on the above side: they are under tension). With this layout, the four resistors can be screen-printed in the same time contrary to the other case that would require a two-step screen-printing. By this method, the reproducibility of the screen-printing and the firing is enhanced. Moreover, this layout allows a differential measurement of the strain, which is essentially independent of the position of the applied force. Within the same thick-film resistor series, both the GFs and the current-noise indices increase with increasing sheet resistivity, while the voltage response of the Wheatstone bridge decreases [6, 7]. Therefore, in most cases 10 kOhms / sq. resistors are used for strain sensors as a useful compromise between sensitivity and relatively low noise, and also because of their relatively low power consumption.

The initial (as-fired) properties of the resistors for the standard firing cycle (850°C, 10 min for DP 2041 and ESL 3414, and 630°C, 10 min for ESL 3114) are given in Table 1. The negative TCR of ESL 3114 is expected due to the wide TCR tolerances for this paste and to the fact that it is adapted to steel substrates, which have a larger TCE than alumina.
TCR for DP 2041 and ESL 3414 are slightly positive: they are well adapted to alumina substrates.

Material	R_s (kOhm)	TCR (ppm/K)	GF_L longitudinal	GF_T transverse
DP 2041	11.0	58.0	11.6	8.1
ESL 3414	8.0	42.0	18.0	10.0
ESL 3114	8.5	-243.0	10.7	8.7

Table 1: Electrical characteristics for the standard schedule

Note: Formulae for the determination of *R*, TCR and GF are described in previous chapter I.4.2.

The observed microstructures (figure 17) differ considerably: the dried structures show an inhomogeneity in function of the particle size. For the three pastes, glass grains are considerably bigger than the conductive particles. However, DP 2041 looks more homogeneous, contrary to ESL series that present sharper and coarser glass grains. These inhomogeneities lead to different microstructures after firing: while DP 2041 has a fine microstructure, ESL 3114 and ESL 3414 exhibit a coarser segregation of conducting regions and glass-only areas. These observations are in accordance with previous work on DP 2041 and ESL 3414 [8].

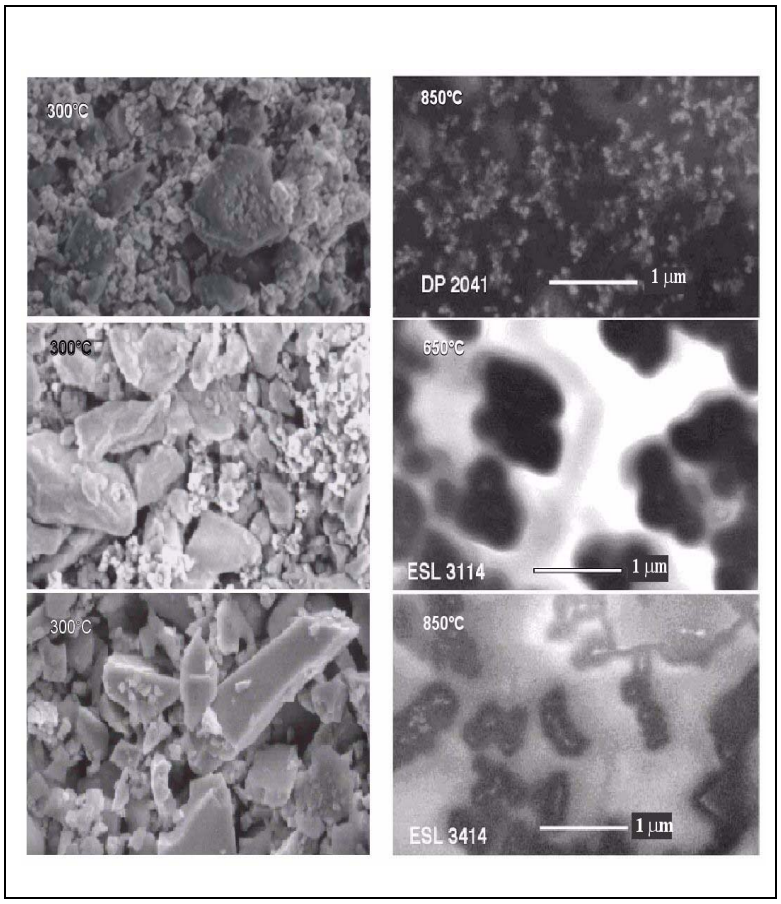

Figure 17: SEM of the surface of the commercial resistors, before and after the firing (same scale for each micrography)

II . 2 . 3 . Sensitivity and stability

II . 2 . 3 . 1 . Sensitivity: Effect of firing schedule

Resistors of each composition are subjected to 7 different firing cycles:
1) "standard" resistor firing cycle, in a belt furnace, with a temperature-dwell of 10 min;
2/3) tube furnace, standard temperature, 1h, N/T;
4/5) tube furnace, standard temperature, 11h, N/T;
6/7) tube furnace, high temperature, 1h, N/T.
"Standard" and "high" firing temperatures are 850 and 950°C for DP 2041 and ESL 3414, and 630 and 700°C for ESL 3114.

Cooling times to 250°C are ca. 10min (standard belt furnace), 5 h (N, cooling in tube furnace), and 20 s (T, quenching by rapidly removing and exposing the samples to air).

The properties are given in figure 18 for the different firing schedules and the effect of each parameter (time, temperature, quenching) is given in table 2.

Changed parameters	DP 2041			ESL 3114			ESL 3414		
	ΔR_s (%)	ΔTCR (ppm/K)	GF_L (%)	ΔR_s (%)	ΔTCR (ppm/K)	ΔGF_L (%)	ΔR_s (%)	ΔTCR (ppm/K)	ΔGF_L (%)
Increasing time	-43	+3	-13	-28	+26	-13	+39	-298	-12
Increasing temperature	-86	+18	-14	-45	+212	-36	/	/	/
Quenching	-3	-43	+2	-2	+45	+6	-40	-1	+6

Table 2: Effect of firing parameters on as-fired properties

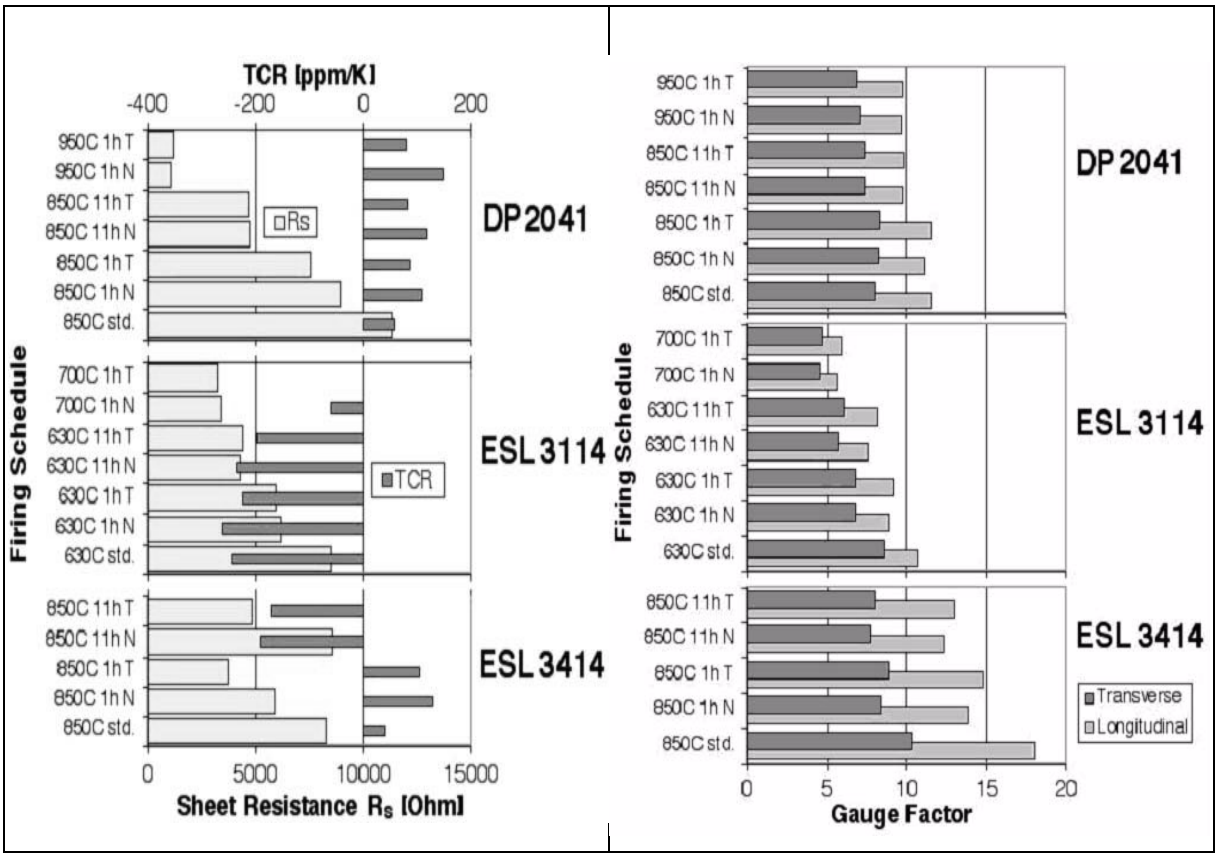

Figure 18: Initial values of sheet-resistance R_S and temperature coefficient TCR (left), initial gauge factors GF (right) as function of firing schedule. Std.=belt furnace; T=tube furnace, quenched; N=tube furnace, furnace cooled

No data is given for ESL 3414 fired at 950°C, as degradation at the terminations was found to occur; SEM observations (figure 19) show a µm-wide glassy area between electrode and resistor devoid of conductive particles.

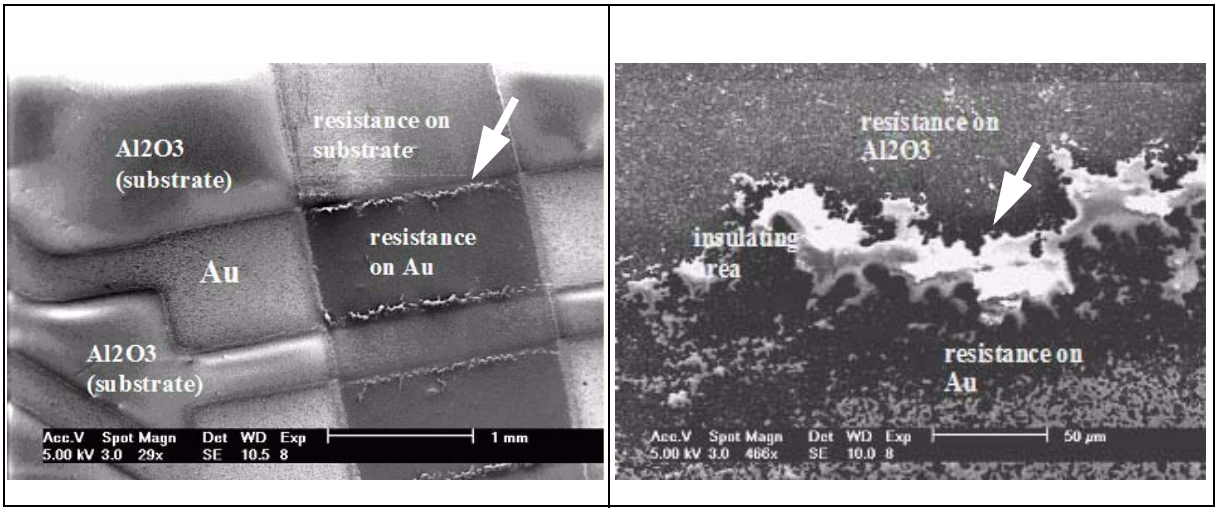

Figure 19: Terminaison effect near the Au-electrodes (ESL 3414, 950°C, 1h, N)

Except in this case, significant termination effects are not observed in this study, which is expected when using Au.
The length of the resistor has a slight influence on the value of sheet-resistance or the TCR; influence that is more visible for high thermal budget. The variations of R_S and TCR as a function of the resistor length for DP 2041 are depicted on figure 20. The same variations are observed on the other pastes (ESL 3414 and 3114). It was predictable in so far as gold electrodes are used. This noble metal is known to have very little interaction with the paste: the diffusion phenomena are negligible. The only variation that we could observe should be due to screen-printing edge effects or it could come from the effect of electrode on short distances (in the case of short resistances), as the gold paste we used (ESL 8837) contains some glass and adhesion promoting oxides that could have a moderate interaction with the piezoresistive paste.
Nevertheless, this kind of electrodes allows us to be relatively independent of the external phenomena (influence of diffusion…). So, the observed modifications will mostly come from the intrinsic evolution of the resistors, as well as (at high temperature) from interactions with the substrate and ambient air.

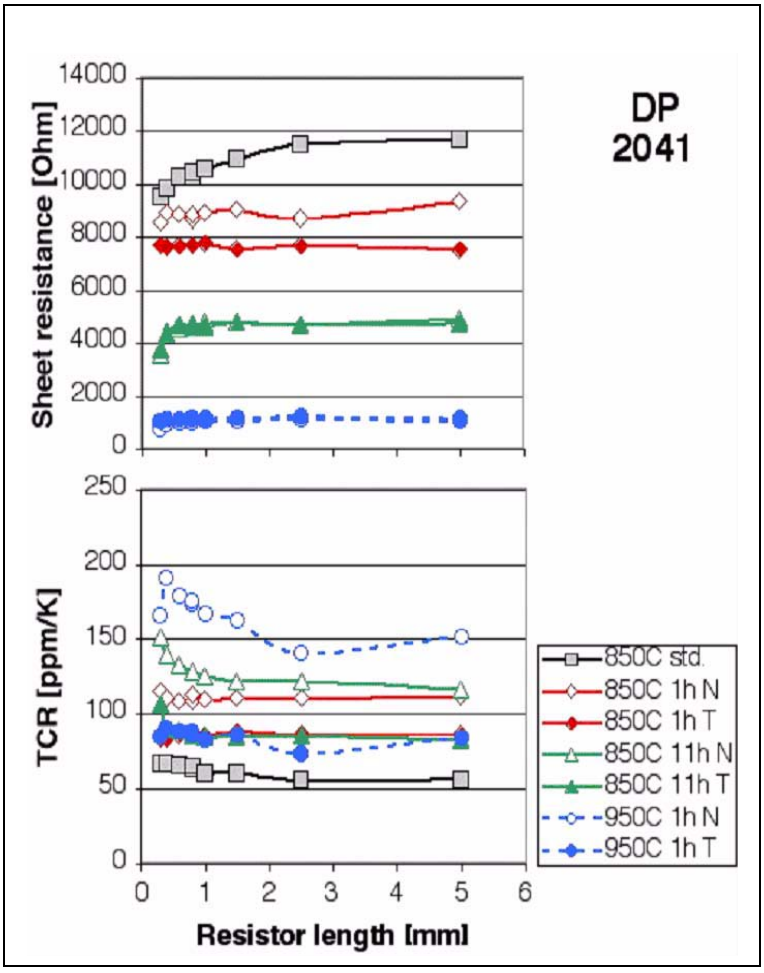

Figure 20: Evolution of R_S and TCR values vs. resistor length (DP 2041)

The effect of the firing schedule is quite different for each composition. Increasing firing thermal budget (temperature, time) causes a strong decrease of R_S for DP 2041, but a small decrease of GF values. ESL 3114 exhibits a much smaller corresponding R_S decrease, but a larger decrease of GF. Quenching DP 2041 influences significantly only its TCR (decreasing).

On the other hand, R_s is strongly decreased for ESL 3414 (this will be subject of future investigations), and TCR increases for ESL 3114. Also, a small but significant increase of GF is observed for ESL 3414 and 3114.
The variations due to an increase of thermal budget (DP 2041 and ESL 3114) are in accordance with results found in the literature [5, 9, 10, 11].

Overfiring the resistors does not radically change the microstructure, but leads to coarsening of the conductive particles for all compositions, which implies diffusion of Ru in the glass. XRD spectra show no apparent change for ESL 3114 (conductive phase: RuO_2 only) and ESL 3414 ($Bi_2Ru_2O_7$ only). In the case of DP 2041, progressive decomposition of $Pb_2Ru_2O_6$ into RuO_2 and PbO (the latter enters the glass) occurs, in accordance with the published stability data [12]. From XRD spectra (figure 21), the mole fraction of Ru in ruthenate (vs. in RuO_2) decreases from 64% (850°C, 1h) to 2% (950°C, 1h). The resulting PbO enrichment of the intergrain glass may contribute to the strong R_s decrease exhibited by DP 2041 [13].

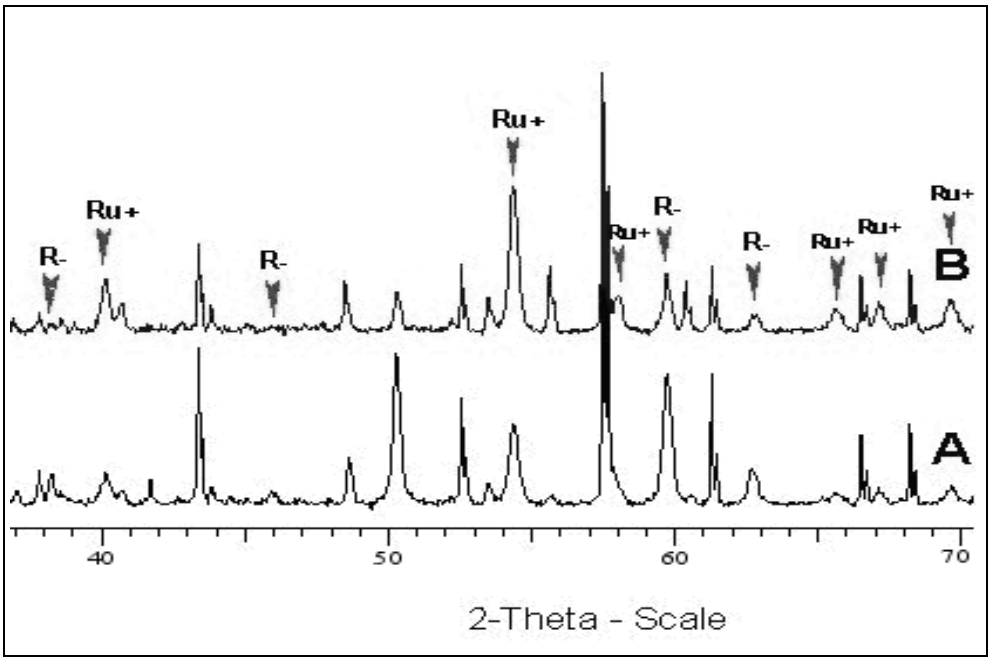

Figure 21: X-ray spectra of the evolution of the ruthenate (Ru-) and RuO_2 (Ru+) phases vs. the firing treatment for DP2041 from 850°C, 1h, N (curve A) to 950°C, 1h, N (curve B)

The arrows show the decomposition of the ruthenate phase ($Pb_2Ru_2O_6$) into RuO_2 and PbO (that is dissolved in the glassy matrix). This phenomenon of dissolution has been explained by Adachi et al [3]. Stability/dissolution of the original conductive phase depends on the composition of the glassy matrix. In the case of DP 2041, the relatively low lead-glass (approximately 63/12/25 %wt : $PbO/SiO_2/B_2O_3$) favoured the dissolution of ruthenate to form ruthenium dioxide. In fact, the tendency to phase decomposition is generally determined by the activity of PbO in the glass melt, but the actual degree of reaction is also governed by kinetics.

Also, firing DP 2041 at 950C 1h precipitates a crystalline phase, on the surface, identified as $ZrSiO_4$ by XRD. This new phase can be distinguished on SEM micrography (figure 22) thanks to its triangular form on the surface.

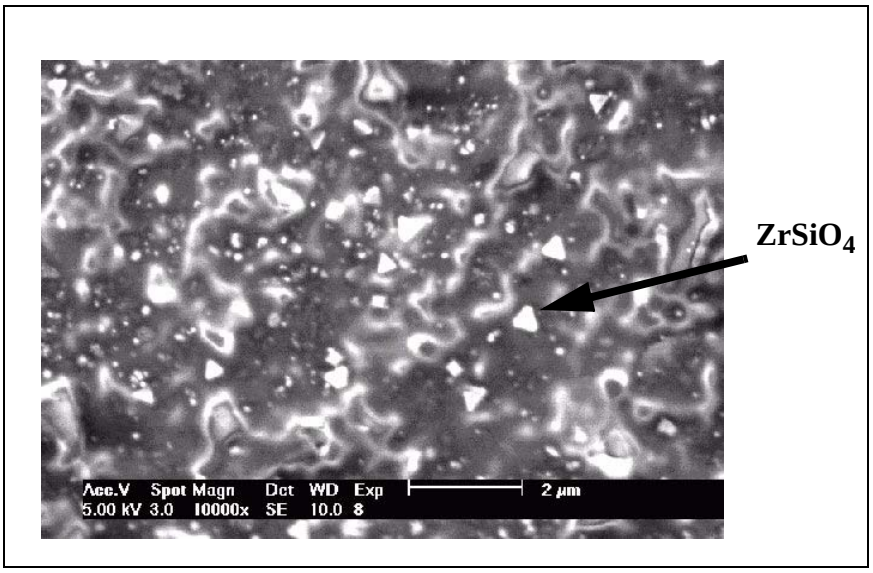

Figure 22: Presence of $ZrSiO_4$ on the surface of DP 2041, 950°C, 1h, N

Note that this phase was already detected in samples fired at 850°C, Std (see chapter II.1.4) but there were no such compounds on the surface.

II . 2 . 3 . 2 . Stability: Post-annealing at 100 and 250°C

After firing, the samples are subjected to long-term annealing cycles at 100 and 250°C in order to ascertain their stability.
Measurements are performed after firing and ex situ during annealing, by periodically removing the samples from the annealing oven.
R_S, TCR and GF values are measured by the same way as previous experiments.

No significant changes in properties are observed upon annealing at 100°C for all pastes. The maximum variation of R_S is < 0.08%. Upon annealing at 250°C, similar results are obtained for GF and TCR. Also, no significant change of microstructure or XRD spectrum is observed. The stability of the microstructure and GF is in accordance with some authors [9], as they explain that GFs of thick-film resistors depend to a greater extent on the microstructure of the material.

However, R_S changes significantly at 250°C and its evolution, given as a function of annealing time in figure 23, is dependent on the firing schedule. No dependence on resistor length was observed, indicating the absence of significant termination effects.

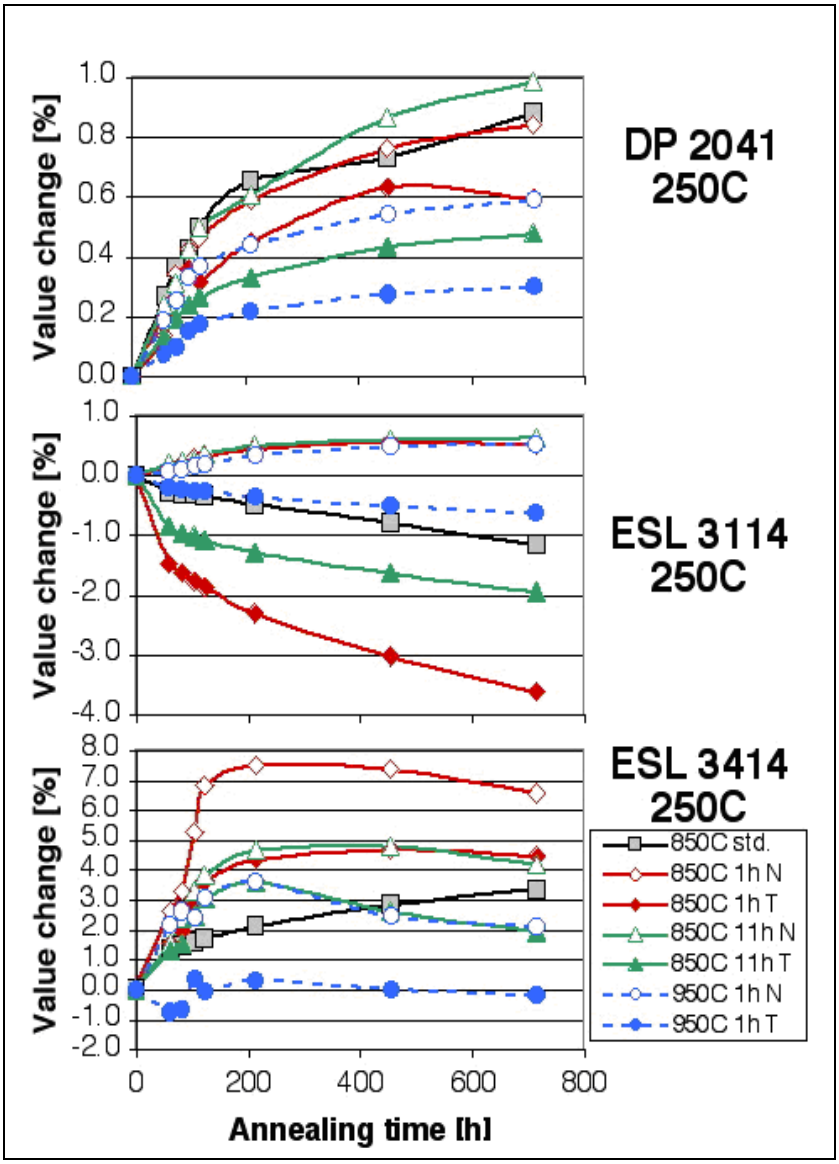

Figure 23: Relative change of sheet-resistance R_S during the annealing

In general, stability for a given cooling rate was found to increase with the firing thermal budget. Increasing the temperature from 850 / 630 to 950 / 700°C had a larger effect than increasing the time from 1 to 11h. The evolution of R_S upon annealing was also found to depend strongly on the cooling rate (furnace or quench). Although the magnitude of the effect varies for different pastes and firing temperatures and times, quenching always shifts the evolution of R_S to lower values, in comparison with the corresponding furnace cooled sample.
DP 2041 (R_S change < 1.0%) was found to be the most stable paste. Even in this case, the observed changes (all positive) are larger than the full-scale piezoresistive response of corresponding sensors using alumina substrates (around 0.3%). ESL 3414 shows similar behaviour, although with poorer stability (changes up to 8%). Except for the short standard firing cycle (10 min), the evolution tends to saturate, and even be partially reversed after ca. 200h, as observed by Cattaneo et al [14].

In spite of the much lower firing temperature of ESL 3114, its thermal stability is comparable to that of DP 2041. Samples made with slow furnace cooling exhibit low positive evolution of R_s upon annealing, which tends to saturate around +0.6%. A similar negative evolution is observed for the sample fired under standard conditions. Quenched samples differ markedly, however, with R_s decreasing strongly upon annealing. In this case, increasing the firing thermal budget significantly improves stability.

At 250°C, possible evolution mechanisms could involve Ru in glass (dissolved or in clusters [15]), or mechanical relaxation. Our investigation methods did not allow direct assessment of Ru in glass, but local rearrangement of Ru in glass during annealing such as precipitation of supersaturated Ru into clusters cannot be ruled out.
Mechanical strain relaxation can be extrinsic (macroscopic thermal mismatch between resistor and substrate) or intrinsic (local thermal mismatch between glass and conductive phase). Extrinsic mismatch between Al_2O_3 and standard 850°C firing resistors is thought to be small, as TCE values given for the glass [16] and RuO_2 (average [17]) are 7…8 and 5 ppm/K, close to the ca. 7 ppm/K value for Al_2O_3. However, the intrinsic, local thermal mismatches are much higher in the case of RuO_2-containing resistors. Rutile RuO_2 has anisotropic TCE values: +9 and -2 ppm/K for the a=b and c axes [17]. Upon quenching, strong tensile strains are therefore expected to be frozen in along the c axis, which can later relax during annealing. We could not verify whether a similar reasoning can be applied to Pb or Bi ruthenate containing resistors, as no TCE data was found for these compounds.

II . 3 . Conclusion

After the analysis of the composition and structure of a typical commercial paste DP 2041, the sensibility and the stability of three usual inks was studied, because of limited available information in literature concerning the effect of firing schedule, particularly of quenching.
The influence of the firing schedule on the properties (R_s, GF and TCR) was found to be different for the three tested compositions. But, R_s seems to be more influenced by the firing conditions contrary to TCR and GF values that are less sensitive. However, ESL 3414 appears to be strongly influenced by these modifications. Upon annealing at 250°C, only R_s changes significantly, and its stability was found to strongly depend on composition and firing schedule. ESL 3414 exhibited the highest changes, whereas DP 2041 and the low-firing ESL 3114 had comparable stability. Increasing the cooling speed by quenching affects both properties and annealing behaviour. This could come from supersaturated Ru in the glass or from frozen-in local strains between conductive phase and glass matrix.
Concerning the structural modifications, the most important phenomenon is the evolution of the conductive phase (ruthenate) into RuO_2 at high temperature in the case of DP 2041.

From a technical point of view, it's evident that these pastes could be optimised. Indeed, their stability could be enhanced with a higher GF. Moreover, they should be modified to be adapted on more elastic substrates (aluminium or steel); that entails a decrease of the firing temperature, and consequently a modification of the composition. In this respect, the results for ESL 3114 are very promising.
These first results will constitute a «starting point» to realise new pastes. The commercial paste results should be considered as our references.
From a scientific point of view, this first step has permit us to show that nanostructure, conduction and properties are intimately linked. By choosing adequate and relevant

composition, structure and firing, we will try to unveil the conduction process that has not been yet elucidated.

References - Chapter II:

1. Baudry H, Franconville F, *Encres sérigraphiables pour haute définition. Rhéologie et impression,* Acta Electronica, 1978, **21**, 283-95.
2. Prudenziati M, *Handbook of sensors and actuators 1*, 1994, **1**, 113-6.
3. Adachi K, Kuno H, *Decomposition of ruthenium oxides in lead borosilicate glass,* J. Am. Ceram. Soc, 1997, **80**, 1055-64.
4. Hrovat M, Belavic D, Samardzija Z, Holc J, *The development of microstructural and electrical characteristics in some thick-film resistors during firing,* J. of materials science, 2002, **37**, 2331-9.
5. Prudenziati M, Morten B, Cilloni F, Ruffi G, *Very high strain sensitivity in thick-film resistors: real and false super gauge factors,* Sensors and Actuators, 1989, **19**, 401-14.
6. Prudenziati M, Morten B, *Piezoresistive properties of thick-film reisitors - an overview*, Hybrid Cicuits, 1986, **10**, 20-23, 37.
7. Hrovat M, Belavic D, Samardzija Z, Holc J, *A characterisation of thick-film resistors for strain gauge applications,* J. Mater. Sci., 2001, **36,** 2679-89.
8. Hrovat M, Samardzija M, Belavic D, Holc J & al, *Microstructural and electrical characteristics of some "overfired" thick-film resistors,* Journal of materials science letters, 2001, **20**, 347-51.
9. Hrovat M, Holc J, Samardzija M, Belavic D, *The influence of firing temperature on gauge factors and the electrical and microstructural characteristics of thick film resistors,* J. of materials science letters, 2001, **20**, 701-5.
10. Hrovat M, Belavic D, Samardzija Z, Holc J, *The development of thick film resistor properties during firing,* in Conf. proceedings. MIDEM, Soc. microelectron. components and mater, Dunajaska, Slovenia, 1999, 169-74.
11. Lee J, Vest RW, *Firing studies with a model thick film resistor system,* in IEEE Transactions on components, hybrids, and manufacturing technology, 1983, **CHMT-6**, 430-5.
12. Adachi K, Kuno H, *Decomposition of ruthenium oxides in lead borosilicate glass*, Journal of the American Ceramic Society, 1997, **80**, 1055-64.
13. Adachi K, Kuno H, *Effect of glass composition on the electrical properties of thick-film resistors,* Journal of the American Ceramic Society, 2000, **83**, 2441-48.
14. Cattaneo A, Marelli M, Prudenziati M, *Effects of refiring processes on electrical and strutural properties of thick-film resistors,* Electrocomponent Science and Technology, 1980, **6**, 165-71.
15. Adachi K, Iida S, Hayashi K, *Ruthenium clusters in lead-borosilicate glass in thick film resistors,* Journal of Materials Research, 1994, **9**, 1866-78.
16. Trubnikov L, *Thermal expansion, vitrification temperature and corrosion behaviour of lead-borosilicate glass,* Refractories and Industrial Ceramics, 2000, **41**, 169-71.
17. Krishna Rao K., Iyengar L, *X-ray studies on the thermal expansion of ruthenium dioxide*, Acta Cryst., 1969, **A25**, 302.

CHAPTER III:

Development of new piezoresistive pastes

The last chapter was dedicated to the study of commercial piezoresistive pastes. The general composition of such pastes has been determined by chemical and structural analyses. On the other hand, the studies of stability have demonstrated that reactions between the components are occurring during the firing, leading to the required electrical properties. The firing conditions have been proved to be of great importance, as stability and electrical behaviour seem to be dependant of them. Although all the phenomena have not yet been elucidated, these first results can be considered as reference and as a starting point for further investigations.
The present chapter is devoted to the selection of parameters to realise new model pastes, whose electrical and structural properties will help us to understand their behaviour. At the end of the chapter, different series of pastes with different technological purposes are proposed in the aim to elucidate the conduction mechanisms. The advantage to realise experimental pastes is the knowledge/control of the exact composition and the possibility to isolate the properties affected by each chosen parameter.
By this way, a manufacturing process has been developed and laid out, process never precisely described in the literature, for this kind of pastes.

III . 1 . Aims: twofold

The realisation of new piezoresistive pastes is encouraged by two interrelated aims:
a technological approach:
- to enhance the properties of the current commercial piezoresistive pastes: to realise a paste used for the same applications (alumina substrate: high firing temperature).
- to manufacture a new generation of piezoresistive pastes adapted to more flexible/sensitive substrates: aluminium, steel..: lower firing temperature.

In this aim, chemical phenomena, which correspond to the reactions between the elements (exchange of atoms) during the elaboration process, together with the influence of different parameters such as the change of conductive grain size, or of the glass composition will be

studied. The resulting electrical properties will be examined in the light of the structural modifications.

a scientific approach:

- to obtain a better understanding of the evolution of the structural, electrical properties and electrical transport mechanism. Firstly, the influence of the process conditions will be investigated. To this end, we will take an interest to the chemical reactions occurring during the sintering and firing steps. On the other hand, a coherence between the electrical transport and its the complex nanostructure will be found. It will be then useful to study and understand the conduction mechanism that take place in such percolative systems in which tunnelling effect between the conductive particles is predominant. At the end of the study, a model of conduction based on a new approach will be validated.

This part will allow us to better understand the evolution of electrical properties and consequently to enhance the properties of piezoresistive pastes.

Analyses of current commercial piezoresistive pastes are considered as reference. The composition of our model pastes will be based on the precedent results.
In order to study the physical, electrical and structural evolutions of piezoresistive pastes, we have chosen judicious parameters for their composition. The following section consists in a detailed description of the different components: their composition, their characterisation and their manufacturing process.

III . 2 . Choice of parameters: composition, characterisation and process

We detected in the precedent chapter that piezoresistive pastes are composed of four parts:
- a lead-borosilicate glass,
- an organic phase,
- a conductive phase,
- diverse additives (oxides).

In this work, we will take an interest in simple systems in order to focus our study on the basic and essential phenomena. No additives will therefore be used.

It is useful to mention that the chosen parameters have specific actions on the properties of piezoresistive pastes:

- the glass composition influences different parameters. The nature of the glass determines the substrate to be used, as it determines the firing temperature and the temperature coefficient of expansion (TCE) of the paste. Indeed, glass and substrate should be compatible to assure good cohesion [1]. Moreover, the stability of the conductive phase is dependent on the glass composition, and the nature of the conductive grains will influence the resistivity of the thick film.

- conductive particle concentration and grain size influence the stability and the electrical properties by modifying GF, TCR and R_S values [1]. The conduction mechanism is consequently mainly dependent on the nature, the grain size and the concentration of the conductive nano-particles.

- the organic vehicle allows to control the rheology of the paste in order to perform the screen-printing, and insures cohesion of the particles during manipulation of the screen-printed substrate after the drying process. The final properties depend on the complete removal of the vehicle.

An itemised description of the different chosen parameters is given hereafter.

III . 2 . 1 . Glass

III . 2 . 1 . 1 . Glass composition

Glass compositions were selected according to their physical properties (TCE, T_g, ...). The choice is representative of a range of temperature based on phase diagram of lead-borosilicate glass as it offers a large melting temperature scale for our tests [2-4]. This glass is not absolutely inert with respect to the conductive phase. From Adachi and Kuno's studies, the stable conductive phase is dependent on the glass composition [5]. The stable phases will be experimentally determined by overfiring the resistors.
Different works have been realised on standard glass composition but less with low firing temperature ones. Of course, low firing temperatures don't favour chemical exchanges. This will allow us to study separately the physical phenomena of conduction from the chemical reactions, and it will be interesting from the point of view of technology.

The three chosen compositions are represented on the phase diagram (figure 1) [2], and corresponds to the following compositions (PbO / B_2O_3 / SiO_2) mentioned in weight percent and molar percent:

glass (a) called V2: 63 / 25 / 12 % wt - 33 / 43.5 / 23.5 % mol

glass (b) called V6: 75 / 10 / 15 % wt - 46 / 20 / 34 % mol

glass (c) called V8: 85 / 10 / 5 % wt - 62 / 24.5 / 13.5 % mol

2 % wt of Al_2O_3 is added to each glass composition in order to avoid a possible crystallisation of silicon oxide into cristoballite phase during the manufacturing process [6]. Indeed, a devitrification of the glass could affect and alter the electrical and structural properties, and could modify the melting temperature of the glass.

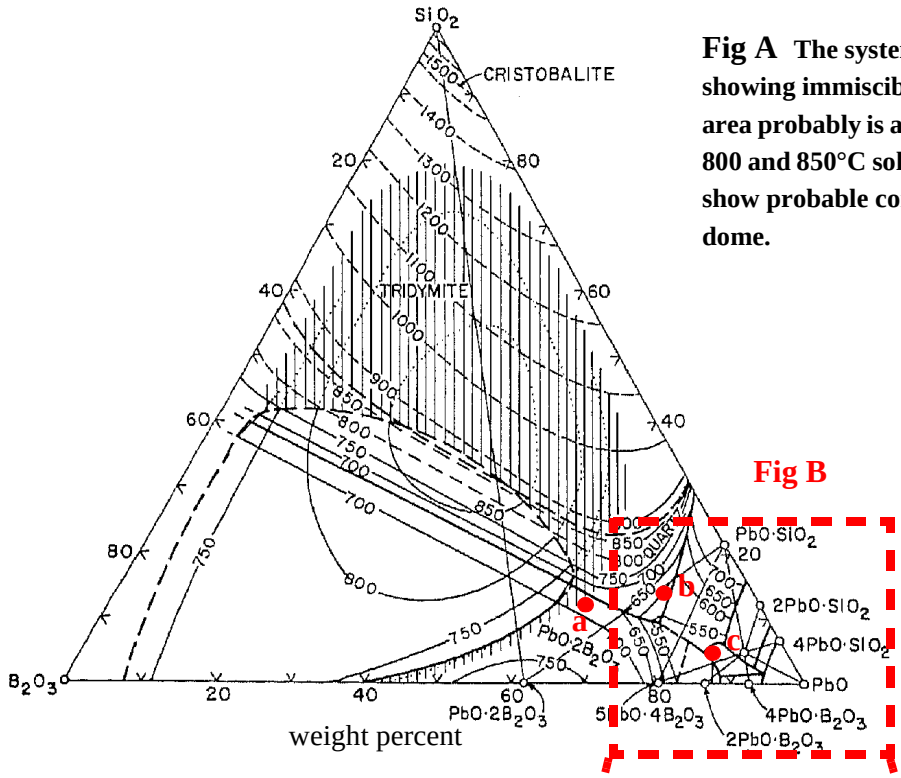

Fig A **The system $PbO-B_2O_3-SiO_2$ showing immiscibility regions. Shaded area probably is a metastable region; 750, 800 and 850°C solid and dotted isotherms show probable contour of two-lquid dome.**

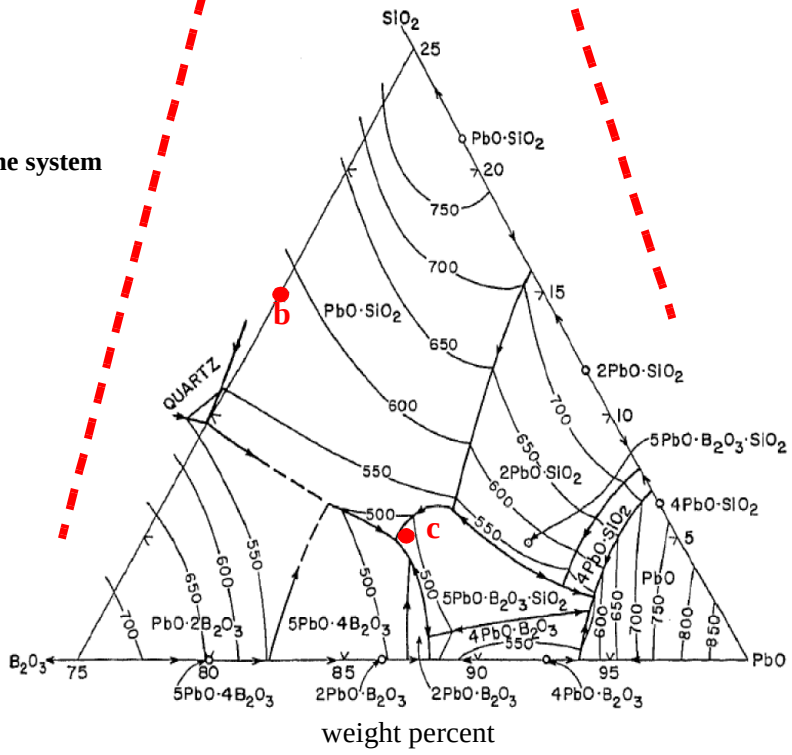

Fig B **High-lead region of the system $PbO-B_2O_3-SiO_2$.**

Figure 1: Phase diagram of the $PbO-B_2O_3-SiO_2$ system from Johnson and Hummel [2]

Glass (a) corresponds to a standard composition often used in the literature [5,7-13] and in the manufacture of commercial high-firing (850°C) compositions, because it fulfils the required properties: its thermal coefficient of expansion is close to the one of alumina, it has a required low viscosity and a suitable surface tension at high-temperatures (800-900°C) [14].
On the opposite, glasses (b) and (c) can be fired at low temperature as represented in figure 1. Glass (c) corresponds to the minimal melting temperature system (500°C). This composition is expected to be compatible with aluminium substrates.

Note that these diagrams on figure 1 are helpful, as they allow us to avoid an immiscibility region for lead oxide compositions below 60 % wt, boron oxide concentration above 30 % wt and silicon oxide below 40 % wt.

These glasses are manufactured in the lab and they are characterised in order to verify that their physico-chemical properties are in accordance with the reference data.

III . 2 . 1 . 2 . Manufacturing process

Different starting powders are used:
- PbO: lead (II) oxide (litharge), 2 microns powder, 99.9+ %, Fluka Chemie GmbH
- H_3BO_3: boric acid, crystalline powder < 10 microns, 99.99+ %, Aldrich Chemical Co
- SiO_2: silicon oxide quartz B600, 2 microns, 99+ %, Sihelco AG
- Al_2O_3: aluminium oxide-alpha, 1 micron, 99.99+ %, Alfa Aesar - Johnson Matthey GmbH

Micrometer powders are preferred in order to optimise the blending before the firing by a homogeneous grain size of the different components. Attention will be turned to the purity of the starting materials (> 99.9%) and to avoiding external contamination or formation of bubbles during the firing coming from carbon residues.

Boric acid (H_3BO_3) is used instead of boron oxide (B_2O_3), because the oxide is very hygroscopic in ambient air and transforms over time into acid. In order to determine the quantity of water in the acid and the decomposition steps of H_3BO_3, a TG / DTA analysis is realised (figure 2):

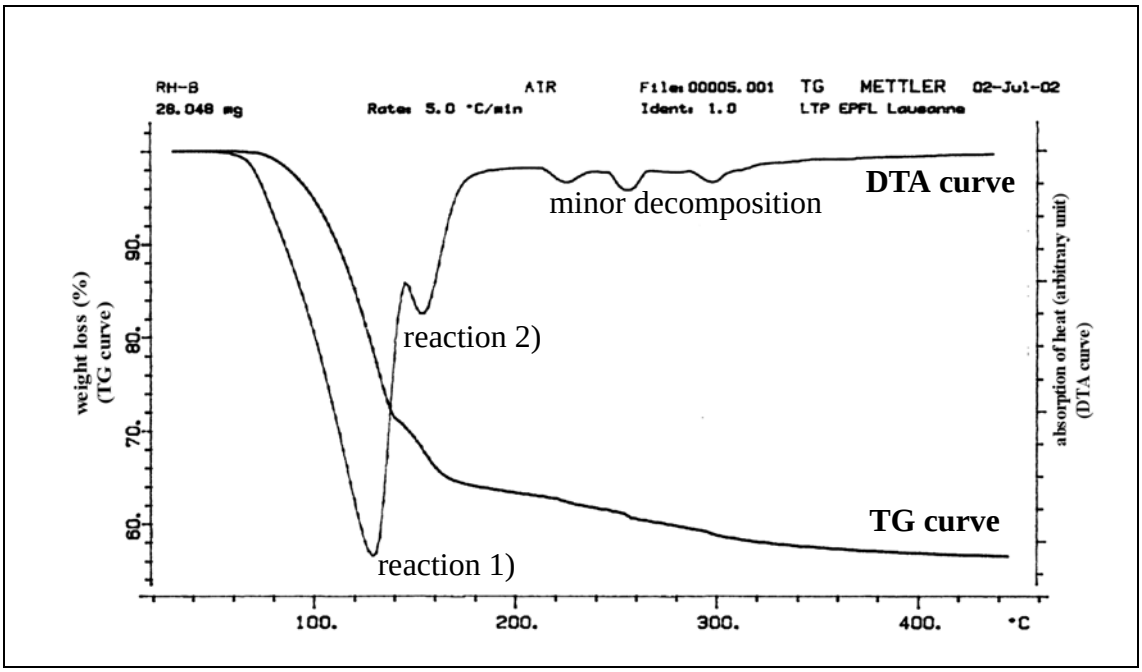

Figure 2: TG / DTA spectra of boric acid dehydratation

From TG analysis, we can estimate that H_3BO_3 contains ~ 42 % wt of water, lost by a two-step reversible stoechiometric decomposition below 400°C:

1) $H_3BO_3 \rightleftharpoons HBO_2 + H_2O$

2) $2\ HBO_2 \rightleftharpoons B_2O_3 + H_2O$

---

1) + 2): $2\ H_3BO_3 \rightleftharpoons B_2O_3 + 3\ H_2O$

Residual peaks above 200°C should be due to the decomposition of other minor impurities (3%wt).

The reversibility of this dehydratation reaction has been observed with IR spectroscopy (figure 3).

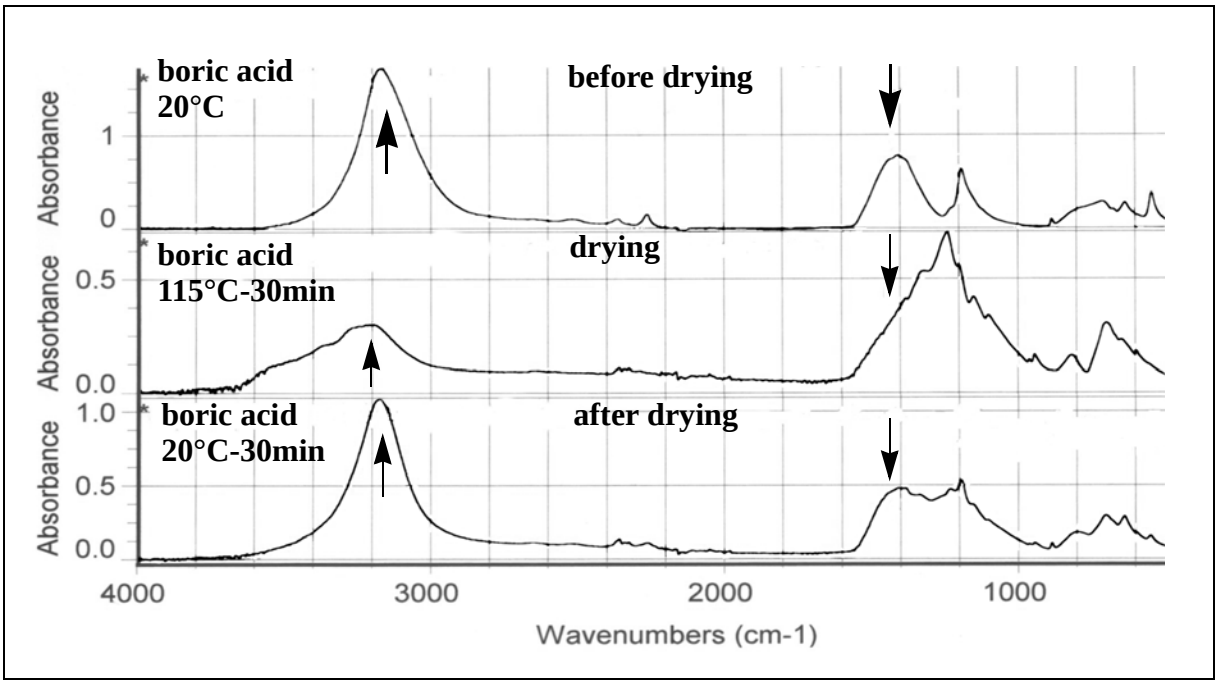

Figure 3: IR spectra of boric acid reversible dehydratation

The evolution of the hydroxy-bonds of H_2O peaks at 3200 and 1400 cm^{-1} contained in the boric acid are observed. Peaks decrease if the acid is heated up at 115°C during 30 min (drying). After this treatment, the compound is left 30 min in ambient air, and the peaks increased again, which underlines the reversibility of the reaction.

Note that water is not totally extracted as the heating temperature was too low (115°C, limited by the apparatus in this study).

In the light of these results, a pre-drying step (~ 400°C) should be included into the fusion cycle of the glass, in order to eliminate the residual water before melting of B_2O_3. Consequently, the weight of the included water will be taken in account in the weighing of H_3BO_3.

The other components were subjected to the same analysis and no significant loss of weight has been detected.

Here are following the steps for the manufacture of the lead-borosilicate glass phase (figure 4). The state of the components at each processing step is given on the right of the diagram, and the characterisation techniques (detailed in the next section) are mentioned on the left.

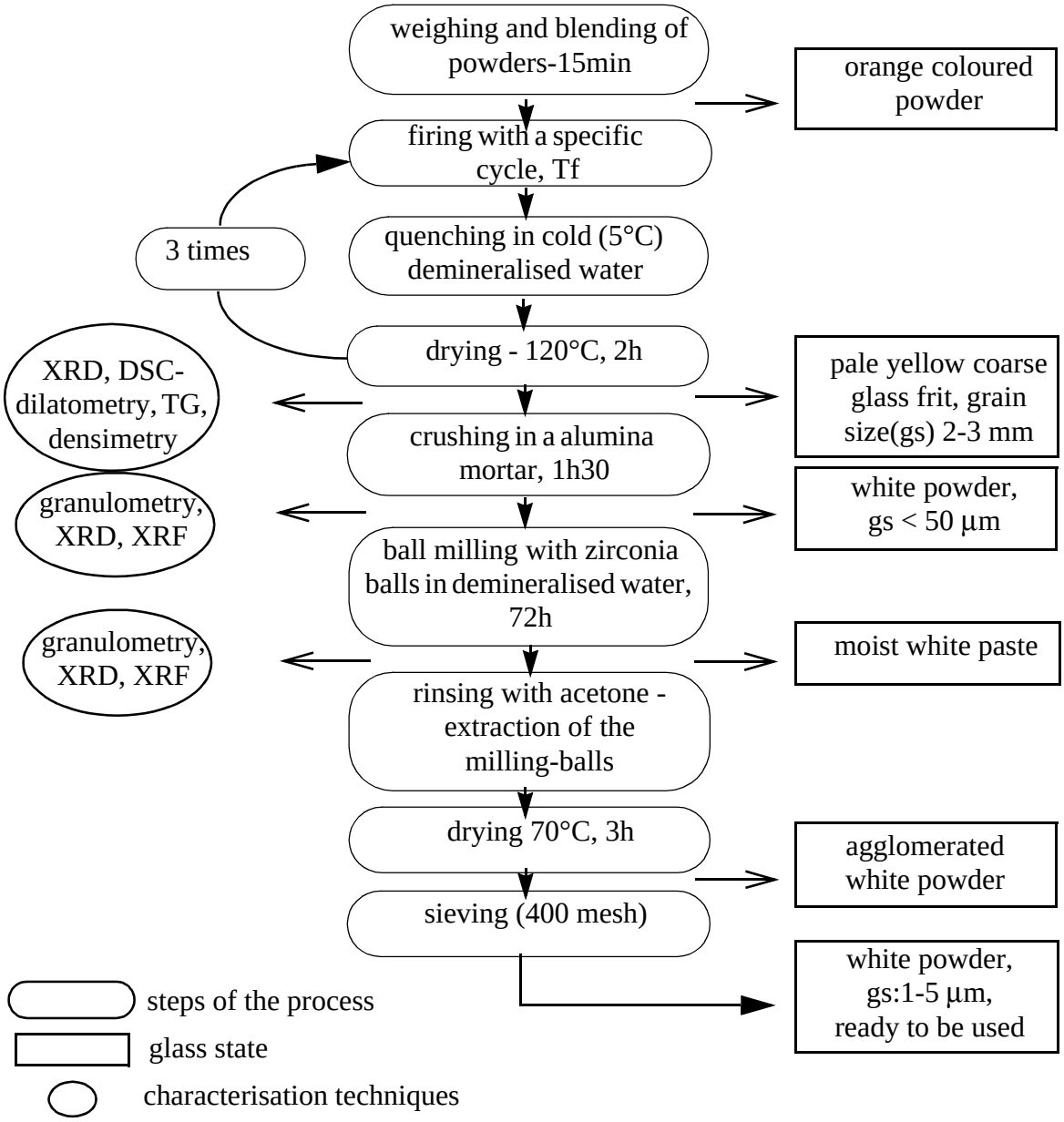

Figure 4: Manufacture process of lead-borosilicate glass frit

Technical details:

- **Blending**

It is realised in a Turbula type T2C - WAB.

- **Firing**

Firing is carried out in a box furnace (Lenton Thermal Designs - 2416CG Eurotherm controller). The powder is poured in a alumina crucible (Al998-001/4: 99,8 % purety, Metoxit AG) in order to avoid external contamination (the diffusion of alumina from the crucible to the glass will be quantified). A crucible is dedicated to each glass composition.
As quenching necessitates manipulation of the crucible at high temperature, it is placed in a machined special refractory steel enclosure (crucible) that can be removed from the furnace

with appropriate tongs. Moreover, the use of a steel enclosure gives additional thermal inertia and insulation to the glass, slowing down its cooling during the manipulation and protecting the alumina crucible from thermal shock. Finally, the steel enclosure protects the user if the alumina crucible accidentally breaks up because of the thermal variations between the furnace and the ambient temperature. A representation of this ingenious system of «double-crucibles» is shown in figure 5:

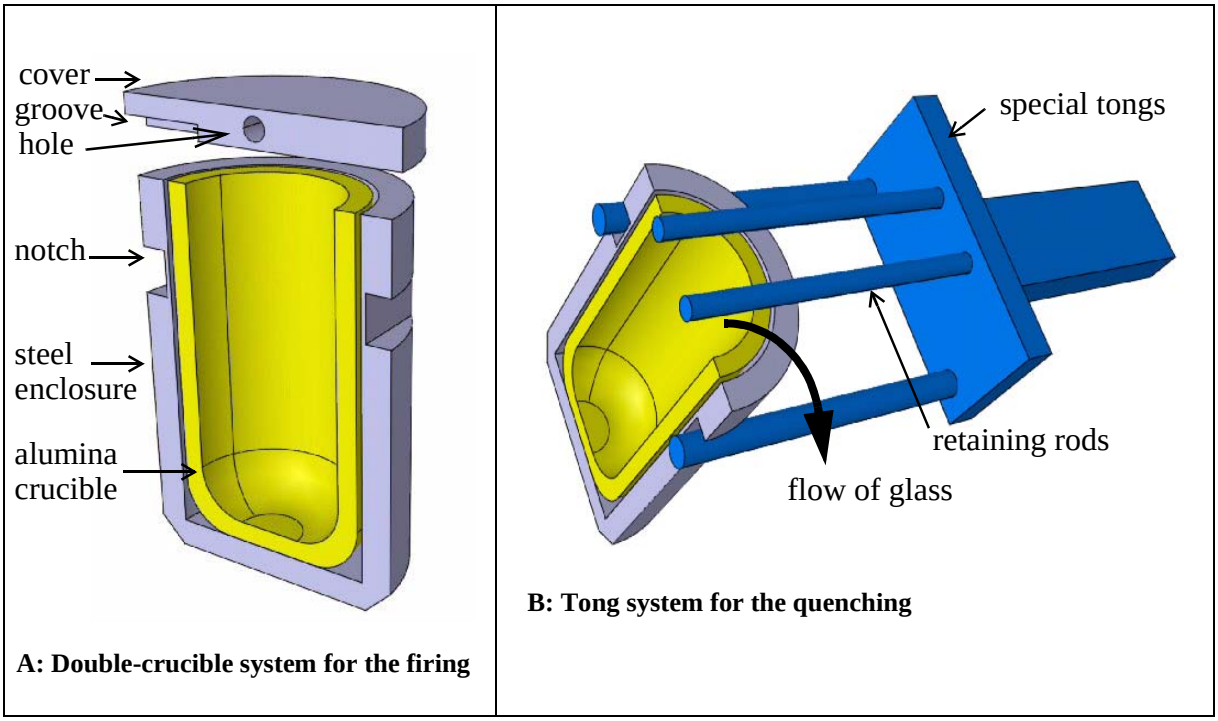

A: Double-crucible system for the firing

B: Tong system for the quenching

Figure 5: Schema of the «double-crucible» system for the glass firing

Figure A represents the double-crucible system with a machined cover. A groove insures air access to the crucible during the firing. A hole machined through the cover allows removing it with a rod, before the quenching. Figure B shows the tong system that allows a safe manipulation. Two retaining rods keep the alumina crucible in place during the quenching.

The powder is then fired in order to obtain a glass. The firing cycle follows appropriate steps adapted to each glass.
All the glass should be fired (melted) three times in order to optimise homogeneity and melting process. Note that the first cycle is different from the two others, as a 420°C-1h dwell temperature, with a smaller 50-420°C slope, is added to favour the elimination of residual water in boric acid.
The adapted cycles corresponding to each glass are depicted in the following figure (figure 6).

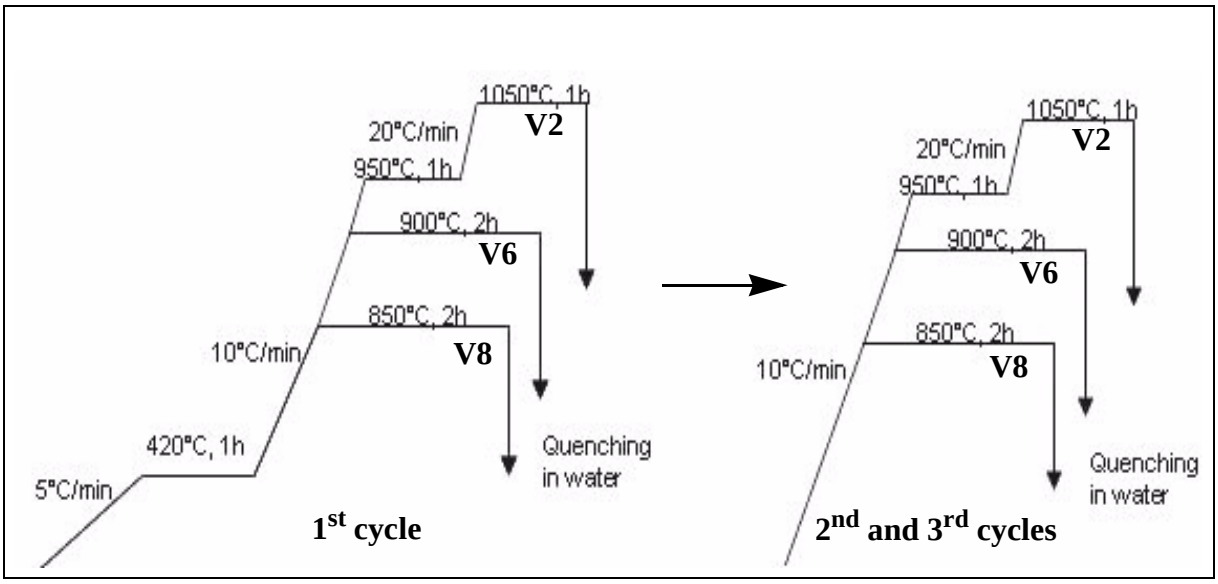

Figure 6: Fusion cycles for the manufacturing of the V2, V6, V8 glasses

A cover should be added on the steel crucible at 700°C (after the elimination of organics), in order to limit lead evaporation occurring from 900°C. This phenomenon is already controlled by the three consecutive cycles, as it is less damaging to heat several times during a short time the glass at high temperature instead of to maintain it at high temperature during a long time.
Although a cover is used, the crucible should not to be hermetically sealed! Indeed, it could stop the air (oxygen) access to the crucible, which can cause a reduction of PbO contained in the glass into non-miscible lead metal that precipitates in the bottom of the crucible. In this case, the reductor can be carbon residues originating of the burnout of organic compounds.
This problem appeared once: the covers stayed stuck on the crucible. The lead balls were collected, and the corresponding mass of Pb_3O_4 (obtained by heating PbO during 24h at 450°C) was added to the glass. It is judicious to add a lead oxide with a higher oxidation degree as it excess of oxygen could serve to oxidise the possible carbon residues into CO_2.

- **Quenching**

Quenching allows to avoid crystallisation of the glass. By cooling it rapidly, the glass stays amorphous. Moreover, a glass frit is obtained by quenching: it improves homogenisation between the firings (the segregation of PbO in the bottom of the crucible is limited) and allows an easier crushing of the glass.
Quenching in cold (5°C) demineralised water enables to maximise thermal shock (cold water) and to limit dissolution and contaminations (demineralised water).

- **Milling**

A first dry crushing is performed in an alumina mortar (Retsch apparatus), which brings little contamination.
A finer grinding is then carried out by ball-milling. The powder is poured in glass bottles with water and 5 mm diameter size zirconia balls. The bottles are placed on rolls (Siemens apparatus) whose speed of rotation is well defined. (If the speed is too high, the balls will stay on the bottle

wall because of the centrifugal speed. If the speed is too low, the balls stay on the bottom of the flask and their inertia is too low to break the particles.)
The process rests on the fact that the inertia of the falling balls will break the glass particles.
Water is used as the liquid because it lowers the strength of the glass: the crushing is easier to perform.

- **Sieving**

An agglomerated powder results in the drying process following the ball-milling. To break up these agglomerates, a screen (400 mesh) is used to sieve the micrometer powder glass.

III . 2 . 1 . 3 . Characterisation

This section is essential to validate the different steps of the process (crushing and milling) by observing their influence on the glass.

This section is devoted to verify that the obtained glasses have the required physico-chemical properties. Also, their thermal properties, sintering behaviour and stability are studied. The glass should be:
- amorphous
- 1-10 µm grain size
- TCE close to alumina (ideally slightly lower so that the resistor is under moderate compression), or steel, or aluminium, respectively: 7 ppm/°C for alumina, 13 for ferritic steel, 17 for austenitic steel, and 24 ppm/°C for aluminium
- not contaminated during the process.

Moreover, it is important to know some other parameters:
- phase transitions: glass transition temperature (T_g), and melting temperature range
- density.

These abovementioned properties can be divided into two groups:
- intrinsic properties that are inherent to the glass such as phase transition, stability...
- extrinsic properties depending on the manufacturing process (crushing and milling).

III . 2 . 1 . 3 . 1 . Intrinsic properties (inherent to the glass)

To this aim, a series of analyses was carried out.

- **Crystalline state of the glass**

XRD is carried out on the glass powder.
If the glass is amorphous, no peak should appear. The results are represented in figure 7. The starting powders of the glass are first represented (PbO, SiO_2, H_3BO_3, Al_2O_3). The spectrum of a non-fired powder glass shows the different peaks corresponding to the above powders. Finally, V2, V6 and V8 melted glasses are represented in the lower part of the graph.

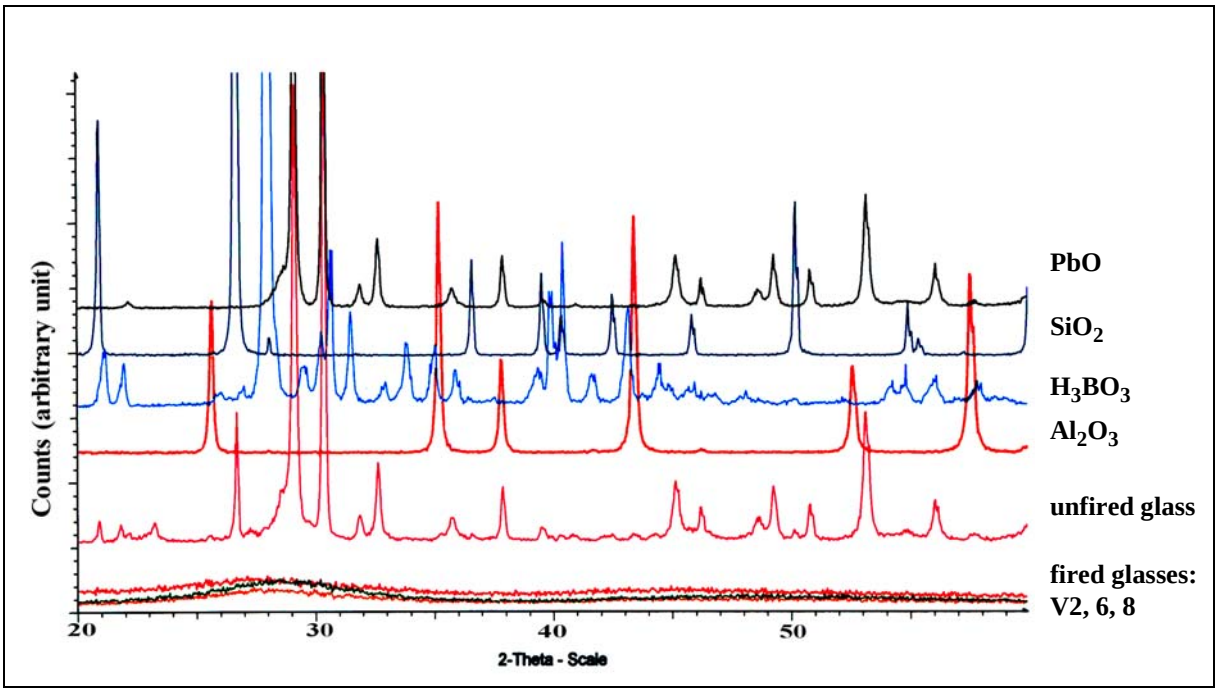

Figure 7: X-ray diffraction of the three manufactured glasses

From the spectra, it is beyond doubt that the V2, V6, V8 are amorphous. For small angles of diffraction, only a short-distance order is detected. It corresponds to the Si-O-Pb or Si-O-Si bonds, for instance.
The melting is supposed to be successful, as none of the initial crystalline powder phases are observed after the firing process.

- **Phase transitions**

The behaviour of each glass during the firing process is studied with DSC analysis. The resulting diagrams are represented in figure 8.

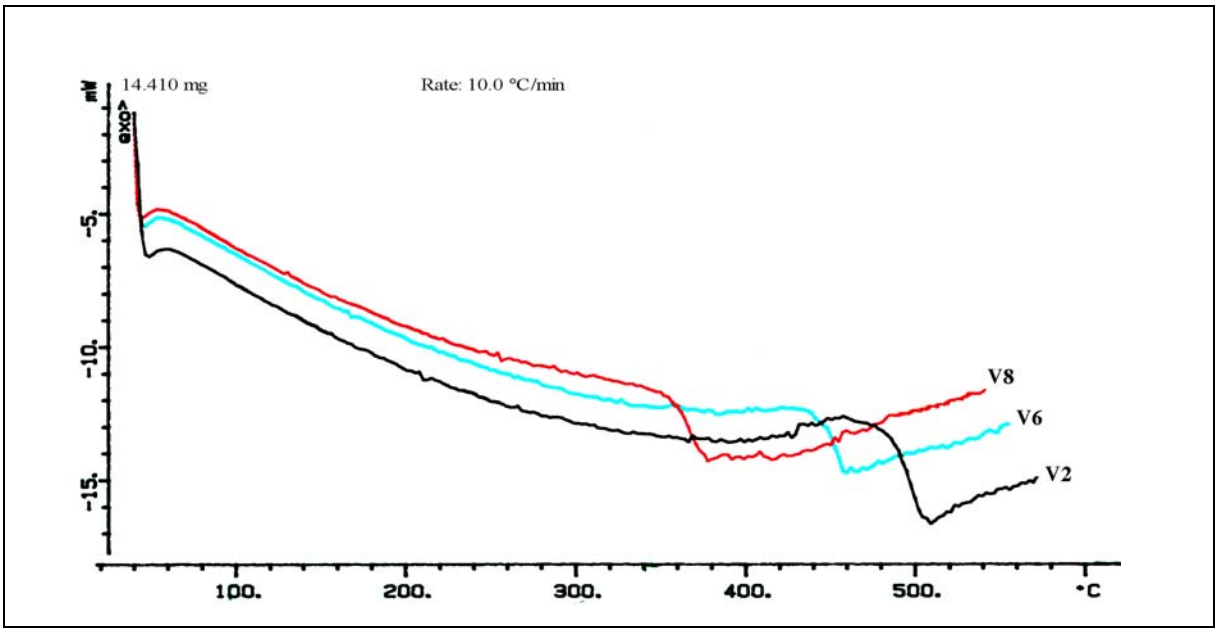

Figure 8: DSC spectra of the V2, V6, V8 glasses

The experiment was realised at 10 °C/min from 50 to 600°C.
The characteristic recess corresponds to the glass transition (T_g) of each glass. No exothermic peak due to crystallisation is observed. Note that the melting step, at T_f, is not clear as it is a progressive phenomenon that does not appear clearly on such DSC spectra. The determination of T_f is arbitrary as it is defined as a temperature corresponding to a chosen viscosity. The most important parameter is T_g as it corresponds to the temperature when the glass begins to transform, to sinter and to adhere to the substrate.

The curves are a little bent: it comes from the calibration of the apparatus.
We can deduce the following approximate T_g values:
- V8: ~ 370°C
- V6: ~ 450°C
- V2: ~ 500°C

As expected, V8 and V6 can be considered as low-temperature glasses, whereas V2 is a standard-high temperature glass. These results are in accordance with the literature [15], even if we observe a difference of 25°C with the T_g values given by Trubnikov et al. They obtained lower values as the heating rate is slower (2.5 °C/min) than ours (10 °C/min) and causes a shift of temperatures.

These DSC results are confirmed by analysis with dilatometry. Each glass powder is pressed in a cylindrical pellet that is placed in the dilatometer and heated. The evolution of the height of the cylinder is determined with displacement sensors (Setaram high temperature dilatometer). T_g and T_f will cause a progressive decrease of the height of the sample. Figure 9 represents the evolution of the height of V8 (% displacement) vs. temperature.

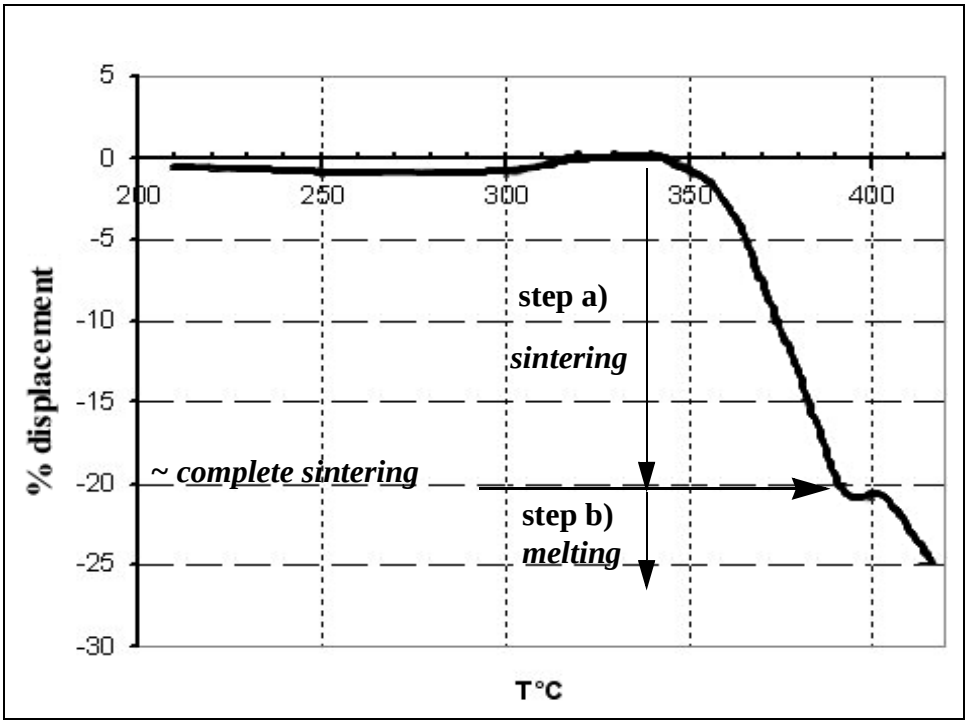

Figure 9: Dilatometry analysis of the V8 glass

Step a) corresponds to T_g, and step b) shows the beginning of melting. The process was then stopped because the melting glass can damage the apparatus.
V2 and V6 show similar behaviour and confirm the DSC results.

The possible difference of temperature between DSC and dilatometry could come from the calibration of the devices.

- **Glass stability**

TG analysis allows to show the importance of the firing conditions. Lead oxide glass firing requires an oxidising environment. Indeed, under reducing conditions (N_2/H_2), PbO contained in the glass can be reduced into lead metal as shown in figure 10.

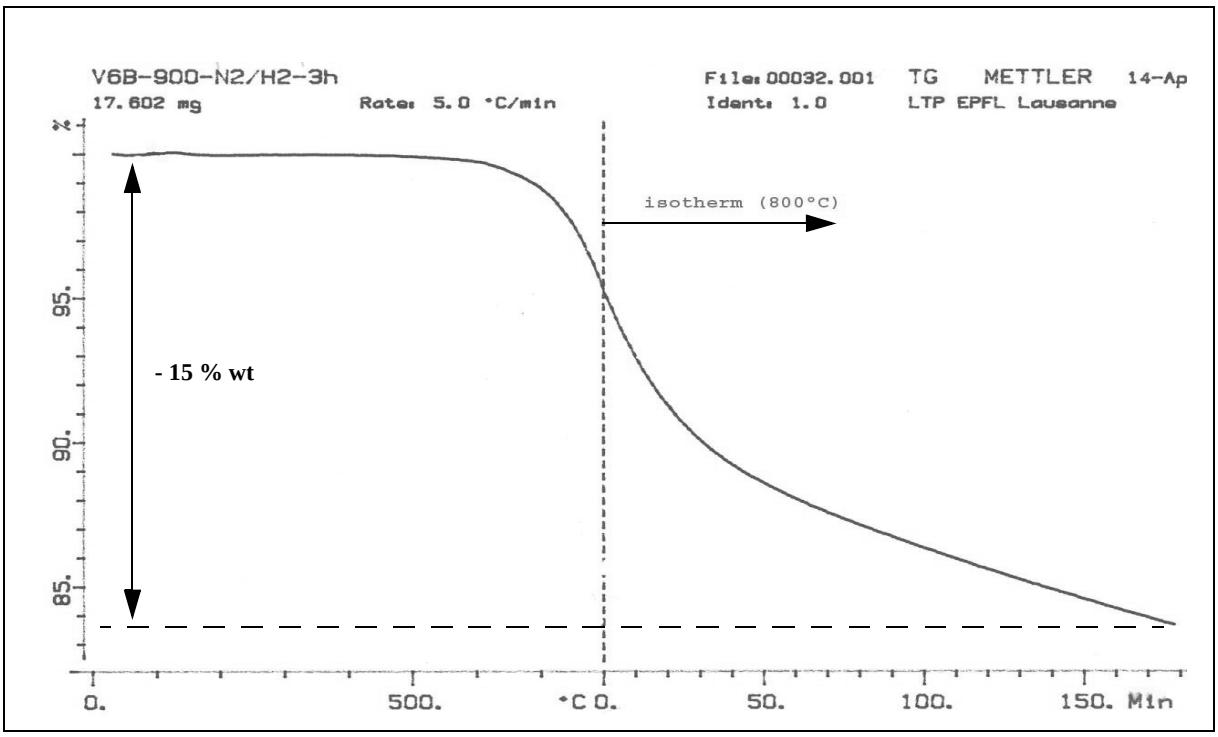

Figure 10: TG of the V6 glass fired under reducing conditions

V6 glass is heated at 5 °C/min from 50 to 800°C, and kept at this temperature during 3 hours. From 800°C, a loss of mass (- 15% wt) is measured. It corresponds to the reduction of PbO into Pb. Indeed, at the end of the experiment, the glass sample has become grey, indicating the presence of precipitated lead.

This reduction is reversible. The same sample was fired in the same temperature conditions but in oxidising environment (air) (figure 11).

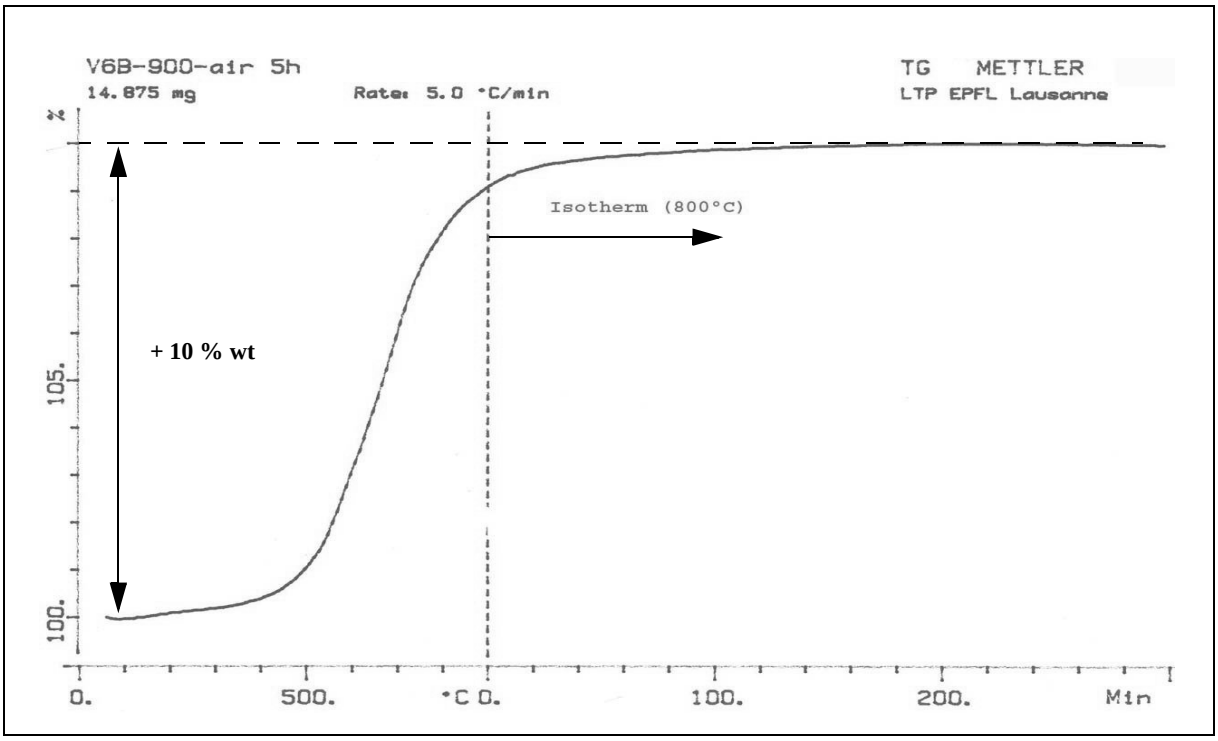

Figure 11: TG of the V6 glass fired under oxidising conditions

From 500°C, lead metal is oxidised into PbO. At the end of the experiment, the sample has become transparent: the grey colour has disappeared.

Besides showing the importance of the firing environment, this last experiment allows to demonstrate that no evaporation of lead was detected during the isotherm, as no loss of mass was measured. The glasses can therefore be considered as stable.

• **Thermal Coefficient of Expansion (TCE) of the glass**

TCE was determined from literature data [15]. A composition TCE diagram is depicted in figure 12. The lines (called isodilates) connecting the points corresponding to compositions (in mole fraction) with the same values of TCE are represented.

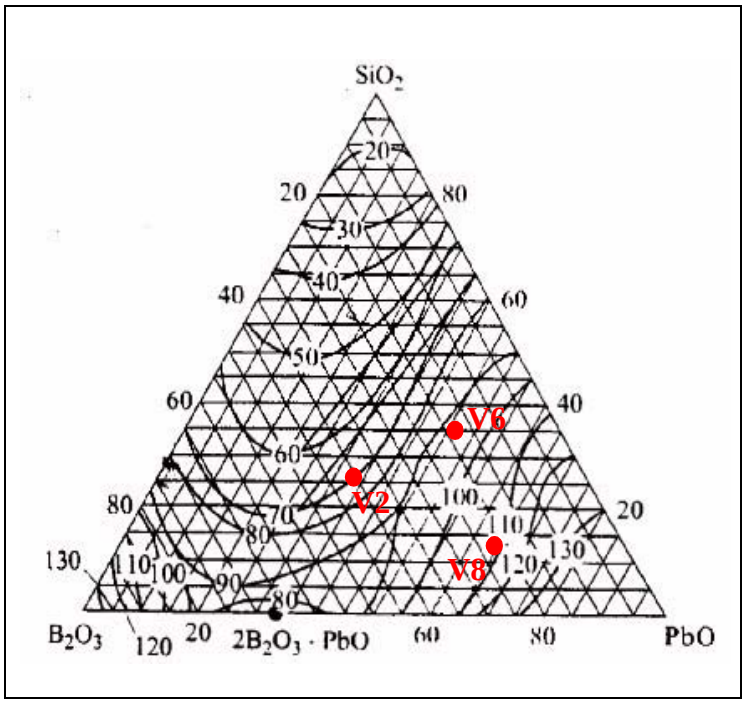

Figure 12: Composition (mole fraction) TCE diagram [15]- The numbers at the curves correspond to the values of the TCE in 10^{-7} K^{-1}

From this system of isodilates, we can deduce the following TCE for each glass:
V2: ~ 7 ppm / °C
V6: ~ 9 ppm / °C
V8: ~ 11 ppm / °C

From these results, we can already suppose problems of incompatibility of the Al_2O_3 substrate with the V6 and V8 systems, as their TCE are too high. In these cases, the fired film is expected to be under tension, which could provoke local cracks. But, remember that the final goal is to use these low firing pastes on substrates with higher TCE (aluminium or steel).

• **Density**

This parameter will be useful for the calculation of the volumic fraction of the glass in the final piezoresistive pastes.
It was determined from the Archimede's principle. It is based on the fact any body plunged in a fluid undergoes a vertical force F_A (push) upward, whose intensity is equal to the weight of the volume of displaced fluid (this volume is thus equal to the immersed volume of the body). we can deduce the following formulae:

$$F_A = (m - m_{app}) \cdot g = V \cdot \rho_{water} = \frac{m}{\rho} \cdot \rho_{water}$$

Then,

$$\rho = \rho_{water} \cdot \frac{m}{(m - m_{app})}$$

m: mass of the glass sample
m_{app}: «apparent» mass of the glass sample plunged in the fluid (water)
ρ_{water}: volume mass of the fluid (water)
ρ: volume mass of the glass sample
V: volume of glass sample
g: gravity

A sample of each glass is obtained by pouring the liquid glass in a graphite mould. After cooling, the sample is extracted, and its density measured.

The estimated densities are:
d_{V2}: ~ 4,56
d_{V6}: ~ 5,30
d_{V8}: ~ 6,10.
The more lead-rich the glass, the higher its corresponding density.

III . 2 . 1 . 3 . 2 . Extrinsic properties (depending on the process)

These properties are resulting from the process and not from the inherent elements of the glass. It is important to know the influence of crushing and milling on the grain size glass. But this kind of treatment can cause contamination of the glass. This is why the pollution of the glass will be quantified.

- **Grain size determination**

The final glass frit should have 1-10 micrometers grain size. In this aim, the glass is subjected to two crushing steps (see figure 4): a crushing in a mortar (1h30) and a ball-milling (72h). Indeed, the crushing in mortar is aimed to rough-hew the starting micrometer glass frit, as the ball-milling is not enough effective.
In figure 13 are depicted the evolution of the grain sizes during the crushing process.

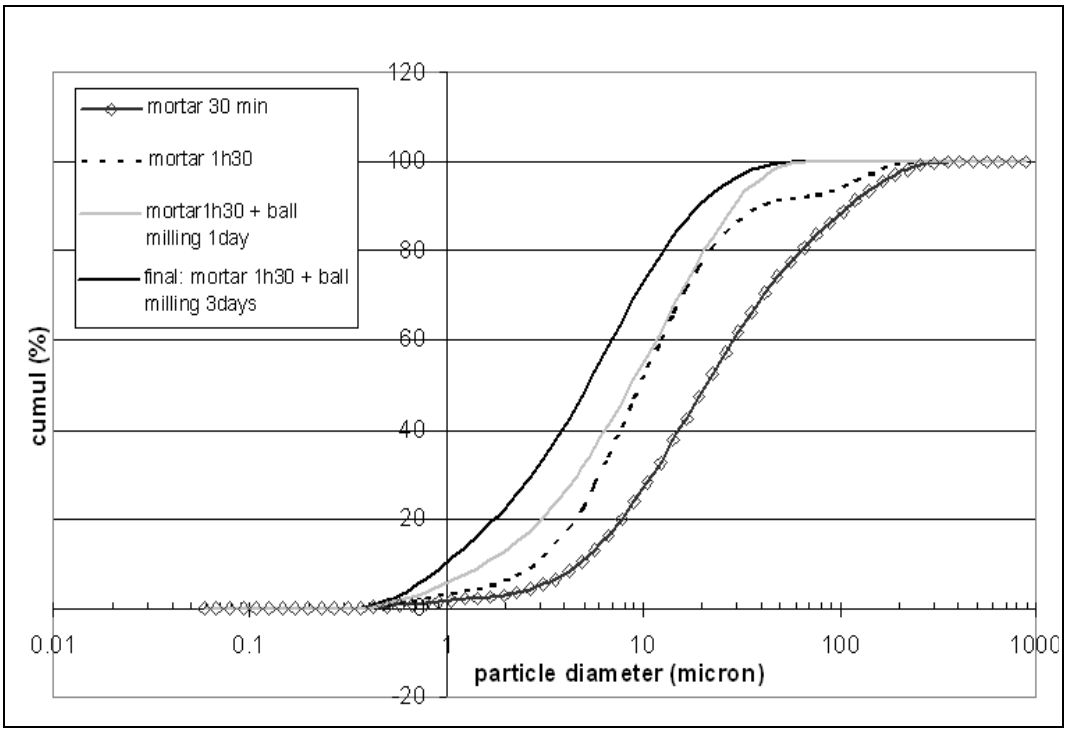

Figure 13: Grain size evolution of the glass during the crushing steps

Measurements were realised with a Malvern Instruments - Mastersizer apparatus. The technique consists in determining the particle size distribution by laser diffraction. 10 nm to 1 mm particle sizes can be detected (with an optimum working for 100 nm - 100 µm particles).

After only 30 min mortar crushing, the particle size is smaller than 500 µm. The increase of crushing time allows to decrease the number of grains with big size (100 µm) and to reduce the dispersion of the particle size (increase of the slope).
Ball milling reduces significantly the diameter of particles (below 10 µm), and three days milling allows to obtain 80% of the grain sizes between 0,5 and 10 µm.
The 20 % remaining biggest particles (> 10 µm) are eliminated by sieving.

- **Contamination from crushing and milling**

These steps are the main source of pollution for a sample.
There are 3 sorts of contamination:
- contamination from the alumina mortar: alumina pollution
- contamination from the ball-milling: ZrO_2 contamination
- carbon contamination from the wear of the polyethylene (PE) flasks during the ball-milling.

No detected crystalline phase (Al_2O_3 or ZrO_2) were observed on XRD spectra. The contamination with alumina was so low that it isn't measurable. The pollution from ZrO_2 was estimated from XRF measurements to be 0,8 % wt, which is satisfactory.

The most important and disturbing pollution was carbon contamination coming from the wear of the PE flasks initially used for the ball-milling. The polymer particles can provoke bubbles or carbon inclusions in the glass during the firing, which can modify the piezoresistive

properties of the pastes. These grey particles are easily visible to the naked eye if a thin layer of glass is fired. This is a simple way to verify that no carbon is present.
In order to avoid this kind of problem, the PE flasks were replaced by pyrex bottles, whose plastic cover was protected with a machined plug, on which a sapphire (Al_2O_3) plate was glued.

III . 2 . 1 . 3 . 3 . Summary of the glass properties

The following table presents the physico-chemical properties of the three manufactured glasses:

	V2	V6	V8
Composition $PbO/B_2O_3/SiO_2+Al_2O_3$	63 / 25 / 12 + 2 %wt 33 / 43.5 / 23.5 + 2 % mol	75 / 10 / 15 + 2 %wt 46 / 20 / 34 + 2 % mol	85 / 10 / 5 + 2 %wt 62 / 24.5 / 13.5 + 2 %mol
crystalline state	amorphous	amorphous	amorphous
T_g (vitrous transition): °C	500	450	370
density	4.56	5.30	6.10
TCE: ppm/°C	7	9	11
grain size: µm	0.5 to 10	0.5 to 10	0.5 to 10

Table 1: Manufactured glass properties

III . 2 . 2 . Organic phase

The organic phase should fulfil two conditions:
- to assure the required rheological properties for the screen-printing,
- to assure the cohesion between the particles after the drying.

The rheological properties are obtained by the association of a volatile and a non-volatile phase. The cohesion is only assured by the remaining non-volatile phase (polymer).

III . 2 . 2 . 1 . Manufacturing process

The used compounds are (figure 14):
- terpineol, anhydrous: $C_{10}H_{18}O$, Fluka Chemie GmbH - 99,95% purity (solvent)
- ethyl-cellulose, ethoxyl content 48%, 300 cps: Fluka Chemie GmbH (polymer).
(These two phases were determined in chap II).

Terpineol

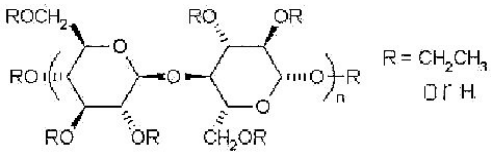

Ethyl cellulose

Figure 14: molecular representation of the organic components

Ethylcellulose is progressively added to the terpineol heated at ~ 40°C. The final mixture should be composed of 2,6 % wt of polymer.
The blend is homogenised by magnetic stirring during two hours. A transparent «gel» with the required viscosity is then obtained. Conductive (see the following section) and glass powders are added and mixed to obtain a paste (see part III.3) that can be used to characterise the organic phase behaviour.

III . 2 . 2 . 2 . Characterisation

- **Decomposition**

A first step is to study the decomposition of the organic phase. All the organics should be burned out before any phase transformation of the glass (here, below T_g) to avoid that carbon particles stay embedded in the glassy matrix.
TG analyses are then carried out to verify that the temperature of complete burnout is below the T_g of each glass.
In figure 15 are represented TG spectra of two kinds of cellulose: 46 and 300 cps.

Note that the denominations of the 300 or 46 cps ethycellulose correspond to the viscosity of a 5% solution of each ethylcellulose in a 80 / 20% toluene / ethanol solution.

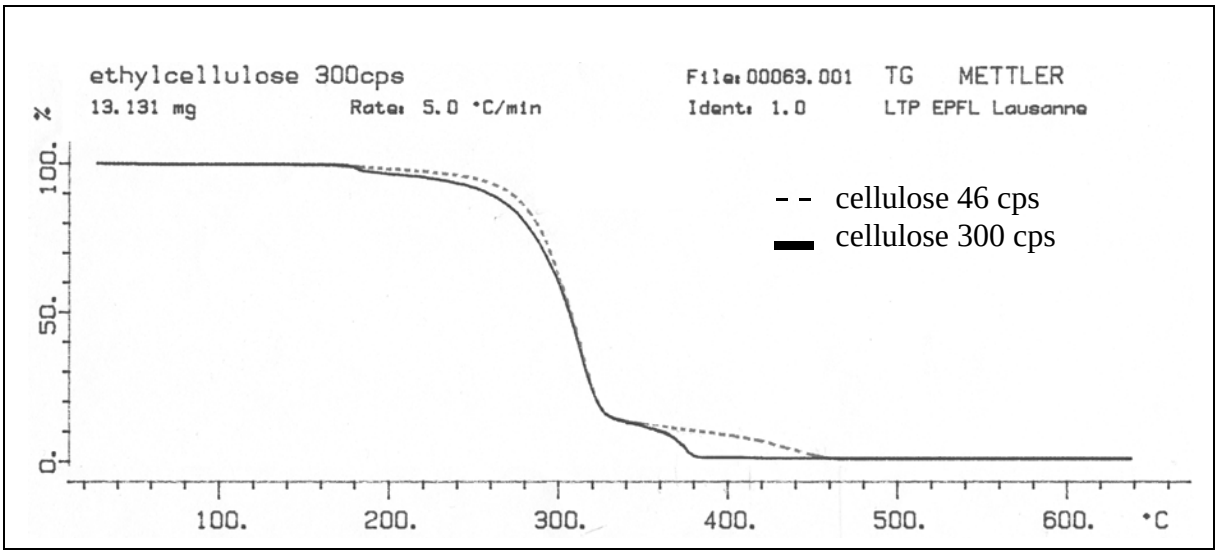

Figure 15: TG spectra of different ethylcelluloses

Although 46 cps cellulose is currently used for standard piezoresistive pastes, this polymer can not be used for low-firing temperature pastes (V8 pastes, for instance), as for this V8 glass, cellulose should burn out before 370°C. Whereas 46 cps cellulose is not adequate, 300 cps cellulose is totally burnt at 380°C. It could be acceptable if the paste firing cycle is adapted to optimise the burnout of the organic before 370°C (for instance, the heating rate can be decreased or an isotherm can be added: see part III.3). Moreover, the quantity of polymer is low, as it represents only 2,6 % wt of the organic phase. The remaining carbon particles should be then negligible at 370°C.

Note that tests with other polymers were carried out. For example, PEMA - poly(ethyl methacrylate - is burned out below 360°C, but its rheological properties were not appropriate. Other organic compounds such as organic phosphate esters could be suitable, but their burnout generates permanent residues (like phosphate) that can modify the properties of the films.

- **Rheological behaviour**

The second step was to verify that the mixture of solvent and polymer confers the required rheological properties to the paste. Indeed, as explained in chapter I, the paste should be characterised by a pseudoplastic or a moderate thixotropic behaviour. Pseudoplastic or thixotropic fluids are similar in behaviour, in that viscosity decreases by applying shear stress, but thixotropy implies hysteresis (figure 16). The thixotropic effect is characterised by two possible values of viscosity, corresponding to an increase or a decrease of shear rate, or by a non recovery of the initial viscosity after shearing. Thus, the more a thixotropic ink is sheared, the more the viscosity is degraded. One understands why the thixotropy is harmful to the reproducibility of the screen printed films.

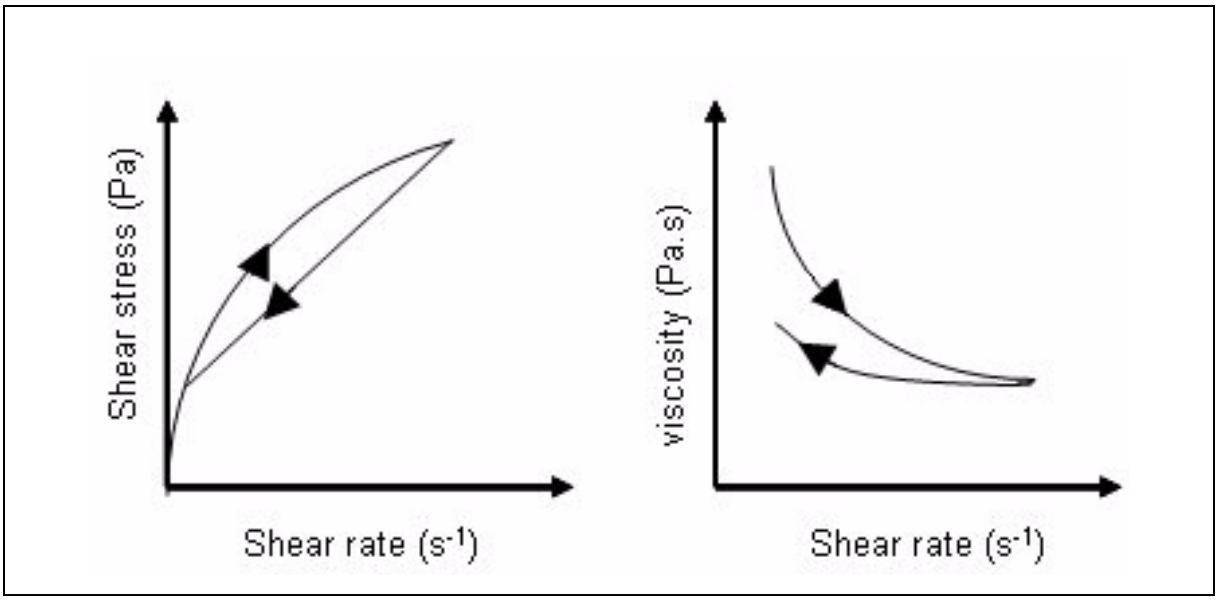

Figure 16: Thixotropic behaviour

A simple mean to validate the rheological behaviour of our pastes is to compare them to the behaviour of an usual commercial paste (DP 2041).
In this aim, we used a HAAKE viscosimeter with a cone-plate system type C20-4° (α = 4°) (figure 17). This geometry (cone-plate) is adapted to characterised high viscosity samples and does not require important quantities of paste for the test.

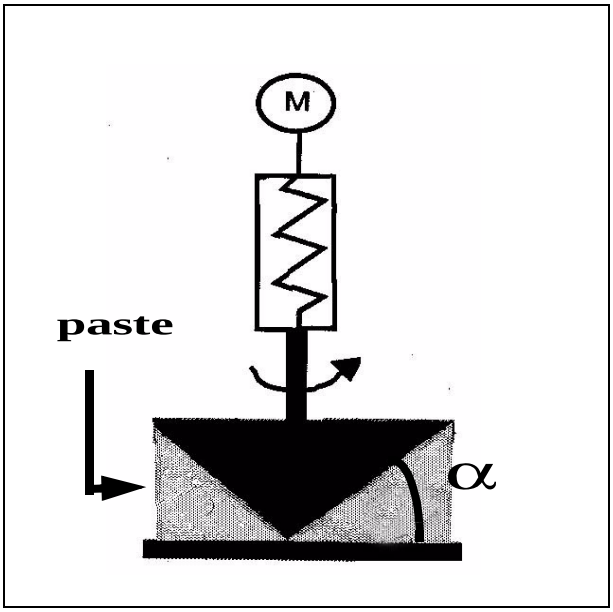

Figure 17: Description of the cone-plate system

Figures 18 and 19 represent the rheological behaviour of respectively a commercial paste (DP2041) and a paste realised in our lab.

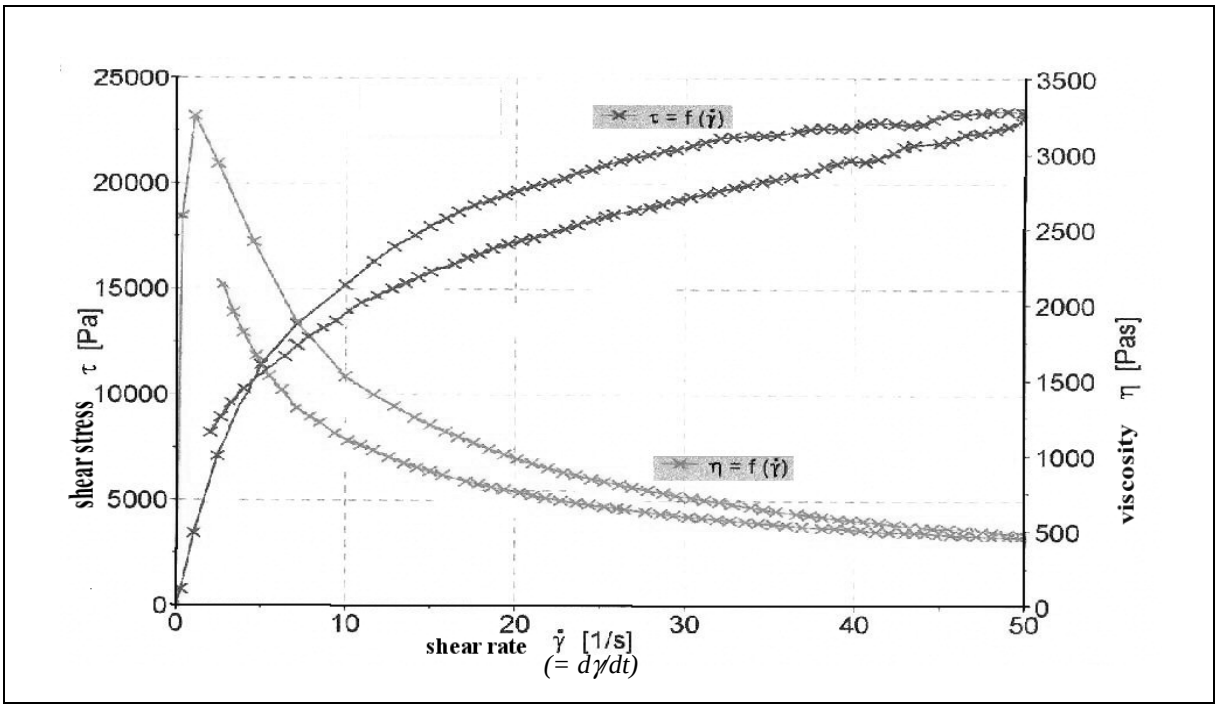

Figure 18: Rheological behaviour of an usual commercial paste (DP 2041)

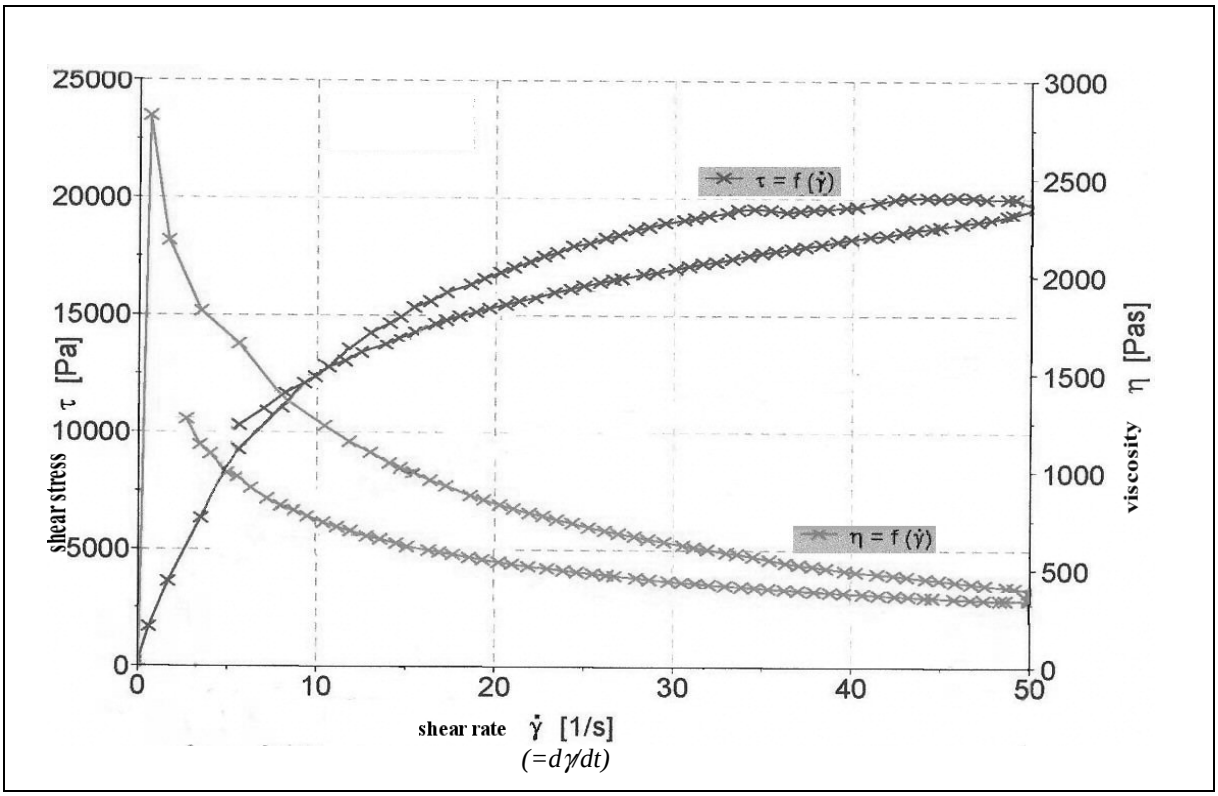

Figure 19: Rheological behaviour of an experimental paste

η represents the viscosity (Pa.s).
τ corresponds to the shear stress (Pa).
$d\gamma/dt$ is the shear rate (s^{-1}). It corresponds to the squeegee motion on the screen to let the paste go through it, which induces friction. This friction is reproduced when the paste is between the

two plates of the cone-plate rheometer. When the plate stay fixed and the cone turns, each layers of the paste moves by following the adjacent one at a different speed because of the frictional forces. A velocity gradient develops inside the ink, and it is called the shear rate.

These three above variables are linked by the following formula:

$$\eta = \frac{\tau}{\dot{\gamma}}$$

From figures 18 and 19, we can deduce that both pastes have a moderate thixotropic behaviour, as a hysteresis is observed with the $\tau = f(d\gamma/dt)$ curve. Moreover, at the end of the shear test, the sample does not recover its initial viscosity ($\eta = f(d\gamma/dt)$ curve).
It is confirmed that the rheological behaviour of the experimental paste is similar to that of DP 2041, although the maximal shear stress value for the maximal shear rate is lower for the first one. However, the obtained rheology of the paste is satisfactory for screen-printing, as the behaviour meets the following requirements for high quality and reproducible printability [16,17]:
- a high viscosity at low shear rate
- a low viscosity and a high shear stress at high shear rate
- a sufficiently reversible behaviour to achieve a reproducible layer.

Comment:
Some measurement problems can be due to a crack of the fluid at the middle of the angular slit, which contributes to drive the fluid to the exterior of the angular slit (figure 20).

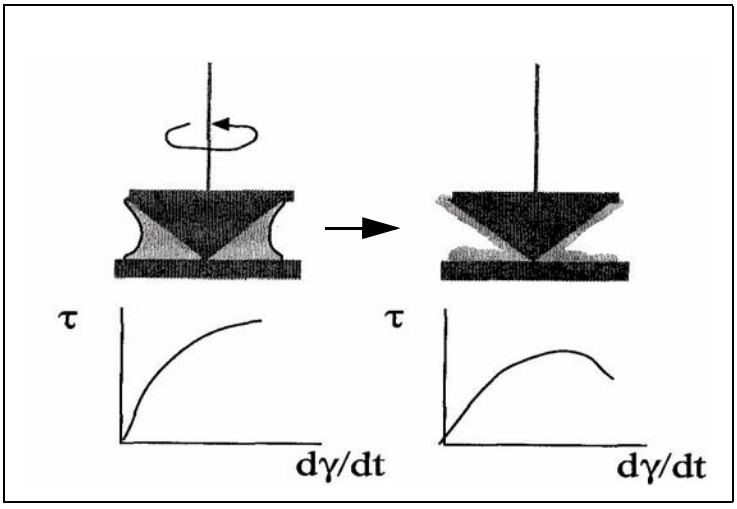

Figure 20: Measurement problem resulting in a crack of the fluid

We met this phenomenon in the case of inhomogeneity of the paste or if the shear rate is too high. A resulting curve is represented in figure 21.

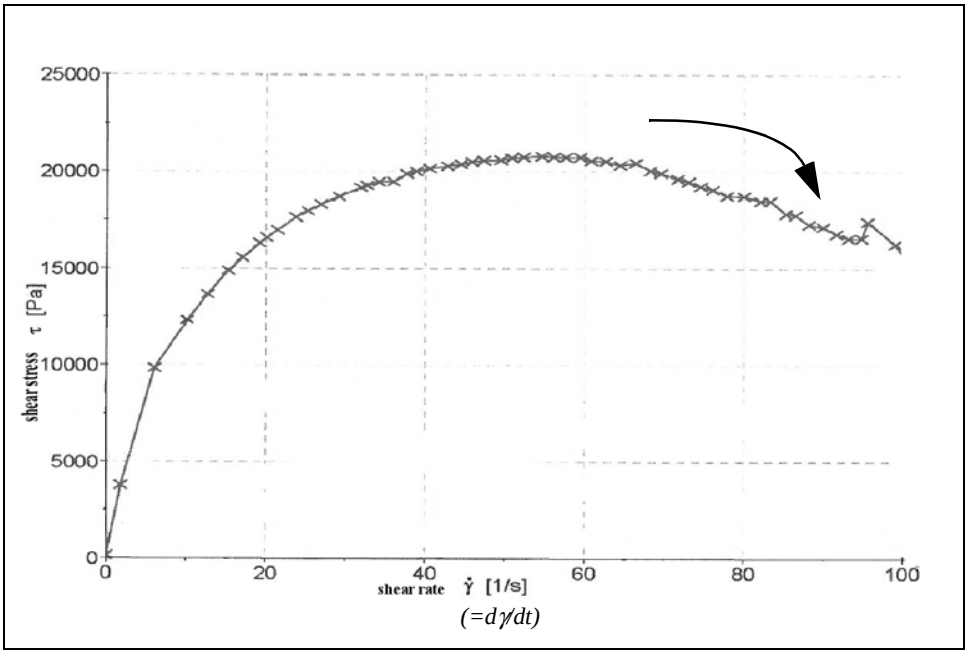

Figure 21: Example of a non valid measurement

At high shear rates, we note a decrease of the shear stress value. At the end of the test, the phenomenon described in figure 20 is observed. It corresponds to a disorganisation / destruction of the molecular structure of the polymer. However, this is observed in «extreme conditions» as, during screen printing, the shear stress does not exceed 50 or 100 s^{-1} [18].

From these experiments, the chosen organic composition can be accepted, in the following proportions:
2,6% wt of ethyl cellulose 300 cps in terpineol.

III . 2 . 3 . Conductive phase

This phase constitutes one of the most important parameters together with the glass in piezoresistive paste compositions, as the electrical values and conduction process depend on it.

III . 2 . 3 . 1 . Selected compounds

Different size of RuO_2 powders are selected:
- 400 nm: Ruthenium (IV) oxide, anhydrous, >99.95 %, Alpha Aesar - Johnson Matthey GmbH.
- 40 nm: Ruthenium (IV) oxide, anhydrous, >99.95 %, Riedel-de Haën.

Two ranges of grain sizes are chosen to study their influence on electrical properties. Moreover, the increase of the specific surface area of the conductive phase could favour the reactions (and a possible dissolution) between the components.

Note that we limit our study on the influence of only one kind of conductive compound. In other words, the influence of lead ruthenate ($Pb_2Ru_2O_6$) will be not analysed. This chosen binary compound will allow to easily detect a possible exchange of lead atoms between the glass and RuO_2. Indeed, if ruthenate phase is produced, it will be easily detected by XRD. This will simplify the observations of possible interactions.

III . 2 . 3 . 2 . Characterisation

• Structure

RuO_2 has a rutile structure in which ruthenium atoms are in a body-centred cubic (bcc) configuration and oxygen atoms form octahedra including a ruthenium element in each center. Figure 22 represents the rutile structure showing RuO_6 octahedron with a single unit cell (left picture), and the right one represents the rutile structure showing many RuO_6 octahedra sharing corners. The view is down the c axis.

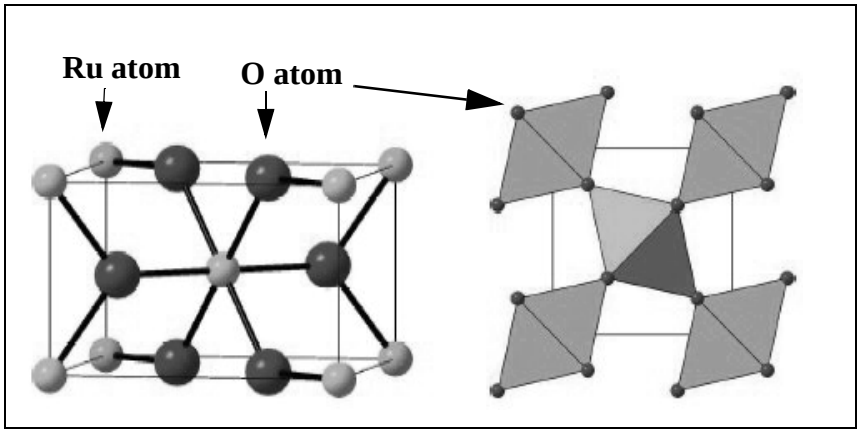

Figure 22: Rutile structure of RuO_2

Ru-based systems are the most used thick film resistors. These oxides are highly conductive materials with good stability when fired even at high temperatures in air. It is normally presumed that they are also stable within the resistors. However, in certain conditions (depending on T_f, glass composition...), there is extensive evidence of exchange reactions of the conductive phase and the surrounding glassy matrix during the firing, as previously explained.

• Composition

This compound is 99.95 % pure. No contamination has been detected, and the X-ray diffractogram (figure 23) shows well-defined sharp peaks, which demonstrate the high degree of crystallinity of the sample.

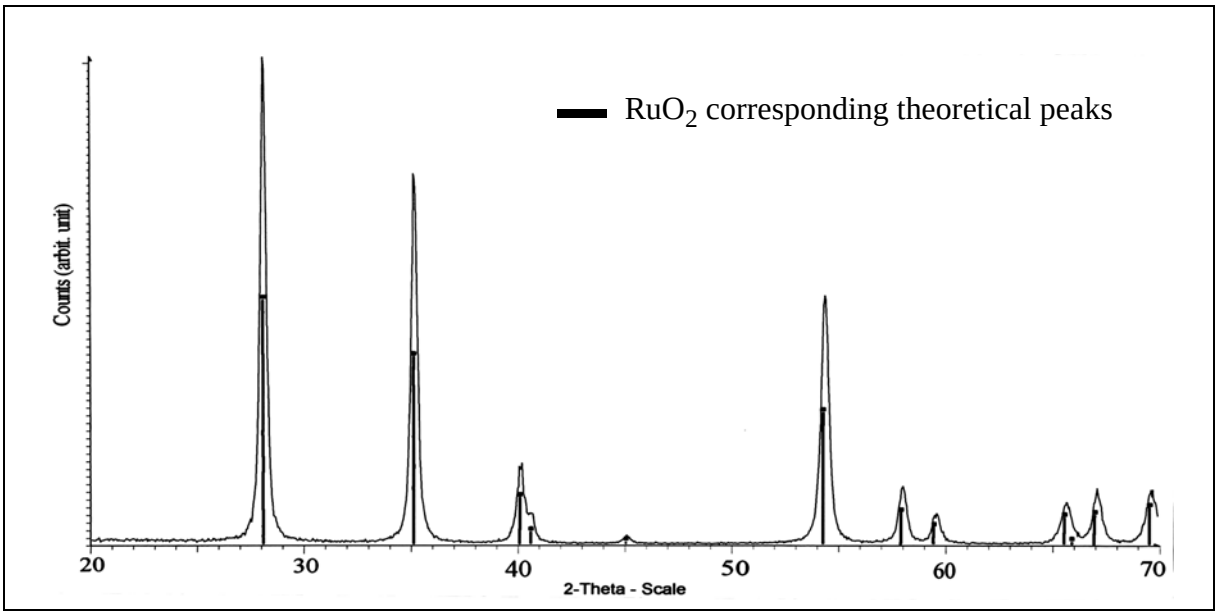

Figure 23: X-ray diffraction of RuO_2 powder (40 nm)

In addition, TG analysis confirmed the anhydrous state of the sample as no weight loss has been detected.

- **Grain size**

The 40 nm sample was observed with TEM and shows a dispersion of spherical particles of ~50nm size. The particles size distribution seems to be homogeneous (figure 24).

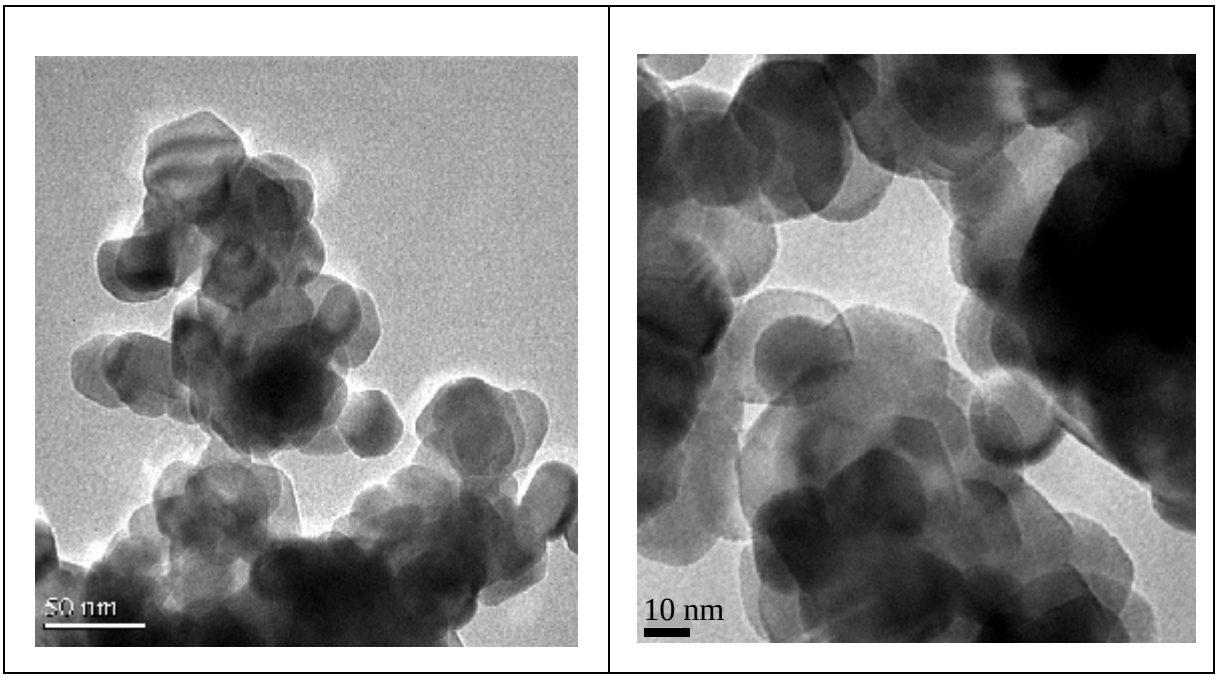

Figure 24: TEM observation of RuO_2 powder (40 nm)

The observation of the supposed 400 nm particles is less evident. SEM observations show that the particles are in reality constituted of agglomerates of smaller particles that form a final grain of 400 nm. These agglomerates can be considered as a single particle. Figure 25 shows the form of such agglomerates, whose the geometry is very variable and not so well defined as the one of the 40 nm particles.

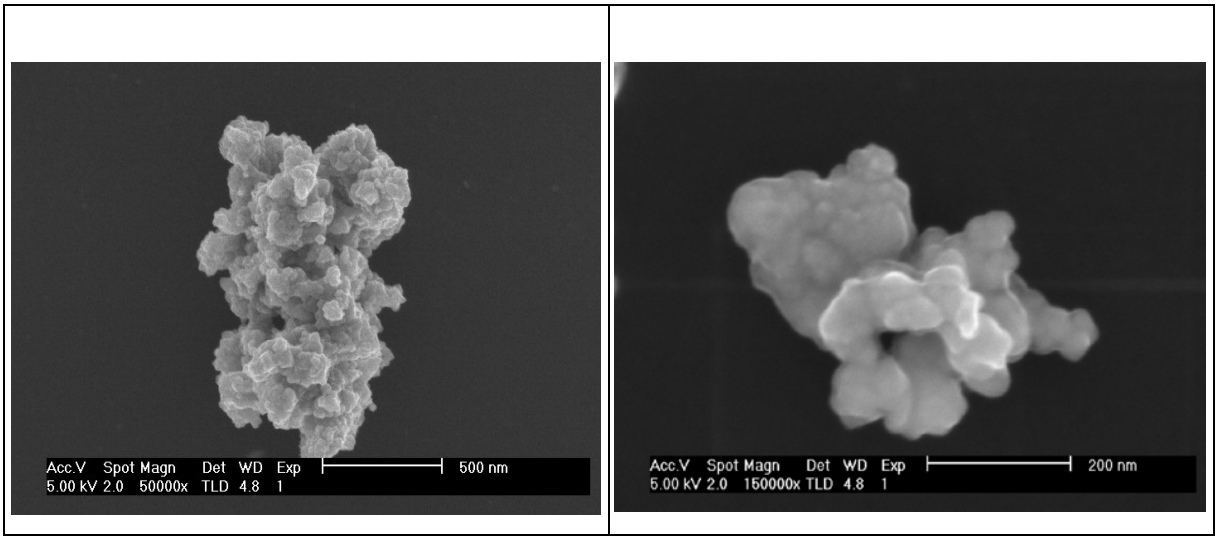

Figure 25: SEM observation of RuO_2 clusters (400 nm)

From these results, small particles can be considered as 40 nm grains and the bigger agglomerates as 400 nm grains.

III . 2 . 3 . 3 . Chosen parameters

We chose concentrations of the conductive phase based on literature data. The corresponding volume fractions of RuO_2 vs. glass vary from 0.23 to 0.045. The intermediate concentrations will be adjusted according to the first electrical results.
This different concentration samples will allow us to study the evolution of the electrical properties (R_s, GF, TCR), and the electrical behaviour close to the percolation threshold. Our results will be interpreted in the frame of a model of conduction based on a nonuniversal tunnelling percolation theory (exposed in chapter IV).

III . 2 . 4 . Summary of the chosen parameters

The main parameters of each phase composing a piezoresistive paste are summarised in the following table.

	glass phase			conductive phase	organic phase
nomenclature	V2	V6	V8	--	solvent + binder
composition	$PbO/B_2O_3/SiO_2$ + 2%wt Al_2O_3			RuO_2	terpineol + ethylcellulose 300 cps
characteristics	1 to 10 µm amorphous			40 and 400 nm	--
	high T_f ~ 700°C	low T_f ~ 600°C	very low T_f ~ 500°C	possible reactions with the glass	pseudoplastic behaviour burnout below 380°C

Table 2: Main parameters of the components of piezoresistive pastes

These three phases will be mixed together with appropriate concentrations to form piezoresistive pastes that will be fired at different temperatures T_f, according to their glassy matrix. This last step is described in the following section.

III . 3 . Paste manufacturing process

III . 3 . 1 . Manufacturing steps

III . 3 . 1 . 1 . General process

In figure 26, are described the successive steps to manufacture a piezoresistive paste from the three chosen phases (glass, conductor and organics).

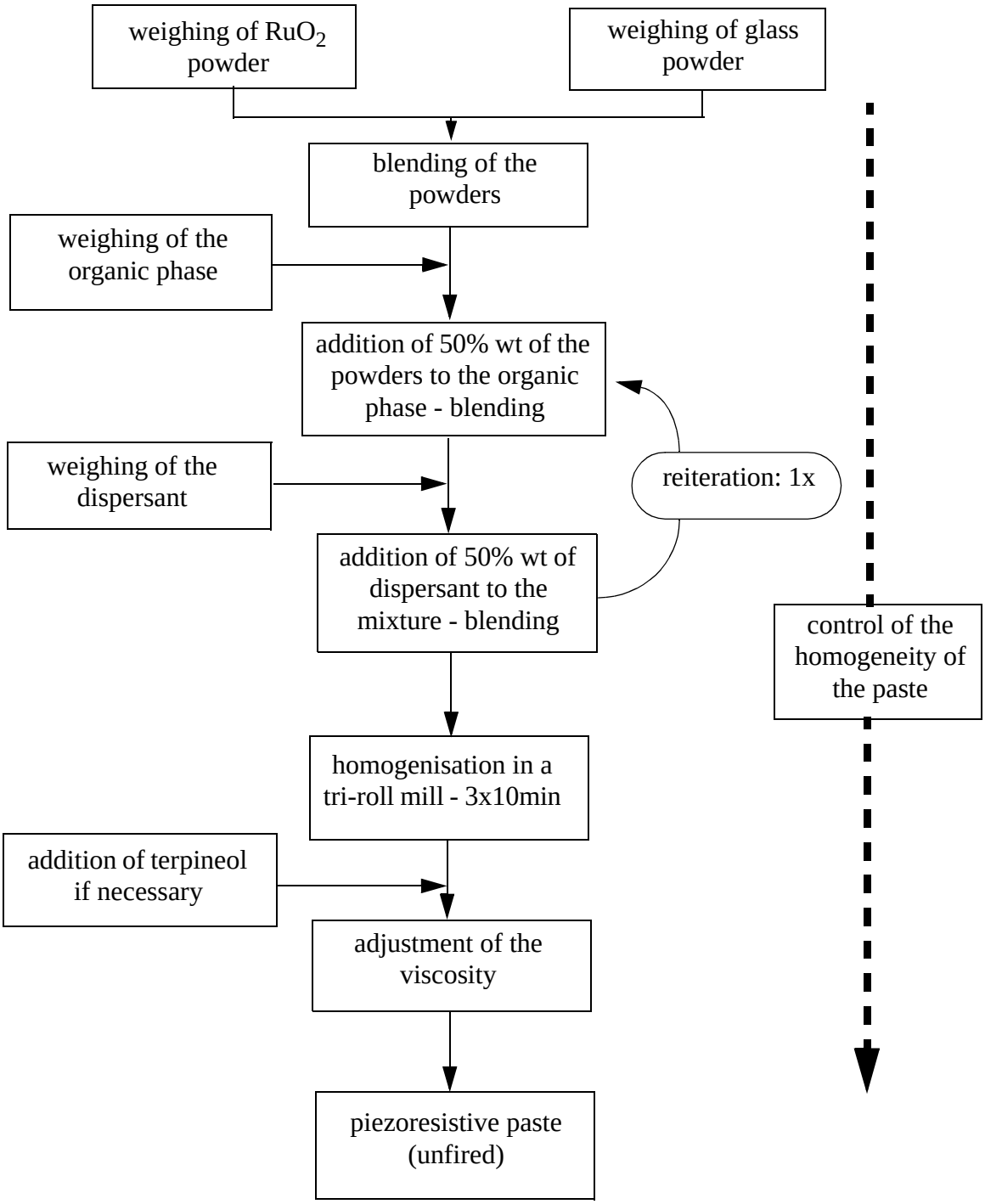

Figure 26: Manufacturing process of piezoresistive pastes

At the end of the process, a black smooth viscous paste is obtained and ready to be screen-printed. It should be stored hermetically to avoid solvent evaporation that could affect viscosity.

III . 3 . 1 . 2 . Details of the process

• technical details

- blending: it is realised by hand with a spatula.
- the powder is integrated into the organic phase in two steps to optimise the homogenisation and to allow the solvents to wet each particles.
- dispersant: to avoid agglomerates, a dispersant is added. The used compound is acetylacetone, $CH_3COCH_2COCH_3$, >99,9 % - Sigma-Aldrich Chemie GmbH.
- homogenisation: it is carried out with a EXACT three roll mill (figure 27-A), which is composed of three in-line rolls separated by small adjustable gaps (figure 27-B).

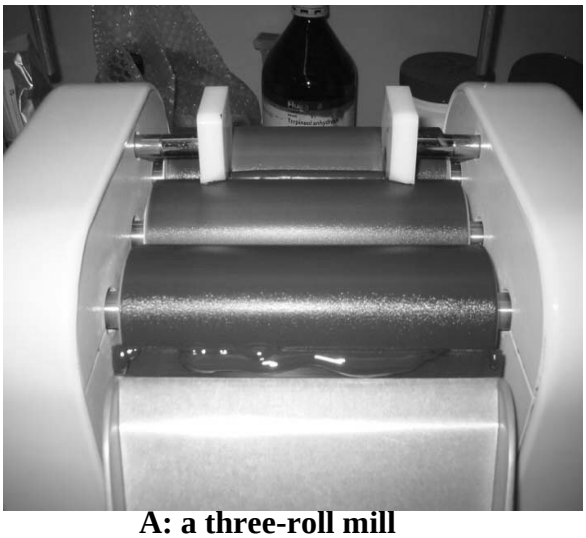

A: a three-roll mill

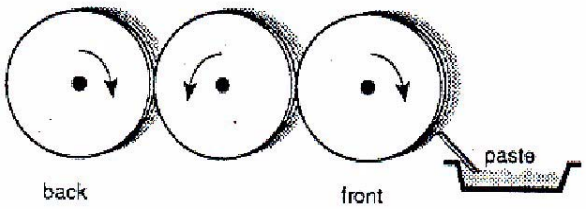

B: roll action

Figure 27: A three-roll mill and schematic view of the roll action

The rolls rotate in opposite directions at different speeds relative to each other. A take off blade scrapes the ink off the front roll, and the paste is collected in a chute. This cycle is repeated several times until the desired dispersion is obtained. In order to limit contamination, the rolls are in alumina. Care must be taken if the ink contains metal powders which might be converted into flakes if too high stresses are applied during the roll operation (this is not the case for our materials).

- adjustment of the viscosity: during the homogenisation, if the paste is too viscous (it should flow if it is risen up with a spatula), small quantities of terpineol can be added. This modification does not damage the properties of the pastes.

• phase proportions

The electrical properties depend on the concentration of RuO_2 and glass and the rheology depends on the concentration of the organic phase. The quantitative composition is presented in table 3.

	conductive phase	glassy matrix	organic phase
concentration (%wt)	25 to 5	55 to 75	20 (2.6% ethylcellulose + 17.4% terpineol)

Table 3: Quantitative composition of a piezoresistive paste

In addition, 5% wt (vs. the total quantity of powders) of dispersant should be added to avoid agglomerates.

• firing conditions

In order to avoid carbon residues due to process contamination, specific firing cycles should be determined for each series of pastes.
However, all the cycles are similar concerning the zone in which reactions occur in order not to influence the properties. The modifications will be realised for the range of temperature below the softening temperature of the glasses.

To eliminate carbon residues, a solution is to impose a dwell temperature near 500°C (carbon decomposition). However, for this temperature, the glass begins to react, so it is more judicious to decrease the temperature of the dwell but in a same time to increase its duration. The different firing cycles corresponding to each kind of glass are depicted in figure 28.

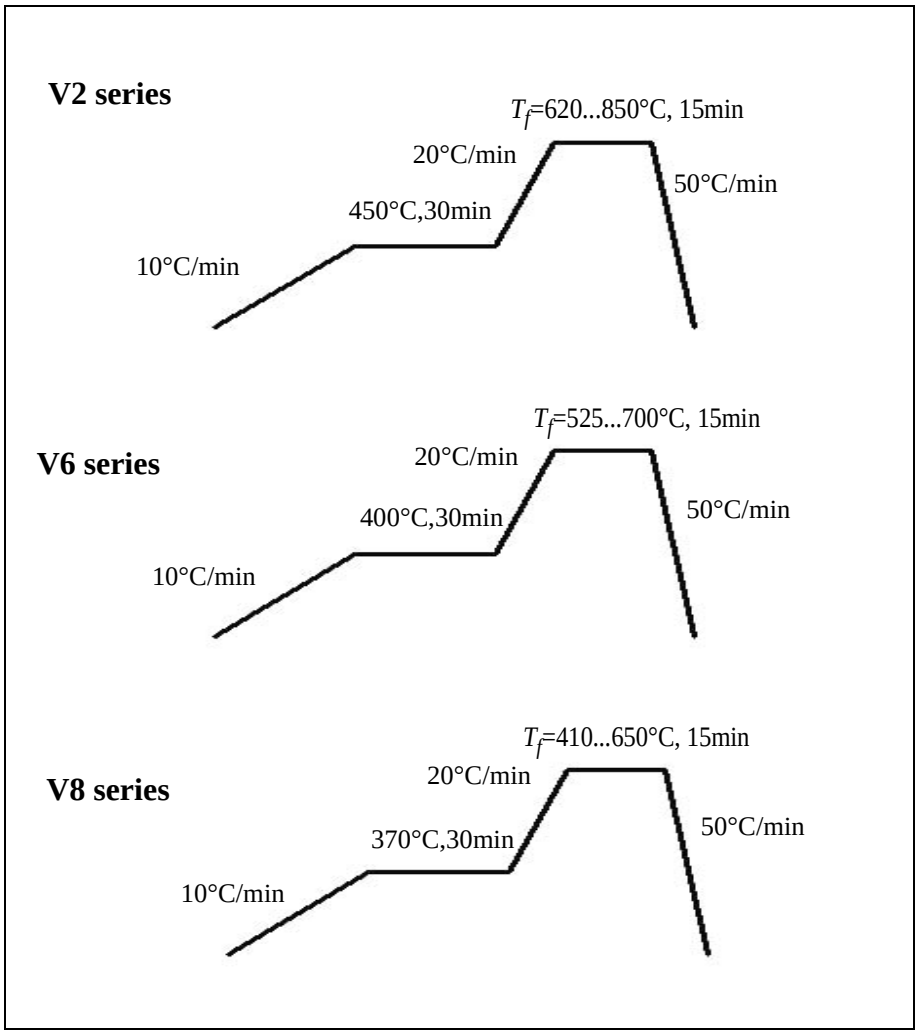

Figure 28: Cycles of firing of the different series of pastes

Each cycle is realised under a flow of dried air.
The mentioned T_f corresponds to the firing temperatures that vary according to the glass composition.
For V2 series, T_f is comprised between 620 to 850°C, with an optimum firing at 700°C.
For V6 series, T_f is comprised between 525 to 700°C, with an optimum firing at 600°C.
For V8 series, T_f is comprised between 410 to 650°C, with an optimum firing at 500°C.

The advantage of these three series of pastes is that they cover a large range of temperatures and that they can be used on different substrates.

III . 3 . 2 . Characterisation

Characterisation of the obtained films is detailed in chapter IV by analysing the influence of different parameters (firing conditions, conductive phase concentrations,...) on the behaviour of the pastes.

However, we can already verify that the obtained thick films are dense after firing, without bubbles, and ~ 10 µm thick (see SEM pictures in chapter IV). Moreover, they give coherent electrical responses that will be presented in chapter IV.
Concerning the study of the phase evolution, any new phase will be easily detected as all the constituents are known (contrary to commercial pastes) and as there is a single conductive phase. To illustrate the simple composition of the obtained pastes, figure 29 shows a XRD spectrum of V6 series piezoresistive paste fired at 700°C.

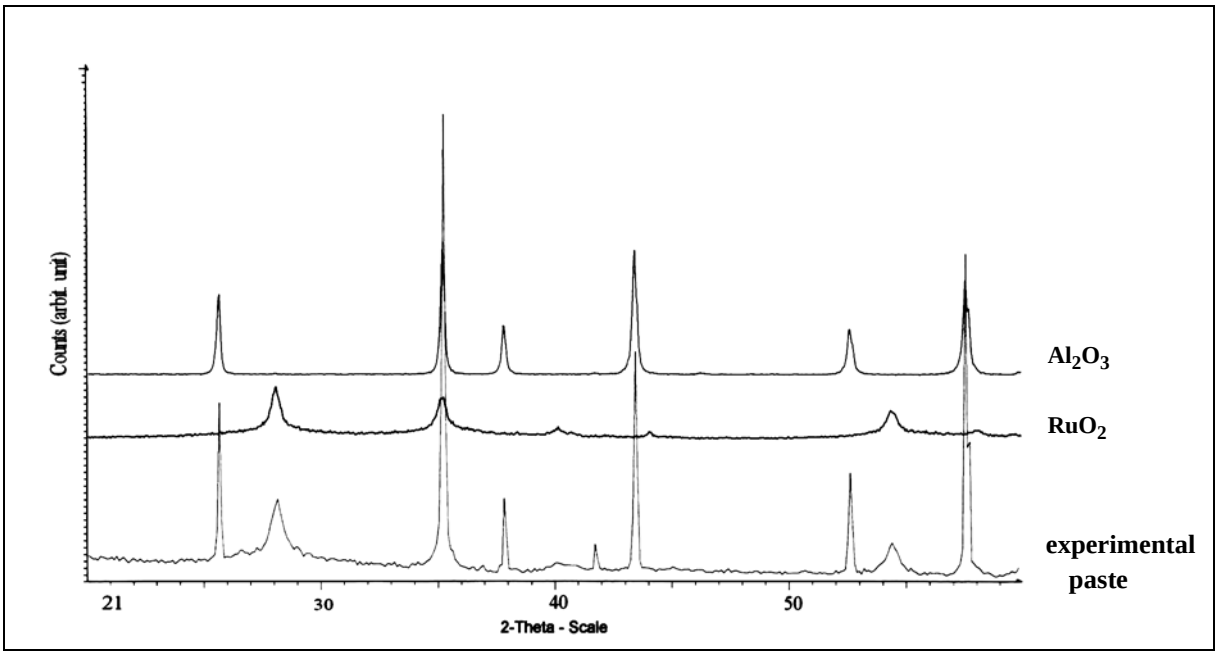

Figure 29: XRD spectrum of an home-made piezoresistive paste fired at 700°C

All the peaks are resolved, and RuO_2 and Al_2O_3 phases are detected. RuO_2 corresponds to the conductive phase whereas Al_2O_3 peaks come from the alumina substrate on which the film is screen-printed. The amorphous glass phase is not detectable, and no other contaminations are observed.

III . 3 . 3 . Conclusion

This part is important, as it allows us to precisely define a manufacturing process for our piezoresistive pastes, and for other thick film compositions in general. It results in the ability to realise different series of pastes with different ranges of firing temperatures. This control on several parameters (glass composition, conductive phase concentration, grain size, firing temperature...) will allow us to direct precisely our research toward the principle of conduction in such systems, and the reactions between the elements and their influence / repercussion on the electrical properties.

References - Chapter III:

1. Prudenziati M, *Handbook of sensors and actuators,* Elsevier,1994, **1**, 118-20.
2. Johnson DW, Hummel FA, *Phase equilibria and liquid immiscibility in the system PbO-B_2O_3-SiO_2,* Journal of the american ceramic society, 1968, **51**, 196-201.
3. Geller RF, Bunting EN, *The system PbO-B_2O_3-SiO.*, Journal Res. Natl. Bur. Std, 1939, **23**, 275-83.
4. Trubnikov IL, *Thermal expansion, vitrification temperature, and corrosion behavior of lead-borosilicate glasses.,* Refractories and industrial ceramics, 2000, **41**, 169-71.
5. Adachi K, Kuno H, *Decomposition of ruthenium oxides in lead borosilicate glass,* J. Am. ceram. Soc., 1997, **80**, 1055-64.
6. Prudenziati M, Morten B, Forti B, Gualtieri AF, Mihai Dilliway G, *Devitrification kinetiks of high lead glass for hybrid microelectronics,* Intern. J. of Inorg. Mat., 2001, **3**, 667-74.
7. Adachi K, Iida S, Hayashi K, *Ruthenium clusters in lead-borosilicate glass in thick film reisitors,* J. mat. res, 1994, **9**, 1866-78.
8. Vest RW, *A model for sheet resistivity of RuO2 thick film resistors,* IEEE Transaction on components, hybrids, and manufacturing technology, 1994, **CHMT-14**, 396-406.
9. Vest RW, *A loading curve model for RuO2 thick film resistors as function of glass viscosity,* Proceedings of the international symposium on microelectronics, ISHM, Orlando, 1991, 418-25.
10. Prudenziati M, Sirotti F, Sacchi M, Tombesi A, Akomolafe T, *Size effects in ruthenium-based thick-film resistors: rutile vs. pyrochlore-based resistors,* Active and passive elec. comp., 1991, **14**, 163-73.
11. Palanisamy P, Sarma DHR, Vest RW, *Liquid-phase sintering in thick-film resistor processing,* J. Am. Ceram. Soc - communications, 1985, **68**, C215-6.
12. Prabhu A, Vest RW, *Investigation of microstructure development in RuO_2-lead borosilicate glass thick films,* Mat. Sc. Res., 1975, **10**, 399-408.
13. Prabhu A, Fuller GL, Vest RW, Solubility of *RuO_2 in a lead borosilicate glass,* J. Am. Ceram. Soc - discussions and notes, 1974, **57**, 408-9.
14. Palanisamy P, *Influence of substrates on microstructure development in thick film resistors,* PhD Thesis, Purdue University, 1979.
15. Trubnikov IL, *Thermal expansion, vitrification temperature, and corrosion behaviour of lead-borosilicate glasses,* Refractories and industrial ceramics, 2000, **41**, 169-71.
16. Riemer DE, *The direct emulsion screen as tool for high resolution thick film printing,.....*
17. Riemer DE, *The shear and flow experience of ink during screen printing,* ISHM'87 Proceedings, 1987, 335-40.
18. Baudry H, *Le contrôle rhéologique des pâtes pour déterminer leur aptitude à la sérigraphie,* EMI, 1976, **226**, 38-41.

CHAPTER IV:

Electrical and structural evolution of new piezoresistive pastes

The last chapter was dedicated to the manufacture of piezoresistive pastes with different firing temperatures (for different substrates). At the end of chapter III, our new piezoresistive pastes were considered as ready to be used, as their physico-chemical properties were determined to be sufficient to realise thick-film resistors.
From these previous results, we aim to realise different series of pastes by varying different parameters such as conductive phase grain size, concentration and firing temperature. Structural and electrical properties will be studied, and a coherent relationship will be found between the electrical behaviour (conduction process) and the complex nanostructure. In other words, this key chapter presents the results and their interpretation by a model of conduction based on an unpublished hypothesis.
After having studied the properties of resistors fired according to the standardised cycles depicted in figure 28-III, we will dedicate our interest to their process sensitivity to other firing parameters such as firing time and cooling speed. Furthermore, we will examine the stability of the resistors during long-term storage at elevated temperature. The results corresponding to the different glass phases (V2, V6, V8) will be compared and the most stable pastes will be selected to be integrated in a complete low-firing thick-film system to give a sensor that will be characterised in chapter V.
(For the properties of the glasses see Table 1, p77.)

IV . 1 . Sample description - experiments

IV . 1 . 1 . Sample description

We have three categories of piezoresistive pastes: V2, V6 and V8 pastes (characterised by their glassy matrix). For each type, appropriate concentrations of the conductive phase were chosen: the corresponding volume fractions of RuO_2 vs. glass vary from 0.23 to 0.03 for each

conductive particle size (40 nm and 400 nm). The obtained pastes will be then fired at different temperatures adapted to the glass compositions.
The volume fraction x of RuO_2 is determined as following:

$$x = \frac{V_R}{V_R + V_G}$$

V_R: total volume of RuO_2 particles
V_G: total volume of the glass

The chosen parameters corresponding to each class of pastes are summarised in table 1.

	RuO_2 grain size	RuO_2 concentration (volumic fraction)	Firing temperature (°C)
V6-paste	40 nm	0.23 - 0.15 - 0.11 - 0.09 - 0.08 - 0.075 - 0.07- 0.067 - 0.06 - 0.055 - 0.05 - 0.045 - 0.03	from 525 to 700°C, with 25°C steps
	400 nm	0.23 - 0.15 - 0.11 - 0.095 - 0.085 - 0.08 - 0.075 - 0.073 - 0.07 - 0.06 - 0.055 - 0.05 - 0.03	
V2-paste	40 nm	0.11 - 0.08 - 0.075 - 0.067 - 0.065 - 0.06 - 0.055	from 620 to 850°C, with 25°C steps
	400 nm	0.11 - 0.09 - 0.08 - 0.075 - 0.071 - 0.07 - 0.067 - 0.06 - 0.055	
V8-paste	40 nm	0.11 - 0.09 - 0.08 - 0.075 - 0.072 - 0.07 - 0.069 - 0.067 - 0.065	from 410 to 650°C, with 25°C steps
	400 nm	0.11 - 0.09 - 0.08 - 0.077 - 0.075 - 0.072 - 0.07 - 0.065 - 0.06 - 0.055	

Table 1: Selected parameters for each category of piezoresistive pastes

Note that the choice of the concentrations is not systematic as the intermediate concentrations were adjusted according to the first results.
The firing schedules are presented in chapter III.3.1.

Used nomenclature for the fired samples:
To simplify the name of the samples, the following notation was adopted:
for instance, a V6-paste with 0.23 volume fraction of 40 nm RuO_2 grain size and fired at 600°C will be called: P0.23-6-40-600C
with P: piezoresistive paste
0.23: volume fraction of RuO_2
6: glass composition (V6)
40: conductive grain size (40 nm)
600C: firing temperature (600°C).

From the results, selected samples will be exposed to the same thermal treatments as the commercial pastes (see chapter II.2.3). Indeed, the samples are subjected to different cooling rates, and different dwell-firing temperatures. The stability of the electrical and structural properties will be studied during long-term high temperature storage at 250°C.
The firing parameters and the choice of the samples for the annealing step will be deduced from the previous results, and will be described in details in section IV.6.

This different concentration samples will allow us to study the evolution of the electrical properties (R_s, GF, TCR), and the electrical behaviour close to the percolation threshold. From our results, an origin of the conduction mechanism that we will be explained in the following section will be proposed.

IV . 1 . 2 . Measurements

The same layout as chapter II.2 is used together with the same termination material (ESL 8837 Au). Moreover, the electrical measurements and structural observation techniques are also identical. For this characterisation step, all the pastes are screen-printed on alumina substrates in order to obtain comparable results, particularly to have the same sensitivity between each sample for gauge factor measurements.

IV . 2 . V6-paste category: low firing temperature system

This V6-series is the most characterised and studied of our categories. Its results are the most representative and will be used to define the conduction mechanism. Different parameters have been chosen for the study the behaviour of the pastes: the grain size and the concentration of the conductive particles and the firing temperature.
This section allows us to analyse their influence on the electrical results and principally on the the resistivity value. Moreover, structural observations are presented to explain the obtained electrical responses. These first results will allow us to characterise the conduction process.

IV . 2 . 1 . Link between the influence of parameters and the conduction mechanism

This section is dedicated to determine the conduction mechanism in such percolative systems. We will mainly take an interest to the evolution of the resistivity and consequently to the influence of the volume concentration of RuO_2.

IV . 2 . 1 . 1 . Influence of the volume concentration of RuO_2

In figure 1, we plot the resistivity as a function of RuO_2 volume concentration x for different values of T_f and for both RuO_2 grain diameters (see caption for more details). At low T_f, the blending curves display a strong enhancement of ρ as x is reduced and asymptotically approach infinite as x becomes equal to a critical value x_c. This behaviour is typical of a percolation transition according to which ρ versus x can be expressed as a power law equation:

$$\rho = \rho_0 (x-x_c)^{-t} \qquad (1)$$

where ρ_0 is a prefactor and t is the transport critical exponent [1,2].
The value of x_c can be then determined by fitting Eq.1, from the different obtained samples.

Before presenting the detailed analysis of our resistivity data in terms of Eq. 1, let us first discuss the overall behaviour as function of T_f and x.

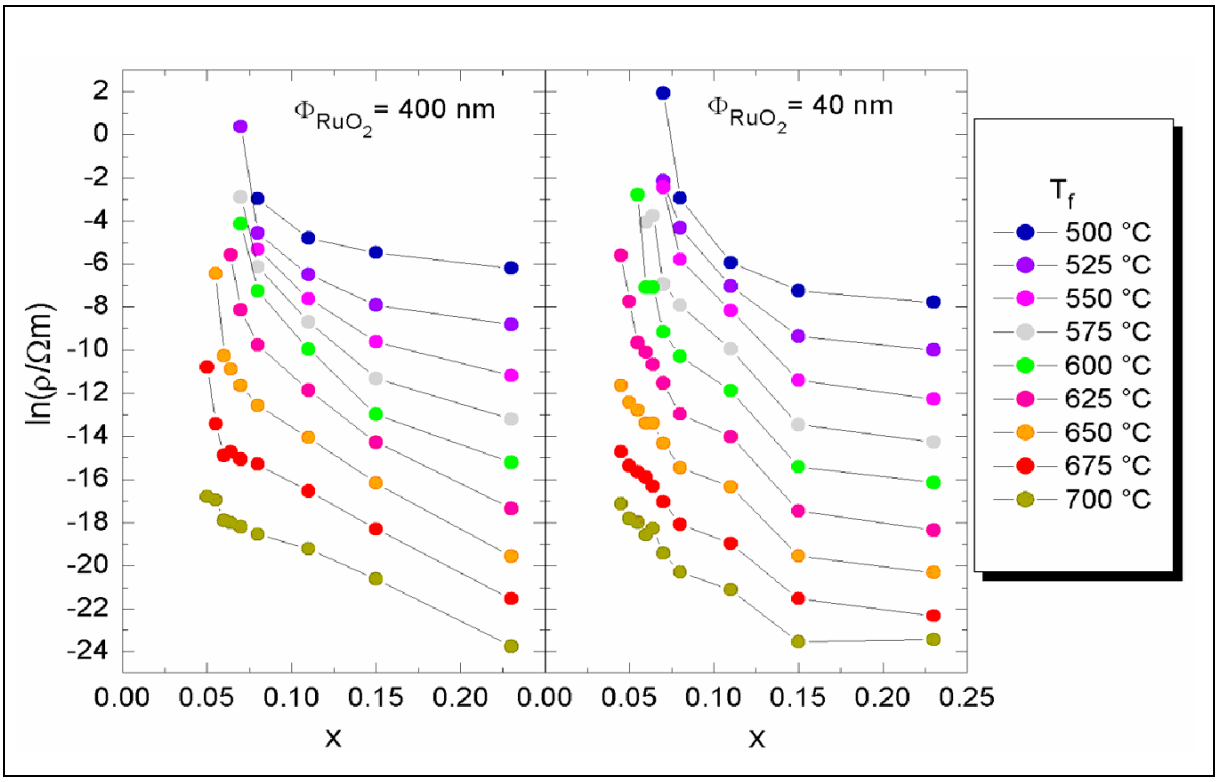

Figure 1: Resistivity vs. RuO_2 volume concentration *x* for various thick-films for different T_f and for 400nm and 40nm RuO_2 grain sizes (beware: the curves are manually shifted along the lnρ-axis for clearer results)

According to various studies [3-5], it is expected that packing of smaller conducting particles around much larger glassy grains would reduce x_c, since less RuO_2 is needed to establish a percolating path. However, as it is clear from figure 1, the percolation transition of the nominal 400 nm TFRs is not much different from that of the 40 nm samples. This is an indication that the mean grain size is certainly lower than 400 nm, coherently with the discussion of chapter III. Upon rising T_f, both series of TFRs display a lowering of the percolation threshold, and for T_f > 675 °C for the 400 nm TFRs and T_f > 625 °C for the 40 nm TFRs no revealing sign of percolative divergence is visible for the concentrations used in the present study.
The phenomenon of the shift of the percolation threshold x_c with the firing temperature may have different explanations. One of these is the chemical interaction between the original RuO_2 grains with the glass leading to the formation of a new conducting phase such as $Pb_2Ru_2O_6$. The degree of diffusion of such phase inside the glass grows with T_f, leading to a modified microstructure made of RuO_2 grains surrounded by a T_f-dependent halo of $Pb_2Ru_2O_6$ nanoparticles. This kind of reactions have already been observed in TFRs fabricated with high firing temperatures [6,7], but it is quite unrealistic that they could take place also in V6-samples, as the firing temperatures were not high enough to initiate the chemical reaction.

However, to investigate this possibility, we performed X-ray measurements aimed to detect possible signatures of the presence of a $Pb_2Ru_2O_6$ phase.
To this end, we report, in figure 2, our X-ray analysis on a 6.4% of RuO_2 volume fraction resistor at T_f = 600 °C and T_f = 700 °C. In both cases, the signals associated to the RuO_2 phase are clearly discernible (peaks labelled by the letter R), together with the peaks labelled by the letter S ascribed to the Al_2O_3 substrate. There is no evidence for the formation of other

conducting phases such as $Pb_2Ru_2O_6$, although we cannot exclude from our x-ray measurements that nano-sized particles of $Pb_2Ru_2O_6$ around the RuO_2 particles could eventually be present [8]. However, similar x-ray profiles have been obtained also for TFRs fired at 700 °C for much longer times (1 hour), so we can conclude that there is no evidence for variation of the conducting phase concentration with T_f.

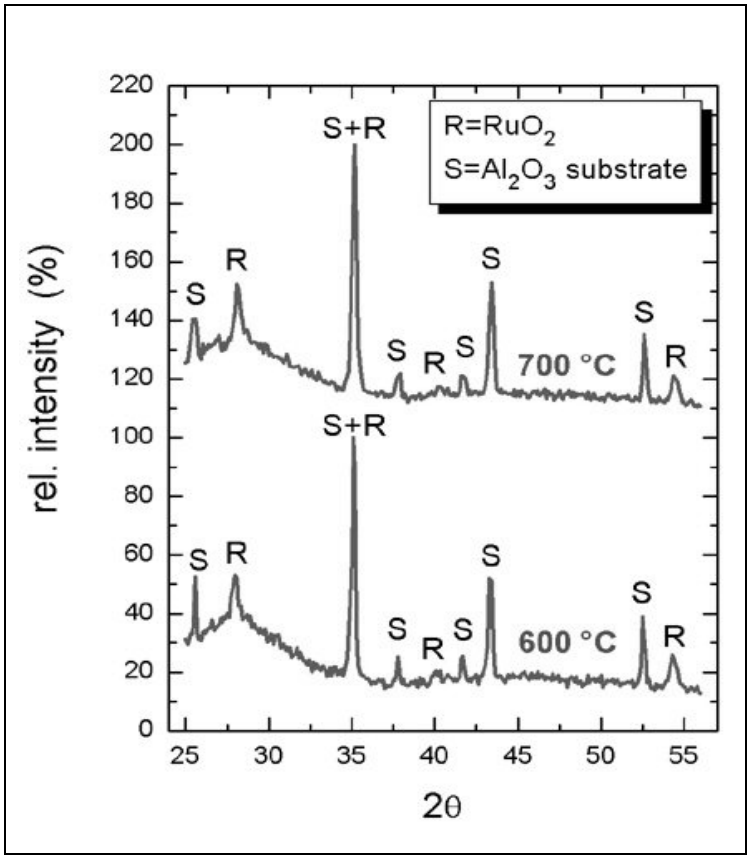

Figure 2: X-ray spectra of V6-sample (6,4% of RuO_2) fired at 700 and 600°C-15min

The behaviour is due to microstructural changes, and therefore driven by physical, rather than chemical, RuO_2-glass interaction. For example, the lowering of x_c upon rising T_f could be explained by the fact that the viscosity of the glass decreases with T_f and allows to disperse homogeneously the nanoparticles of RuO_2. This homogeneous dispersion (if we are not in an extreme situation to avoid reaction with the substrate, as described later) increases the number of conductive paths. This is a possible interpretation. In fact, according to some authors [9], rearrangement of the conductive particles can lead to either formation of new chains and a lowering of the resistivity and of x_c or to a break up of some chains and to an increased resistivity / x_c. The observation of the structure modifications will be more detailed in future sections (IV.2.1.2 and IV.2.3.1.1).

IV . 2 . 1 . 2 . Characterisation of transport percolation: determination of *t*

In order to investigate in greater detail the percolation properties of the V6-series, we have fabricated and measured additional samples at relatively low T_f, where the percolating behaviour is more pronounced (see figure 1). The resulting transport measurements are reported in figure 3 for both 40 and (nominal) 400 nm cases.

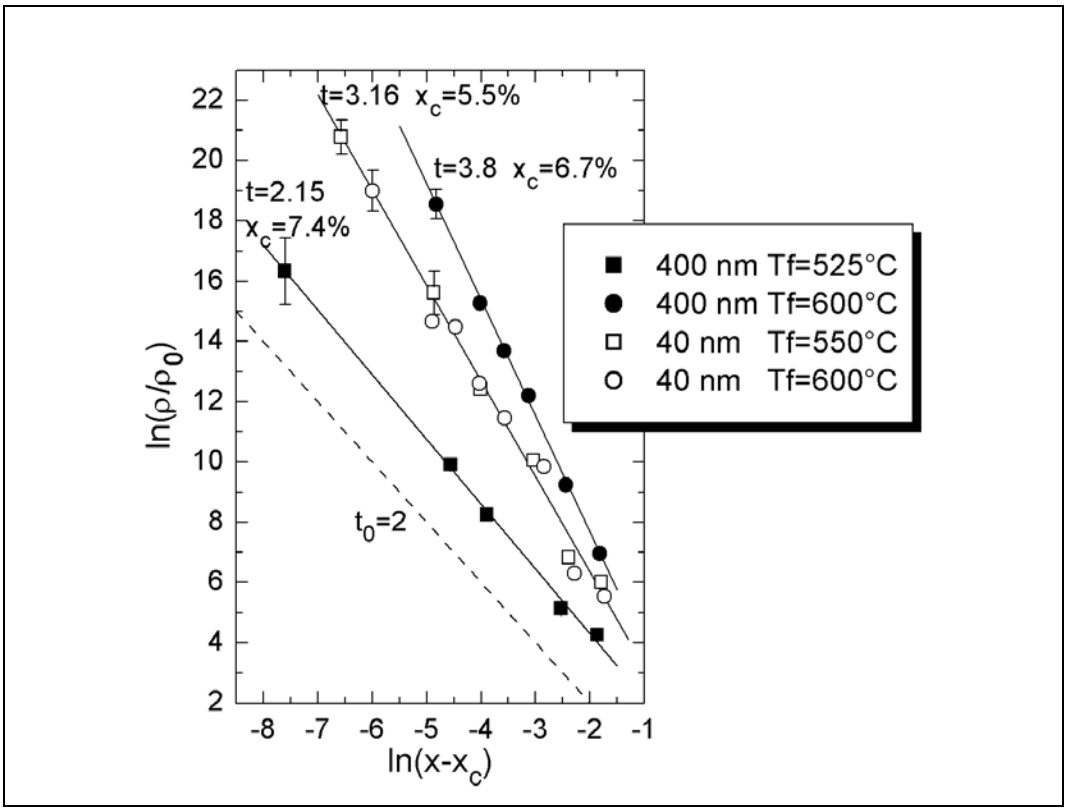

Figure 3: ln-ln plot of the resistivity as a function of RuO_2 volume concentration - The dashed line with the slope *t*=2 corresponds to universal behaviour of transport

As shown in the ln-ln plot of figure 3, all series satisfy the power law equation (1). The critical concentration x_c, the prefactor ρ_0, and the resistivity exponent t have been determined by a non-linear curve fitting to Eq. 1. The fitting results are reported in figure 3 and will be summarised later in table 2 (in section IV.2.2).
The two 40 nm size series have the same value of the transport exponent (t ~ 3.16) independently of the firing temperature. On the contrary, the 400 nm size series have t ~ 3.8 for T_f = 600°C and t ~ 2.15 for T_f = 525 °C. This latter value is close to the exponent t_0 ~ 2 expected to be the universal value characterising all three dimensional percolating systems irrespectively of their microscopic composition [6-11].
As we shall discuss in the following sections, the observation of t values different from t_0 ~ 2 indicates that the percolating transport in the V6-system is of nonuniversal type, and it is qualitatively different from that described by the standard theory of transport percolation.

Before speculating on the origin of the non-universality, it is interesting to discuss the relation between the exponent t and the microstructure of our samples as determined by SEM analysis. We chose some representative samples knowing that there is no difference for the 40 nm size series, whatever T_f, contrary to 400 nm series, for which T_f could be an influencing parameter on the behaviour of the transport (see comment on figure 4).
Concerning the chosen volume concentration x, we selected x = 0.08 as it seems to be an optimal value: it is a good compromise to avoid the perturbations due to extreme concentrations (too high values of resistivity...).

If we observe by SEM the surface of two series of V6-paste with RuO_2 volume fraction $x = 0.08$, with the firing temperature T_f is 525°C and 600°C for the 400 nm grain size paste (figures 4-1(a) and 4-1(b), respectively), while T_f = 550°C and 600°C for the 40 nm grains size series (figures 4-2(a) and 4-2(b), respectively), it appears that universal behaviour ($t \sim 2$) is found for more clustered samples (figure 4-1a) while the nonuniversal behaviour ($t \neq 2$) is observed when the conducting phase is more dispersed in the glass (figure 4-1b).

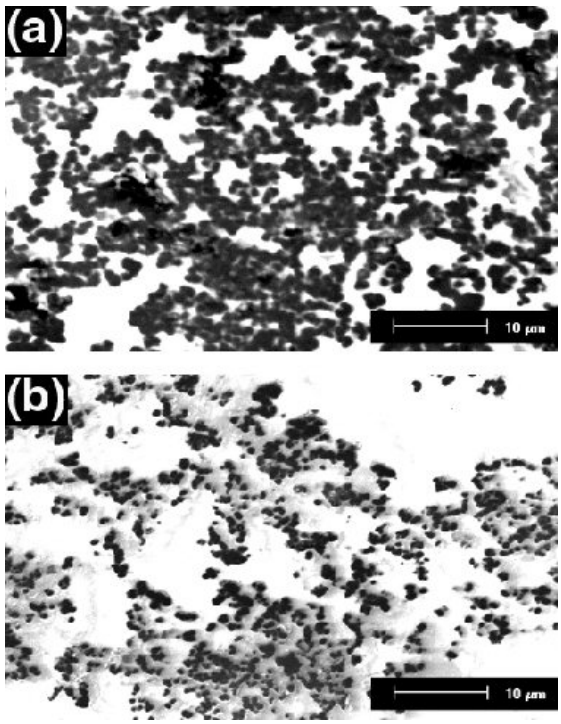

1- 400nm grain size, fired at 525°C (a) and 600°C (b)

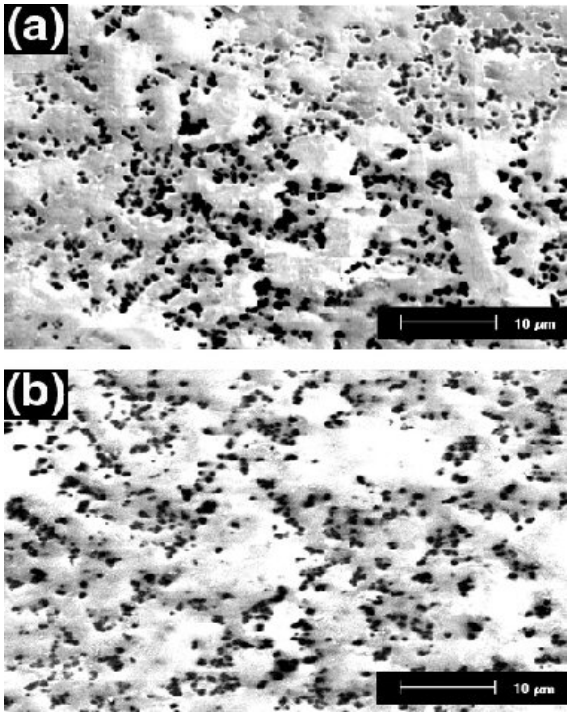

2- 40nm grain size, fired at 550°C (a) and 600°C (b)

Figure 4: SEM observation of the surface of a V6-paste (x=0.08) for different grain sizes and different T_f

In the images, dark areas indicate highly conducting regions rich of RuO_2 clusters, while the white zones are instead made of insulating glass (which tends to charge up in the SEM). The grey regions surrounding the RuO_2 clusters indicate that some conduction is present, although much lower than the dark areas, which we ascribe to finer RuO_2 particles dispersed in the glass [12]. At the length scale shown in the figures, the conducting and insulating phases are not dispersed homogeneously, with the RuO_2 clusters segregated between large glassy regions of few micrometers in size. This segregation effect in TFRs is well known and it is due to the large difference in size between the fine conducting particles and the much coarser glassy grains employed in the preparation of the resistors [13]. The segregated structure explains also the quite low values of x_c reported in figure 3.

Concerning the effect of the firing temperature, it is interesting to note that, for the 40 nm size series, there is not much qualitative difference in the microstructure between 550 and 600°C, while, for the 400 nm series, it appears that the conducting phase is more clustered at low firing temperature than at high T_f, where the appearance of grey regions indicate larger RuO_2

dispersion in the glass. (Note that the observed phenomenon of charging-up can distort slightly the observation by masking some conducting areas.)

There seems to be therefore a correlation between (non) universality and microstructure: the more dispersed microstructure is found only in the nonuniversal (t > 2) samples. This interpretation is coherent with the nonuniversality of 40 nm series, which indeed displays a large amount of RuO_2 dispersion evidenced by the grey regions in figures 4-2a and b. The microstructure has therefore a primary role for the onset of nonuniversality.

IV . 2 . 1 . 3 . Limits of the universality of the transport

The appearance of nonuniversal values of t (>2) is not surprising as it has already been experimentally observed in several materials. This is illustrated on figure 5 where we have collected about 100 different values of the critical exponent t and the critical threshold x_c measured in various composites including carbon-black-polymer systems [7,14-33], oxide-based thick film resistors (TFRs) [3,4,13,34-42], and other metal-inorganic and -organic insulator composites [33,43-52].

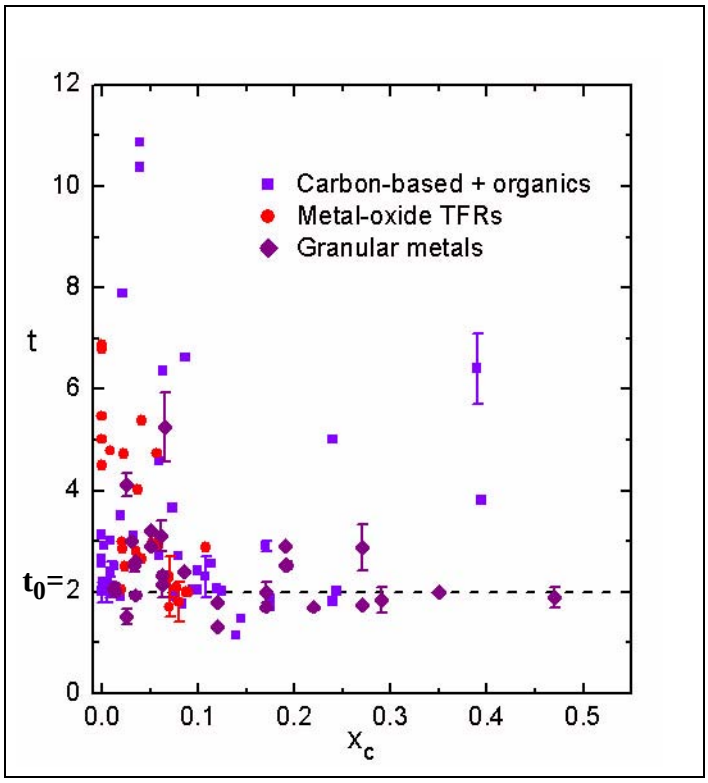

Figure 5: Collection of critical exponent values *t* and corresponding critical threshold concentration x_c for various disordered conductor-insulator composites

(The dashed line denotes the universal value t_0=2.0)

It is clear that, despite that many of the t-values reported in figure 3 are close to $t_0 \sim 2.0$, almost 50 % of the measured critical exponents deviate significantly from universality by displaying $t \neq t_0$.

Examining all the data reported in this figure, one observes that the lack of universality is not limited to a particular class of materials, although the granular metals have somewhat less spread values of t compared to the carbon-black and TFRs composites. Another important

observation is that for the vast majority of the cases, the nonuniversal critical exponent is larger than t_0, and only few data display $t < t_0$. Finally, there is no clear correlation between t and the critical concentration value x_c.
With the accumulation of experimental reports of nonuniversality, various theories have been proposed in order to find an origin to this phenomenon [16,53–56]. These theories are reviewed in the following sections.

IV . 2 . 1 . 4 . Models of conduction in percolative systems

The electrical behaviour as function of the structure will be interpreted in the frame of a model of conduction based on a nonuniversal tunnelling percolation theory. Before presenting our original proposition, it would be useful to examine the different models of conduction proposed for percolative systems in the literature. The origin of these models rests on the universality or nonuniversality theories [53-56].

IV . 2 . 1 . 4 . 1 . Random-resistor network models of transport universality

Let us consider a system with conductive particles dispersed randomly in an insulating matrix. The theoretical description of this situation is based on random-resistor networks (RRN) models where the particles occupy random positions on a regular lattice (see figure 6). Two neighbouring particles are electrically connected if there is a bond between them. If the bond is absent, the conductance g between the particles is zero.

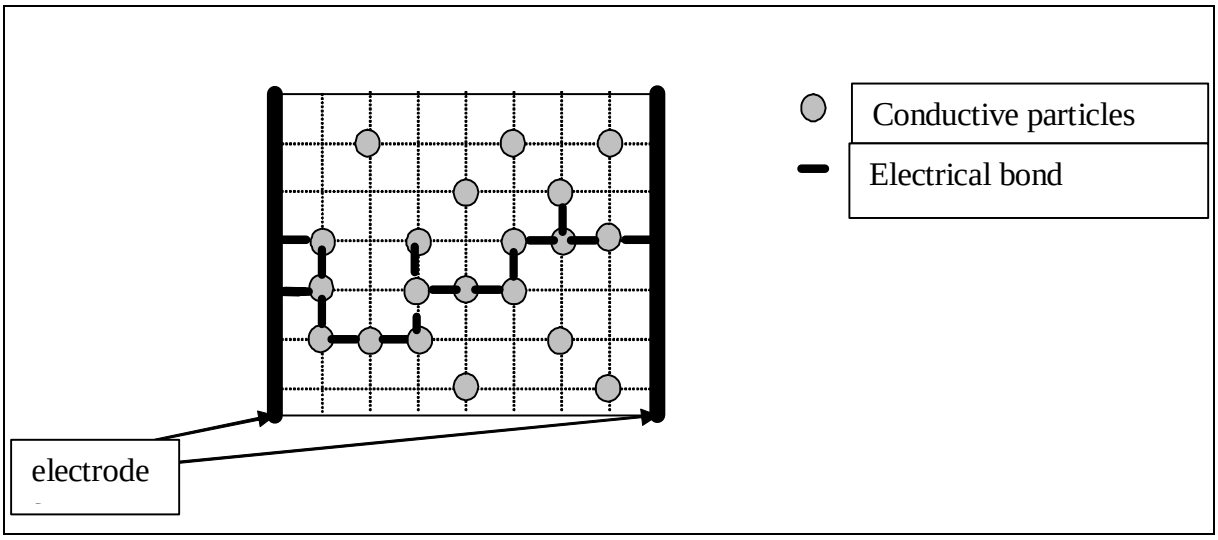

Figure 6: Illustration of a percolative system

Hypothesis: The conductance and the distance between the electrical bound particles are constant.

In general, the local conductance g between two particles can be expressed as following:

$g = 1/R$ (with $g \to 0$ if $R \to \infty$, R: resistance)

$g = \sigma_{loc} \cdot S/l$ (if $l \to 0$, g increases as $R \to 0$)

with σ_{loc} : local conductivity between two particles, l : distance between two particles, and S: the cross section.

The mathematical representation of such RRN is the following one:
p: the probability that the conductance $g \neq 0$ between two neighbouring particles.
(1-p): the probability that $g = 0$.

If the electrical bonds and their conductances are uniform (figure 7.a), and according to the percolation theory in RRN, the theoretical bulk conductivity Σ follows the power law equation, in the vicinity of p_c (the critical probability for percolation) [57]:

$$\Sigma = \Sigma_0 \cdot (p - p_c)^t \ , \qquad (2)$$

where Σ_0 is a prefactor. Close to the percolation threshold, t is universal ($t = t_0 \sim 2$), for all three dimensional lattices. This situation holds true also if the values of g change from bond to bond and have a distribution function centred about some mean value g_0 (see figure 7.b, for example). Hence, contrary to p_c which depends on microscopic details (microstructure, topology), t is expected to be independent of microscopic details and an external perturbation like an applied strain would have no effect. For this reason it is said to be universal [1,2].
.

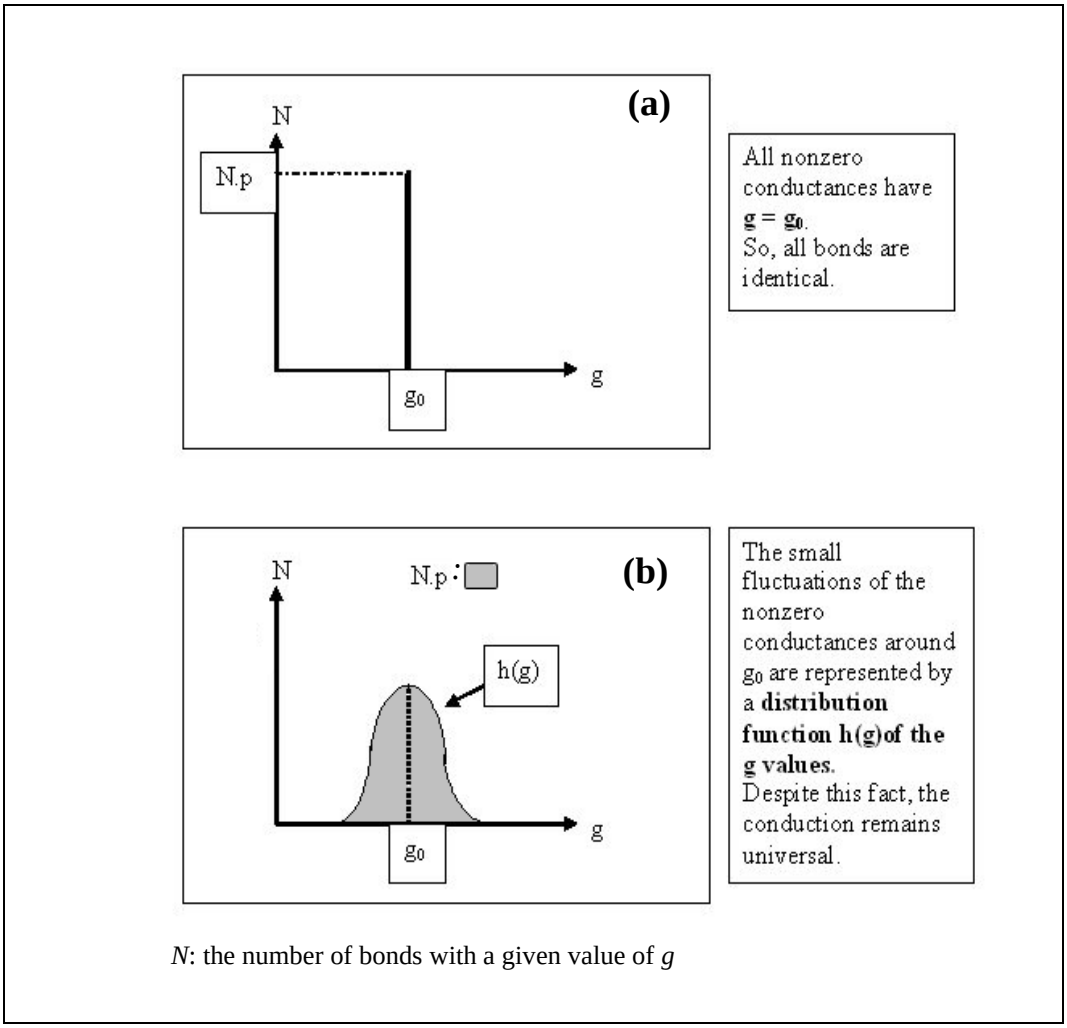

Figure 7: Representation of the power law equation, in case of universal transport

In real systems, Eq. 2 is translated into:

$$\sigma_{bulk} \sim \sigma_0 \cdot (x - x_c)^t \qquad (3)$$

where, σ_{bulk} is the bulk conductivity of the composite with a x volume fraction of conducting phase. σ_0 is a constant, x_c is the critical concentration below which the composite has a zero conductivity, and t is the critical exponent. In terms of resistivity, Eq.3 corresponds to the Eq.1, with $\rho = 1/\sigma$ and $\rho_o = 1/\sigma_o$.

IV . 2 . 1 . 4 . 2 . Models of nonuniversality

As discussed above, transport universality is found as long as the distribution function of bond conductances is well behaved and is characterised by a mean value and (weak) fluctuations about it, as in figure 7.b. In this case, close to the bond percolation threshold p_c, the theoretical conductivity Σ of the network behaves as Eq. 2, with $t = t_0 \sim 2$.
As first noticed by Kogut and Straley [53], universality can break down if the distribution function $h(g)$ of bond conductivities diverges for $g \to 0$. In particular, if $h(g)$ has a power law divergence for small g (figure 8) of the form:

$\lim_{g \to 0} h(g) \propto g^{-\alpha}$, where $\alpha < 1$ [53],

then, universality is lost for sufficiently large values of the exponent α [53]. For lattices of dimension D, the resulting conductivity critical exponent is [5,8,12]:

$$t = t_0 \qquad \text{if } (D-2)\cdot\omega + \frac{1}{1-\alpha} < t_0 \qquad (4)$$

or

$$t = (D-2)\cdot\omega + \frac{1}{1-\alpha} \qquad \text{if } (D-2)\cdot\omega + \frac{1}{1-\alpha} > t_0 \qquad (5)$$

where $t_0 \sim 2$ is the universal value, and ω is the correlation-length exponent ($\omega = 4/3$ for $D = 2$, and $\omega \sim 0.88$ for $D = 3$).
For $D = 3$ and by using $t_0 \sim 2$ and $\omega \sim 0.88$, the value of α beyond which universality is lost is: $\alpha_c = 1 - 1 / (t_0 - \omega) \sim 0.107$.

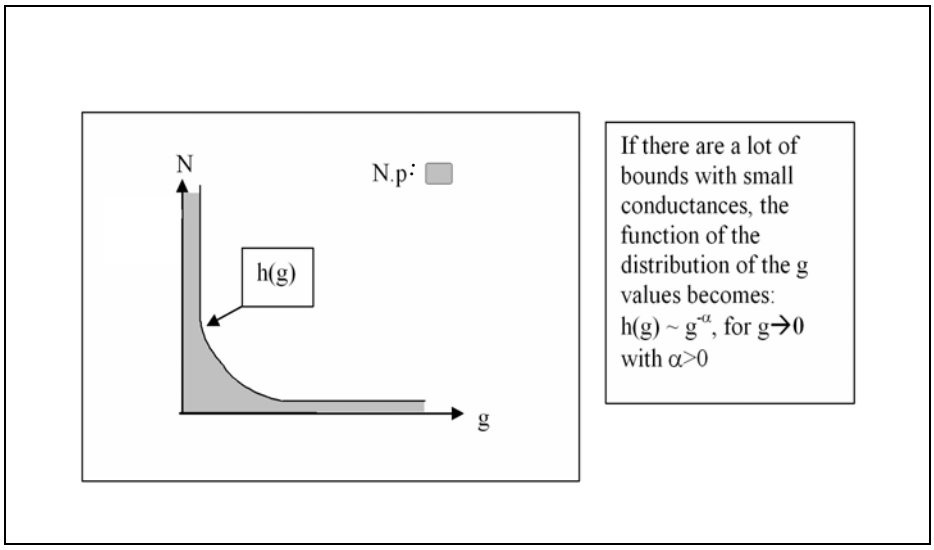

Figure 8: Mathematical representation in case of nonuniversality

The physical origin of the parameter α has been investigated by various authors. In the following, we review two important models, which have been proposed to apply to various kinds of percolating systems.

- **Random Void Model (RVM)**

In this model, current flows through a conducting medium embedding insulating randomly placed spheres [54] (figure 9).

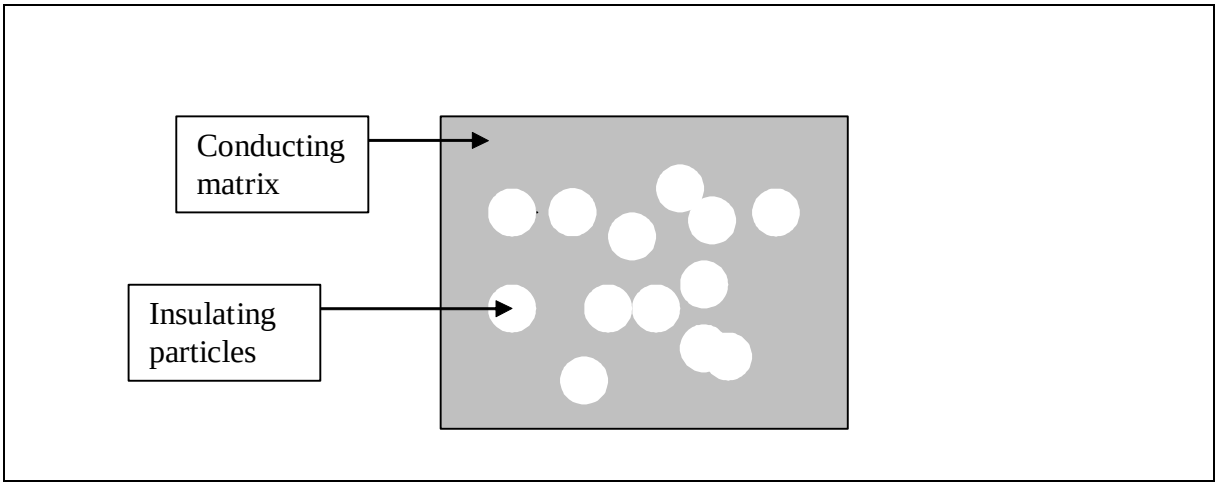

Figure 9: Random void model representation

When mapped into a RRN, it is found that the conductance g of the conductive path between two glass particles depends on the conductive channel width δ between them, with $g \sim \delta^{3/2}$, which leads to a distribution function $h(g)$ of the form $h(g) \sim g^{(-\alpha)}$, where $\alpha = 1/3$ [54]. Hence, in this case, $\alpha > \alpha_c$ ($\alpha_c = 0.107$ for 3 dimensional systems), and according to Eq.5, t is non universal with $t \sim 2.4 > t_0$.

The RVM applies principally to composite where the linear size of the conducting particles is much smaller than that of the insulating grains so that the conducting phase can be approximated by a continuum. In other terms, there are small insulating particles in an electrical continuum. If we consider the structure in the range of macroscopic scale, the TFR structure can be represented by a RVM (figure 10-a). On the opposite, in the case of microscopic scale, this model is not representative (figure 10-b) as we should consider conductive particles in an insulating matrix (the phases are inverted).

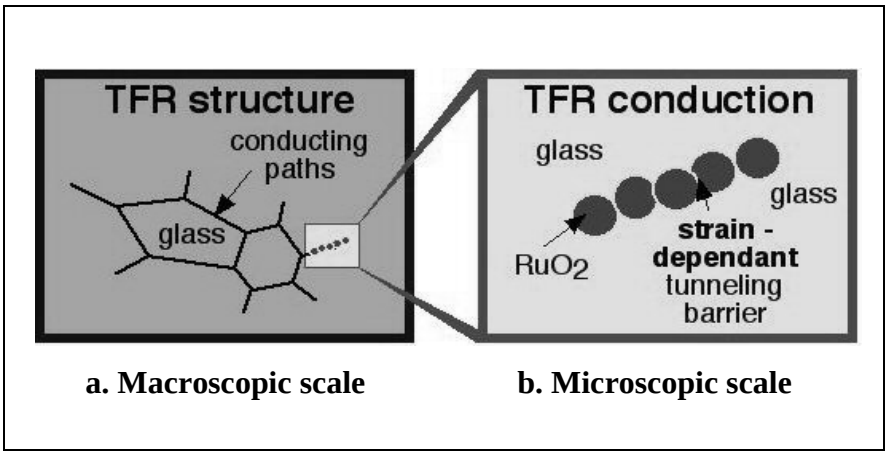

Figure 10: Correlation between the RVM model and the structure

- **Tunnelling percolation model (or inverted random void model)**

This model of transport nonuniversality is based on an inverted random void model in which current flows by a tunnelling process between conducting spheres immersed in an insulating medium (figure 11) [55].

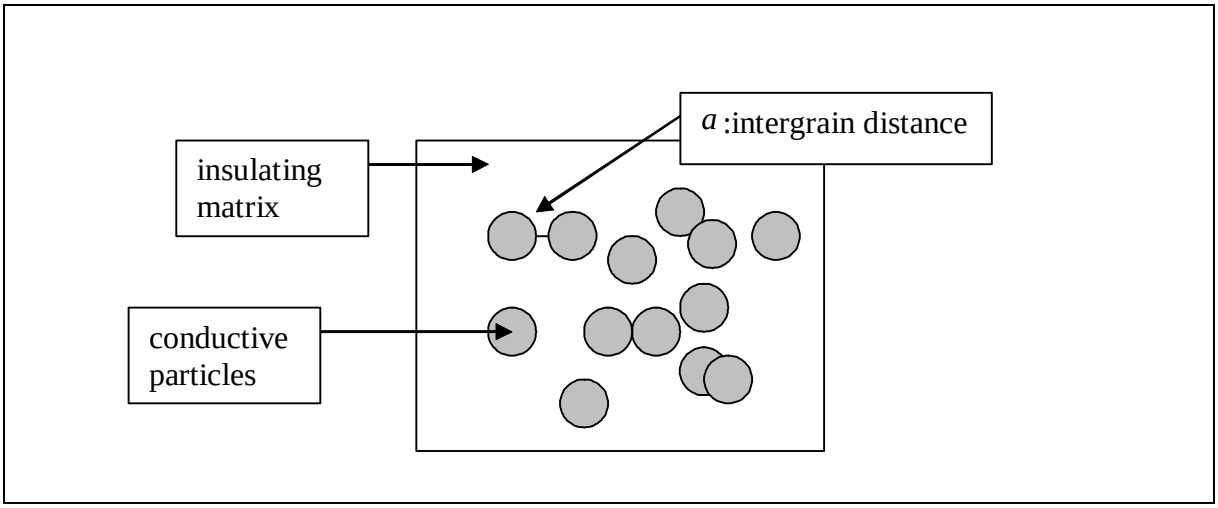

Figure 11: Balberg model representation

This model can be applied to composites in which intergrain tunnelling is the main microscopic mechanism of transport (carbon-black-polymer composites or oxide-based TFRs).

For this case, it has been found that *h(g)* is proportional to $g^{(-\alpha)}$, if $g \to 0$. More exactly, it follows the expression [55]:

$$h(g) = \frac{1-\alpha}{g_0}\left(\frac{g}{g_0}\right)^{-\alpha} \qquad (6a)$$

But, with $\alpha = 1 - (\xi / 2) / (a - \Phi)$ (6b)
(contrary to the random void model where $\alpha = 1/3$), *a* is the distance between two neighbouring particles, Φ is the diameter of the particles, ξ is tunnelling factor and g_0 is constant. To clarify the expression of α, figure 12 shows the corresponding *a* and Φ parameters:

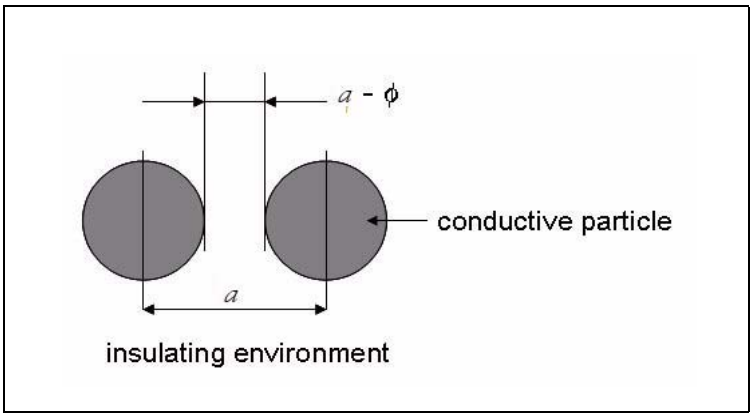

Figure 12: Representation of the *a* and Φ parameters used in the expression of α for two conductive particles under strain

Contrary to the other mentioned model, the tunnelling-percolation model of Balberg predicts that the critical exponent *t* acquires an explicit dependence on a microscopic variable (the mean-tunnelling distance *a*), which can be altered by a suitable external perturbation.
So, if transport nonuniversality is driven by tunnelling, it would be possible to change the value of *t* by applying a pressure or a strain to the composite. Conversely, when a material belongs to some universality class, its exponent is expected to be independent of microscopic details and an applied strain would have no effect.

The nonuniversality is not driven by geometrical factors as in the random void model, but rather than by physical parameters such as ξ and *a*. These can be different depending on the composite and can be modified by a suitable external perturbation. In fact, in the case of an applied pressure or strain, the mean tunnelling distance (a-Φ) would change leading to a modification of the critical exponent *t*. The detection of such an effect would be a direct signature of a tunnelling-percolation-like mechanism of transport nonuniversality.

Comment: The two models could coexist together if the continuum phase of a random void system is made of non-sintered conducting particles interacting through tunnelling processes. In this situation, the different proposed theories could account for the variety of nonuniversal exponents shown in figure 5.

IV . 2 . 1 . 5 . Consequences of the tunnelling-percolation model: piezoresistivity

As noted in the previous section, the tunnelling-percolation theory [55] predicts an explicit mean tunnelling distance dependence of the transport exponent *t* (see Eqs. 5 and 6b). On the

contrary, the random void model gives a value of t different from $t_0 \sim 2$ but nevertheless independent of the microscopic parameters. Hence, one could decide which of these two models explains the measured nonuniversal values of t in the V6-series by applying a strain to the composite. A nonzero variation of t due to the applied strain would unequivocally indicate that transport in these systems is of tunnelling-percolation type.

Let us see in more details what the tunnelling-percolation model would imply in terms of the piezoresistive response.
The piezoresistive factor Γ is defined by the following equation:

$$\Gamma = d\ln(\rho)/d\varepsilon \qquad (\rho : \text{resistivity and } \varepsilon: \text{applied strain}) \qquad (7)$$

where, $\rho = \rho_0 (x-x_c)^{-t}$ is the resistivity of the system. By taking the logarithm of both sides, one has: $\ln(\rho) = \ln(\rho_0) - t \ln(x-x_c)$. So, by applying Eq. 7, it is found that

$$\Gamma = d\ln(\rho)/d\varepsilon = \Gamma_0 - dt/d\varepsilon \ \ln(x-x_c) \qquad (8)$$

with $\Gamma_0 = \dfrac{d\ln\rho_0}{d\varepsilon}$.

In obtaining Eq. 8, we have implicitly supposed that x_c does not depend on the applied strains. We will come back to this point later (in the end of section IV.2.2).

Now, it is clear that if t depends on the mean tunnelling distance a, then the applied strain would modify a ($a \rightarrow a(1+\varepsilon)$) and $dt/d\varepsilon$ would be different from zero. As a consequence, Eq. 8 predicts a logarithmic divergence of Γ at $x=x_c$. More precisely, by combining Eq. 8 with Eqs. (4,5) and Eq. 6b, the tunnelling-percolation mechanism of nonuniversality gives:

$$\Gamma = \Gamma_0 \qquad \text{if } t = t_0 \sim 2 \qquad (9a)$$

or $\Gamma = \Gamma_0 - dt/d\varepsilon \cdot \ln(x-x_c)$ if $t > t_0$ (9b)

where, according to Eqs. 5 and 6b:

$$\frac{dt}{d\varepsilon} = \frac{1}{1-\alpha} = \frac{a-\Phi}{\xi/2}. \qquad (10)$$

In the following section, we analyse the possibility that the piezoresistive response in our V6-system follows Eqs. 9 by performing gauge factor measurements.

IV . 2 . 2 . Determination of GF - Measurements

We will use the same series of samples used in figure 3, that show universal and nonuniversal behaviours. The GF measurements were realised with the same technique (cantilever beam) described in chapter II.2. We determined the piezoresistive response by recording $\Delta\rho/\rho$ vs. ε. Indeed, remember that the piezoresistive factor Γ can be expressed as:

$\Gamma = \dfrac{\Delta\rho}{\rho \cdot \varepsilon}$ (see chap I.3.2.1, for a detailed definition)

Figure 13 shows the corresponding results for representative samples (400 nm size series, T_f = 600 °C). Note that the substrate tensile strain $\varepsilon > 0$ along the main cantilever axis were induced by applying different known weights on the free end of the cantilever (the cantilever

bar is clamped at the opposite end). Compressive strains ($\varepsilon < 0$) were obtained by weights applied in the opposite face of the cantilever. In the whole range of applied strains (up to about $|\varepsilon| = 4,5 \times 10^{-4}$), $\Delta\rho/\rho$ changed linearly and symmetrically with ε, indicating the absence of false strain responses due to elastic faults of the resistive films [58]. Moreover, no cracks have been detected with SEM observations.

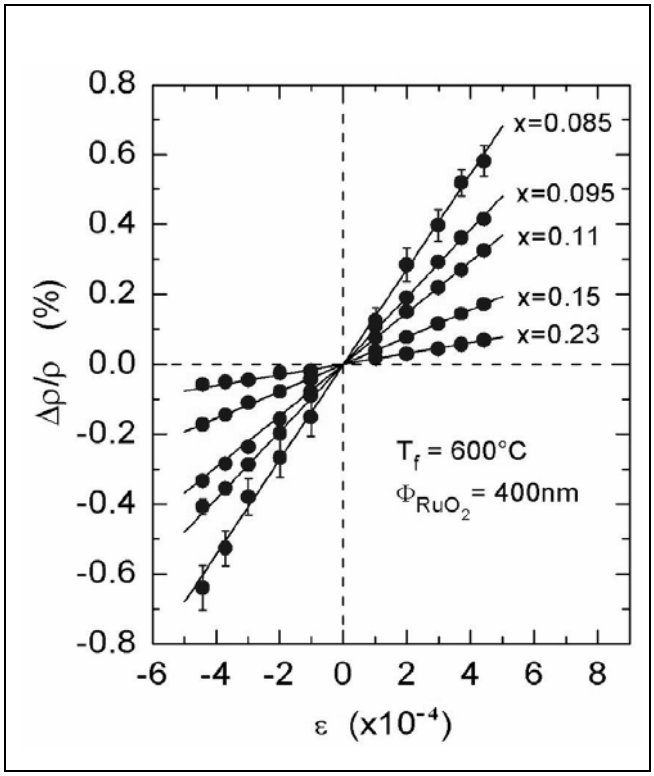

Figure 13: Resistivity variation of the 400 nm series (600°C) as a function of strain and for different RuO_2 volume concentrations

As the RuO_2 concentration x decreases, the resistivity change ($\Delta\rho/\rho$) increases. We can already mention that high concentrations will be less interesting as the amplitude of the signal is weaker because of the high conductivity of the corresponding samples. Note that the transport exponent for the 400 nm (600°C) series is $t = 3.84$, that is much larger than $t_0 = 2$. Hence the enhancement of the slope of $\Delta\rho/\rho$ as x decreases could well be one signature of a divergence of Γ as $x \to x_c$.

From figure 13, we can determine Γ for each concentration as it corresponds to the slope of each straight line. The results are reported in figure 14, where Γ is plotted as a function of x for both 400 nm and 40 nm series.

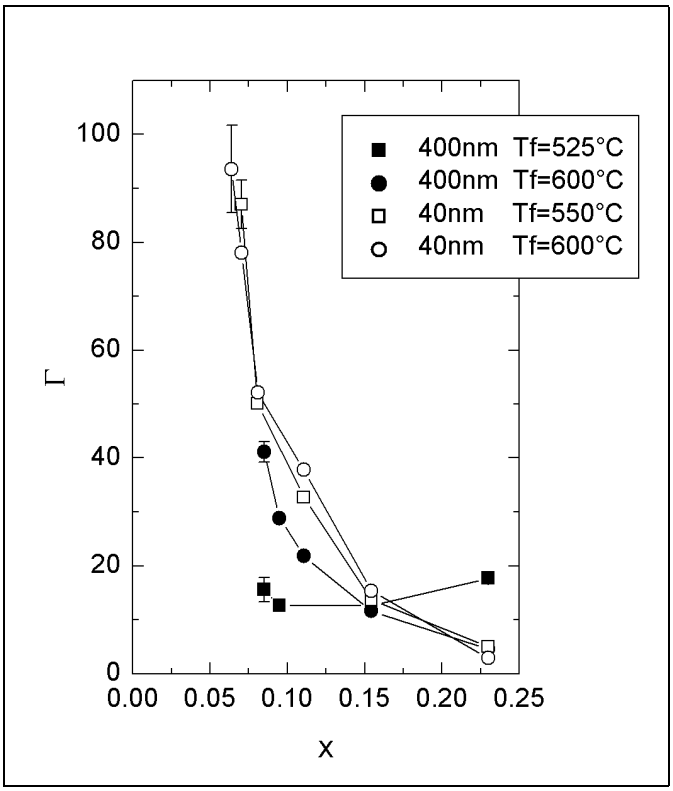

Figure 14: Piezoresistive factor plotted as a function of RuO_2 volume concentration *x*

With the exception of the 400nm-525°C sample which displays an almost constant piezoresistive response, the other series clearly diverge at the same critical concentration x_c at which the conductivity goes to zero. According to the tunnelling-percolation theory, Γ should follow one of the two 2 cases (see section IV.2.1.5):

$$\Gamma = \Gamma_0 \qquad \text{if } t = t_0$$
$$\text{or} \quad \Gamma = \Gamma_0 - dt/d\varepsilon \cdot \ln(x-x_c) \qquad \text{if } t > t_0$$

The last case predicts a logarithmic divergence at the percolation threshold ($x = x_c$) when the exponent t is nonuniversal.

Then, if $dt/d\varepsilon$ is nonzero, we expect a logarithmic divergence of Γ at $x = x_c$. A representation of this idea is shown in figure 15 where $\Gamma-\Gamma_0$ is plotted as a function of $\ln(x-x_c)$ with x_c values extracted from the conductivity data. In the entire range of concentrations, and for all the series Γ is rather well fitted by the previous mentioned expression.

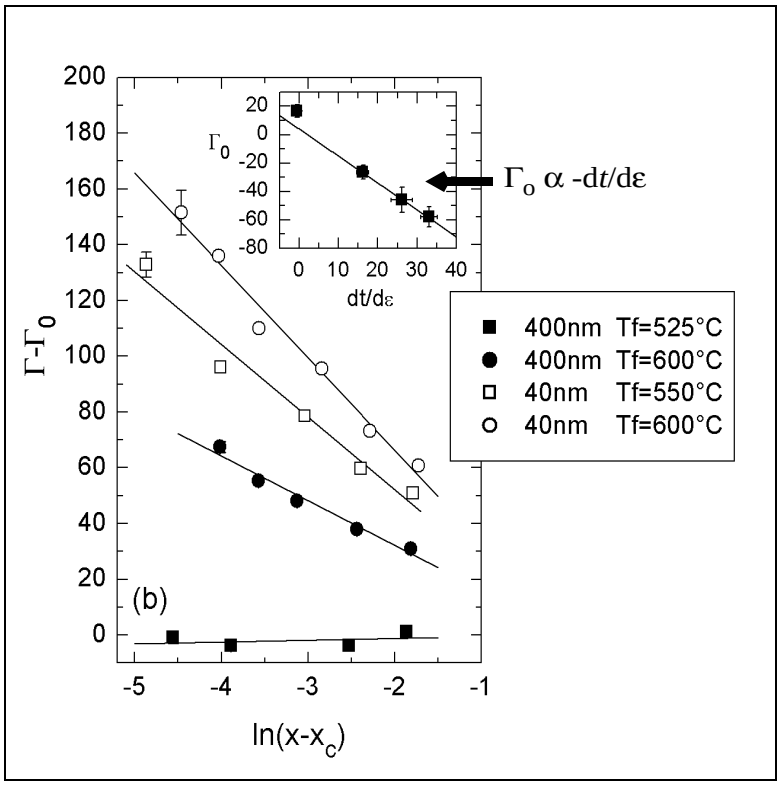

Figure 15: Γ-Γ_0 as function of ln(x-x_c)
Solide lines correspond to the fits to the previous equation

The 400nm-525°C series, which has exponent t = 2.15 ± 0.06 close to the universal value, has no x dependence of Γ (dt/dε = 0), while the other series, characterised by nonuniversal exponents, display a logarithmic divergence of Γ as $x \to x_c$, as their slope is nonzero. This is in agreement with the expectations of the tunnelling-percolation theory.

The different obtained parameters are summarised on table 2:

RuO_2 grain size	T_f	x_c	ln(σ_0 [ohm.m])	t	Γ_0	dt/dε
400 nm	525 °C	0.0745	11.1 +/- 0.3	2.15 +/- 0.06	16.5 +/- 4.5	-0.6 +/- 1.2
400 nm	600 °C	0.0670	14.2 +/- 0.2	3.84 +/- 0.06	-26.4 +/- 4.8	16.2 +/- 1.5
40 nm	550 °C	0.0626	14.3 +/- 0.5	3.17 +/- 0.16	-45.9 +/- 9.0	26.1 +/- 2.7
40 nm	600 °C	0.0525	13.7 +/- 0.7	3.15 +/- 0.17	-57.9 +/- 7.2	33.0 +/- 2.1

Table 2: Determined parameters for representative samples

Note however that in RuO_2-based TFRs the large difference between the bulk moduli of RuO_2 (~ 270 GPa) and of the glass (~ 40-80 GPa) leads to local strain variations so that the dt/dε values of 40 nm series and 400nm-600°C series in table 2 are not simply equal to 1/(1-α) (Eq.10) but incorporate also the effect of the strain heterogeneity [59]. The tunnelling-

percolation picture is able to explain also the change of sign of Γ_0 which from positive for the universal series becomes negative for the nonuniversal ones (see inset of figure 15). In fact an effective medium calculation [61] with the tunnelling-percolation distribution function *h(g)* (Eqs.6) leads to $\Gamma_0>0$ when $t = t_0$ and $\Gamma_0<0$ when $t > t_0$ [60], in agreement with the experimental results (see table 2).

The fit of our piezoresistive data provides a good agreement with the tunnelling-percolation model. However, a divergent piezoresistive response has been claimed be due to a ε dependence of x rather than to a ε dependence of the transport exponent t [4].

To verify this hypothesis, we decided to fit the results according to the extreme cases. Let us first assume, contrary to our hypothesis, that the change of $(x\text{-}x_c)$ is dominant, e.g. t remains essentially constant:

$$\Gamma = \Gamma_0 - \frac{t \cdot d\ln(x - x_c)}{d\varepsilon} = \Gamma_0 - t \cdot \frac{dx}{d\varepsilon} \cdot \frac{1}{x - x_c}$$

We will show that this does not match our results well.
For the particular case of RuO_2-based TFRs, one finds that for small values of the RuO_2 concentrations x:

$dx / d\varepsilon \sim -Ax$ [4,22,60],

where A is function of the bulk moduli of the glass and the RuO_2 particles. A is zero if the bulk moduli of each phases are identical, engendering that $dx/d\varepsilon$ is null. In our case, the bulk modulus of RuO_2 ~ 270 GPa, whereas the one of the glass ~ 40 - 80 GPa.

We obtain then:

$$\Gamma = \Gamma_0 + At\frac{x}{x - x_c} = K_1 + \frac{K_2}{x - x_c} \qquad (11)$$

with $K_1 = \Gamma_0 + At$ and $K_2 = Atx_c$.

In figure 16, we have plotted the Γ values as a function of $1 / (x\text{-}x_c)$ with the same critical concentrations of x_c extracted from the resistivity data on figure 3.

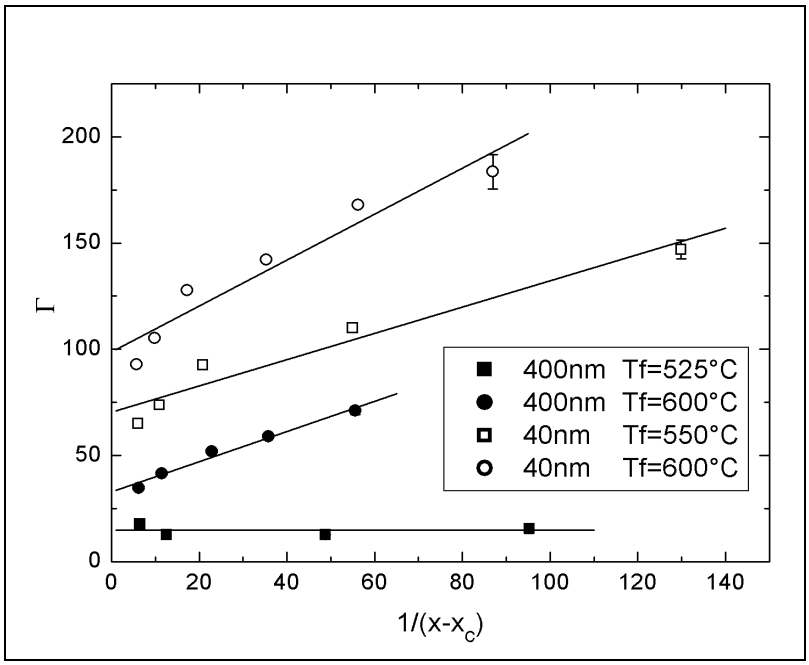

Figure 16: Piezoresistive factor Γ plotted as a function of $1/(x-x_c)$ with tentative fits to Eq. 7 (solid lines)

(*The data related to different series have been shifted vertically by +30 for clarity.*)

According to Eq. 11, Γ should follow a straight line as a function of $1/(x-x_c)$ which, although being rather correct for the 400nm-600°C series, is manifestly not true for the other samples. In addition, the 400nm-525°C series remains almost constant, implying that $A=0$ for this case, contrary to the premises of Ref. 4. In addition to the bad fit with our data, the reasoning of Ref.4 is based on a misunderstanding of the actual physical meaning of x appearing in Eq. 1. In fact, x should be considered just as an operative estimate of the probability (concentration) p of intergrain junctions with finite resistances present in the sample [1,2]. Current can flow from one end to another of the composite as long as a macroscopic cluster of junctions spans the entire sample. Instead of x, an equally valid variable describing the intergrain junction probability p would have been the concentration in weight of RuO_2, which is manifestly independent of applied strain (and of the elastic properties of the material), in our resistor material.

The reasoning of Refs. 22 and 4 is therefore nonconsistent with the physics of percolation. However, one could tentatively argue that the applied strain actually changes the concentration p of junctions by breaking some of the bonds. This situation could be parameterised by allowing a p dependence of x so that $dx/d\varepsilon \sim (dx/dp)(dp/d\varepsilon)$. Also in this case however, one would end with a $1/(x-x_c)$ divergence of Γ which we have seen to lead to poor fits for our data (figure 16). In addition, the values of the applied strains in our measurements are so small ($\varepsilon \sim 10^{-4}$) that their effect is that of changing the value of the tunnelling junction resistances without affecting their concentration p, so that one realistically expects that $dp/d\varepsilon=0$. This is confirmed by the results of figure 13 which show no deviation from linearity for the entire range of ε values.

In conclusion, we have observed a divergence at x_c of the piezoresistive factor Γ for the samples displaying nonuniversal values of the transport exponent t. We have verified that the divergence is of logarithmic form and is rather well fitted by Eqs. 9, which implies a ε dependence of t. This

finding is in full agreement with the tunnelling-percolation model of Ref.55, according to which transport nonuniversality is driven by strong fluctuations of the intergrain tunneling distances.

After having validated our hypothesis based on the tunnelling-percolation model, complementary studies were carried out to characterise the V6-paste.

IV . 2 . 3 . Complementary studies: *R* and TCR evolution

After having elucidated the conduction mechanism, it would be interesting to study the influence of different parameters (T_f, grain size...) on the electrical properties. These additional observations could, in one hand, give further interpretation of the conduction process, but in the other hand, characterise our V6-based system to compare it to commercial pastes.

IV . 2 . 3 . 1 . Evolution of *R*

IV . 2 . 3 . 1 . 1 . Influence of the firing temperature

In figure 17, we show the room temperature resistivity ρ as a function of T_f for the 400 nm (a) and 40 nm (b) cases and for several values of *x*. Independently of the RuO_2 grain size, ρ depends only weakly on T_f for large RuO_2 concentrations, while for lower values of *x* a maximum is discernible at firing temperatures not much larger than the melting temperature of the glass. In this region, the position of the maximum shifts at lower T_f values as the concentration *x* is lowered. For even lower values of *x*, the resistivity exceeds the maximum measurable value (about 10^3 Ohm · m) for $T_f < 600$°C. This behaviour and in particular the presence of a maximum of ρ has already been reported by other authors [12], and it is probably due to enhanced intergrain tunnelling distances driven by penetration of the glassy phase between the RuO_2 grains.

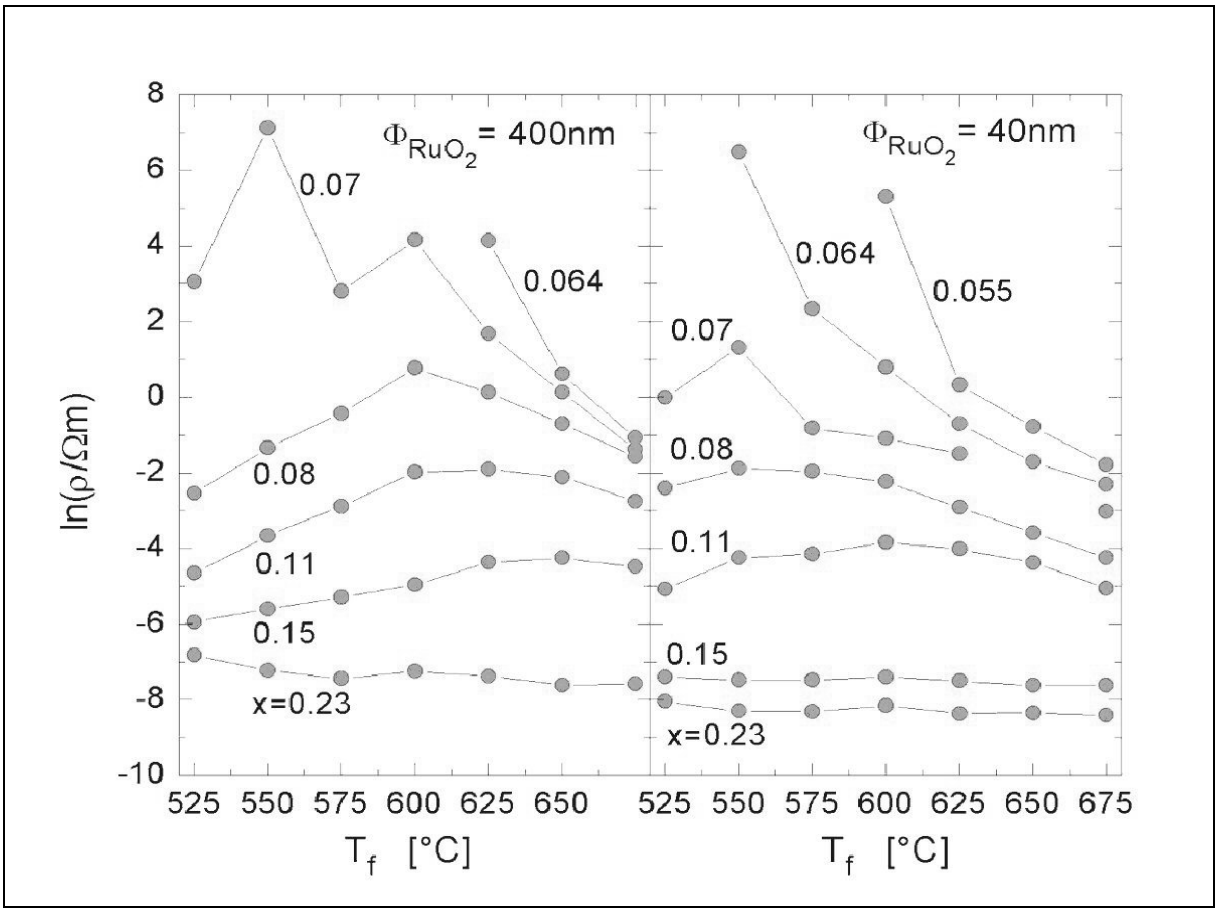

Figure 17: Resistivity values as a function of the firing temperature T_f for 400nm (a) and 40nm (b) RuO_2 grain sizes and for different values of the RuO_2 volume concentration *x*

Moreover, the resistivity is less dependent of the grain size. For a same concentration of RuO_2, the 400 nm size has an higher value of ρ than 40 nm. It is predictable as the specific surface area is larger for smaller particles and favours the flow of the current through the paste [5]. Indeed, as explained in section IV.2.1.1, the increase of the specific surface of the conductive grains favours conductive chains, what can be explained by geometric considerations.

Moreover, although the influence of the grain size and T_f has already been observed by SEM surface observations (see figure 4), the influence of T_f can be emphasised by a cross section observation of the same paste (figure 18). In the same way, we can observe on a cross section of a 400 nm size series fired at 500 and 700°C (x=0.11).
Warning: the white particles correspond to the RuO_2 grains whereas the grey phase represents the glass, contrary to the previous figure. This inversion of colours is due to a phenomenon of charge in the case of insulating matrix. In fact, the most representative figures correspond to the one of figure 18. In this case, the phenomenon of charge is reduced by a carbon coating of the surface which allows to the emitted electrons to be drained out and don't disturb the observations.

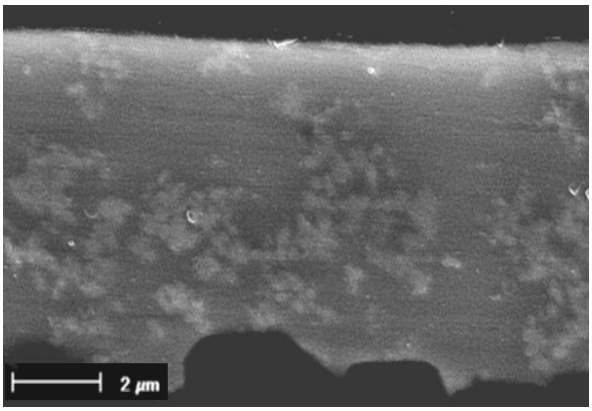

T_f = 525°C

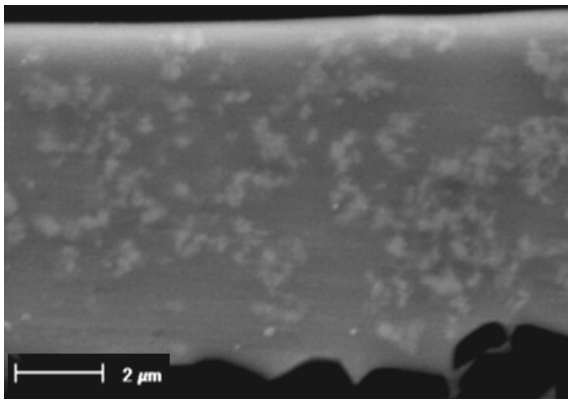

T_f = 700°C

Figure 18: SEM of a cross section of a 400 nm grain size series at 525°C and 700°C (the substrate is on the bottom)

As in figure 4, these images show that for low T_f, the RuO_2 particles seem to be more clustered than for 700°C. For high T_f, the glass wets the particles and separates them by progressively dispersing the clusters.

However, if we observe in details the fired paste (700°C), we can see that the dispersion is not homogeneous. Figure 19 show that the thick film resistor can react with the substrate at high temperature.

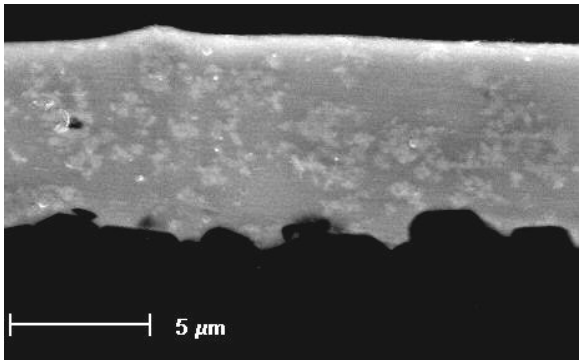

T_f = 525°C

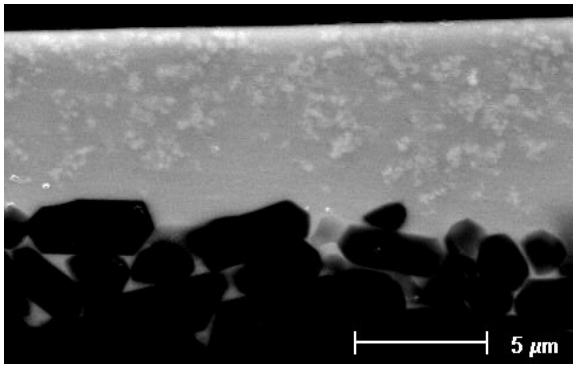

T_f = 700°C

Figure 19: SEM of a cross section for low and high T_f : reaction with the substrate (the substrate is on the bottom)

At 700°C, because of its low viscosity, the glass can react with the glassy phase of the alumina substrate and penetrate around the grains, which causes a surface desegregation of the alumina as observed in figure 20. The glass probably reacts also with the alumina grains themselves, leading to an enrichment in aluminium of the glass close to the substrate. This modification of the bottom layer (called by some authors the «dead layer» [62]) generates a thin area (1 µm) where no RuO_2 particle is detected and that is presumed to be rich in Al_2O_3. This phenomenon

has already been mentioned by several authors in the case of overfired systems [63] and refers to a probable dissolution of the alumina substrate into glass [64].
It has been demonstrated that this modification can disturb the electrical behaviour, particularly for samples whose glass composition is poor in alumina [64].

This additional complementary observation to the one on figure 4, emphasise the fact that, the lowering of x_c (figure 1) could be due to a microstructural changes driven by physical, rather than chemical, RuO_2-glass interactions. For example, prior to the firing cycles, the RuO_2 grains are in form of clusters dispersed among the glassy grains. From the electron transport point of view, each cluster is an effective large particle whose size depends on several factors such as the quantity and nature of the organic dispersant, the mixing procedure, etc.. During firing, the glassy grains start to soften and eventually they wet the RuO_2 clusters, starting to penetrate inside the clusters and to separate the original particles. At sufficiently high firing temperatures (and depending on the firing time) the initial clusters are completely broken up in the glass. In this situation, the percolation threshold is given by the small RuO_2 particles rather than by the large RuO_2 clusters, and it can be considerably lower than that at the first stage of firing. This mechanism could qualitatively explain the gradual lowering of x_c increasing with T_f shown in figure 1, although it is not excluded that, at very high firing temperatures, the glass viscosity is so low that the heavier RuO_2 particles may fall towards the bottom of the TFR (or the inverse case if the glass reacts with the substrate), leading to a non-homogeneous distribution of the phases. In this case, the effective RuO_2 concentration at the bottom is not the same than at the top of the sample, and x_c appears to be effectively lowered [65]. This latter possibility could be verified by SEM observations of the vertical cross-section of the samples. Whereas the phenomenon of reaction with the substrate is presented in figure 20, we were not able to obtain clear SEM images in the case of sedimentation of RuO_2, that could be favoured as the conductive phase is denser (d ~7) than the glass (d ~ 5).

IV . 2 . 3 . 1 . 2 . Influence of the dwell-time of firing

Figure 20 shows the dependence of the firing dwell time on the resistivity value. Increasing time of firing causes a decrease of resistivity. This can be explained by the fact that the increase of time favours the kinetics of reactions [63].
Moreover, the variation between 15 minutes and 1 hour seems to be more important for 40 nm grain size, as the specific area is more important.

These observations can be extended to all the samples and can be compared to the behaviour of the commercial piezoresistive pastes studied in chapter II.
However, no new phase (like lead-ruthenate) was detected by X-ray analysis. We can presume that the generated new phase might be too small to be detected. In fact, the absence of new phase is in accordance with the phase diagram of Adachi and Kuno (figure 24) that shows the stability of the RuO_2 phase. In this case, the evolution of the values vs. the firing time could be due to microstructural effects like modification of the surface of the particles or local dissolution phenomenon.

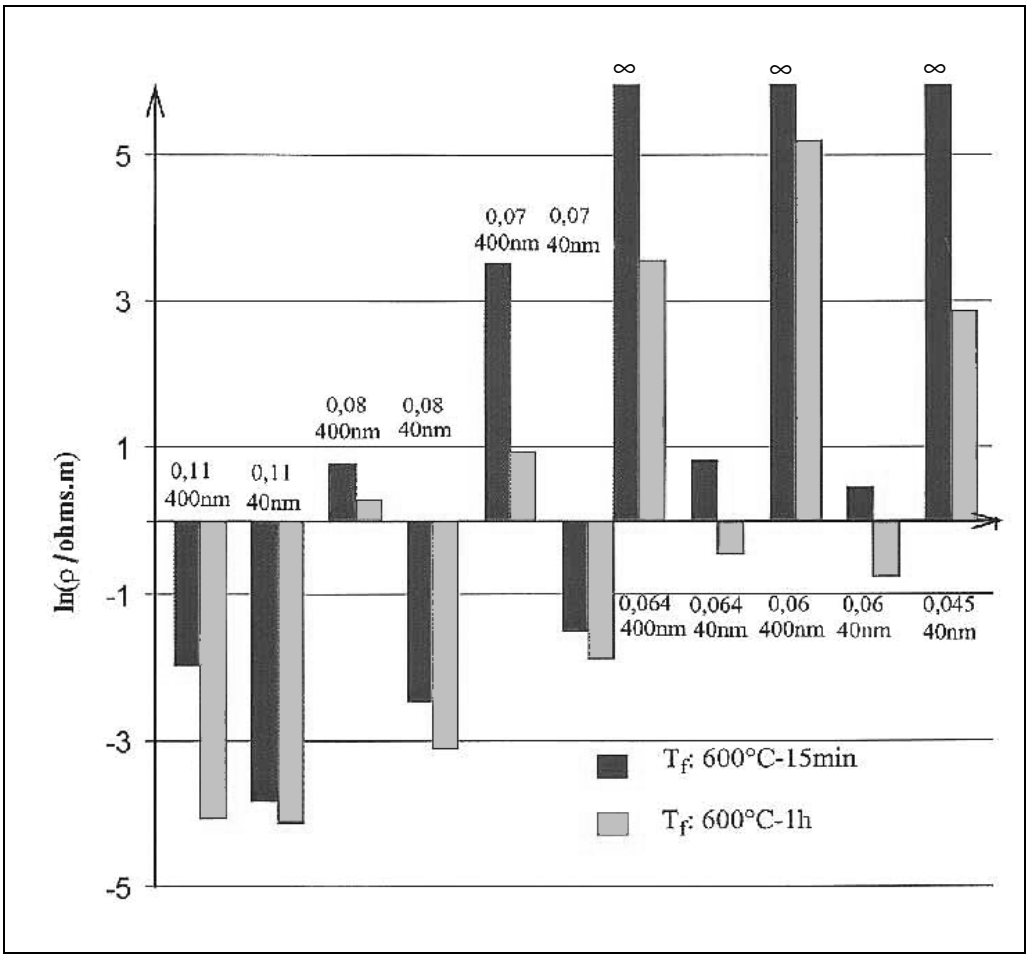

Figure 20: Influence of the dwell-firing time on the resistivity value for V6-samples fired at 600°C

Note that the ln-values superior to 5.5 correspond to values of resistances too large to be measured with our apparatus (noted ∞ on the graph).

IV . 2 . 3 . 2 . Evolution of TCR

At this stage of the study, the evolution of TCR is less important than *R* and GF behaviour. However, we pay attention to the influence of T_f and the concentration of RuO_2 on the behaviour of TCR in order to characterise the obtained pastes for future applications (figure 21).

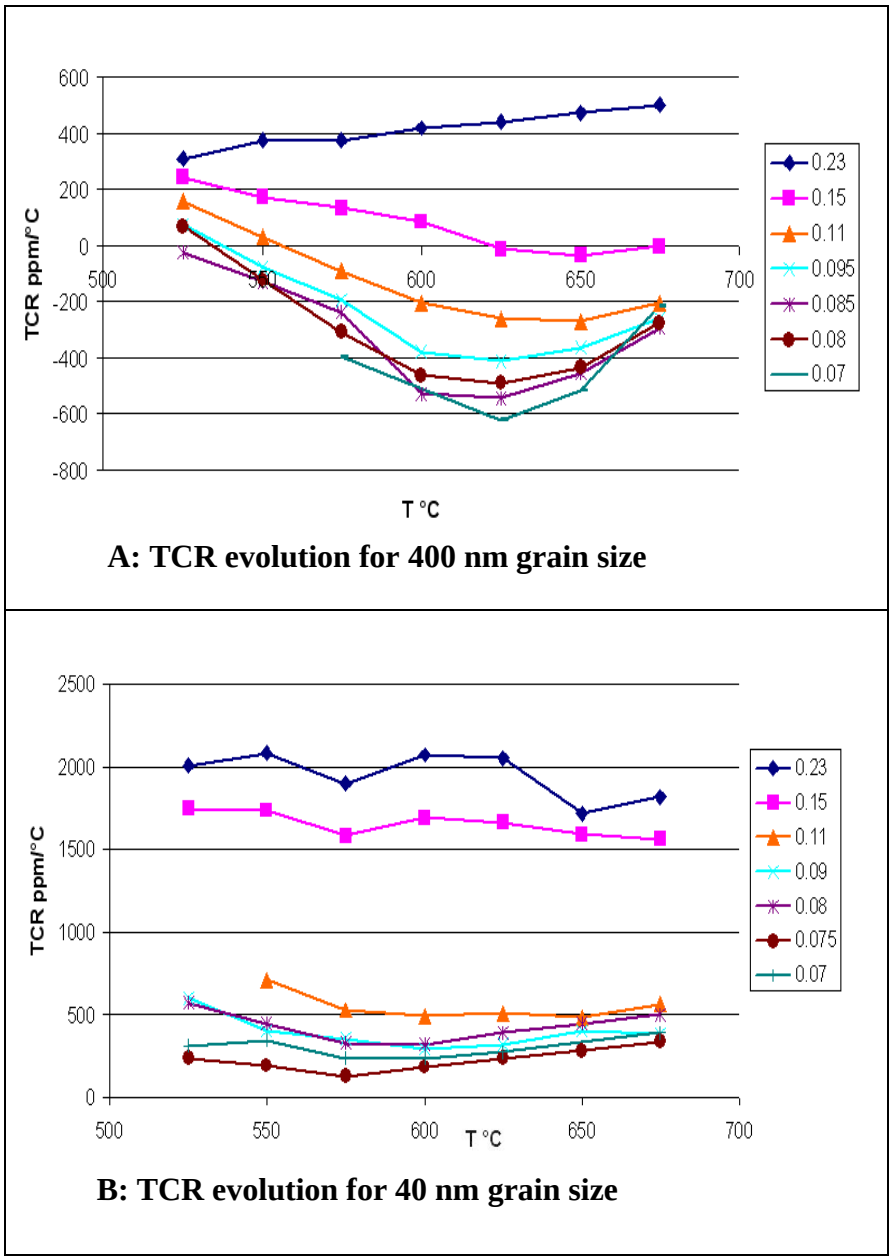

Figure 21: TCR evolution of V6-series for 400 nm (A) and 40 nm (B) grain size pastes

TCR values stay stable whatever T_f, although it is less obvious with 400 nm grain size. In this case, we observe a minimum around 600°C that is stronger for low concentrations.
For 40 and 400 nm size, TCR values are high for high RuO_2 concentrations. This is coherent with the resistivity behaviour, as to a high resistivity (low concentration) corresponds a low TCR value [5].
Moreover, for a same resistivity value, TCRs corresponding to 40 nm grain size are higher than TCRs of 400 nm grain size, as referred in the literature [5]. This phenomenon is represented in figure 22, in which the corresponding TCRs of 40 and 400 nm grain size for three representative firing temperatures are plotted. (Note that the same behaviour will be observed for the other series of glass). This difference of TCR shows that the 40 and 400nm-resistors can be considered as two different materials, which shows the influence of the grain size on the TCR values.

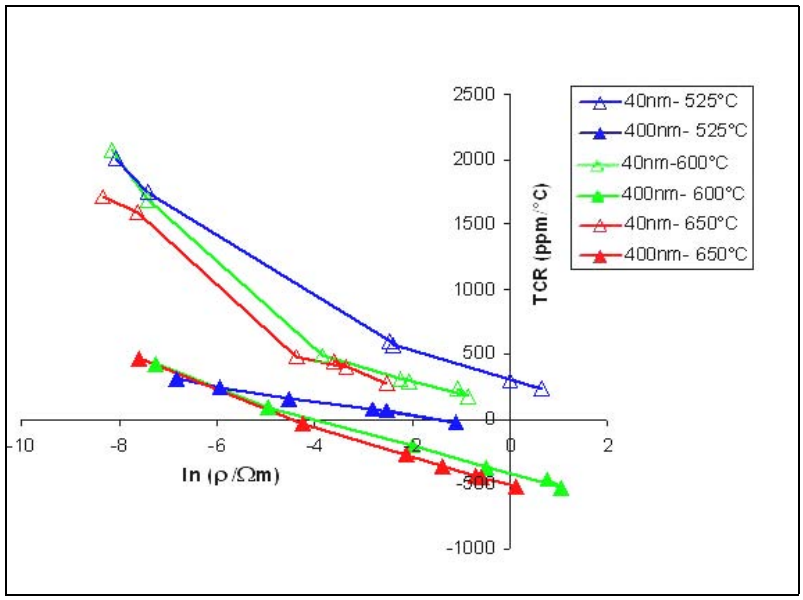

Figure 22: TCR evolution vs. lnρ for the V6-series for different firing temperatures

From these observations, we can assume that this V6-series covers a large range of TCR values and it supposes that it could be used for different applications.

IV . 2 . 4 . Conclusion

The V6-paste series can be considered as our reference concerning piezoresistive pastes realised in our lab. This section allowed us to characterised them and to validate our hypothesis.

On the one hand, we showed the influence of different parameters (T_f, grain size, concentration, dwell time) on the main electrical properties (R, TCR and GF). Structural analysis gave a possible interpretation of the results. At the end of this part a percolative mechanism for this kind of systems was emphasised.

On the other hand, we aim to validate our hypothesis by studying the GF behaviour.
We took an interest to conductivity and piezoresistivity measurements in disordered RuO_2-glass composites close to the percolation threshold. We have found that the fabricated samples display both universal and nonuniversal behaviour of transport. The corresponding piezoresistive responses changed dramatically depending on whether the composites were universal or not. For the composites with $t \sim 2$, the piezoresistive factor Γ showed no dependence upon the RuO_2 volume fraction x, whereas the nonuniversal composites displayed a logarithmic divergence of Γ near the percolation threshold. We have interpreted the piezoresistivity results as being due to a strain dependence of the conductivity exponent when this was nonuniversal.
As discussed, a logarithmic divergence of Γ was found to be fully consistent with the tunnelling-percolation model of nonuniversality proposed by Balberg a few years ago. According to this theory, when the tunnelling distance between adjacent conducting grains has sufficiently strong fluctuations, the exponent t acquires a dependence upon the mean tunnelling distance a. An applied strain could so disturb the piezoresistive response and engender a variation of t.

In view of such agreement between theory and experiments, we conclude that the origin of nonuniversality in RuO_2-glass composites is most probably due to a tunneling-percolation mechanism of nonuniversality.
We have brought forth a microscopic formulation to the phenomenological level proposed by Balberg, and we can now assert that TFRs are nonuniversal compounds showing transport exponent t larger than the universal limit value $t = 2.0$. This exponent t depends on strain and leads to a logarithmic divergence of the gauge factor.

The possibility of influencing t by external means (e. g. strain) has never been studied so far.
We have proposed a new way to investigate percolative systems by studying the behaviour of piezoresistive pastes.

IV . 3 . V2-paste category: high firing temperature system

The same experiments and measurements as the previous series are carried out.
For this case, the interpretation of the results is more ambiguous. These series of V2-paste characterised by its higher firing temperature differs from the V6-series as its percolative behaviour is not so well defined.

IV . 3 . 1 . Electrical behaviour: influence of parameters

IV . 3 . 1 . 1 . Influence of the firing temperature

Figure 23 shows the variation of the resistivity as function of T_f for different volume concentrations of the RuO_2 for 400 nm and 40 nm.

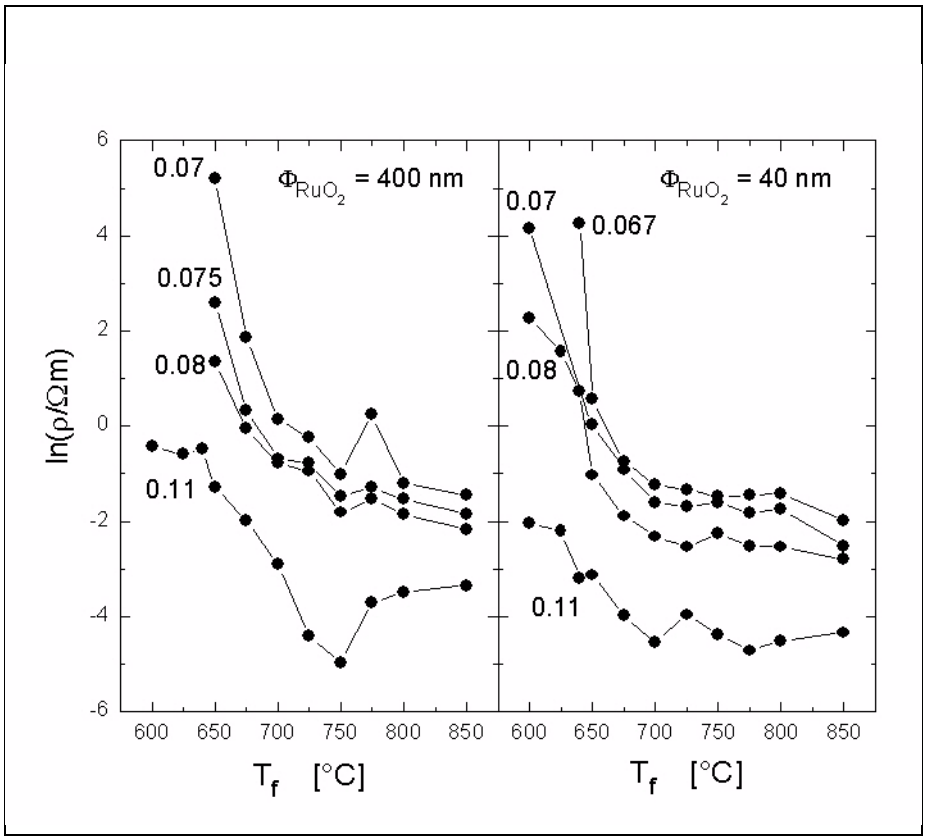

Figure 23: Resistivity evolution in function of T_f for 400nm and 40nm RuO_2 grain size and for different volume concentrations of RuO_2

The behaviour of this V2-paste appears to be different from the V6-series, as no maximum is discernible at optimal temperature (here ~ 700°C). In fact, it behaves more like small concentration of V6-series. Indeed, whatever the concentration is, the resistivity value increases when T_f decreases. This phenomenon is less marked with high concentration (x = 0.11).
The increase of the resistivity occurs for T_f < 750°C for 400 nm grain size and for T_f < 700 °C for 40 nm. It could be explained by the fact below these firing temperatures, the glass does not wet all the conductive particles and this creates an inhomogeneous system for low temperatures.

SEM images (figure 24) illustrate the homogenisation of the structure with the increase of T_f.

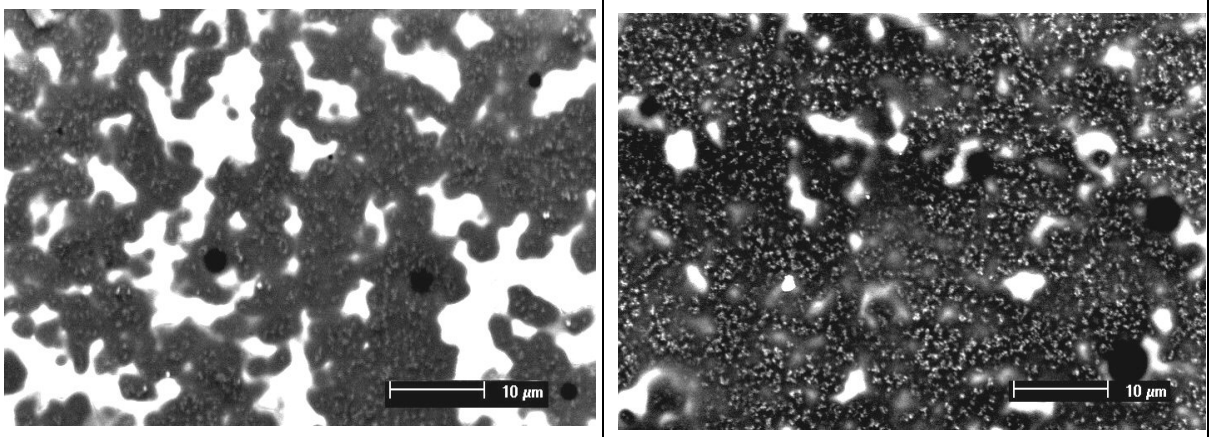

Figure 24: SEM observations of the surface of a V2-paste (x=0.11, 400nm) fired at 640°C (left) and 800°C (right)

At low temperature (640 °C) RuO_2 particles seem more clustered. We can discern some charged up glass areas. On the opposite, at 800°C, the paste seems more homogeneous and the insulating zones decrease significantly. From the both images, it is easy to imagine that the resistivity could be lower for high firing temperatures.

Moreover, the decrease of resistivity with T_f could be due to the apparition of a new conductive phase (such as lead ruthenate). But, we did not detect new phase by X-ray analysis. In spite of the high temperature, no ruthenate apparition is favoured. This was predictable if we consider the diagram of stability from Adachi and Kuno (figure 25), which shows the stability of the conductive phase in function of the glass composition for T_f ~ 850°C.

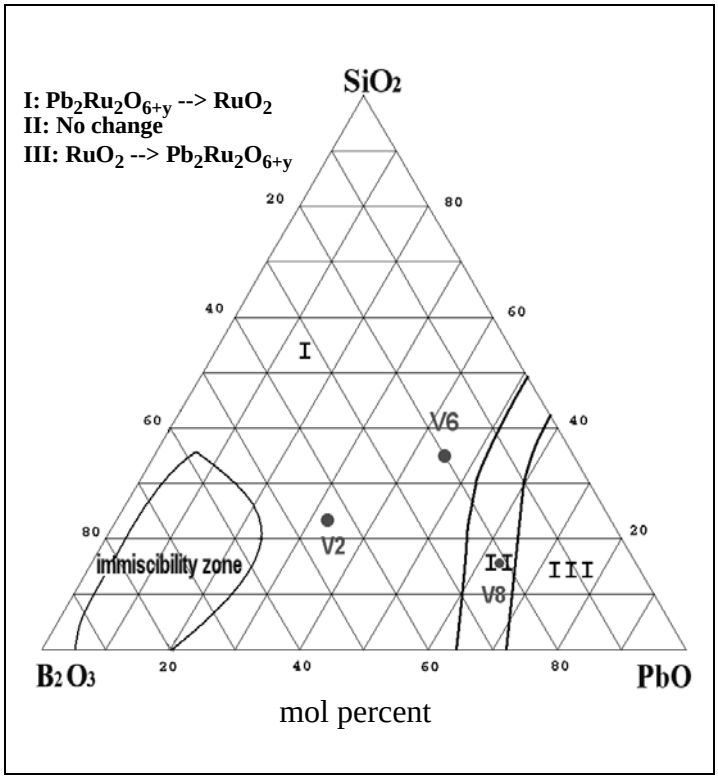

Figure 25: Stability of the conductive phase in the PbO-B_2O_3-SiO_2 system (850°C) [66]

Adachi and Kuno [66,67] showed that in glasses poor in PbO, the ruthenate phase disappears and RuO_2 is formed (region I) while for PbO-rich glasses, the RuO_2 reacts with the PbO from the glass and forms $Pb_2Ru_2O_{6+y}$ (with y~0, see chapter I.3.1) (region III), as presented in figure 24. Between these two regions (region II), they did not see a significant evolution of the RuO_2 to ruthenate ratio, presumably because the driving force for this evolution was too low.
If we plot our glass compositions (V6, V2 and V8), we can see that V2 and V6 glasses are in the region where the RuO_2 phase is stable, this explains then why no new phase is detected. And V8 lies more or less on the boundary between the RuO_2 and ruthenate fields.

IV . 3 . 1 . 2 . Influence of the volume concentration of RuO_2 - Determination of the nature of the transport

In figure 26, we plot the resistivity as a function of RuO_2 volume concentration *x* for different values of T_f and for both RuO_2 grain diameters (see caption for more details).

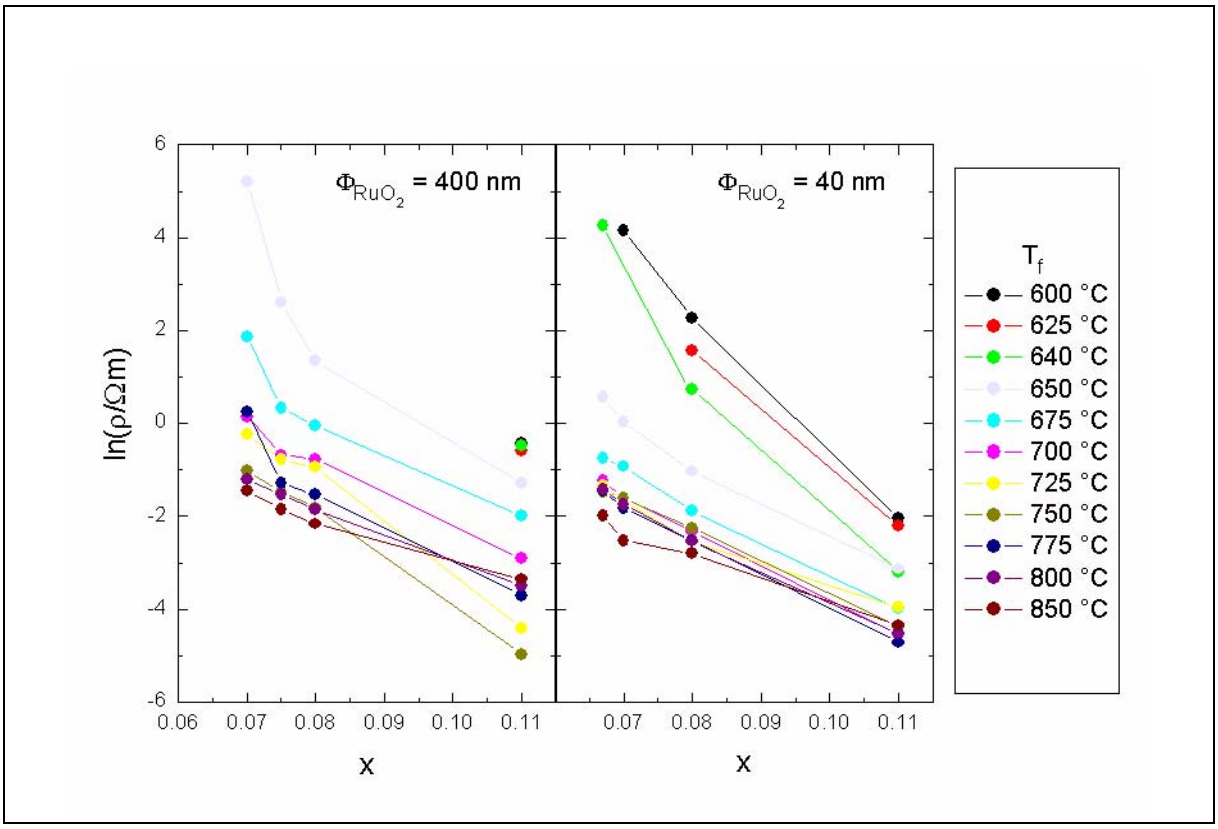

Figure 26: Resistivity as function of RuO_2 volume concentration *x* for various thick-films for different T_f and for 400nm and 40nm RuO_2 grain sizes

The situation seems less clear than the V6-series, as the percolation threshold is not observed for the most of the cases.
For the 400 nm case, the percolation transition is quite clear for T_f < 700 °C while it disappears for higher values of T_f. But, for the 40 nm series, the situation is even more peculiar since no clear signal of a percolation transition is visible at any value of the firing temperature.

For 40 nm case, it appears that the chosen concentrations are not close enough to x_c.
For the 400 nm series, we can discern a percolative behaviour for low temperatures and particularly for 650°C. But, we were not able to measure additional values for lower *x* as the resistance values were too high.
However, we can try to determine some parameters for the 400nm-650°C series. The fitting of the previous results gives the following parameters, if we consider that:

$$\rho = \rho_0 (x-x_c)^{-t}$$

where ρ_0 is a prefactor and *t* is the transport critical exponent [1,2].

We obtain:
$\ln\rho_0$ = -8.2 +/- 0.3
t = 2.2 +/- 0.1
x_c = 0.068 +/- 0.0002

For this situation, the transport seems to be universal ($t \sim 2$). The determination of x_c allows to show that the chosen concentrations for 400 nm are close to the percolation threshold.

For the other samples the situation is not enough clear to be correctly interpreted. Moreover, no structural difference between the samples was detected.

In conclusion, we can suppose that the behaviour is percolative for $T_f < 700°C$, but the lack of values and the limits of the measurements don't allow us to validate this hypothesis.
Moreover, we should mention that the used V2-glass was polluted with carbon particles coming from the PE flasks during the ball-milling. Despite of a refining process of the glass to eliminate the carbon residues, it is possible that some pollution remained in the paste and disturbed the electrical measurements by modifying the conductivity. Indeed, the expected volume concentrations of conductive grains may be undervalued, which could explain why we are so far from x_c.
In addition, some incoherences of electrical measurements can be explained by the presence of isolated bubbles in the bulk of the paste as shown by SEM observation of a cross-section of a 400nm-700°C series (figure 27). (Note also some substrate-resistor interactions, like the V6-series).

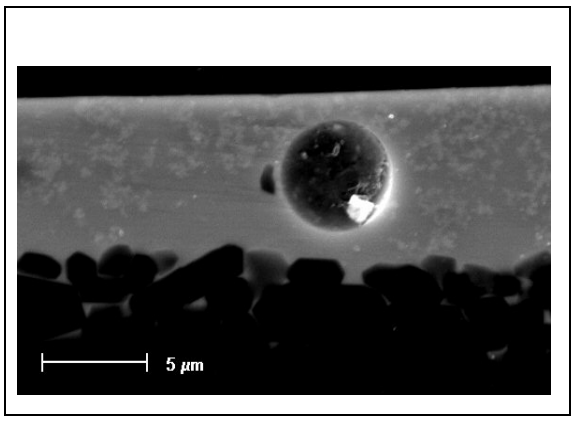

Figure 27: SEM observation of a cross-section of a 400 nm sample (the substrate is on the bottom)

It is evident that from the previous results, a piezoresistive study will be not consistent.
However, we can have a look at some complementary results, such as the behaviour of the TCR that is presented in the next section.

IV . 3 . 2 . Complementary study: evolution of TCR

Figure 28 shows the influence of T_f and the concentration of RuO_2 on the behaviour of TCR.

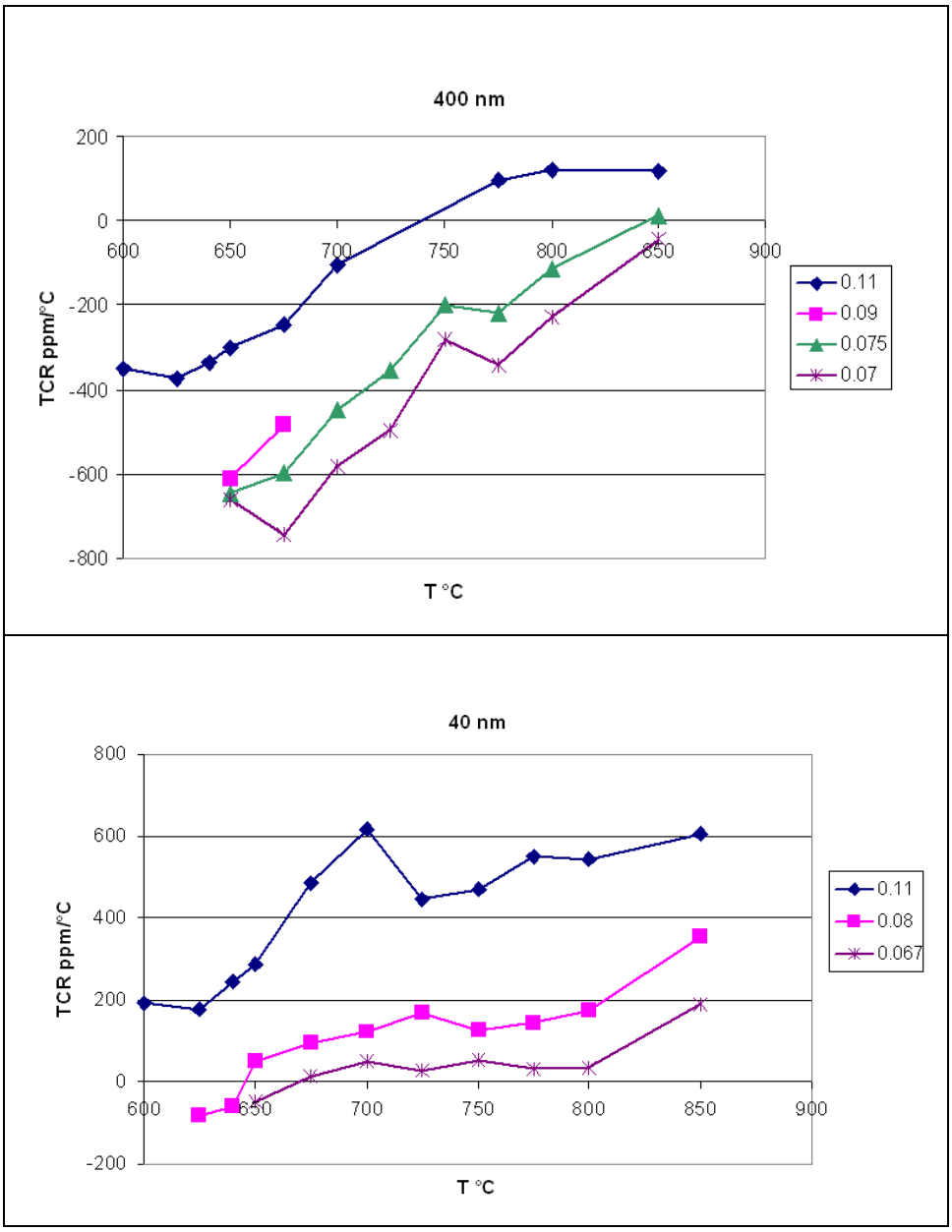

Figure 28: TCR evolution vs. T_f of V2-series for 400 nm (top) and 40 nm (bottom) grain size pastes

The evolution of TCR depends on the grain size. 40 nm series seems more stable contrary to 400 nm, whose TCR increases when T_f is high. Nevertheless, some similitudes with the V6-series remain.

For both sizes, TCR values are high for high RuO_2 concentrations. This is coherent with the resistivity behaviour, as to a high resistivity (low concentration) corresponds a low TCR value [5]. Moreover, for a same concentration of RuO_2, TCRs corresponding to 40 nm grain size are higher than TCRs of 400 nm grain size, as referred in the literature [5].

At last, 40 nm pastes give positive TCR whereas for 400 nm, TCR values are mainly negative.

Note that few values are given for T_f < 650°C because of the instability of the measurements, which leads to important errors.

Despite of some instability, we can assume that this V2-series covers a large range of TCR values. Note that TCR values for 40 nm and for moderate concentrations lie in a practically usable range as they are included in the range 0 - 150 ppm/°C.

IV . 3 . 3 . Conclusion

It is evident that the V2-series behaviour is less evident than the previous series (V6-paste). It comes from the fact that the chosen x seem too far from the x_c threshold. So, no distinct percolative behaviour was emphasised (except for low temperatures). Concerning the electrical transport, the only analysed series (V2-400nm-650°C) shows an universal transport. But this result should be confirmed by other samples.

It appeared that the results were not so relevant than the previous series as the V2-glass was initially polluted by carbon particles coming from the process, that could disturb the electrical behaviour.

Although this series does not allow to completely reinforce our previous results, some signs of percolative behaviour are nevertheless present. Moreover, without considering the theoretical aspect, this series offers an interesting range of TCR values (that could be latter improves by additives) and it would be useful for technological goals.

IV . 4 . V8-paste category: very low firing temperature system

The V8-series is characteristic by its very low T_f. During the study of the influence of parameters, we met technological problems (drift of the values). It is evident that the aim of this section is not to study the electrical behaviour but to understand and resolve the technological difficulties.

IV . 4 . 1 . Study of *R*: influence of parameters

IV . 4 . 1 . 1 . Influence of T_f

As previous series, we plot the resistivity in function of T_f for different concentrations and grain sizes of RuO_2 (figure 29).

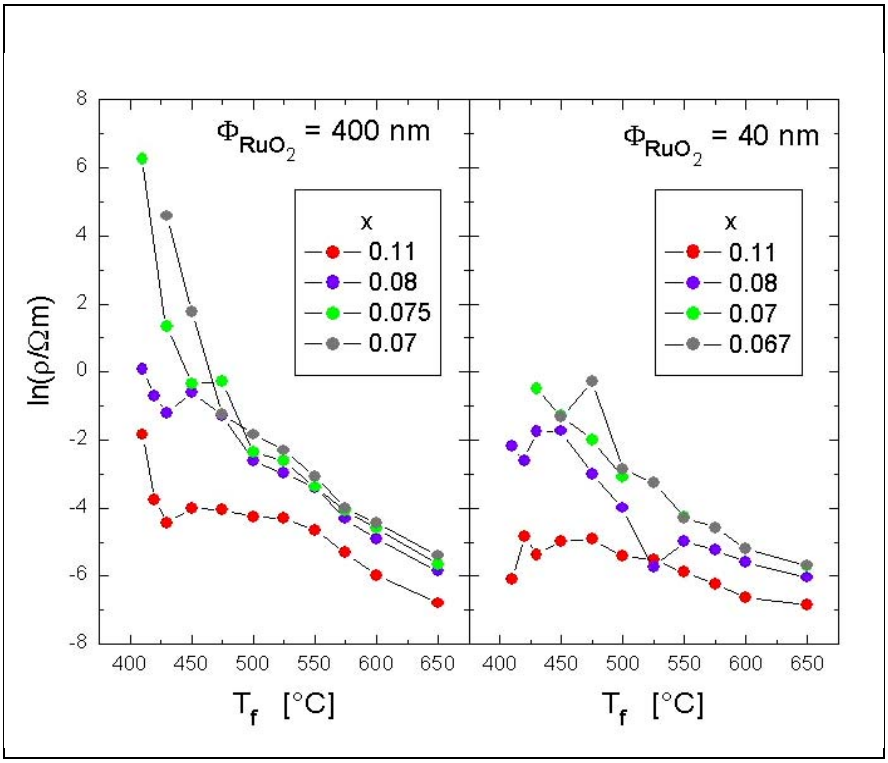

Figure 29: Evolution of the resistivity vs. T_f for 400 and 40 nm size RuO_2

The 400 nm series presents the same behaviour as the 400 nm-V2 series. Indeed, whatever the concentration, the resistivity value increases when T_f decreases (except for high concentrations (x = 0.11)).
The phenomenon is less marked for the 40 nm series, as we probably chose concentrations x too far from x_c.

SEM images (figure 30) illustrate the homogenisation of the structure with the increase of T_f.

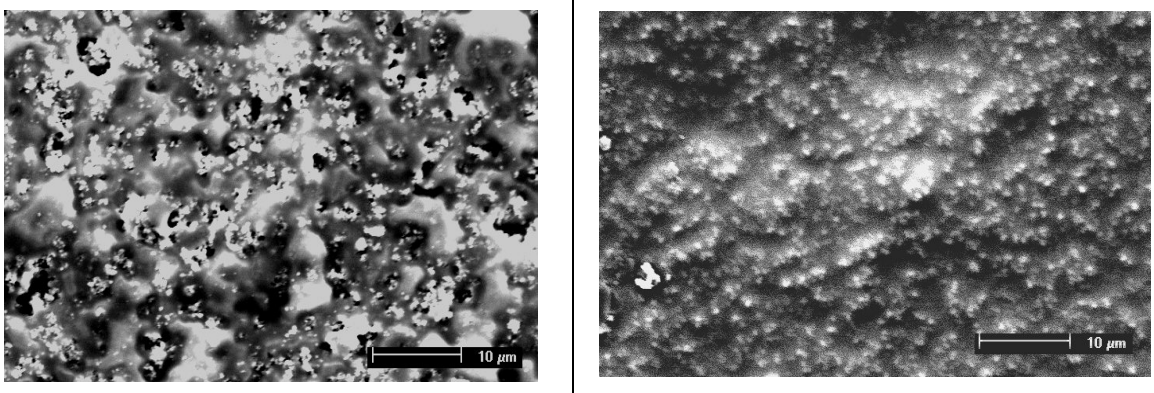

T_f = 420 °C **T_f = 650 °C**

Figure 30: SEM observations of the surface of a V8-paste (x=0.11, 400nm) fired at 420°C (left) and 650°C (right)

At low temperature (420 °C), the RuO_2 particles seem more clustered. We can discern some charged up glass areas. On the opposite, at 650°C, the paste seems more homogeneous and the insulating zones decrease significantly. From both images, it is easy to imagine that the resistivity could be lower for high firing temperatures, as observed with the previous series.

Moreover, we did not detect new phase by X-ray analysis (as expected from figure 25).

IV . 4 . 1 . 2 . Influence of RuO_2 concentration

The evolution of the resistivity vs. the RuO_2 concentration for different T_f and grain sizes is represented in figure 31 .

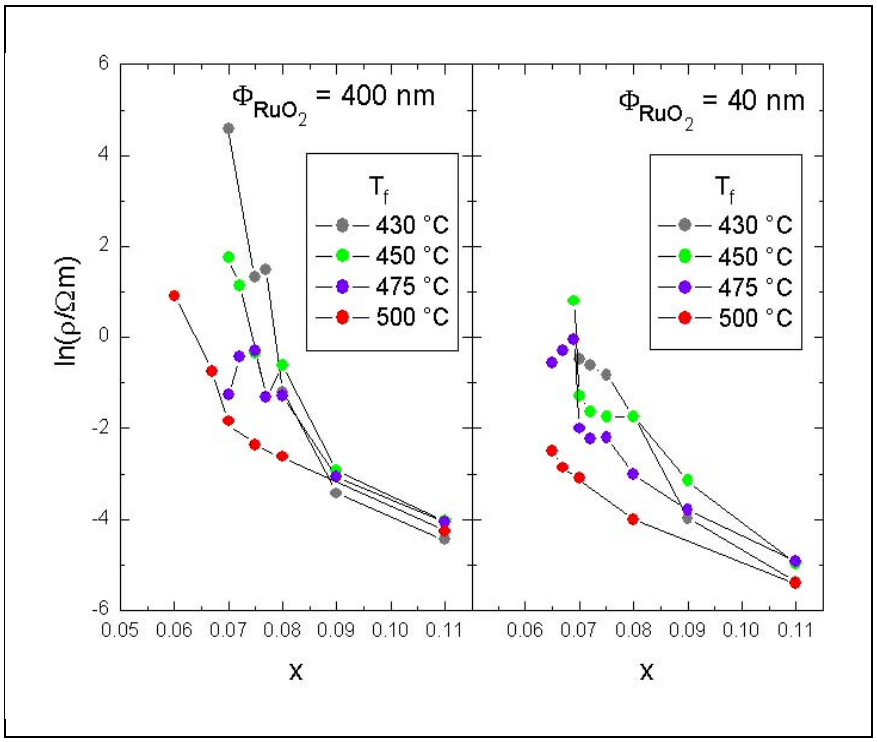

Figure 31: Resistivity vs. RuO_2 volume concentration x for different T_f and for 400 and 40 nm grain sizes

The situation looks like the V2-series, as the percolation threshold is not pronounced for most of the cases.
For the 400 nm case, the percolation transition is quite clear for low T_f values. But, for the 40 nm series, the situation is even more peculiar since no clear signal of a percolation transition is visible at any value of the firing temperature.

For the 40 nm case, it appears that the chosen concentrations are not enough close to x_c.
For the 400 nm series, we could discern a percolative behaviour for low temperatures, but the obtained results are not usable as each point is marked by an important error. The results issue of a possible interpretation would be not representative of the system behaviour. This is why no precise studies directed to the understanding of the electrical transport will be carried out for the V8-series.

Consequently, the main goal of this section will be to try to interpret the instability of the results and to try to improve on this situation.

IV . 4 . 1 . 3 . Origin of the instability of the measurements

It is probable that this instability comes from the too different TCE values of the paste and the substrate. Indeed, the TCE value of the V8 glass was estimated to be 11 ppm/°C, whereas the TCE of Al_2O_3 is 7 ppm/°C (see Chapter III). It is evident that the film is subjected to non negligible tensile strains from the substrate, which can create localised cracks in the resistance that have been observed by SEM (figure 32).

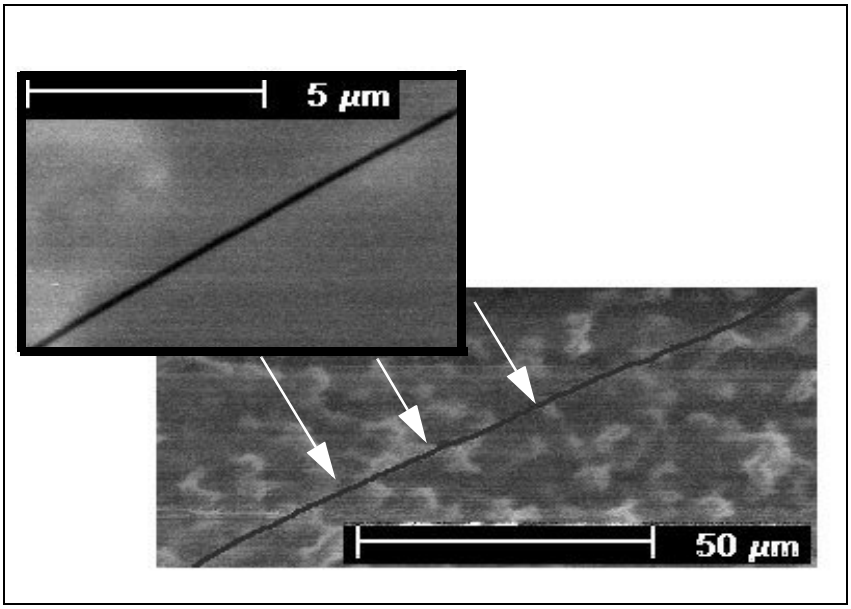

Figure 32: SEM of a crack on the surface of a V8-series resistance

These cracks are not negligible as the amplitude of their propagation stretches along several micrometers.
Moreover, we can attribute this instability to isolated bubbles similar to the one observed for the V2-series (figure 27). It could come from the fact that the softening temperature of the glass is very close to the removal threshold of the organics. Despite of the optimised firing process, some bubbles can remain. But it does not seem to be the major disturbing parameter.

In order to validate our hypothesis of cracks, the evolution and the stability of the gauge factor value will be studied.

IV . 4 . 2 . Study of the instability: Piezoresistive response

Evolution of GF is a good indicator for the study the stability of a film according to the applied strain. The appearance of cracks in the bulk of the system will be emphasised by a drift of the signal.
The aim is firstly to apply a strain (like for the other series) and to observe if there is an hysteresis or a shift of the values between the initial state (before applying a load) and the final state (after loading).

IV . 4 . 2 . 1 . Identification of the instability

The GF measurements were realised with the same technique (cantilever beam) described in chapter II.2. Increasing loads (from 0 to 80 g) were applied to the end of the alumina cantilever. The behaviour of several samples is represented in figure 33.

Notation:

we will use the nomenclature defined in the beginning of this chapter by mentioning the different cantilevers as following:

« volume concentration-grain size-glass-T_f-$GF_{L \text{ or } T}$ »

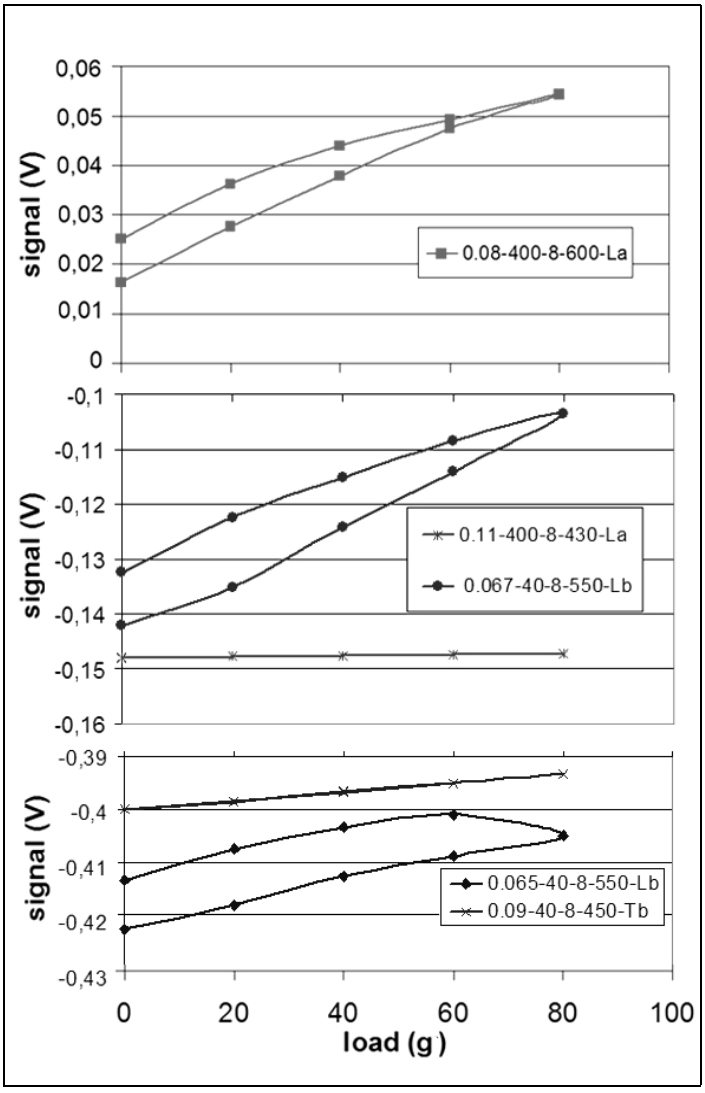

Figure 33: Evolution of the piezoresistive response for different V8-samples

We observe that the majority of the samples shows a hysteresis: the signal at the end of the loading cycle increases. This could be explained by the apparition or lengthening of cracks that modify the electrical response.

However, some rare samples present a linear evolution (0,09-40-8-450), whereas some others (0,11-400-8-430) do not seem to be influenced by a load, because of their probable too high concentration.

Whatever the behaviour is, no apparent correlation between the concentration or T_f has been found.

A complementary study carried out on several cycles (three successive cycles) allows showing that the more critical cycle is the first loading during which the cracks are generated. We observe a stabilisation for the two following cycles (figure 34).

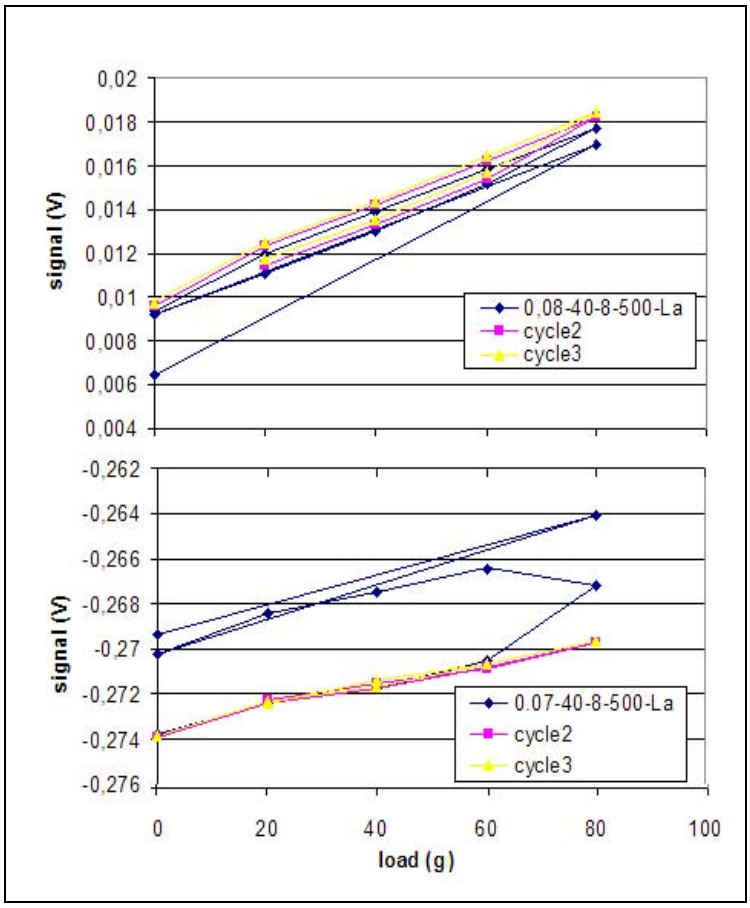

Figure 34: Evolution of the instability during three following cycles

In figure 34, the behaviour of two representative samples (medium concentration and optimal T_f) is shown. It appears that all the cracks seem to appear during the first cycle, as the two following cycles are reproducible. But it is evident that after the first cycle, the signal is permanently modified.

Moreover, if the samples are left at room temperature without strain during few days, we observe an increase of the resistivity value of ~ 16% for $x = 0.08$, and ~ 18% for $x = 0.07$. This behaviour shows that an embrittling of the film can be expect during time, and particularly a phenomenon of stress corrosion, as observed in previous studies [68-70]. These last results show that the 0.08 sample seems to be more stable, which is in accordance with the results on figure 34 that show a lower hysteresis for $x = 0.08$.

IV . 4 . 2 . 2 . Proposition of solutions

In order to avoid this inconvenient, different solutions can be proposed. It is possible:
- to decrease the strain (load) to minimise the cracks,
- to use a substrate with a closer TCE than the V8-pastes,

- to measure the signal by subjecting the cantilever to compressive strains instead of tension that amplify the strains in the bulk.
- to modify the composition of the V8-glass in order to change its TCE by adding some modifiers (amorphous SiO_2, for instance).

Among these propositions, some of them are easier to carry out than others. We will take an interest to the two first solutions. The third one was tried in one case, but gave inconsistent results: it is probable that the initial cracks provoke false gauge effects, as compressive strain can close the cracks and create new contacts modifying the gauge factor evolution. The last solution will be the topic of future studies.

IV . 4 . 2 . 2 . 1 . Decrease of strain

To avoid cracks, we decided to observe the behaviour of some samples by applying different decreasing loads: 80, 40 and 20 g. Note that before applying each load, the cantilever is unloaded. It will allow us to stabilise the existing cracks, with the large initial load, and use the decreased load for GF measurement. The evolution of the two previous samples is depicted in figure 35.

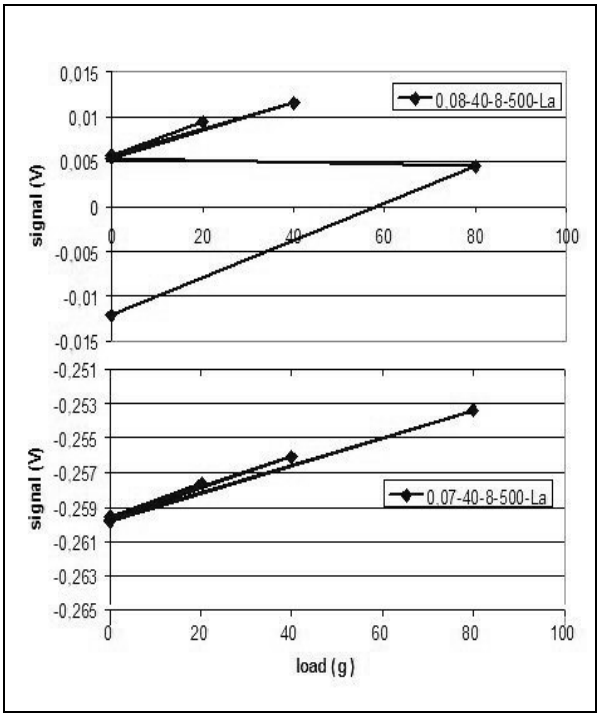

Figure 35: Piezoresistive response during three cycles with decreasing loads

So that the samples were observed in the same conditions, the first cycle consists in applying a load of 80 g that generate cracks.
These two samples are representative, as the first (0,08-40-500-La) show a strong deviation of the signal for 80 g, whereas 0,07-40-500-La presents a relatively linear signal that it is less influenced by cracks.
Whatever the samples are, the lower loads (20 and 40 g) don't seem to generate cracks. Note that the very low loads (20 g) lead to measurement precision issues due to the correspondingly very low electrical response.
An appropriate solution would to decrease the applied strain and to apply a 40 g load.

Between the figures 34 and 35, we detect a shift of the signal if we compare the final value of figure 34 and the initial value of figure 35. These values should be the same, as the different experiments were carried out successively (but they were separated by a phase of rest during 15 days). We suppose that the samples (and the cracks) propagation over time is due to stress corrosion effects due to ambient humidity and thermal tensile strain [69,70].

IV . 4 . 2 . 2 . 2 . Change of the substrate

The second solution was to change the alumina substrate by an other material characterised by a closer TCE of the resistor film.
A possible candidate could be ZTA (Zirconia Toughened Alumina) whose TCE is 9 ppm/°C. Although its TCE is yet lower than the one of V8, it could be considered as a good compromise as ZTA material is chemically close of the alumina substrate. Indeed, for example, some measurements on alumina and ZTA substrates show relatively similar results in the case of commercial pastes, such as DP 2041 [71].
The same cycles as figure 34 were realised to compare the results.
In figure 36, the three successive cycles corresponding to the alumina substrate and to the ZTA substrate are depicted. All the values are normalised to obtain comparable results. Indeed, to realise the cycles, we applied a maximum load of 40 g. But, the used ZTA cantilevers were thinner than the alumina ones: the thickness were ~ 0,3 µm (0,635 µm for alumina). So, as the main material constants are nearly the same as alumina (elastic modulus E* ~ 340 GPa, Poisson's ration ~ 0.23), the resulting surface strain along the main cantilever axis, corresponding to a determined load, becomes four times higher than the strain for alumina. This comes from the following expression of the strain ε:

$\varepsilon = 6\, M\, g\, d / (E^*\, b\, h^2)$ (for more details, see chapter II.2)

where h is the thickness.
As, $h_{ZTA} = (h_{Al_2O_3} / 2)$, then we obtained that $\varepsilon_{ZTA} = 4\, \varepsilon_{Al_2O_3}$. So, the strain corresponding to a load of 40 g for a ZTA cantilever, corresponds to a strain generated by a load of 160 g on the alumina cantilever. This is why the scales are different from both substrates, which justifies a standardisation of the values (figure 36).

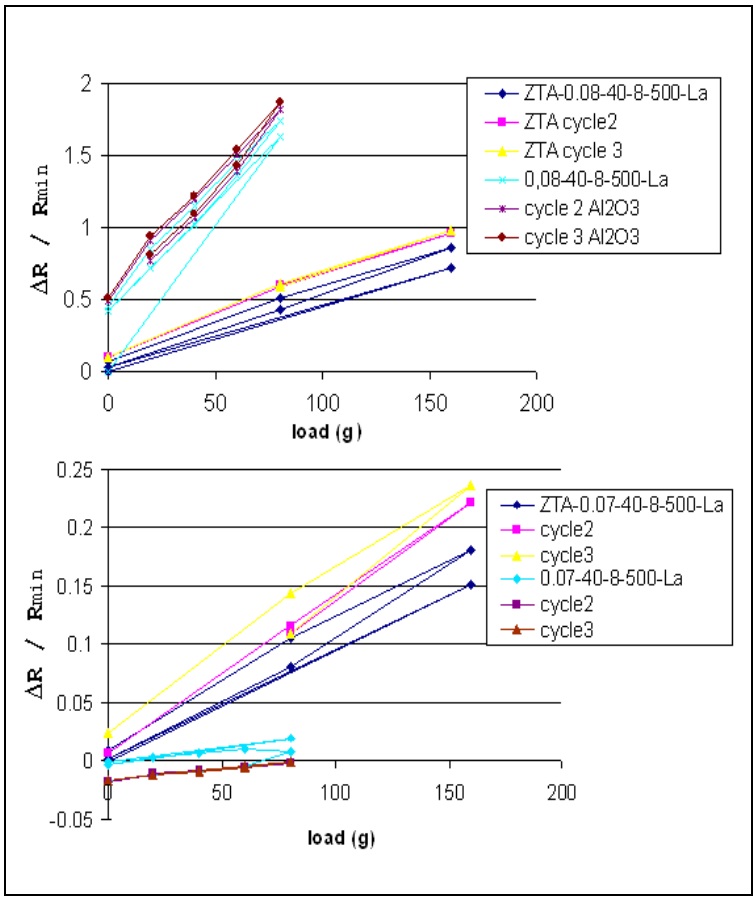

Figure 36: Piezoresistive response with a ZTA and an alumina substrates

If we compare the values with the same load, we can observe the results with ZTA substrate appears to be more stable. Although a hysteresis persists, high loads don't provoke important and irreversible modifications of the behaviour.
It is evident that the stability could be optimised as the TCE of ZTA is not the same as the TCE of alumina, but it was interesting because of its comparable properties.

Moreover, we can suppose that the residual instability could come from internal microscopic strains between the different phases of the paste (glass and RuO_2), as explained in chapter II.

IV . 4 . 2 . 3 . Conclusion

This study allows to show the importance of the substrate in thick-film technology. In our case, the TCE of the V8-series is too high compared to that of alumina, which leads to cracks in the resistor. This affects the piezoresistive response, which shows a non negligible drift, as referred in the literature [72]. However, the initial cracks embrittle the material (humidity, oxidation) and an instability seems to be always present.

To decrease the applied strain, we can use a different substrate (with a TCE > 11 ppm/°C, such as ZrO_2 or steel) to give stability to the system. But, this implies to develop compatible dielectrics to avoid the chemical interactions between this kind of substrate and the resistors (see chapter V and outlook).

Therefore, an extensive study of piezoresistivity in this series could not be carried out, as the obtained results are not representative as dependent on external perturbations.
However, we can study the evolution of TCR value that remains coherent.

IV . 4 . 3 . Complementary study: evolution of TCR values

Figure 37 shows the influence of T_f and the concentration of RuO_2 on the behaviour of TCR.

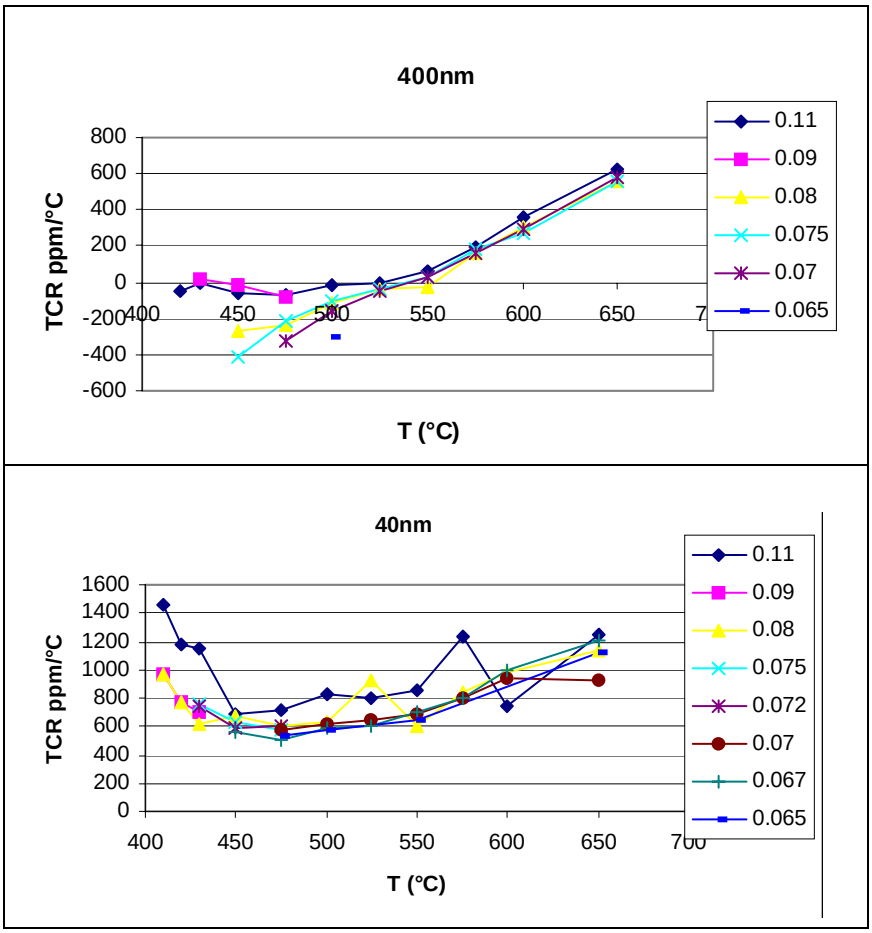

Figure 37: TCR evolution vs. T_f of V8-series for 400 nm (top) and 40 nm (bottom) grain size pastes

The evolution of TCR depends on the grain size. 40 nm series seems more stable contrary to 400 nm, whose TCR increases when T_f is high. However it retains some similitudes with the V2-series.
For a same concentration of RuO_2, TCRs corresponding to 40 nm grain size are higher than TCRs of 400 nm grain size, which is also the case for our results on V6 and V2 systems, and as referred in the literature [5]. Moreover, TCRs for the 400nm-series are little dependent on the concentration except for low temperatures.
At last, 40 nm pastes give positive TCR whereas for 400 nm, TCR values are both negative and positive.

An interesting technological point is that we observe a zone of stability where TCR remains constant. For 40 nm size, it corresponds to the range: 475 - 550°C (TCR ~ 600 ppm/C°). Whereas for 400 nm, the range is: 500 - 550°C with a TCR value ~ 0 ppm/°C.

The study of TCR is interesting as some TCRs are close to 0. We can expect that the samples stay more or less stable in this range of temperatures that is one of the required properties to realise a sensor.

Note: TCR values on ZTA substrate are little higher than values on alumina, which was predictable as the higher thermal expansion of ZTA induces a piezoresistive shift of the TCR [71]. Figure 38 shows this discrepancy between each case, although the values are relatively close, which is in accordance with previous measurements [73]. The coherence between the values show that the measurements can be considered as representative.

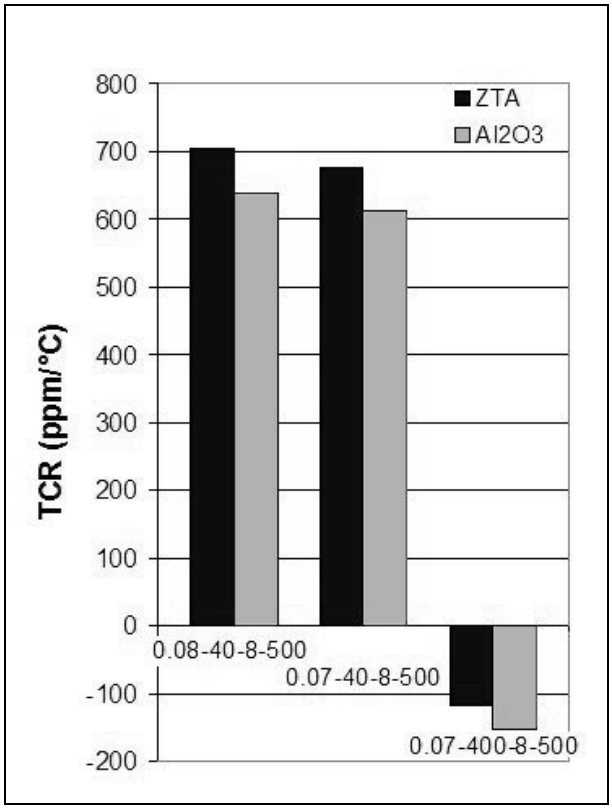

Figure 38: TCR values of V8-pastes (T_f = 500°C) on ZTA and alumina substrates

As we were limited by the available quantities of ZTA substrates, we chose optimal concentrations (0.07 and 0.08) and optimal T_f (500°C).

IV . 5 . Conclusion

The three chosen series of pastes (V6, V2 and V8 pastes) offer complementary results by their different behaviour.
The V6-series allows us to validate our hypothesis that the exponent *t* can depend on strain and leads to a logarithmic divergence of GF. We conclude that the origin of nonuniversality in RuO_2-glass composites is probably due to a tunnelling-percolation mechanism of nonuniversality.
The V2-paste category shows more ambiguous results as its percolative behaviour is not clearly established. Although this series does not allow to completely reinforce our previous results,

some signs of percolative behaviour are nevertheless present. Additional samples are needed to define it more precisely.
The very low T_f of V8 led to technological problems, because of its instability (cracks) due to its TCE being too high for the alumina substrate. We took an interest to propose solutions to decrease this instability. These problems did not allow a precise study of the electrical transport.

IV . 6 . Sensitivity to firing conditions and stability studies

The last part of the study of new piezoresistive pastes is dedicated to the evaluation of their firing sensitivity and stability. In coherence with the study of commercial pastes (chapter II), similar experiments were realised. We will first study the effect of the firing schedule on representative samples. Stability will then be qualified by measuring the influence of a post annealing high temperature storage (250°C).

IV . 6 . 1 . Effect of the firing schedule

IV . 6 . 1 . 1 . Samples and experiments

In order to limit the number of samples, we selected «10 kOhm» compositions (giving ca. 10kOhm resistance for a square resistor with a typical fired thickness of 10 µm) for each category to be coherent with the study of commercial pastes (chapter II). For each concentration, the two different grain sizes are selected (40 and 400 nm). Each sample is fired at low, medium (optimal) and high temperature according to its glass composition, except for the V8-system, which was fired at low and especially high temperatures to favour chemical reactions.
Selected samples and conditions of firing are summarised in table 3.

samples	T_f (°C)		
0.11-400-6	525	600	675
0.08-40-6			
0.11-400-2	640	675	750
0.08-40-2			
0.11-400-8	420	650	800
0.11-40-8			

Table 3: Selected samples and initial conditions of firing

V6 and V2 series are subjected to different firing cycles with a temperature dwell time of 15 min. The cooling rates have been modified:
1) «standard» resistor firing cycle, with a cooling rate of ~ 50 °C/min (see cycles as described in chapter III.3) (n);
2) «quenching», with a cooling rate of ~ 300 °C/min (T);
3) «slow», with a cooling rate of ~ 2 °C/min (L).

As the V8-series is prone to cracking, it was not significant to subject it to the same experiments. However, we will study the its sensitivity to firing by increasing the time of the temperature dwell (3h).

The influence of the firing parameters will be studied through the evolution of *R* / TCR values and GF values. The same measurement techniques as in chapter II.2 are used.
In addition, structural analysis will allow to interpret the electrical results.

IV . 6 . 1 . 2 . Processing sensitivity on the V6-system

IV . 6 . 1 . 2 . 1 . *R* and TCR evolution

- **Influence of the cooling rate vs. T_f**

In figure 39 is depicted the evolution of *R* and TCR values for the both grain size series (400 - 40 nm) for each firing conditions.

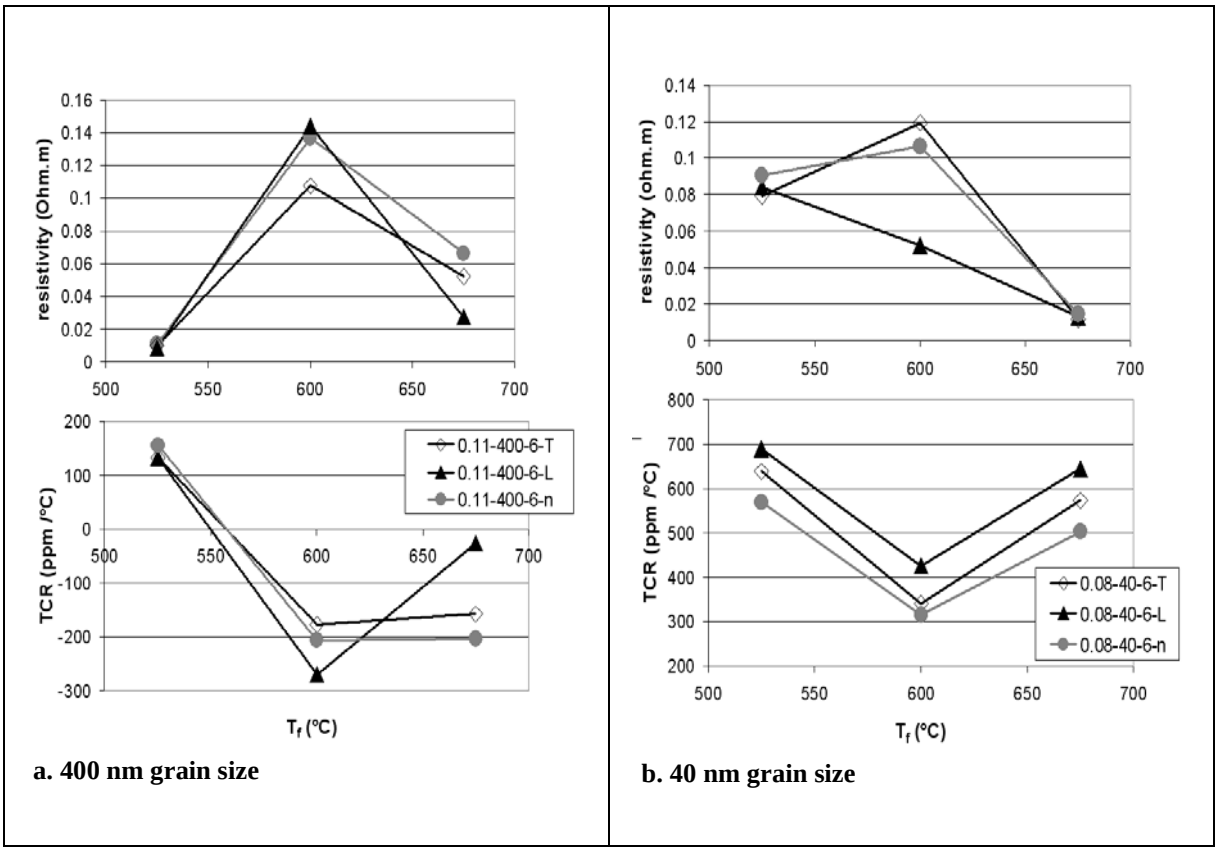

a. 400 nm grain size

b. 40 nm grain size

Figure 39: *R* and TCR evolution of 400 (a) and 40nm-V6 series (b) for the different cooling rates

Whatever the grain size, the same trend is observed. High resistivity values are correlated to low TCRs for each selected parameter.
According to the coherence of the results, we decide to study mostly the evolution of the resistivity values, as it will be easier to interpret *R* results (after that, the reasoning could be transposed to the TCR evolution).

Resistivity values reach a maximum for optimal / intermediate temperatures. We cannot deduce anything from the effect of the cooling rate. However, we can affirm that the corresponding *R* values for a given temperature are more or less dispersed. Indeed, for 400 nm size fired at low temperature, the discrepancy between the different values is low. The disparity increases for higher T_f.
A nearly opposite behaviour is observed for the 40 nm size series as the less dispersed values correspond to high T_f.

This behaviour can be explained by a phenomenon of diffusion of the conductive nanoparticles. If we consider the following Einstein's equation that expresses the brownian motion, we can explain the disparity of the results vs T_f:

$$D = \frac{kT}{F}$$

D: diffusion coefficient (m^2/s)
k: Boltzmann's constant ($1.39.10^{-23}$ J/K)
T: temperature (K)
F: frictional coefficient (kg/s)

For 400 nm, *F* is high because of the agglomerates present at low T_f. In this case, the diffusion is slow, or even nonexistent. So, no variation is detected whatever the cooling rate as the system can be considered as motionless.

On the contrary, for 40 nm-high temperature, *F* is small, and *D* high. However, no difference of the *R* values between the different firing conditions are detected as the system has become homogeneous because of the diffusion. For 40 nm-675°C, the three systems can be considered as stable and they are not more influenced by the cooling rate and their *R* values are similar.

For low temperature-40 nm size, the *R* values are more influenced by the cooling rate if we compare the more significant disparity with the results for the 400 nm-series. It comes from the smaller size of the particles that are more subjected to the diffusion. In this case, a motion can already been detected.

The same evolution is observed for high temperature-400nm size. *F* is small, and *D* is high but the system has not yet reached an equilibrium. In this case, the cooling rate still influences the values.

For optimal / intermediate temperatures, we can observe an intermediate situation. The glass wets the particles and disperses the agglomerates. *F* and *D* are characterised by medium values. In this case, we suppose a competition between a physical phenomenon (diffusion) and a chemical one (reactions).

Note that no specific correlation is found between the different cooling rates for a same T_f, but we will study it more in detail in the following part.

Another interpretation is that the evolution of the values can be due to some microscopic local strains between the particles, as explained for the commercial pastes.
The remaining strain can be extrinsic (macroscopic thermal mismatch between resistor and substrate) or intrinsic (local thermal mismatch between glass and conductive phase). Extrinsic

mismatch between Al_2O_3 and optimal 600°C firing resistors is thought to be small, as TCE values given for the glass [74] and RuO_2 (average [75]) are 8...9 and 5 ppm/K, close to the ca. 7 ppm/K value for Al_2O_3. However, the intrinsic, local thermal mismatches are much higher in the case of RuO_2-containing resistors. Rutile RuO_2 has anisotropic TCE values: +9 and -2 ppm/K for the a=b and c axes [75]. Upon quenching, strong tensile strains are therefore expected to be frozen in along the c axis (which could later relax during annealing).

- **Influence of the temperature-dwell time vs. the cooling rate**

In order to better explain the situation, we should isolate these two parameters and realise a more precise study on a single concentration for the optimal temperature. In this case, we would be able to explain the variation of the values vs the cooling rate.

A first step is to verify that the cooling rate is an influent parameter. We would like to dissociate the influence of slow cooling and long dwell temperature time. For 40 and 400 nm- grain sizes, and optimal T_f: 600 °C, we will firstly determine intermediate points by carrying out complementary cooling rates such as 0.5 and 20 °C/min, to confirm the trend. In the same time, the temperature-dwell time is increased (to 5h) to show that even for low cooling rates, the cooling phase is not merely an extension of the dwell-time. Indeed, for lower cooling rates, we remark that the temperature-dwell time is inevitably increased as the slope of the cooling is low. So, the samples stay during ~ 45 min at 600°C, instead of 15 min for the other samples (n and T). By comparing 15 min and 5 h dwell-time results, we will determine whether the cooling rate can be considered as a determining parameter or if it is due to a longer firing time. In this second case, the values should remain identical. It will allow knowing whether the cooling rate or the dwell time has more incidence on R and TCR values.

Figure 40 summarises the results of both experiments for both size series at 600 °C, as it depicts the evolution of *R* and TCR values for complementary cooling rates and the corresponding values for a temperature-dwell time of 5 h compared to 15 min dwell-time.

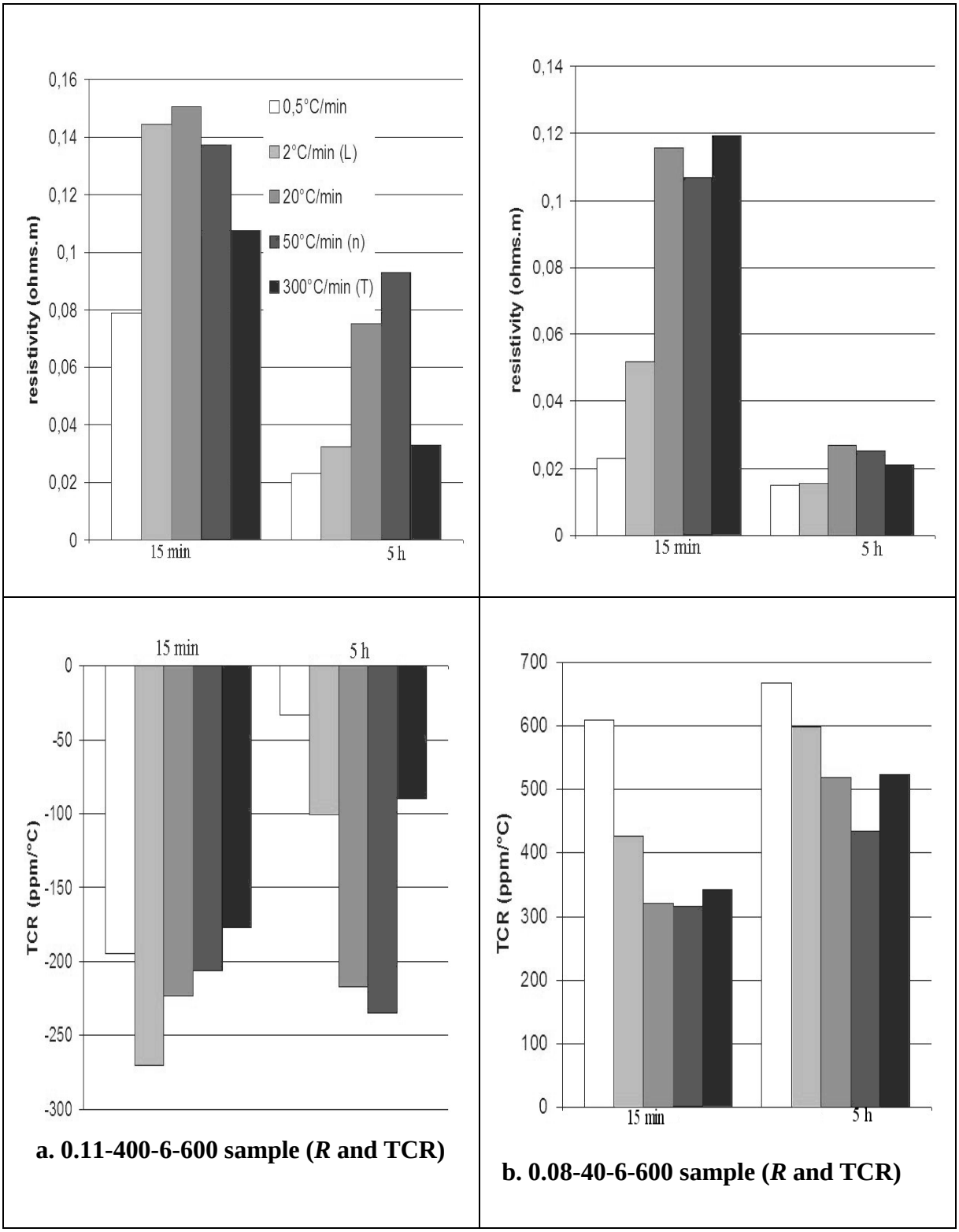

a. 0.11-400-6-600 sample (*R* and TCR)

b. 0.08-40-6-600 sample (*R* and TCR)

Figure 40: Influence of the dwell-time and of the cooling rate on *R* and TCR values (the caption is the same for each graph)

Both sizes show coherent and similar evolutions.

The complementary points allow to find a correlation between the different cooling rates for a same T_f, as the resistivity values increase when the cooling rates increase. At high cooling rates, this trend is reversed. This is observed on all 4 sets of samples. The opposite and coherent effect with the evolution of resistivity is obtained with TCR values, if we consider the possible errors of measurements (for instance, the higher the cooling rate, the lower the stability for the measurements. This is mostly the case for quenched samples).
The same trend is observed for 400 nm-size, but less marked.
The fact that the *R* values decreases for high cooling rates shows that several mechanisms concerning the evolution take place during the cooling step, namely mechanical (due to the material strain) and chemical evolution (due to the interaction with the particles).

Concerning the influence of the dwell-time, we observe that the values differ vs. the dwell-time. An increase of the dwell-time leads to a decrease of the resistivity value. It could be expected as increasing the time can favour the reactions and the generation of nanoconductive particles that could provoke a decrease of the resistivity.
We can deduce that the dwell-time seems more influent than the cooling rate.
Note that whatever the dwell-time is, the same trend remains: *R* values increases when the cooling rate increases (except for high cooling rates) (and the opposite for TCR), but for 5h-dwell, the *R* values are less dispersed (and consequently less influenced by the cooling rate).
Moreover, the difference between the *R* value of 15 min and 5 h seems to increase when the cooling increases (less marked for 400 nm-series). It shows that in the case of quenching, the cooling rate has nevertheless a small influence on the values, contrary to for low cooling rate, for which the values are nearly the same: in this case, the cooling rate has no more incidence. An equilibrium is reached.

We can conclude that there is a combined influence of the cooling rate and the dwell-time on *R* and TCR values.
The observations are the same as the 400 nm size but less marked. It could be due to the decrease of reactivity because of the smaller specific surface. A possible evolution to an equilibrium is less probable.
Moreover we observe that the most incoherent results correspond to the quenched values. This was predictable because of the high remaining intrinsic strains.

Whatever the conditions, no new phase or difference between the samples was observed by X-ray and SEM analysis, except for the series fired at 525°C. For this case, we can see the influence of the cooling rate. It emphasizes the fact that a slowly cooled rate sample stays at high temperature during longer time that a quenched sample. It allows in this case an improvement of the melting of the glass that is not complete when the sample is quenched (figure 41).

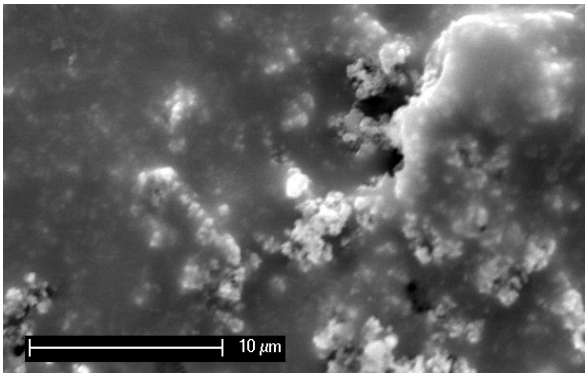

a. Quenched sample (T)

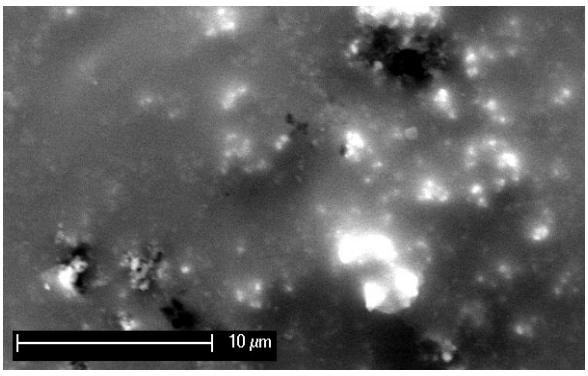

b. Slowly cooled sample (L)

Figure 41: 0.11-400-6-525 samples: quenched (a) and slowly cooled (b)

Quenched sample shows some agglomerates not yet wetted by the glass. On the contrary, if the cooling rate is decreased, the sample remains at high temperature during a longer time. A more homogeneous resistor is then obtained (although some agglomerates subsist because of the low T_f).

These results seem coherent with the behaviour of commercial pastes as the quenching decreases the resistivity values whereas an increased dwell-time decreases them.

IV . 6 . 1 . 2 . 2 . GF evolution

Similar experiments were carried out on cantilevers to measure the piezoresistive response.
Because of the lower number of samples, we chose to fire the cantilevers at optimal and high temperatures, as the low temperature seems less interesting (the glass not completely melted, poor diffusion...).
As explained for commercial pastes, the GF values are less influenced by the firing conditions. Figure 42 shows the evolution of the value of the longitudinal GFs (transversal GFs show the same trend) for quenched and slowly cooled 0.11-400 and 0.08-40 samples fired at 600 and 675°C.

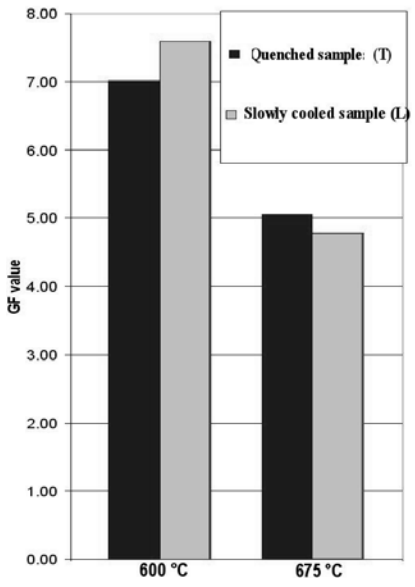

a. GF_l for 400 nm series

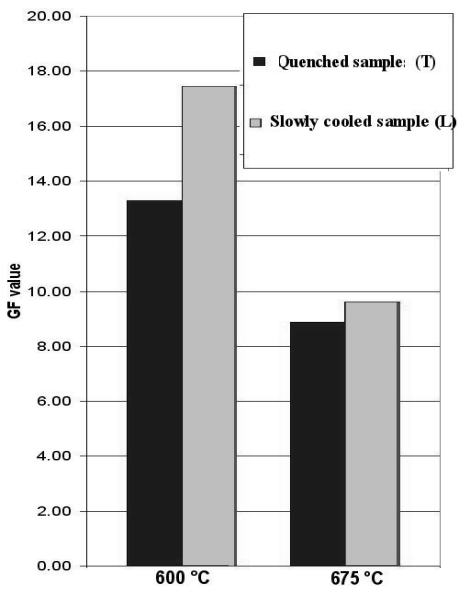

b. GF_l for 40 nm series

Figure 42: Evolution of the longitudinal GF for 400 (a) and 40 nm series (b)

We cannot conclude on the effect of the cooling rate. But the samples seem little influenced. Like commercial pastes, an increase of T_f provokes a decrease of the GF value which is coherent with the resistivity results, as high resistivity should generate high GF. It proves that the results are coherent with the previous measurements (*R* and TCR values).

IV . 6 . 1 . 3 . Processing sensitivity on the V2-system

IV . 6 . 1 . 3 . 1 . *R* and TCR evolution

This study is less detailed than the previous one, as the nearly same behaviours are observed. In figure 43 is depicted the evolution of *R* and TCR values for the both grain size series (400 - 40 nm) for each firing condition.

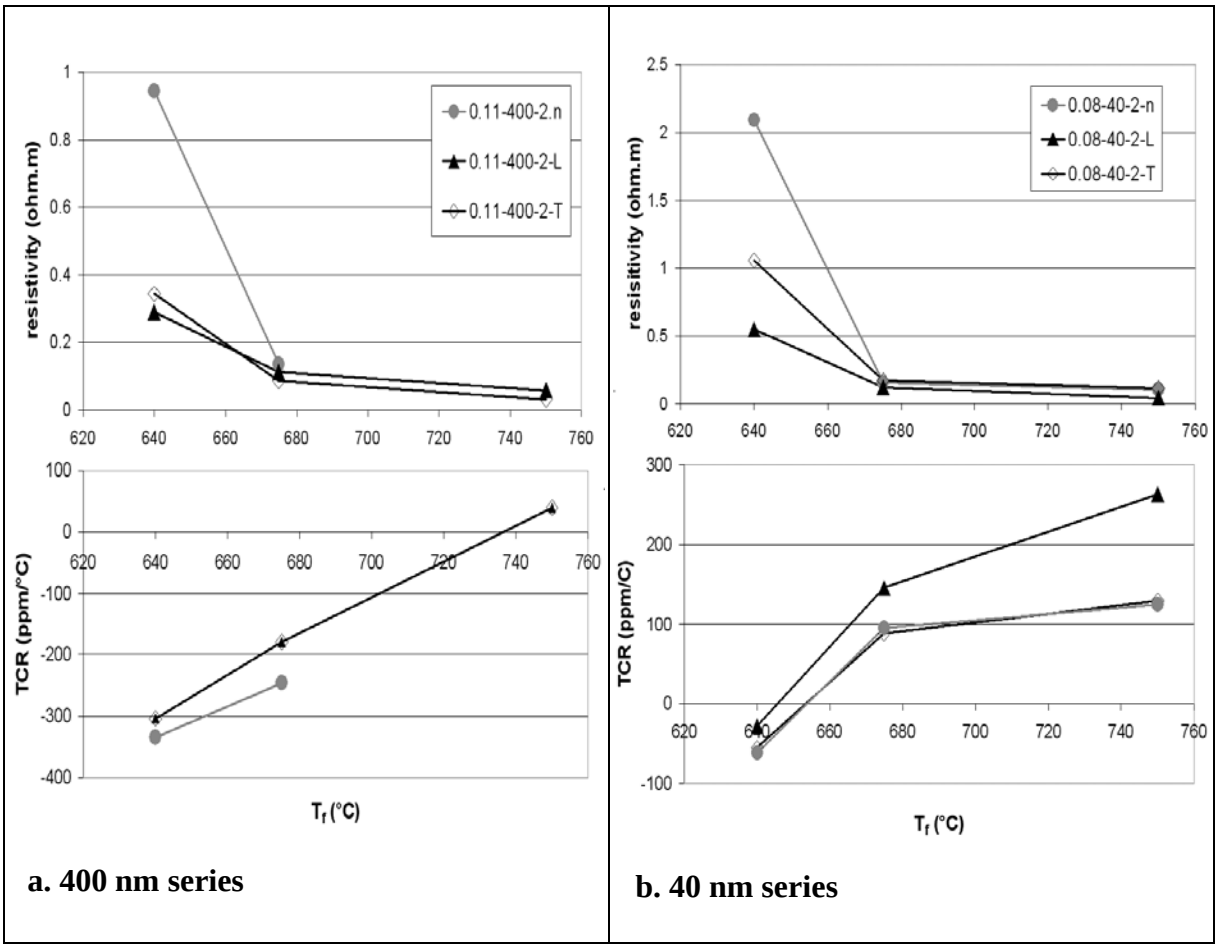

Figure 43: *R* and TCR evolution of 400 (a) and 40 nm-V2 series (b) according to the cooling rate

It is shown that the resistivity values decrease when T_f increases, whatever the cooling rate. The opposite and coherent trend is observed for TCR values.
For intermediate and high T_f, the discrepancy of the *R* values is very low. The samples seem not influenced by high T_f. In fact, it appears that at low T_f, the particles already diffuse contrary to the V6-series. Indeed, as T_f is higher for the V2-series, we can suppose that for low T_f the situation of the system corresponds to the intermediate situation of the V6-system (600 °C). In this case, for low T_f (640 °C), the *D* and *F* values are medium, and the particles can be influenced by a diffusion phenomenon. At intermediate temperature (675°C) the system has already reached an equilibrium.

Concerning the influence of the cooling rate on the resistivity values (mostly for low T_f, no correlation can be found because of the lack of points). It was the same situation for the previous V6-system.

Concerning the structural behaviour, SEM images show that the quenching leads to less homogeneous systems (figure 44). The same behaviour is observed whatever T_f.

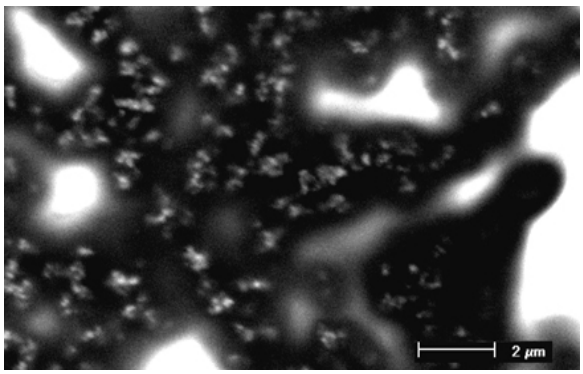

a. Quenched sample (T)

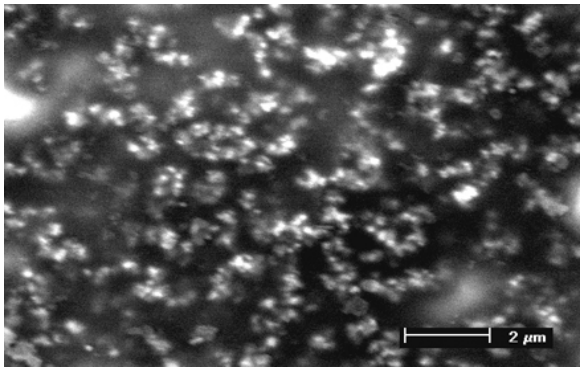

b. Slowly cooled sample (L)

Figure 44: 0.11-400-2-675 samples: quenched (a) and slowly cooled (b)

We can expect that the behaviour of the V2-series would be the same as the V6-series if we had realised some complementary cooling rates.

IV . 6 . 1 . 3 . 2 . GF evolution

Figure 45 shows the evolution of the GF_L values for quenched and slowly cooled 0.11-400 and 0.08-40 samples fired at 675 and 750 °C.

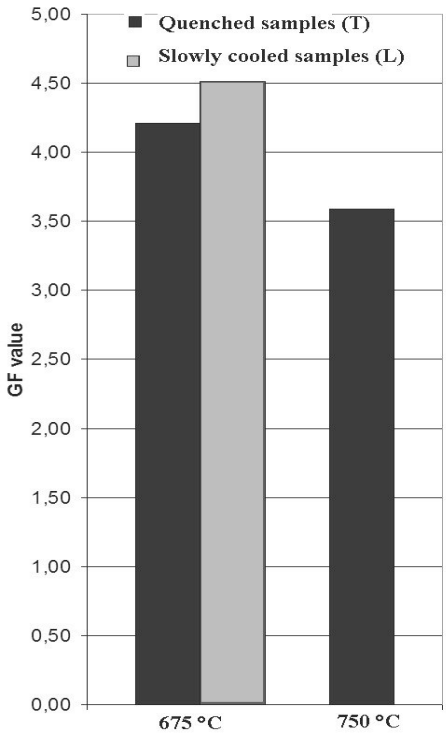

a. GF_L for 400 nm series

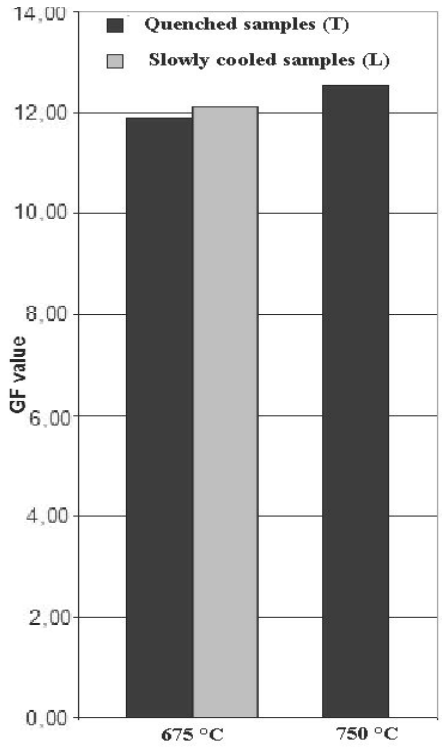

b. GF_L for 40 nm series

Figure 45: Evolution of longitudinal GF for 400 (a) and 40 nm series (b)

The trend seems to be the same as the V6-series mostly for the 400 nm grain size, as an increase of T_f provokes a decrease of the GF value, which is coherent with the resistivity results, as high resistivity should generate high GF. It proves that the results are coherent with the previous measurements (*R* and TCR values).
For 40 nm size, the phenomenon is less marked and should be confirmed by additional experiments.

IV . 6 . 1 . 4 . Processing sensitivity on the V8-system

We reported that the V8-system is characterised by unstable measurements because of technological problems (cracks). Subjecting these samples to such «extreme» firing conditions would not bring significant results, as it could accentuate the instability.

However, we did decide to take an interest on the evolution of the microstructure, and to study the influence of the temperature and dwell-time. This was prompted by the fact that V8 lies at the boundary between the RuO_2 and $Pb_2Ru_2O_6$ stability fields.

Firstly, we observed in the previous section that the system appears more homogeneous for high temperature (650°C) (figure 30). Moreover, if the 400 nm series is fired at high temperature (650°C) during 3h, a new phase can be detected by X-ray analysis (figure 46).

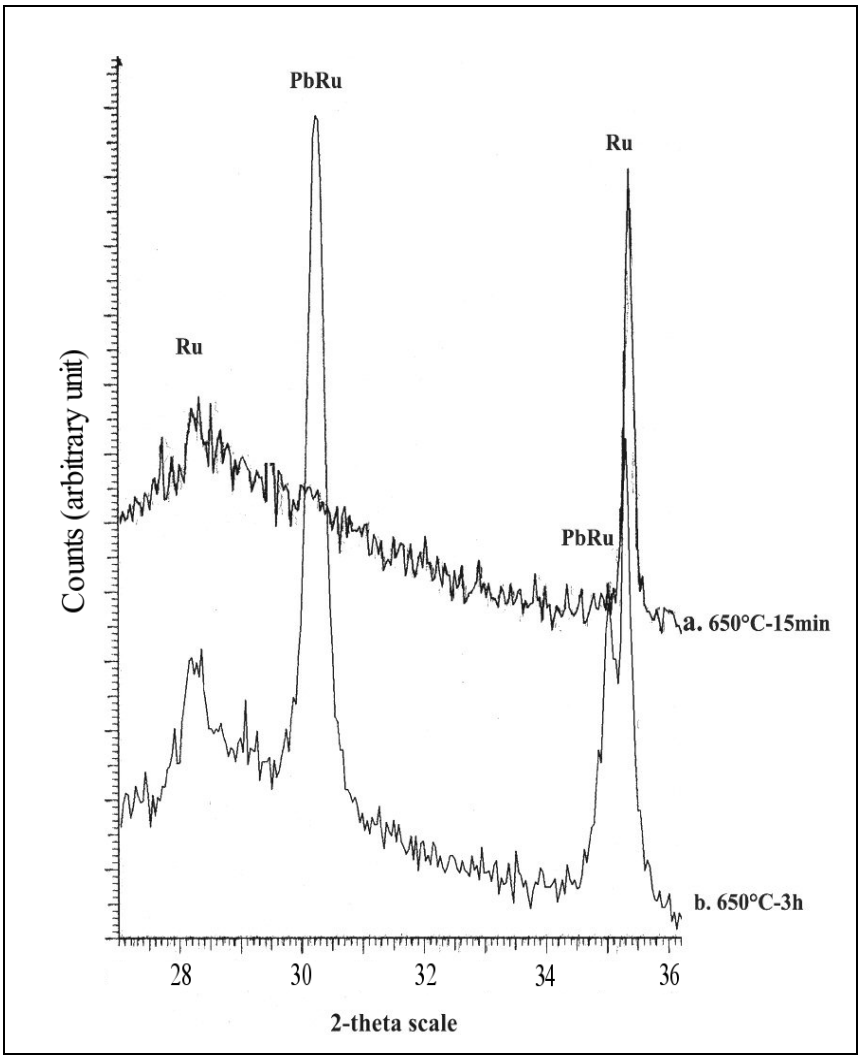

Figure 46: X-ray spectra of 0.11-400 sample fired at 650°C during 15 min (a) and 3 h (b)

The additional peaks (PbRu) correspond to the $Pb_2Ru_2O_6$ phase. However, no new phase is detected for the 40 nm-series (Ru corresponds to RuO_2 peaks).

In a second time, we decided to over-fire the same sample (800°C-15min) to determine the predominant parameter (temperature of firing or dwell-time) for the formation of lead ruthenate (figure 47).

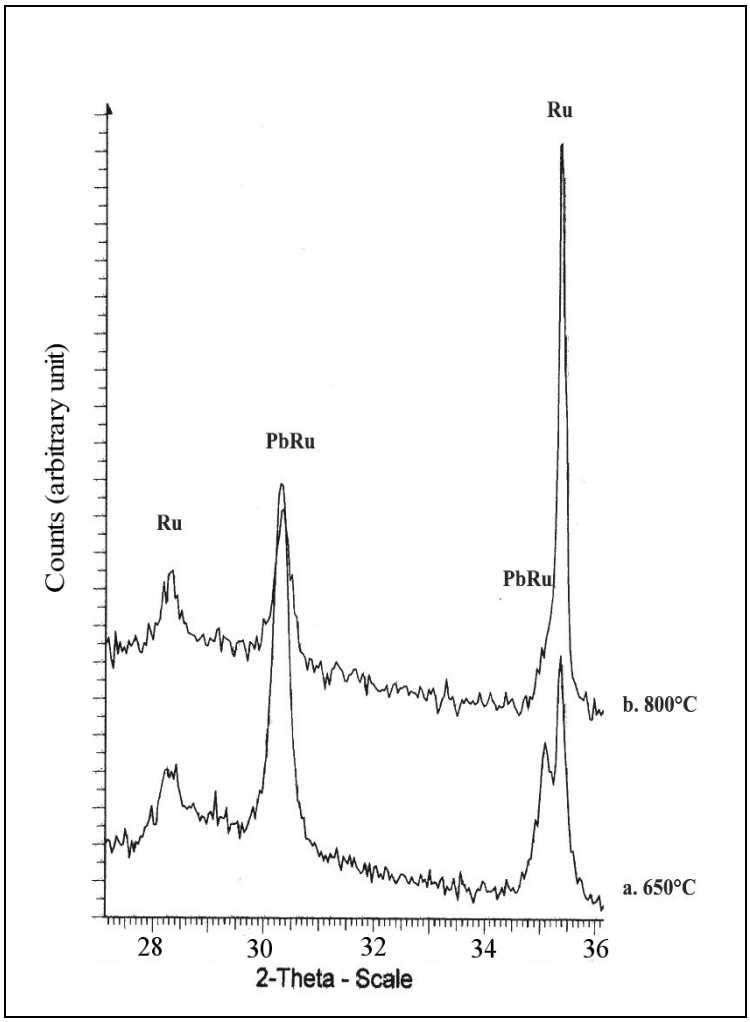

Figure 47: X-ray spectra of 0.11-400 sample fired at 650°C-3h(a) and 800°C-15min(b)

If we compare the ruthenate peaks, it appears that the peaks corresponding to the 650°C-3h sample are more important than the one fired at 800°C-15min. Apparently, increasing the dwell time has more effect than increasing the firing temperature in promoting ruthenate formation.

Note that it is easy to observe the increase of ruthenate. On the other hand, we should observe a proportional decrease of RuO_2, but this behaviour is not predominant.
This new phase can be explained by the fact that ruthenate phases are more stable in high-lead glasses [12]. Moreover, according to Morten et al [76,77], the decomposition of lead-ruthenate into RuO_2 is expected for firing temperatures between 800 and 1000°C, which indicates that the ruthenate is also thermodynamically favoured at low temperatures. In our case, at 650°C during 3h, the components tend to reach an equilibrium. Then, the ruthenate phase is favoured. At 800°C, 15min, the driving force for ruthenate formation decreases. No increase of ruthenate is expected at this temperature as in the range 800-1000°C, the RuO_2 phase is favoured.
Moreover, for this glass composition, the conductive phase compound should be stabilised, if fired at 850°C, as showed in the diagram of stability of Adachi and Kuno (figure 25). Indeed, the V8 glass composition corresponds to a stable system in which the initial conductive phases should remain stable around 850°C.

SEM analyses allow to illustrate the fact that some structural modifications occur when the 400nm-samples are fired during 15 min and 3 h (figure 48).

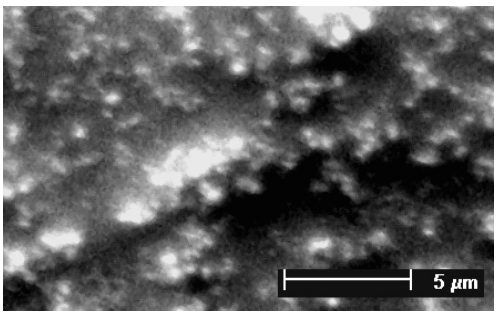

a. 0.11-400-8-650°C - 15 min

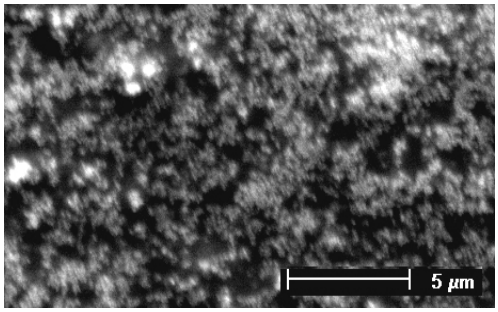

b. 0.11-400-8-650°C - 3h

Figure 48: SEM surface observation of a 400 nm sample fired at 650°C during 15 min (a) and 3 h (b)

It is evident that the sample fired during 3h shows a finer microstructure. The conductive particles are smaller and their concentration seems higher.

A strange and incoherent result is that no new phase is detected for the 40 nm series, despite of the fact that several samples were tested. Yet such reactions should be favoured in the case of smaller conductive particles as the corresponding specific area is more important, which is not the case. This phenomenon could be explained by a less favoured nucleation of the ruthenate phase with smaller particles of RuO_2. Indeed, it could be due to the difference of morphology and size of the two series of RuO_2 powders that can affect their surface reactivity.
Another explanation is that a possible new phase is generated but the nanoparticles are too small and too isolated to be detected.

IV . 6 . 1 . 5 . Conclusion

R, TCR and GF values are coherent as a high resistivity is associated to a low TCR and to a high GF, which shows that the obtained values are representative.
V6 and V2-series are in accordance with the results of the commercial pastes. Indeed, coherent behaviour is observed: the increase of the cooling rate increases the resistivity values, whereas the increase of dwell-time decreases them. We observe a combined influence of the cooling rate and the temperature dwell-time on *R* and TCR values.
The evolution of the values can be explained by diffusion phenomenon and local microscopic strains due to important cooling rates.
On the opposite, low cooling rates allow to homogenise the microstructure of the resistors.

Concerning the V8-series, the influence of dwell-time and temperature were studied, whereas the effect of the cooling rate were not because of the instability of the resistor. A new phase (lead ruthenate) was detected for the only 400 nm-series.

IV . 6 . 2 . Post annealing study - stability in high-temperature storage

After firing, the samples are subjected to long-term annealing cycles at 250°C in order to ascertain their stability.
Measurements are performed after firing and ex situ during annealing, by periodically removing the samples from the annealing oven.
R, TCR and GF values are measured by the same way as previous experiments.

In general, 40 and 400 nm size series are characterised by the same trend. This is why only representative samples will be presented in the following study. The chosen samples are:
- 0.11-400-6 for low, medium and high temperatures (corresponding to the previous experiments),
- 0.08-40-2 for low, medium and high temperatures (corresponding to the previous experiments),
- 0.08-40-8 and 0.07-40-8 at 500°C as they were not subjected to «extreme» firing conditions.

Moreover, we will take an interest only on the evolution of the electrical properties, as no significant change of microstructure or XRD spectrum was observed.

IV . 6 . 2 . 1 . Evolution of *R*

The following figures (49, 50, 51) show the evolution of the *R* value during the annealing time, for the V6, V2 and V8 series.

.

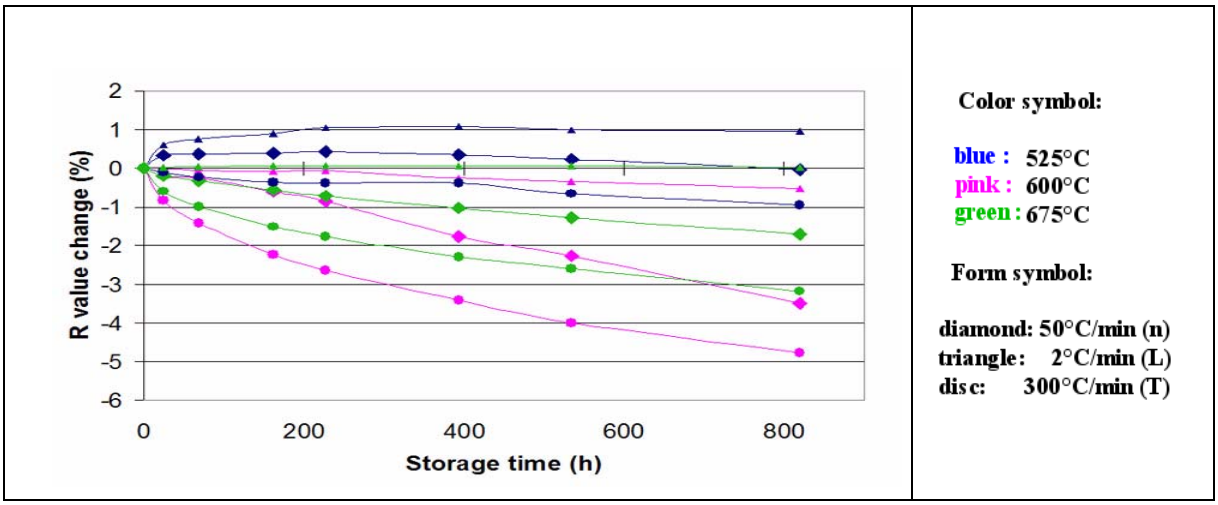

Figure 49: Relative change of the resistivity of the 0.11-400-6 sample during the annealing

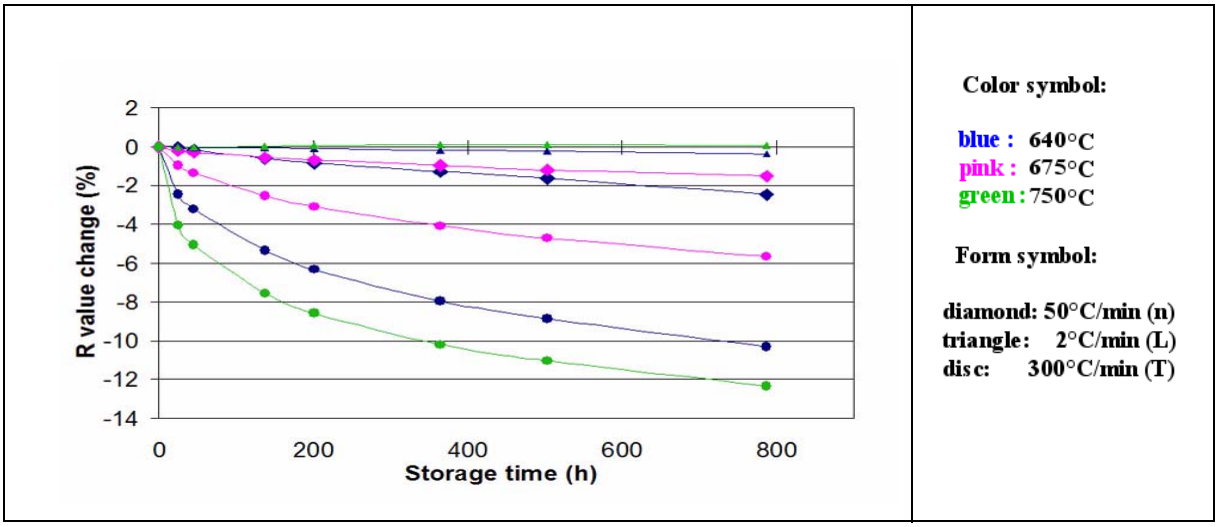

Figure 50: Relative change of the resistivity of the 0.08-40-2 sample during the annealing

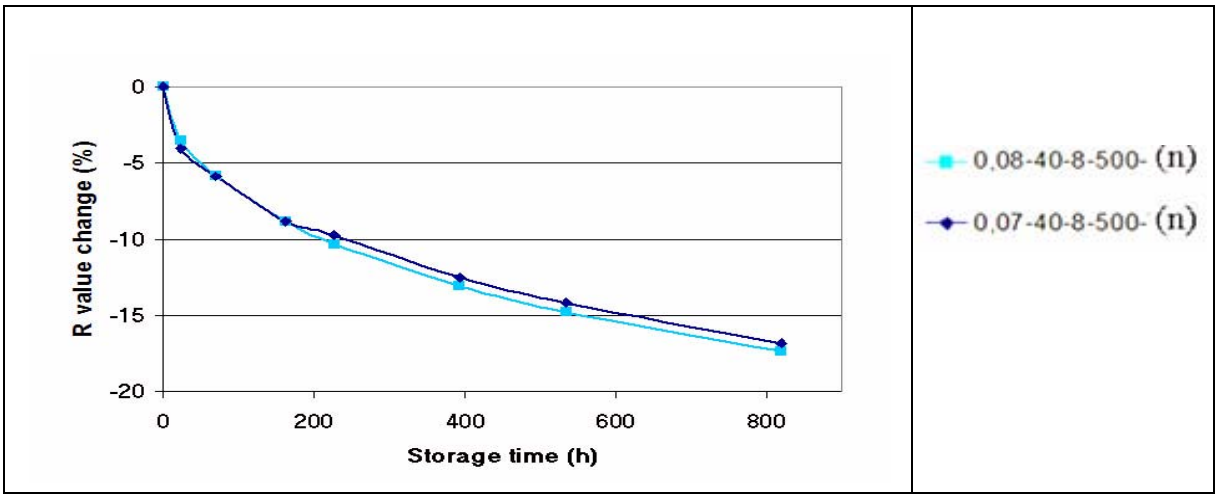

Figure 51: Relative change of the resistivity of the 0.08 and 0.07-40-8-500°C sample during the annealing

Concerning the V6-series (figure 49), the slowly cooled samples (triangles) show a relatively good stability (< 1%) of the *R* value during the annealing time. On the opposite, the quenched samples (discs) show a decrease of the *R* value (variation ~ 5 %). For the 40 nm grain size, this instability is more marked (variation ~ 10 %). Moreover, we can observe that the samples fired at low T_f (525 °C) are the most stable, whatever the cooling rates.

Concerning the V2 series (figure 50), the same trend as the V6-series concerning the influence of the cooling rate is observed, with more significant variations (maximum ~ 10 %) and a more marked difference between quenched and slower cooled samples. However, contrary to the previous series, the firing temperature does not seem to influence the stability.
This behaviour is observed for both particle sizes, although the 400nm series appears to be more stable (variation < 3%).

The V8-series (figure 51) shows the most important instability (~ 18%), which was predictable from the very low firing temperature of the glass. The evolution is identical for both samples. They show a progressive decrease of the *R* value, and they don't seem to be stabilised after 800h of annealing, contrary to the two previous series. The regularity of the progression of the *R* values emphasizes the fact that the behaviour of these samples is governed by a continuous phenomenon that evolves and that could be compared to a strain relaxation occurring at 250°C. During the high temperature storage, the strains can relax, phenomenon that is shown by a decrease of the standard deviation of the resistivity value vs. the storage time. In fact, the high temperature storage allows to relax the strains and to decrease the influence of humidity, which leads to a stopping of the progression of the cracks.

If we compare the three series,V6 and V2-categories appear the most stable during the annealing time. This emphasises the fact that few microscopic strains were generated during the firing process. Moreover, after an annealing time of 800 h, the values seem to be stabilised, contrary to the V8-samples.

IV . 6 . 2 . 2 . TCR evolution

The following figures (52, 53, 54) show the evolution of the TCR values during the annealing time, for the V6, V2 and V8 series.

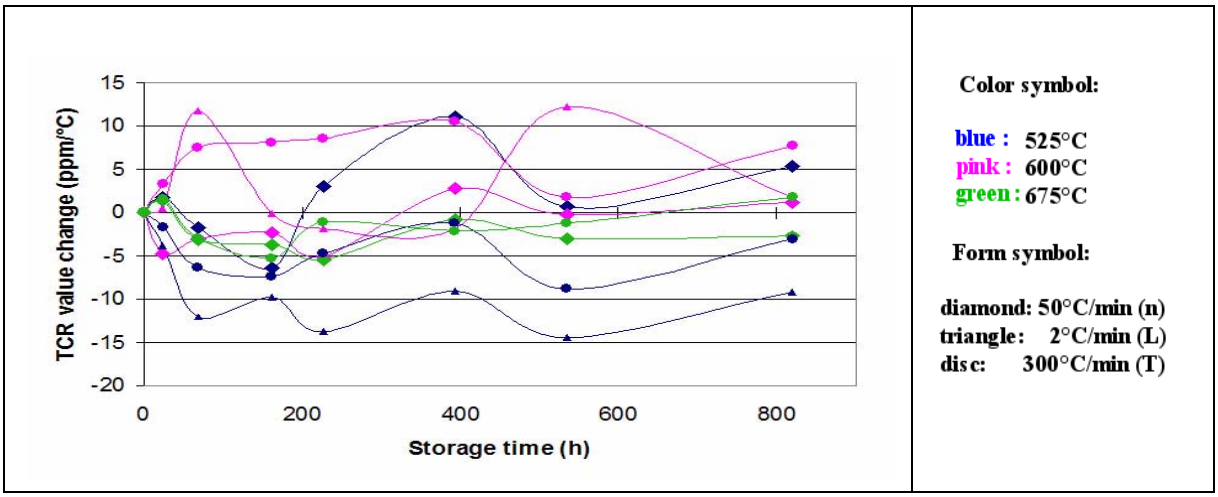

Figure 52: Relative change of TCR of the 0.11-400-6 sample during the annealing

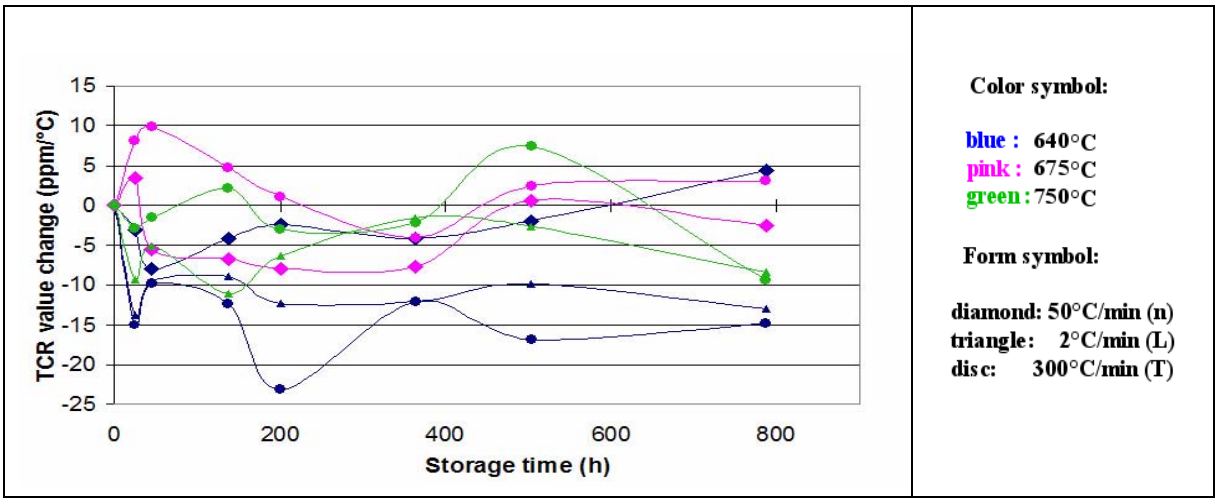

Figure 53: Relative change of TCR of the 0.08-40-2 sample during the annealing

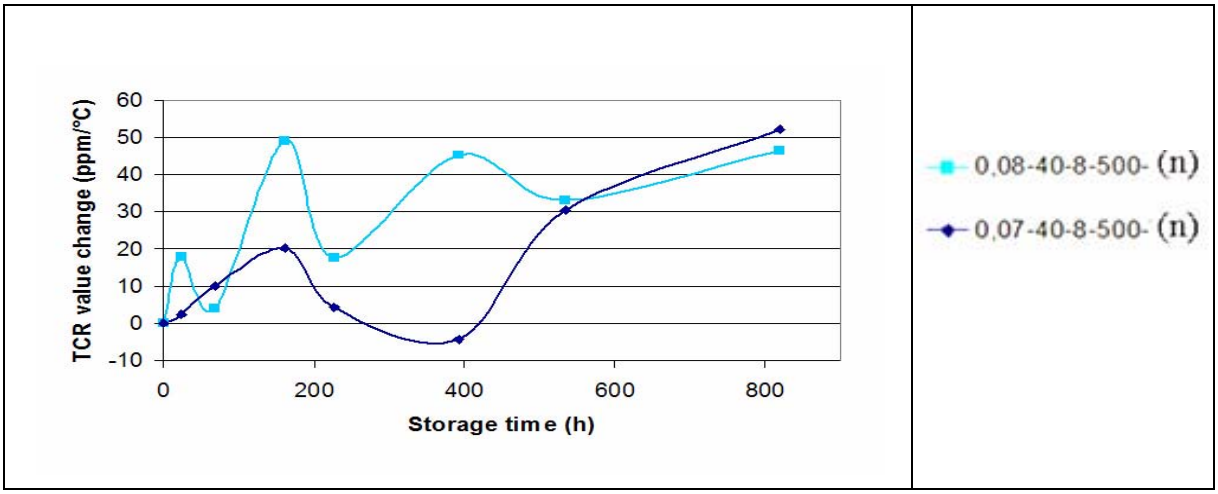

Figure 54: Relative change of the TCR of the 0.08 and 0.07-40-8-500°C sample during the annealing

Concerning the V6 and V2-series (figures 52, 53), they are characterised by the nearly same trend as their maximum variation is about 10-15 ppm/°C. Although it is difficult to emphasise a trend, it seems that the samples fired at high temperature appear to be more stable. This trend is validated by both particle sizes, even if the 40nm-V6 series seems to be the less stable (TCR change > 30 ppm/°C).
However, no correlation has been found between the stability and the cooling rates.

The variations of V8-TCR values (figure 54) are more significant (until 50 ppm/°C), the time of annealing does not seem to stabilise them. But it subsists a coherence between the *R* and TCR values as *R* decreases during the annealing whereas TCR increases.

IV . 6 . 2 . 3 . GF evolution

The following figures (55, 56) show the evolution of the longitudinal GF values during the annealing time, for the V6 and V2 series.
To present clearer results, only the evolution of GF_L is presented, knowing that the GF_T evolution follows the same trend.
No results are presented for the V8-series, because of its remaining instability (presence of cracks). The incoherence of the GF value is due to the cracks that lead to a continuous drift of the values.

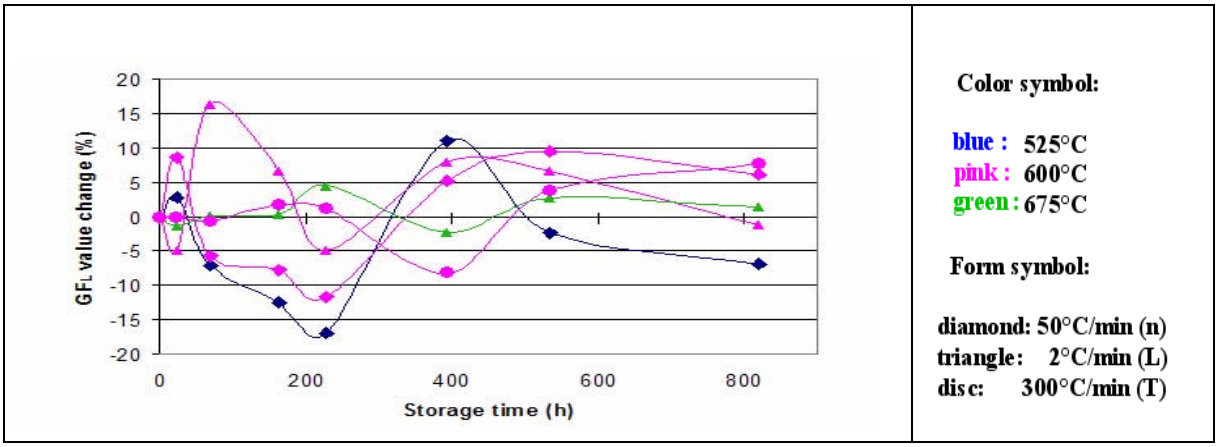

Figure 55: Relative change of the Gf_L value of the 0.11-400-6 sample during the annealing

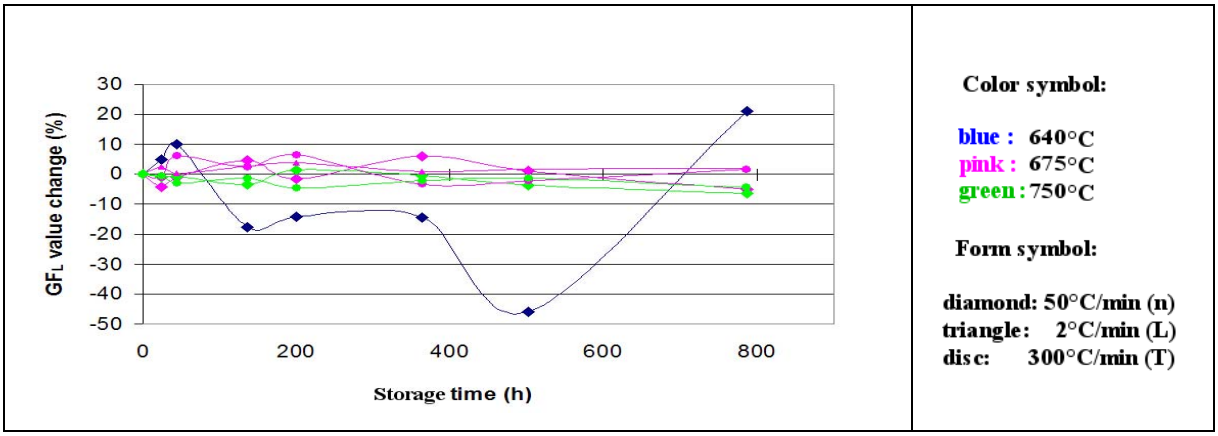

Figure 56: Relative change of the GF_L value of the 0.08-40-2 sample during the annealing

If we exclude the 0.08-40-2-640°C sample, the V6-series shows a more important variation (~15 %) than the V2-series (< 10%). This behaviour is due to the fact that the V2-series is less influenced by the annealing because of its higher T_f process. The instability of the 0.08-40-2-640°C sample could be due to its low firing temperature (640 °C).
Concerning the V6 series, the 40 nm grain size shows a less important variation (< 15%) than the 400nm grain size.
Whatever the series are, the GF values seem to be stabilised after 800 h of annealing.

IV . 6 . 2 . 4 . Conclusion

Upon annealing at 250°C, similar results are obtained for GF and TCR. Also, no significant change of microstructure or XRD spectrum is observed. The stability of the microstructure and GF is in accordance with some authors [78], as they explain that GFs of thick-film resistors depend to a greater extent on the microstructure of the material.

However, *R* changes significantly at 250°C and its evolution is dependent on the firing schedule. The evolution of *R* upon annealing was also found to depend strongly on the cooling rate for commercial and home-made pastes. The slower the cooling rate is, the more stable the *R* value is. This observation is common to the commercial and experimental pastes.
Moreover, in general, stability of commercial pastes for a given cooling rate was found to increase with the firing thermal budget. Our pastes depend on the firing temperature but their behaviour differs. Indeed, for the V6-series, decreasing the firing thermal budget significantly improves stability, while for the V2-series the firing temperature does not seem to influence the stability.

It is evident that these new series of pastes are not as stable as DP2041 (*R* change < 1.0%). Their variations are much similar to the ESL3414 or 3114 pastes. Like commercial pastes, the evolution tends to saturate, and even be partially reversed after ca. 200h, as observed by Cattaneo et al [79].
If we compare the three experimental pastes, in spite of the much lower firing temperature of V6, its thermal stability is comparable to that of V2. These two experimental pastes can be compared respectively to ESL 3114 and DP 2041, because of their difference of firing temperature. The pastes based on the V8 glass present the higher instability, because of its lowest firing temperature.

At 250°C, possible evolution mechanisms could involve Ru in glass (dissolved or in clusters [12]), or mechanical relaxation. Our investigation methods did not allow direct assessment of Ru in glass, but local rearrangement of Ru in glass during annealing such as precipitation of supersaturated Ru into clusters cannot be ruled out.
Mechanical strain relaxation can be extrinsic (macroscopic thermal mismatch between resistor and substrate) or intrinsic (local thermal mismatch between glass and conductive phase), as explained before, which can later relax during annealing.

IV . 7 . Conclusion

These three different series of pastes allow us to study different aspects of the thick-film technology.
The V6-category was used to validate our hypothesis about the conduction mechanism. It appears that the nonuniversal behaviour of tunnelling-percolation mechanism can be demonstrated by applying an external force to the system - aspect that has never been described in the literature.
Moreover, we showed that the electrical properties are depend on different parameters such the conductive concentration, T_f or the dwell time.
The V2-series study emphasized our hypothesis concerning the conduction mechanism, although the results were more ambiguous.
The V8 system was too instable to realise the same study and we preferred to find solutions to decrease the internal strains due to difference of TCE between the different materials. Moreover, the hypothesis of cracks due to thermal strains was validated by a more regular and less anarchic evolution of the values of the paste at 250°C.

Whatever the paste category is, structural analysis does not in general reveal the apparition of new phases, but shows a dependence of the microstructure vs. T_f. Also, reactions between the substrate and the glass of the resistor were observed at high T_f, leading to a modification of the homogeneity of the bulk resistor and thereby to a change of the electrical values.

After the analysis of the properties of these new pastes, their stability was studied, because of limited available information in literature concerning the effect of firing schedule, particularly of quenching and to compare them to the commercial paste stability.
The influence of the firing schedule on the properties (*R*, GF and TCR) was found to be different for the three tested compositions. But, their corresponding values were coherent as a high resistivity is associated to a low TCR and to a high GF.
V6 and V2-series are in accordance with the results of the commercial pastes. Overall, the increase of the cooling rate increases the resistivity values, whereas the increase of dwell-time decreases them. In fact, we observe a combined influence of the cooling rate and the temperature dwell-time on *R* and TCR values.
The evolution of the values can be explained by diffusion phenomenon and local microscopic strains due to important cooling rates.
However, V8 appears to be strongly influenced by the dwell-time and temperature. A new phase (lead ruthenate) was detected only for the 400 nm-series. The absence of this new phase for the 40 nm-series could be explained by the difference of morphology between the two series of particles that can influence the nucleation.

Upon annealing at 250°C, only *R* changes significantly, and its stability was found to strongly depend on composition and firing schedule. V8 exhibited the highest changes, whereas V2 and V6 had comparable stability.
Modifying the cooling speed and the firing temperature affects both properties and annealing behaviour. This could come from supersaturated Ru in the glass or from frozen-in local strains between conductive phase and glass matrix.

From a scientific point of view, this first step allowed to show that nanostructure, conduction and properties are intimately linked. By choosing adequate and relevant composition, structure and firing, we proposed a new way to unveil the conduction process that has not been yet elucidated. But this trend should be confirmed by other complementary experiments.

From a technical point of view, it is evident that these pastes could be optimised through better stability, higher GF or adapted TCR. However they present a large range of applications because of their different T_f and their different TCRs. Thanks to this particularity, these pastes could be used on different substrates.
Some applications will be then presented in the following chapter.

References - Chapter IV:

1. Stauffer D, Aharony A, *Introduction to percolation theory*, Taylor and Francis, London, 1994.
2. Sahimi M, *Heterogeneous materials I: linear transport and optical properties*, Springer, New York, 2003.
3. Carcia PF, Ferretti A, Suna A, *Particle size effects in thick film resistors*, J. Appl. Phys., 1982, **53**, 5282-8.
4. Carcia PF, Suna A, Childers WD, *Electrical conduction and strain sensitivity in RuO_2 thick film resistors*, J. Appl. Phys., 1983, **54**, 6002-8.
5. Tamborin M, Piccinini M, Prudenziati M, Morten B, *Piezoresistive properties of RuO_2-based thick-film resistors: the effect of RuO_2 grain size*, Sensors and Actuators A, 1997, **58**, 159-64.
6. Clerc JP, Podolskiy VA, Sarychev AK, Eur. Phys. J. B, 2000, **15**, 507.
7. Soares BG, Gamboa KMN, Ferreira AJB, Ueti E, Camargo SS, J. Appl. Polymer Science, 1998, **69**, 825.
8. Adachi K, Iida S, Ishigame J, Sekihara S, *Microstructural glass modifications in as-fired and high-voltage-surged thick-film resistors*, J. Mater. Res., 1991, **6**, 1729-35.
9. Hrovat M, Samardzija Z, Holc J, Belavic D, *Microstructural, XRD and electrical characterization of some thick film resistors*, Journal of materials science: materials in electronics, 2000, **11**, 199-208.
10. Batrouni GG, Hansen A, Larson B, Phys. rev. E, 1996, **53**, 2292.
11. Normand JM, Herrmann HJ, Int. J. Mod. Phys. C, 1995, **6**, 813.
12. Adachi K, Iida S, Hayashi K, *Ruthenium clusters in lead-borosilicate glass in thick film resistors*, J. Mater. Res., 1994, **9**, 1866-78.
13. Pike GE, in Electrical Transport and Optical Propertiesof Inhomogeneous Media, edited by J. C. Garland and D.B. Tanner (American Institute of Physics, New York, 1978), 366.
14. Flandin L, Chang A, Nazarenko S, Hiltner A, Baer E, J. Appl. Polymer Sci., 2000, **76**, 894.
15. Dziedzic A, Inform. MIDEM **31**, 2001, 141.
16. Heaney MB, *Measurement and interpretation of nonuniversal critical exponents in disordered conductor-insulator composites*, Phys. Rev. B, 1995, **52**, 12477-80.
17. Flandin L, Prasse T, Schueler R, Schulte K, Bauhofer W, Cavaille JY, Phys. Rev. B, 1999, **59**, 14349.
18. Rubin Z, Sunshine SA, Heaney MB, Bloom I, Balberg I, Phys. Rev. B, 1999, **59**, 12196.
19. Nakamura S, Saito K, Sawa G, Kitagawa K, Jpn. J. Appl. Phys., 1997, **36**, 5163.
20. Mandal P, Neumann A, Jansen AGM, Wyder P, Deltour R, Phys. Rev. B, 1997, **55**, 452.
21. Celzard A, Mc Rae E, Mareche JF, Furdin G, Dufort M, Deleuze C, J. Phys. Chem. Solids, 1996, **57**, 715.

22. Carmona F, Mourey C, J. Mater. Sci., 1992, **27**, 1322

23. Carmona F, Canet R, Delhaes S, J. Appl. Phys. 1987, **61**, 2550.

24. Czarczynska H, Dziedzic A, Licznerski BW, Lukaszewicz M, Seweryn A, Microelectron. J., 1993, **24**, 689.

25. Kubat J, Kuzel R, Krivka I, Bengston S, Prokes J, Stefan O, Synthetic Metals, 1993, **54**, 187.

26. Adriaanse LJ, Brom HB, Michels MAJ, Brokken-Zijp JCM, Phys. Rev. B, 1997, **55**, 9383.

27. Chen CC, Chou YC, Phys. Rev. Lett., 1985, **54**, 2529.

28. Quivy A, Deltour R, Jansen AGM, Wyder P, Phys. Rev. B, 1989, **39**, 1026.

29. Van der Putten D, Moonen JT, Brom HB, Brokken-Zijp JCM, Michels MAJ, Phys. Rev. Lett., 1992, **69**, 494.

30. Chakrabarty RK, Bardhan KK, Basu A, Phys.Rev. B, 1991, **44**, 6773.

31. Hindermann-Bishoff M, Ehrburger-Dolle F, Carbon, 2001, **39**, 375.

32. Foulger SH, J. Appl. Polymer Sci., 1999, **72**, 1573.

33. Fournier J, Boiteux G, Seytre G, Marichy G, Synthetic Metals , 1997, **84**, 839.

34. Angus HC, Gainsbury PE, Electronic components, 1968, **9**, 84.

35. Vest RW, Conduction Mechanisms in Thick-Film Microcircuits Final Technical Report, ARPA Order (PurdueResearch Foundation, Ind., 1975), 1642.

36. De Jeu WH, Geuskens RWJ, Pike GE, J. Appl.Phys., 1981, **52**, 4128.

37. Bobran K, Kusy A, J. Phys. Condens. Matter, 1991, **3**, 7015.

38. Szpytma A, Kusy A, Thin Solid Films, 1984, **121**, 263.

39. Kusy A, Physica B, 1997, **240**, 226.

40. Listkiewicz E, Kusy A, Thin Solid Films, 1985, **130**, 1.

41. Kubov´y A, J. Phys. D: Appl. Phys., 1986, **19**, 2171.

42. Dziedzic A, Materials Science, 1987, **13**, 199.

43. Chiteme C, McLachlan DS, Phys. Rev. B, 2003, **67**, 024206.

44. Lee SI, Song Y, Noh TW, Chen XD, Gaines JR, Phys. Rev. B, 1986, **34**, 6719.

45. Youngs IJ, J. Phys. D: Appl. Phys., **35**, 2002, 3127.

46. Abeles B, Pinch HL, Gittleman JI, Phys. Rev.Lett., 1975, **35**, 247.

47. Deptuck D, Harrison JP, Zawadzki P, Phys. Rev.Lett., 1985, **54**, 913.

48. Mamunya YP, Davydenko VV, Pissis P, Lebedev EV, Eur. Polymer J., 2002, **38**, 1887.

49. Song Y, Noh TW, Lee SI, Gaines JR, Phys.Rev. B, 1986, **33**, 904.

50. Chen YJ, Zhang XY, Cai TY, Li ZY, Chin.Phys. Lett., 2003, **20**, 721.

51. Maaroufi A, Haboubi K, El Amarti A, Carmona F, J. Mater. Sci., 2004, **39**, 265.

52. Sun J, Gerberich WW, Francis LF, J. Polymer Sci. B, 2003, **41**, 1744.

53. Kogut PM, Straley JP, J. Phys. C: Solid State Phys., 1979, **12**, 2151.

54. Halperin BI, Feng S, Sen PN, Phys. Rev. Lett., 1985, **54**, 2391.

55. Balberg I, Phys. Rev. Lett., 1987, **59**, 1305.

56. Balberg I, Phys. Rev. B, 1998, **57**, 13351.

57. Kirkpatrick S, *Percolation and conduction,* Rev. Mod. Phys., 1973, **45**, 574-88.

58. Prudenziati M, Morten B, Cilloni F, Ruffi G, Sens. Actuators. 1989, **19**, 401.

59. Grimaldi C, Ryser P, Straessler S, *Gauge factor enhancement driven by heterogeneity in thick-film resistors,* J. Appl. Phys., 2001, **90**, 322-7.

60. Grimaldi C, Maeder T, Ryser P, and Straessler S, J. Phys. D: Appl. Phys., 2003, **36**, 1341.

61. Vionnet-Menot S, Grimaldi C, Maeder T, Straessler S. Ryser P, *Tunneling-percolation origin of nonuniversality: Theory and experiments,* Phys. Rev. B, 2005, **71**, 064201-1-12.

62. Kuo CY, Blank HC, Proceedings of the ISHM Symposium - Montgomery, 1968, 153-60.

63. Hrovat M, Samardzija Z, Holc J, Belavic D, *Microstructural and electrical characteristics of some «overfired» thick-film resistors,* J. mat. sc. lett., 2001, **20**, 347-51.

64. Prudenziati M, Morten B, Cilloni F, Ruffi G, Sacchi M, *Interactions between alumina and high lead glasses for hybrid components,* J. appl. phys, 1989, **65**, 146-53.

65. Ewen PJS, Robertson JM, *Percolation model of conduction in segregated systems of metallic and insulating materials: application to thick film resistors,* J phys. D: Appl. Phys., 1981, **14**, 2253-68.

66. Adachi K, Kuno H, *Decomposition of ruthenium oxides in lead borosilicate glass*, J. Am. Ceram. Soc., 1997, **80**, 1055-64.

67. Adachi K, Kuno H, *Effect of glass composition on the electrical properties of thick film resistors,* J. Am. Ceram. Soc., 2000, **83**, 2441-48.

68. Maeder T, Jacq C, Birol H, Ryser P, *Strength of ceramic substrates for piezoresistive thick-film sensor applications,* European microelectronics and Packaging Symposium, Prague-june 2004, in press.

69. Adams R, McMillan PW, *Review static fatigue in glass,* J. of Mat. Sci., 1977, **12**, 643-57.

70. Lü BT, *Fatigue strength prediction of soda-lime glass,* Theoretical and applied fracture mechanics, 1997, **27**, 107-14.

71. Maeder T, Grimaldi C, Ryser P, *Properties of thick film resistors on dielectric and metal substrates for piezoresistive sensors,* IMAPS conference - Poland, 2003.

72. Abe O, Taketa Y, Haradome M, *The effect of various factors on the resistance and TCR of RuO2 thick-film resistors--Relation between the electrical properties and particle size of constituents, physical properties of glass and firing temperature,* Electrical Eng. in Japan, 1989, **109**, 12-18.

73. Jacq C, Maeder T, Menot-Vionnet S, Birol H, Saglini I, Ryser P, *Integrated thick-film microelectronics applied on different material substrates*, EMPC conference - Belgium, 2005, in press.

74. Trubnikov L, *Thermal expansion, vitrification temperature and corrosion behaviour of lead-borosilicate glass*, Refractories and Industrial Ceramics, 2000, **41**, 169-71.

75. Krishna Rao K., Iyengar L, *X-ray studies on the thermal expansion of ruthenium dioxide*, Acta Cryst., 1969, **A25**, 302.

76. Morten B, Masoero A, Prudenziati M, Manfredini T, *Evolution of ruthenate-based thick film cermet resistors*, J. Phys. D: Appl. Phys, 1994, **27**, 2227-35.

77. Morten B, Prudenziati M, Sacchi M, Sirotti F, *Phase transitions in Ru based thick-film (cermet) resistors*, J. Appl. Phys, 1988, **63**, 2267-71.

78. Hrovat M, Holc J, Samardzija M, Belavic D, *The influence of firing temperature on gauge factors and the electrical and microstructural characteristics of thick film resistors*, J. of materials science letters, 2001, **20**, 701-5.

79. Cattaneo A, Marelli M, Prudenziati M, *Effects of refiring processes on electrical and strutural properties of thick-film resistors*, Electrocomponent Science and Technology, 1980, **6**, 165-71.

CHAPTER V:

Applications

It is undubitable that our piezoresistive pastes show a large range of values concerning the electrical properties, which allows diverse applications described in this chapter. The nature of our pastes presents the advantage to be used on different substrates such as steel or aluminium as expected at the beginning of this work.
Moreover, the large range of applications will be emphasised by the fact that even the less interesting samples (resistors with poor properties: high TCR, ...) could be used for specific applications.

The following table summarises the obtained values according to the paste-series.
(For the detailled properties of the glasses, see table 1, p77).

	RuO_2 grain size (nm)	**Process temperature (°C)**	***R* value (kOhms)**	**TCR value (ppm/°C)**	**GF value**	**TCE (ppm/°C)**
V6-series	40	525 to 675	0.03 to 100	+80 to +2000	2 to 30	9
	400		0.08 to 500	-600 to +500	3 to 15	
V2-series	40	640 to 775	0.8 to 200	-60 to +600	7 to 20	7
	400		1.5 to 500	-600 to +100	4 to 16	
V8-series	40	420 to 650	0.32 to 54	+470 to +1200	8 to 17	11
	400		0.1 to 55	-410 to +620	3 to 17	

Table 1: Property range of our experimental piezoresistive pastes

This table confirms that the three categories of pastes offer a large range of applications.

From this table, we can extract some interesting samples whose electrical properties meet our requirements for piezoresistive sensing, which are:
- Sheet resistance ~ 10 kOhms
- TCR value ~ 0 ppm/°C
- GF value > 10
- diverse TCE and firing process temperatures to be adapted on different substrates.

The most promising samples are presented in table 2.

	samples	T_f (°C)	*R* value (kOhms)	TCR value (ppm/°C)	GF value
V6-series	0.09-40	600	15	290	14
	0.075-40	625	15	230	16
	0.07-40	625	20	250	10
	0.06-40	650	20	190	13
	0.055-40	675	20	190	22
	0.03-40	650	20	150	20
	0.11-400	675	8	-90	7
	0.085-400	550	11	-128	5
V2-series	0.11-40	640	5	240	13
	0.08-40	700	10	100	15
	0.07-40	750	15	-18	18
	0.067-40	750	18	52	18
	0.06-40	700	5	13	17
	0.11-400	700	5	-100	5
	0.09-400	750	15	-165	7
V8-series	0.08-400	500	6	-115	6
	0.075-400	500	7	-100	10
	0.07-400	500	12	-150	15

Table 2: Most promising experimental pastes for piezoresistive sensors

We observe that, for each series, the grain size of the conductive phase seems to be a decisive factor for electrical properties.

V . 1 . First prototype on aluminium substrate: load cell

V . 1 . 1 . Prototype

A simple prototype force sensing beam was built on aluminium substrate (figure 1). The used resistor was the 0.08-40-6-575°C with the following properties:
R = 14 kOhms
GF = 15
T_f = 575 °C

The used dielectric (to avoid short circuit between the conductor and the aluminium substrate) was realised in our lab and is composed of the V6-glassy matrix to assure an optimised compatibility between the resistive and dielectric pastes.

Figure 1: Single resistor fired onto aluminium beam

This force sensing cell was characterised (figure 2), and found to be surprisingly good, given the fact we used «simple» aluminium. Use of stronger alloy could be possible and would potentially yield reasonably good force cells.

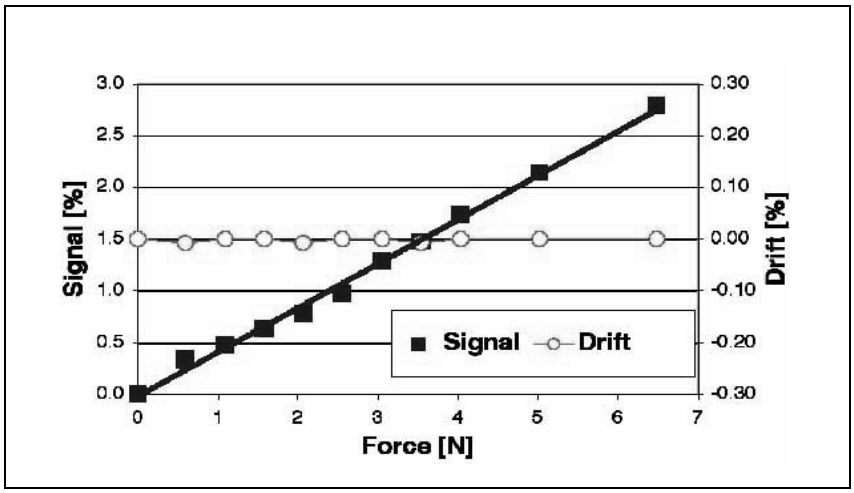

Figure 2: Electrical response of the prototype

Note that the dielectric based on the V6-glass was filled with TiO_2. This «filler» was used to stabilise the dielectric and to avoid the infiltration of the conductor and resistor through it. The addition of TiO_2 is used as a mechanical filler and as a modifier of the TCE.
Nevertheless, it is important to mention that the observed values of resistance were higher than the expected one's, which shows that the dielectric should be optimised.

V . 1 . 2 . Additional tests on aluminium alloy and stainless steel substrates

Preliminary and promising studies [1] were carried out on other mechanically interesting substrates, such as aluminium alloy ($AlMgSi_{0.5}$, TCE = 24 ppm/°C), aluminium-silicon composites (Osprey CE9, Osprey CE11 and Osprey CE17, TCE = 9 , 11 and 17 ppm/°C), and ferritic stainless steel 1.4016 (TCE = 11 ppm/°C).
The 0.075-400-8 sample was fired on them in the range of 500-525°C.

(Note that the obtained values on alumina substrate for these temperatures were respectively 7 and 5 kOhms and -100 and -50 ppm/K for 500 and 525 °C).

Moreover, in order to match the TCE of the substrates and the resistor and to isolate the two materials, a dielectric layer was screen-printed on the surface of the substrate. This dielectric was realised with the same V8-glass with different fillers in 40-50 %vol (alumina, cristobalite or quartz) that serve to dimensionally stabilise the layer and to control its TCE.
Whereas this study presents *R* and TCR results, no measurement for the piezoresistive response was realised.

The *R* and TCR results are summarised in table 3:

substrate material	dielectric composition	T_f (°C)	*R* value (kOhms)	TCR value (ppm/°C)
Al alloy	V8 + quartz	525	20-40	-50
Al-Si composite	V8 + alumina	525	25	-100
Stainless steel 1.4016	V8 + alumina	500	15	-100

Table 3: *R* and TCR values of the 0.075-400-8 resistor as a function of substrate material

Note that the surface of the stainless steel was pre-oxidised during 1h-900°C to create an oxide layer on the substrate surface, thereby improving the adherence of the dielectric thick-film on substrate. This thermal treatment does not affect the electrical properties.

These results show that our experimental low-firing compositions have demonstrated promising electric properties and chemical stability. Future work should concentrate on developing dielectric with finer filler particles (< 20 µm), on improving the adherence on stainless steel substrates by surface treatment or incorporation of adherence promoters, and on measuring and optimising the gauge factor of the resistors for piezoresistive sensing applications.

V . 2 . Determination of the heating flux from a laser in a hermetic packaging (glass substrate)

This example makes use of the high TCR observed in some samples, especially the 40 nm ones, to make PTC (Positive Temperature Coefficient) thermistors.

V . 2 . 1 . Purpose of this study

The aim of this study is to solder a hermetic packaging based on two different components: a glass base and a metal cover without heating the interior in order to allow sealing of sensitive items such as organic compounds or biological samples. The sealing by laser was chosen, because of the optimum hermeticity obtained by this technique (in opposite to sealing by glue or elastomer seal) [2].
In this case, a metallic conductor + solder rim is screen-printed on the glass substrate and the passage of the laser diode locally melts the solder, which seals the packaging after cooling.

V . 2 . 2 . Problems of soldering - role of resistors

However, this technique leads to local overheating of the materials and could destroy the glass compound. Moreover, the diffusion of the heat inside the packaging could deteriorate the inside electronic components.
To quantify the diffusion of the heat through the glass substrate, several V8-resistors have been screen printed on the surface of the glass as depicted on figure 3. They are called *R1*..*R5*.
R1 and *R3* measure the heating flux near the solder joint, whereas *R2*, *R4* and *R5* determine the temperature of zones more distant from the laser.

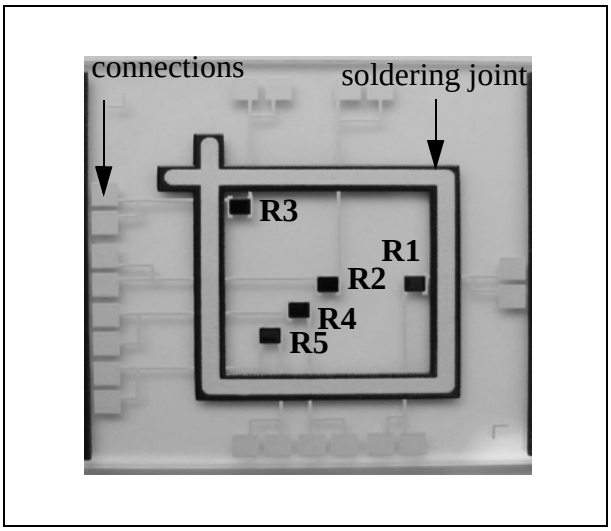

Figure 3: V8-resistances on the glassy base

Note that to favour local absorption of the laser beam and to increase heating efficiency, the soldering joint is screen-printed on a black dielectric film. This black film is composed of the V8-glassy matrix in which Co_3O_4 has been added to obtain the dark colour.
By this way, we expect that the black film will absorb the maximum of heat and thus limit the heat diffusion inside the packaging.

Concerning the resistors, we used 0.11-40-8 samples fired at 500°C. Indeed, this resistive composition exhibits adequate properties for this application, as it is characterised by a low *R*-value (~ 300 Ohms, for T_f ~ 500 °C), a high TCR value (~ 800 ppm/°C), and the low firing temperature characteristic of the V8 compositions. This high TCR value shows a great dependence of the temperature, which is unwanted in the case of piezoresistive compositions as it leads to a parasitic signal, but is advantageous for use as PTC thermistors, as it will be sensitive to a small modification of the temperature of the glass substrate. Moreover, the corresponding TCE of the V8-series and of glassy base are relatively compatible.
Another advantage is that such PTC resistors with low firing temperature are not available in commercial pastes.

V . 2 . 3 . Determination of the heating flux through the substrate

V . 2 . 3 . 1 . Validation of the technique of measurement

Firstly, the screen-printed resistances were tested in function of the temperature to verify their reliability. Figure 4 shows the evolution of the *R*-value vs. the temperature of the substrate for the resistance *R1*.

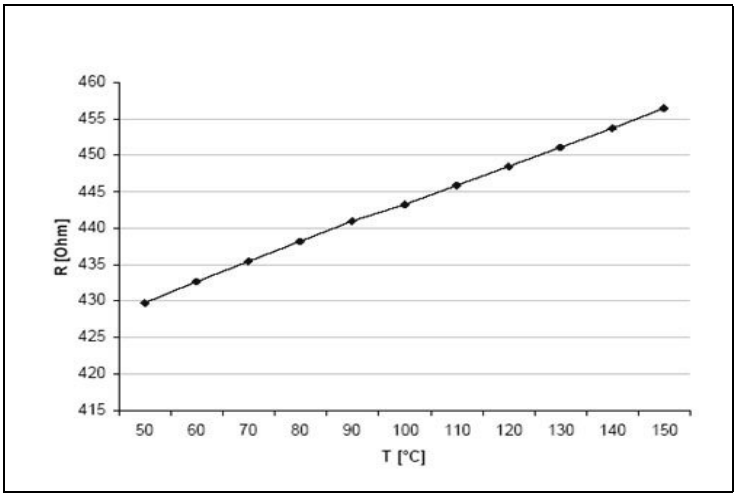

Figure 4: Evolution of the R1-value vs the temperature

We observe a linear reproducible evolution of the *R* value vs. the temperature. The five screen-printed resistors present the same behaviour [3]. We can deduce that the further experiments could be representative.

V . 2 . 3 . 2 . Some results

Different tests were realised to characterise the thermal flux in the packaging.

- **Evolution of the temperature of the glassy base in function of the run speed of the laser spot on the joint.**

Figure 5 shows the *R1*-response in function of time for different speeds of the spot.
t = 0 corresponds to the situation where the spot is on the right bottom corner of the joint. The spot moves with different speeds to reach the right top corner.

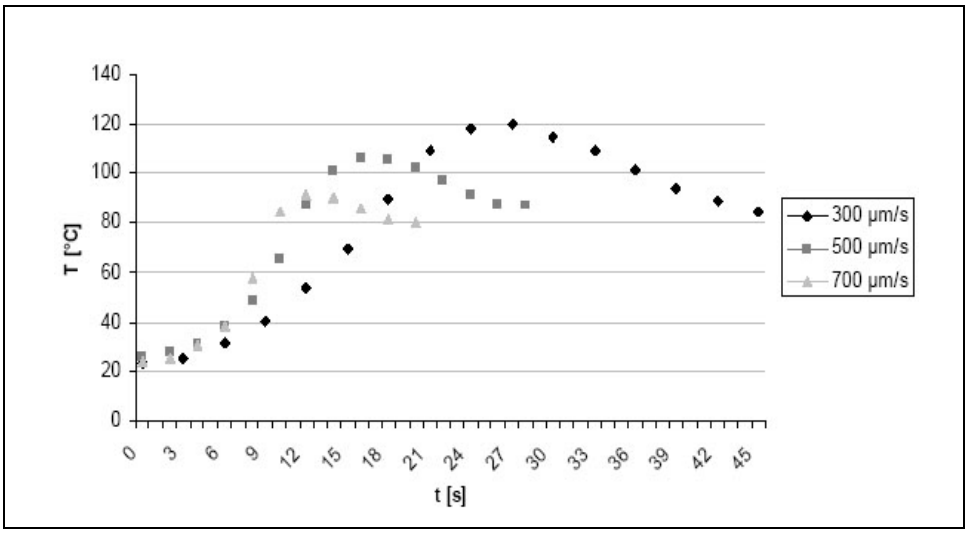

Figure 5: Evolution of the temperature (determined by *R1*) vs. time for different run speed of the laser spot

We observe that the maximum temperature is inferior to the temperature of the spot (140 °C), and it depends strongly on the run speed of the spot. A future solution to avoid an overheating of the substrate would be to increase the speed of the spot.

- **Evolution of the heat flow through the glassy base in the case of a fixed laser spot.**

These series of resistance allow determining the thermal diffusion when the spot keeps still. We decided to fix the spot on the left bottom corner (near *R5*) and to study the evolution of the temperature vs. time for the *R5, R4* and *R2* resistors placed respectively at 4.3, 6.6 and 9 mm from the spot (figure 6).

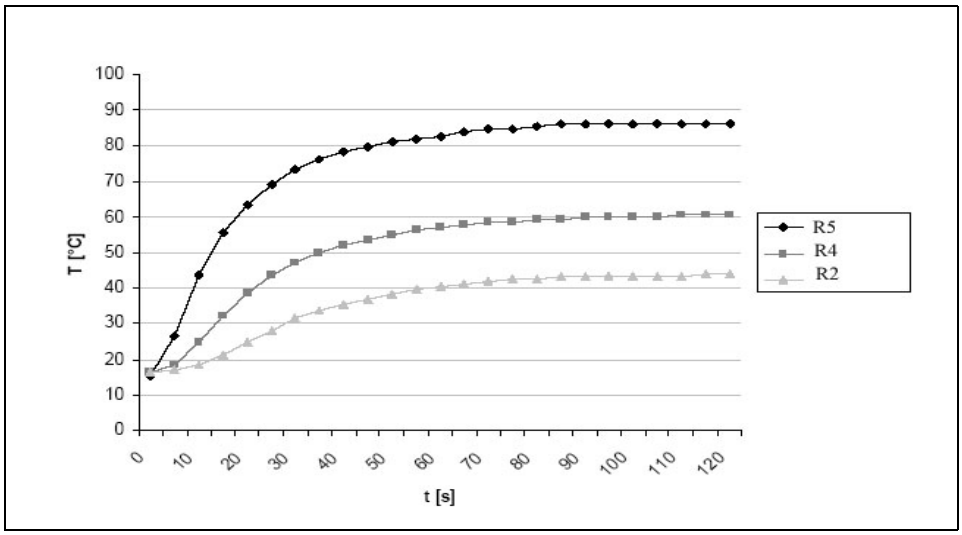

Figure 6: Evolution of the temperature vs. time for *R5, R4* and *R2*.

We observe that the temperature becomes stable after 90 seconds. This maximum temperature decreases strongly if the distance between the spot and the resistances increases.

These two previous experiments will help us to determine the optimal parameters for laser soldering.

In addition to the fact that this application shows that pastes with non appropriate properties for piezoresistive sensors can be even used, this experiment showed a good adherence of the V8-glass on the glassy substrate.

V . 3 . Future applications

V . 3 . 1 . A force sensing device for ligament balancing assistance in total knee arthroplasty (steel substrate)

This can be considered as a future application for our V6- or V8-resistors on steel. Until now, the V8 glass was used to realise the crossover dielectric paste to apply on the steel substrate and fired at 500°C, as commercial dielectric pastes do not support the strains imposed by the substrate.
A further step could be to use a V6- or V8-piezoresistive paste (because of its higher TCE) with a high GF and a processing temperature from 500 to 650°C. A compromise will have to be found between optimisation of steel mechanical properties (ideal: < 500°C, martensitic steel) and of the stability of the resistors, which is much better for V6-based ones.
Note that for martensitic steels, 750°C is the absolute maximum firing temperature, as they undergo disruptive phase transformation if heated above this limit. For austenitic steels, the TCE mismatch is still quite large. Therefore, dielectrics should contain a high TCE filler, such as quartz.
At present DP 2041 commercial paste is used but it is not optimum as its T_f is 850°C.

A brief description of the device follows.

V . 3 . 1 . 1 . Purpose of this study

The aim of this study was to resolve some problems of tibio-femoral misalignment and ligamentous imbalance encountered in the case of total knee arthroplasty (TKA) [4,5]. Indeed, ligament balancing in TKA is believed to have an important influence on the joint stability and prosthesis lifetime.
While current surgical tools and navigation systems help to achieve a precise alignment and placement of the prosthesis, the ligamentous force balance is still qualitatively assessed by the surgeon through manual trial movements of the limb. An objective and quantitative intraoperatively measurement of the forces acting within the knee would help the surgeon to improve the accuracy of the ligament balancing procedure, thus ensuring a good joint stability and an increased prosthesis lifetime. Within this framework, we developed a new force-sensing device for TKA. Indeed, unlike other systems reported in the literature [6-13], this device offers simultaneously the advantage of real-time and precise measurements, keeping the patella in its anatomical place and minimal bone resection, which helps to preserve the joint line.

V . 3 . 1 . 2 . Method of measurement

The developed force-sensing device consists of two sensitive plates, one for each condyle, and a tibial base plate, which is fixed by customised surgical pins. Due to its small size and thickness (6 mm), the device entirely fits inside the tibio-femoral gap with the patella in its anatomical

place after an initial tibial precut. Lateral and medial wedges are used to adjust the device thickness to the tibio-femoral gap. Each sensitive plate contains three deformable bridges instrumented with strain gauges by using thick-film piezoresistive pastes (figures 7 and 8). Applying a load in the sensitive area generates a vertical reaction force and a deformation in each bridge, which is measured by the piezoresistive sensors. The bridges are designed for a maximal total load of 500 N, which offers a sufficient safety margin, since passive loads acting in the knee joint during the surgery are expected to vary between 0-100 N.
Thick-film piezoresistive sensors [14] are used instead of standard bonded metallic strain gauges, which are space consuming and difficult to sterilise.
Applying a load in the sensitive area of the device deforms the instrumented bridges proportionally to the amplitude of the reaction forces generated in each bridge pillar. The amplitude and location of the applied load can thus be determined from the static equilibrium conditions. Based on the measurements of force amplitude and on the contact location of each condyle, the parameter characterising the ligament balance, (called the varus-valgus moment of the tibio-femoral forces) can be computed [15].
Teflon insulation cables and medical connectors are used to ensure the device's autoclavability. Furthermore, the sensitive plates are coated with a 10 µm parylene layer which makes the device operational in an aqueous environment and fully biocompatible.

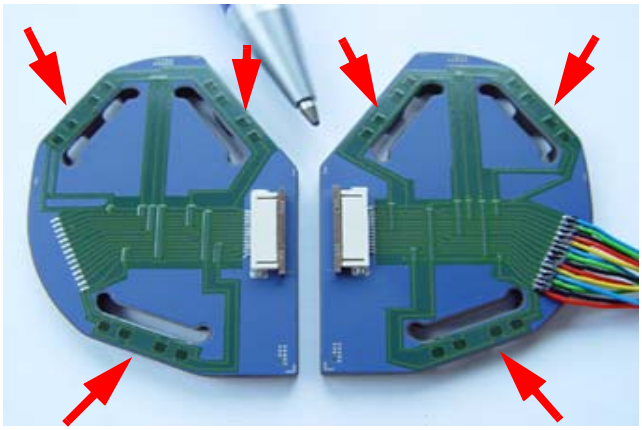

Figure 7: Sensitive plates of the force sensing device (the arrows show the bridges)

a. Deformable bridge with the 4 piezoresistors
(corresponding to the arrows on figure 7)

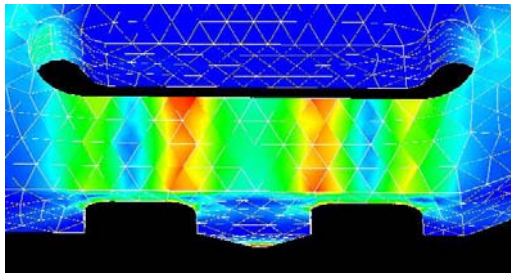

b. Representation of the applied strain on the material by finite element modeling
(green:negative, bleu:zero, and yellow/red:positive)

Figure 8: Deformable bridge

V . 3 . 1 . 3 . Validation of the device

To validate the system, ex situ and in situ studies should be carried out [15].

- **Intrinsic accuracy (ex situ studies)**

The intrinsic accuracy of the device was evaluated by loading the sensitive area with weights ranging from 0 to 100 N applied at 20 evenly distributed locations.
The intrinsic accuracy of 1.4 N of maximum force amplitude and 0.6 mm of local error (which corresponds to a 3 % relative error on the active measurement range), as well as the measurement range of 0-500 N seem to be appropriate for this application.

- **Tests on plastic bones (in situ studies)**

To determine whether the device is suitable for the purpose of ligament balancing, a control experiment was performed with plastic bones equipped with adjustable springs, which represented the collateral ligaments (figure 9). The tension of the springs was tuned to simulate ten different degrees of ligamentous imbalance.
The plastic bone experiment showed the device's suitability for the purpose of ligament balancing as the measured varus-valgus moments were proportional to the applied spring force differences.

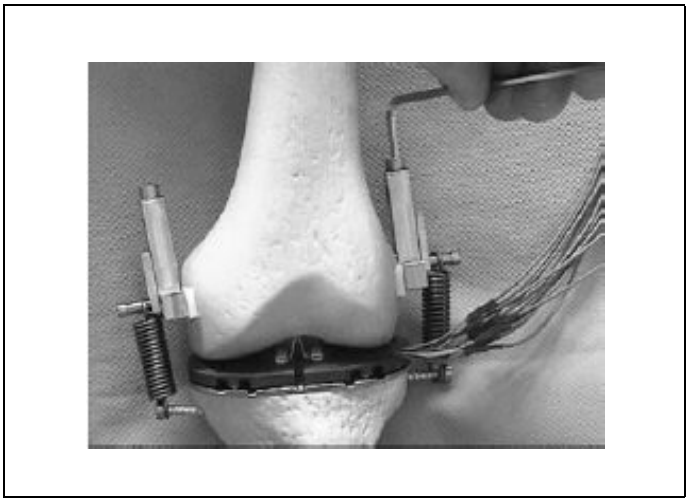

Figure 9: Plastic bone experiment

- **Cadaver Experiments**

To make quantifiable measurements of what surgeons describe as a balanced knee joint, we measured the tibio-femoral forces and moments in a balanced and an unbalanced condition.
The cadaver experiments demonstrated the adequacy of the measurement scale (0-500N) as well as the consistency between the acquired data and the surgeon's perception. In addition to measurements in discrete positions, the device allows continuous measurement during full knee flexions.

The proposed force-sensing device for ligament balancing in TKA provides not only the amplitude of the tibio-femoral contact forces but also their varus-valgus moment, the main parameter characterising the ligament balance.

Thanks to its quantitative and precise measurements, the developed force-sensing device has the potential to improve the quality and repeatability of the ligament balancing procedure in TKA. Further cadaver experiments will be performed to confirm these results and to quantify the benefit of using such a device compared to the manual approach.

V . 3 . 2 . A pressure membrane sensor (steel substrate)

V6 and V8 series could be used because of their low T_f, as this kind of substrates doesn't allow processing temperatures significantly above 650°C because of the phase transformation or softening of the steel between 750 and 900°C.

V . 3 . 2 . 1 . Purpose of this study

The aim of this study is to replace the alumina pressure sensor (figure 10) that doesn't present the best properties. Indeed, the use of steel substrates could allow to obtain:
- a higher signal due to its high elasticity (span for alumina: 2.4 mV/V, and for steel: 3.5 mV/V),
- a higher safety factor. At very high overpressures, the membrane deforms plastically, reducing the stress and thus allowing higher overloads. Moreover, failure behaviour is much more predictable, as the whole structure does not fail, as the case of Al_2O_3 (figure 11)..

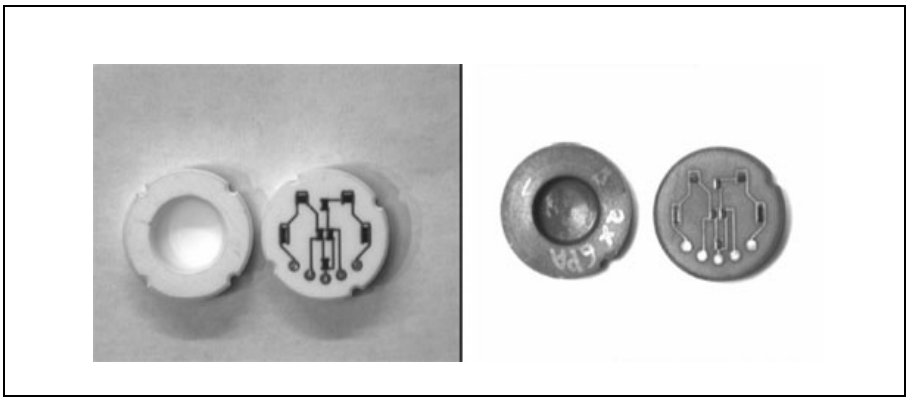

Figure 10: Both side view of alumina (left) and steel (right) pressure sensors

As presented in figure 10, the applied pressure is determined by the wheatstone bridge screen printed of the surface of the material.

In the case of too high pressure, we obtain different behaviours (figure 11).

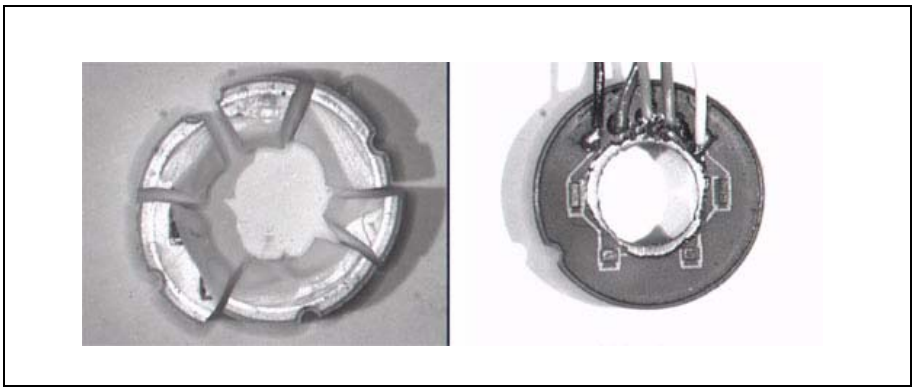

Figure 11: Alumina (left, P_N=200bar) and steel (right, P_N=40bar) pressure sensors after destruction

In the case of alumina, the break up goes through the bulk of the sensor, whereas for the steel one, the damages are only limited to the membrane. For alumina and steel membranes, the safety factor is respectively of 3.5 and 25 vs. the nominal pressure, P_N.

The following picture (figure 12) shows the intermediate state for a low pressure (P_N=20bar) steel sensor before the break up, which shows the plastic deformation of the material (that is not possible in the case of alumina).

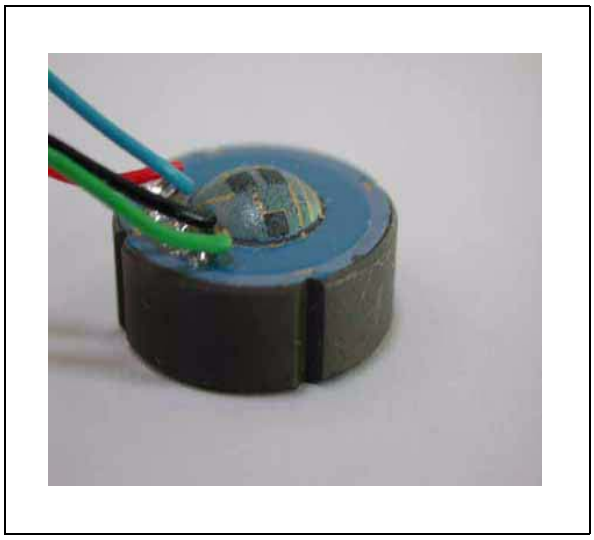

Figure 12: Plastic deformation of a steel membrane sensor before rupture

V . 3 . 2 . 2 . Disadvantage of the used commercial pastes

For the same reasons as the previous application (arthroplasty), the present used commercial pastes show a too high T_f. In the case of ferritic steel, a V6-paste could be suitable because of its adequate TCE, although its T_f around 650 °C is little too high. In fact, we should find a compromise between the properties of the resistors and the substrate. Regarding T_f, the V8-system could be more appropriate but it seems less stable. On the opposite, although the V6-system is characterised by an higher (but suitable) T_f, it presents more stable properties.
Nevertheless, a V8-paste could be proposed for austenitic or martensitic steels because of its higher TCE and its lower T_f values.
Note that the martensitic stainless steels are more suitable for this kind of pressure sensor due to their very high elastic properties and relatively good temperature stability.

Different samples could be proposed in the V6-series:
0.075-40-6-625, 0.06-40-6-650 or 0.03-40-6-650, as they are characterised with:
R ~15-20 kOhms
T_f ~ 650 °C
TCR values comprised between 100 and 250 ppm/°C according to the cateory of the steel (austenitic, ferritic, or martensitic).
The V8-samples should be still optimised as their properties don’t fully satisfy to the above mentioned conditions.

V . 4 . Conclusion

The diverse applications proposed in this chapter show that successful results can be obtained with our home-made piezoresistive pastes.
Our new piezoresistive pastes have already found present applications on more flexible substrates (steel or aluminium) that can be used in different domains (medical, industrial...). Moreover, it was shown that higher filler loadings can lead to compositions set aside other applications that don't use the piezoresistive effect, such as low-firing PTC thermistors.

As explained previously, other complementary studies are needed to optimise these series of low firing temperature pastes (improvement of the adherence, of the TCE ...), although these first results already offer some interesting and promising perspectives.

Some ideas concerning future improvements will be described in the last part of this thesis.

References - Chapter V:

1. Jacq C, Maeder T, Menot-Vionnet S., Birol H, Saglini I, Ryser P, *Integrated thck-film hybrid microelectronics applied on different material substrates,* EMPC 2005, Brugges, Belgium, in press.

2. Nicollin V, *Etude d'un pakaging étanche et de son indutrialisation*, rapport interne de projet de diplôme - EPFL, 2005.

3. Rey C, *Etude d'un pakaging étanche et de son indutrialisation*, rapport interne de projet de semestre - EPFL, 2005.

4. Fehring TK, Valadie AL, *Knee instability after total knee arthoplasty*, Clin. Orthop., 1994, **299**, 157-62.

5. Moreland JR, *Mechanisms of failure in total knee arthroplasty,*. Clin. Orthop., 1988, **226**, 49-64.

6. Attfield SF, Warren-Forward M, Wilton T, Sambatakakis A, *Measurement of soft tissue imbalance in total knee arthroplasty using electronic instrumentation,* Med. Eng. Phys., 1994, **16**, 501-5.

7. Davy DT, Kotzar G, Berilla J, Brown RH, *Telemetrized orthopaedic implant work at Case Western Reserve University,* Implantable Telemetry in Orthopaedics, 1990, 205-19.

8. D'Lima DD, Patil S, Steklov N, Colwell CW, *In vitro measurement of dynamic soft-tissue balance during total knee arthroplasty with an instrumented tibial prosthesis,* in Trans. 50th annual meeting of Orthopaedic Research Society, San Francisco, 2004, 301.

9. Kauffman KR, Kovacevic N, Irby SE, Colwell CW, *Instrumented implant for measuring tibiofemoral forces*, J. Biomech., 1996, **29**, 667-71.

10. Morris BA, D'Lima DD, Slamin J, Kovacevic N, Arms SW, Townsend CP, Colwell CW, *E-Knee: evolution of the electronic knee prosthesis*, J. Bone Joint Surg. Am., 2001, **83-A**, 62-6.

11. Takahashi T, Wada Y, Yamamoto H, *Soft-tissue balancing with pressure distribution during total knee arthroplasty*, J. Bone Joint Surg., 1997, **79**, 235-9.

12. Wallace AL, Harris ML, Walsch WR, Bruce WJ, *Intraoperative assessment of tibiofemoral contact stresses in total knee arthroplasty,* J. Arthroplasty, 1996, **13**, 223-77.

13. Winemaker MJ, *Perfect balance in total knee arthroplasty: the elusive compromise,* J. Arthroplasty, 2002, **17**, 2-10.

14. Prudenziati M, Morten B, *The state of the art in thick-film sensors,* Microelectr. J., 1992, **23**, 133-41.

15. Crottet D, Maeder T, Fritschy D, Bleuler H, Nolte LP, Pappas IP, *Development of a force amplitude- and location-sensing device designed to improve the ligament balancing procedure TKA,* IEEE Trans. Biom. Eng., in press.

Conclusion and outlook

Conclusion

The main technological goal of this work was to develop a new generation of piezoresistive pastes characterised by a low firing temperature process, in order to adapt them on aluminium or steel substrates instead of alumina that presents less interesting mechanical properties.
To reach this goal, it was then inevitable to understand the behaviour of these pastes during the firing and to correlate the evolution of the structure with the obtained electrical properties. The study of these properties and the control of the components of these new pastes allowed us to understand the conduction process between the conductive nanoparticles through the nanocomposite, and to validate an unpublished hypothesis.

During this work, different results have been obtained concerning technological and more theoretical goals.
The structural analysis of standard commercial piezoresistive pastes allowed us to determine the main components of a piezoresistive paste and to understand their role. In fact, thick-film resistors consist of a percolating network of conducting oxide nanoparticles dispersed in an insulating glassy matrix. The nature and the relative concentrations of the metallic and the glassy phases as well as the fabrication procedures are key ingredients governing the thick-film resistors electrical and piezoresistive properties. The tailoring of these factors and the knowledge of their effects on the properties are therefore of primary importance in the production of reliable thick-film sensor devices.
From these results, different lead borosilicate glassy matrix were synthesised in order to decrease the firing temperature process of the new pastes. At the end of this first part, a detailed manufacturing process, that never been fully explained previously, was proposed.

A second part was dedicated to the study of the behaviour and the characterisation of our new piezoresistive pastes. Three series of model pastes were realised with different firing temperatures: a high (T_f = 700°C, called V2-series), a low (T_f = 600°C, called V6-series) and a very low (T_f = 500°C, called V8-series) firing process temperature were obtained.
The control of several parameters (glass composition, conductive phase concentration, grain size, firing temperature...) allowed us to direct precisely our research to emphasise the principle

of conduction in such percolative systems and the reactions between the elements and their influence / side-effect on the electrical properties.

The three chosen series of pastes (V6, V2 and V8 pastes) offer complementary results by their different behaviours.
From the point of view of theoretical goals, our novel hypothesis based on the Balberg model has been successfully validated. Indeed, we took an interest to conductivity and piezoresistivity measurements in disordered RuO_2-glass composites close to the percolation threshold. We have found that the fabricated samples display either universal or nonuniversal behaviour of transport. The corresponding piezoresistive responses changed dramatically depending on whether the composites were universal or not. For the composites with the critical exponent $t \sim 2$, the piezoresistive factor Γ showed no dependence upon the RuO_2 volume fraction x, whereas the nonuniversal composites displayed a logarithmic divergence of Γ near the percolation threshold. We have interpreted the piezoresistivity results as being due to a strain dependence of the conductivity exponent t when its value is nonuniversal.
As discussed, a logarithmic divergence of Γ was found to be fully consistent with the tunnelling-percolation model of nonuniversality proposed by Balberg a few years ago. According to this theory, when the tunnelling distance between adjacent conducting grains has sufficiently strong fluctuations, the exponent t acquires a dependence upon the mean tunnelling distance a. An applied strain could so disturb the piezoresistive response and engender a variation of t.
We have brought forth a microscopic formulation to the phenomenological level proposed by Balberg, and we can now assert in view of such agreement between theory and experiments, that TFRs are mainly nonuniversal compounds showing transport exponent t larger than the universal limit $t = 2.0$. This exponent t depends on strain and leads to a logarithmic divergence of the gauge factor.
The possibility of influencing t by external means (e. g. strain) has never been studied so far.
We have proposed a new way to investigate percolative systems by studying the behaviour of piezoresistive pastes.

From the point of view of technological goals, different aims have been reached.
We found a relation between the structure evolution and the electrical properties, which could allow us to optimise our piezoresistive pastes. Indeed, we showed the impact of different parameters (T_f, dwell firing time, RuO_2 grain size and concentration) on the main electrical properties (R, TCR and GF). Structural analysis gave a possible interpretation of the results.
The increase of T_f improves the bulk homogeneity, which engenders a decrease of resistivity. It could be explained by the fact that the intergrain distances are driven by penetration of the glassy matrix between the RuO_2 grains. At sufficiently high firing temperatures (and depending on the firing time) the initial clusters are completely dispersed in the glass.
This phenomenon lowers x_c. In this case, this lowering could be due to microstructural changes driven by physical, rather than chemical, RuO_2-glass interactions. In this situation, the percolation threshold is given by the small RuO_2 particles rather than by the large RuO_2 clusters, and it can be considerably lower than that at the first stage of firing. This mechanism could qualitatively explain the gradual x_c lowering with T_f shown in this work.
Moreover, it has been observed that high firing temperatures could provoke some modifications such as reactions with the alumina substrate leading to segregation of the conductive phase. Moreover, it is not excluded that, at very high firing temperatures, the glass viscosity is so low that the heavier RuO_2 particles may fall towards the bottom of the TFR (or the inverse case if the glass reacts with the substrate), leading to a non-homogeneous distribution of the phases engendering some modifications of the properties (x_c appears to be effectively lowered). This

latter possibility could be established by SEM observations of the vertical cross-section of the samples. Whereas the phenomenon of reaction with the substrate has been observed, we were not able to obtain clear SEM images confirming sedimentation of RuO_2.
On the other hand, the increase of the dwell time and/or firing temperature decreases resistivity, as kinetics of reactions are favoured.
Concerning the RuO_2 parameters, it has been shown that larger grain size pastes presented higher resistivity values. Indeed, the decrease of the specific area of the conductive grains does not favour the current flow through the film. Moreover, the influence of the specific surface area is emphasised by the fact that an increase of it lowers the percolation threshold value (x_c).
The second more important parameter is the conductive phase concentration that shows a percolative behaviour for low concentrations, expressed by an increase of the resistivity when x becomes close to x_c.
Concerning TCR evolution, the results are in correlation with the previous resistivity results. Indeed, high TCRs corresponds to low resistivity values. Moreover, TCRs of small grain size pastes are higher than TCRs of bigger grain size ones for the same resistivity value (the same trend was observed for the resistivity evolution). This difference of TCR shows that the 40 and 400nm-resistors can be considered as two different materials, which shows the influence of the grain size on the TCR values.
The study of the evolution of GF was mainly used to characterised the electrical transport, and the evolution of GF depends on the universality or not, as explained before.
Whatever the paste-category, structural analysis didn't reveal the apparition of new phases, but showed a dependence of the microstructure vs T_f. Indeed, reactions between the substrate and the glass of the resistor were observed, leading to a modification of the homogeneity of the bulk resistor and thus, to a change of the electrical values.

After the analysis of the properties of these new pastes, their sensitivity in function of the process conditions and stability upon annealing were studied, because of limited available information in literature concerning the effect of firing schedule, particularly of quenching and to compare them to the commercial paste sensitivity / stability.
The influence of the firing schedule on the properties (R, GF and TCR) was found to be different for the three tested compositions. But, their corresponding values remained coherent as a high resistivity was associated to a low TCR and to a high GF.
V6 and V2-series were in accordance with the results of the commercial pastes. The increase of the cooling rate increases the resistivity values, whereas the increase of dwell-time decreases them. Moreover, we observed a combined influence of the cooling rate and the temperature dwell-time on R and TCR values. The evolution of the values can be explained by diffusion phenomenon and local microscopic strains due to important cooling rates.
However, V8 appeared to be strongly influenced by the dwell-time and temperature. A new phase (lead ruthenate) was detected for the only 400 nm-series at 650°C. This was prompted by the fact this system lies at the boundary between the RuO_2 and $Pb_2Ru_2O_6$ stability fields. The fact that the nucleation of this new phase was favoured for only 400 nm grain size could be due to morphological parameters of the particles.

Upon annealing at 250°C, only R changed significantly, and its stability was found to strongly depend on composition and firing schedule. V8 exhibited the highest changes, whereas V2 and V6 had comparable stability.
In general, 40 and 400 nm size series were characterised by the same trend.
The evolution of R upon annealing was also found to depend strongly on the cooling rate for commercial and home-made pastes. The slower the cooling rate, the more stable the R value.

Moreover, in general, stability of commercial pastes for a given cooling rate was found to increase with the firing thermal budget.
It is evident that these new series of pastes were not so stable as DP 2041 (R change < 1.0%). Their variations were much similar to the ESL 3114 paste. This trend was expected as ESL 3114 is similar to our experimental pastes because of its low firing temperature (~ 625°C) and its similar conductive phase composition (RuO_2). Like commercial pastes, the evolution tends to saturate.
If we compare the three experimental pastes, in spite of the much lower firing temperature of V6, its thermal stability was comparable to the V2 ones. The pastes based on the V8 glass presented the higher instability, because of its lowest firing temperature.
The stability of the microstructure and GF is in accordance with some authors, as they explain that GFs of thick-film resistors depend to a greater extent on the microstructure of the material. Modifying the cooling speed and the firing temperature affects both properties and annealing behaviour. This could come from supersaturated Ru in the glass or from frozen-in local strains between conductive phase and glass matrix.
At 250°C, possible evolution mechanisms could involve Ru in glass (dissolved or in clusters), or mechanical relaxation. Our investigation methods did not allow direct assessment of Ru in glass, but local rearrangement of Ru in glass during annealing such as precipitation of supersaturated Ru into clusters cannot be ruled out. Moreover, mechanical strain relaxation can be extrinsic (macroscopic thermal mismatch between resistor and substrate) or intrinsic (local thermal mismatch between glass and conductive phase), as explained before, which can later relax during annealing.

Another technological aim has been reached as we were able to manufacture low firing process temperature piezoresistive pastes with different T_f to adapt them on other substrates. It allowed to show that some essential parameters, such as a good compatibility of the TCE of the substrate and the glassy matrix should be taken into account. But the best evidence of the success of our pastes was the realisation of operational prototypes in different fields such as force and pressure sensors on highly elastic substrates. Moreover, promising results were also obtained in the case of PTC thermistors, that can be used for the thermal adjustment of measurement bridge of piezoresistive sensors.

From a scientific point of view, this first step allowed to show that nanostructure, conduction and properties are intimately linked. By choosing adequate and relevant composition, structure and firing, we proposed a new way to unveil the conduction process that has not been yet elucidated. But this trend should be confirmed by other complementary experiments.
From a technological point of view, good properties have been achieved with a low T_f (500-600°C), a reasonable R-value (~ 10 kOhms), and good GF (~ 15). But, it is evident that these pastes could be optimised, as, until now, a compromise should be made between low T_f and stability of the values. Although the stability could be enhanced with a higher GF or adapted TCR, they present a large range of applications because of their different T_f and their different TCRs. Thanks to this particularity, these pastes could be used on different substrates.
To sum up, this work is relevant and innovating as it combines physical, chemical and material phenomena and it is based on a new generation of low temperature piezoresistive inks using standard pastes as reference. In order to validate our work, different functional systems have been presented for applications on metal and even glass substrates.

Outlook

This work has generated some open points that should be studied in more detail in future work and that concern different fields.

- **Optimisation of properties for technological applications**

The very low T_f of V8-based resistors generates technological problems, because of their instability (cracks) on alumina, due to their high TCE values. Alumina is however not their intended use, and their high thermal expansion makes them a good match for metallic substrates such as steels or aluminium alloys.
Moreover, to improve their properties, some modifiers can be added to the glassy matrix to decrease the TCE value. We can for example add a filler with a lower TCE such as Al_2O_3 or amorphous SiO_2 but it could alter the microstructure of the resistor and could react with the glass. Another solution is to consider the diagram proposed by Trubnikov [1] which shows that the TCE can be lowered by only changing the proportions of our three-component glass. For instance, a simultaneous slight decrease of PbO and increase of B_2O_3 can decrease the TCE without considerably changing T_f. But, it leads to moderate changes as, for this system, a decrease of T_f generally increases the TCE.
However, these modifications are not easy to achieve as the improvement of some properties are often obtained to the detriment of other properties that can be negatively affected. In fact, the glass composition corresponds to a subtle equilibrium between different parameters, and it requires more detailed analysis.
In case of promising results study of the conduction mechanism could be carried out to be compared to the V2 and V6 pastes results.

Moreover, it has been shown that the TCR values could be improved to be closer to 0 ppm/°C. The usual approach to adjust the TCR values is to change the chemistry of the paste, namely to include in the ink small amount of additives. Several solutions are described in the literature [2,3,4].
For example, TiO_2, MnO_2, CdO, Rh_2O_3, V_2O_5 can be added as «negative TCR drivers», while conversely CuO and precious metals are used as «positive drivers» [2]. Moreover, the addition of rutile oxides such as TiO_2, GeO_2 or TeO_2 in the glassy matrix increases the resistance and decreases the TCR [3]. In fact, the addition of these compounds increases the thickness of the glass barrier (as the glass viscosity is lowered) and reduces the impurity states in the glass by limiting the solubility of the ruthenium ions.
Another method of compensation of TCR has been described [5]. The authors propose to mix two conductive phases with close resistivity but with opposite TCRs. They use lead ruthenate (TCR positive) and another semi-conductor $Pb_3Rh_7O_{15}$ (TCR negative ~ -300ppm/°C) to obtain an intermediate mixture with the same resistivity but an intermediate TCR.

Concerning the increase of GF values, different parameters can be adjusted. However, this value is mainly linked to the microstructure of the paste and less to the composition of the conductive phase [6-10]. Indeed, it has been observed [6] that commercial piezoresistive pastes like ESL3414 (GF ~ 20) consist of rather large conductive grains in the glassy matrix. The more homogeneous material with many small grains and short distances between the grains will have low GF, while the material with larger average distances between grains will have a higher GF. But, note that this kind of high GF pastes are generally characterised by an important noise index and less table properties. Additionally, more attention should be paid to the analysis of false high GF values that are due to microcraks, as described by Prudenziati et al [10].

Even though a new generation of low-firing temperature piezoresistive pastes has been performed, corresponding low firing temperature dielectrics and conductors should be realised so that the different films, composing a system, should be compatible. Studies about improvements of such dielectrics are in progress in our lab. Indeed, they are composed by the same glassy matrix combined with different fillers (alumina, quartz or cristobalite) to adapt their TCE and to stabilise them dimensionally, avoiding excessive interactions with subsequently deposited conductive and resistive films [11]. Two solutions can be proposed: either the glass is filled with an inert powder to stabilise the glassy matrix in order to limit its spread during the different refirings, or the glassy matrix is filled with a reactive powder that reacts with the glass stabilising it by causing devitrification and/or an increase of its melting temperature.
However, few studies concerning the adaptation of conductive pastes have been programmed until now. Glass frit can be added to such conductive pastes to adjust their T_f, but the difficulty lies in the compatibility between the different films (problems of chemical interactions at the interfaces).

- **Understanding of the physical mechanism of charge transport**

The V2-paste category shows more ambiguous results as its percolative behaviour is not pronounced. Although this series does not allow to completely reinforcing our previous results, some signs of percolative behaviour are even so present. Other samples should confirm this trend. In particularly, complementary x values closer to the x_c threshold should be chosen.

On the other hand, the piezoresistive response could be improved and studied from another point of view if we consider an «extreme» system composed of a polymer/resin matrix in which RuO_2 particles are embedded. In this case, the system is composed by interconnecting stiff conducting and soft insulating phases, and forms a heterogeneous system. Indeed, such metal oxide is characterised by a high value of bulk modulus B (B_{RuO2}: 270 GPa [12]), the glassy phase has a B-value typically in the 40-80 GPa range, depending on composition, and the epoxy matrix is characterised by a very low B-value ~ 3 GPa (Note that it exists other systems, such as elastomer, that are characterised by lower B value). Hence, the metallic phase is much stiffer than the insulating one so that there is a pronounced microscopic heterogeneity in the elastic properties of TFRs. A straightforward consequence of this elastic heterogeneity is that TFRs under an applied macroscopic strain should develop highly variable local strain fields. Higher GF values than those for a homogeneous system are then expected [13]. The behaviour of such pastes could be then the subject of a complementary study.

- **Structural field**

The observation of the evolution of the structure should be studied more precisely by TEM. A particular attention should be given at the interface of the conductive grains (nanometer layer) where new nano-phases can be detected (for example $Pb_2Ru_2O_6$) [14-16]. More detailed studies should be carried out in order to determine precisely the stoechiometry of the lead ruthenate phase that is not trivial as a deficiency in oxygen has been observed leading to a $Pb_2Ru_2O_{6+y}$ composition. The studies of Goodenough and Muller on properties of oxygen deficient pyrochlores have shown that y corresponds in general to 0 [17,18].

Moreover, we could unveil the presence of supersaturated Ru in the glass that could be present in the case of quenched pastes as supposed in our work.
Concerning the V8-series, a new phase (lead ruthenate) was detected by XRD for the only 400nm-series. A TEM observation at the interface of the nano-conductive particles could give complementary information about this new phase.

- **Material synthesis and fabrication of the pastes**

This section concerns the both main phases: the conductive grains and the glassy matrix.
Instead of using commercial RuO_2 grains, we could synthesise them in our lab by a water-based solution-gel route [19]. The used precursors are less expensive than the obtained oxide. For instance, by reacting ruthenium(III)acetylacetonate (which is not soluble in water) with H_2O_2 in a citric acid solution, a stable aqueous Ru-precursor solution can be prepared.
An advantage of this kind of technique is the control of the RuO_2 grain size, a better homogeneity, the nanoscale grains and the lower processing temperatures [20,21]. The use of water as a solvent certainly adds environmental as well as economic benefits. This technique has the advantage to obtain pure components contrary to the most water soluble Ru-compounds that contain chloride ions (if synthesised with $RuCl_3$) which deteriorate the electrical properties of the final produced conductor materials. Once these chloride ions are introduced in the solution, it is not evident to remove them.
In this case, the $RuCl_3$ is precipitated in aqueous solution by an ammoniac solution [22-24]. The obtained precipitate is the ruthenium hydroxide RuO_2,nH_2O that is washed to eliminate the chloride ions then calcined to obtain RuO_2.
A last solution is to oxidise metallic ruthenium in air or oxygen [25].

Another solution to limit the cost of these piezoresistive pastes is to replace the conductive phase by other less expensive oxides. Successful experiments with cadmium oxide thick film resistors (with a lead-cadmium glass system: PbO-CdO-BaO-B_2O_3, T_f ~ 650°C) have been carried out [26], although the use of nonnoble materials for resistor systems makes the resistors more susceptible to atmospheric effects both during firing and subsequent environmental aging. Small amount of RuO_2 was added to the CdO system to obtain an easy regulation of TCR and sheet resistance. Indeed, it was found that very fine particles of RuO_2 coated substantially larger grains of CdO. Thus connection of these areas into conductive chains can be realised by means of very fine particles of RuO_2.

Piezoresistive pastes have been realised with IrO_2 [27] that can be considered as a quite stable phase (non interacting) in high lead glasses, but that is a very expensive material. The high GF and low TCR values observed in the IrO_2 based systems emphasise the interest in continuation of research in resistive systems based on this conductive phase for stable and high performance thick film piezoresistors. Note that this compound can be synthesised by the same sol-gel route as RuO_2 [24].

Concerning the glassy matrix, a major challenge lies in the trend toward environmentally friendly materials. Our potentially toxic lead borosilicate glass should be replaced by a lead-free glass. This problem of toxicity is particularly acute for medical applications because of a possible dissolution of lead in human body. Another reason to replace lead is the fact that this compound is sensitive for firing temperatures above 800°C, which leads to a partial evaporation.
However, we should explain that the manufacture of a lead-free glass with the same properties as the original used (low T_f, high TCE, ...) is not easy to obtain as explained by Prudenziati et al [28] who evidenced a myriad of complex phenomena including devitrification, relevant bleeding of the glass on alumina substrates, anomalous distribution of conductive grains in the glassy matrix and phase separation. Its results emphasise the criticality in the choice of the glass composition for the preparation of lead-free thick-film resistors.

References - Conclusion and outlook:

1. Trubnikov L, *Thermal expansion, vitrification temperature and corrosion behaviour of lead-borosilicate glass,* Refractories and industrial ceramics, 2000, **41**, 169-71.

2. Prudenziati M, *Handbook of sensors and actuators,* Elsevier, 1994, **1**, 85-97.

3. Weissmann R, Chong W, *Glasses for high-resistivity thick-film resistors,* Advanced Engineering Materials, 2000, **2**, 359-62.

4. Inokuma T, Taketa Y, *Control of electrical properties of RuO_2 thick film resistors,* Active and passive elec. comp., 1987, **12**, 155-66.

5. Boonstra AH, Mutsaers CAHA, *Materiaux de résistance,* Brevet français 2 344 936, 1977.

6. Hrovat M, Belavic D, Samrdzija Z, Holc J, *A characterisation of thick film resistors for strain gauge applications,* Journal of materials science, 2001, **36**, 2679-89.

7. Hrovat M, Holc J, Belavic D, Soba S, *An evaluation of some commercial thick film resistor materilals for strain gauges,* Journal of materials science letters, 1994, **13**, 992-5.

8. Tamborin M, Piccinini S, Prudenziati M, Morten B, *Piezoresistive properties of RuO_2-based thick-film resistors: the effect of RuO2 grain size,* Sensors and actuators A, 1997, **58**, 159-64.

9. Carcia PF, Suna A, Childers WD, *Electrical conduction and strain sensitivity in RuO2 thick film resistors,* J. Appl. Phys., 1983, **54**, 6002.

10. Prudenziati M, Morten B, Cilloni F, Ruffi G, *Very high strain sensitivity in thick film resistors: real and false super gauge factors,* Sensors and actuators, 1989, **19**, 401-14.

11. Jacq C, Maeder T, Menot-Vionnet S, Birol H, Saglini I, Ryser P, *Integrated thick-film hybrid microelectronics applied on different materials substrates,* EMPC 2005, Brugges, Belgium, in press.

12. Hazen RM, Finger LW, J. Phys. Chem. Solids, 1981, **42**, 143.

13. Grimaldi C, Ryser P, Straessler S, *Gauge factor enhancement driven by heterogeneity in thick-film resistors*, J. Appl. Phys., 2001, **90**, 322-7.

14. Adachi K, Kuno H, *Decomposition of ruthenium oxides in lead borosilicate glass*, J. Am. Ceram. Soc., 1997, **80**, 1055-64.

15. Horvat M, Holc J, Samardzija Z, Belavic D, *The influence of firing temperature on gauge factors and the electrical and microstructural characteristics of thick-film resistors,* Journal of materials science letters, 2001, **20**, 701-5.

16. Morten B, Masoero A, Prudenziati M, Manfredini T, *Evolution of ruthenate-based thick-film cermet resistors*, J. Phys. D: Appl. Phys., 1994, **27**, 2227-35.

17. Longo JM, Raccah PM, Goodenough JB, *$Pb_2M_2O_{7-x}$ (M= Ru, Ir, Re) - Preparation and properties of oxygen deficient pyrochlores*, Mat. Res. Bull., 1969, **4**, 191-202.

18. Muller O, White WB, Roy R, J. Inorg. Nucl. Chem., 1964, **26**, 2075-86.

19. Pagnaer J, Nelis D, Modelaers D, Vanhoyland G, D'Haen J, Van Bael MK and all, *Synthesis of RuO_2 and $SrRuO_3$ powders by means of aqueous solution gel chemistry*, Journal of the european ceramic society, 2004, **24**, 919-23.

20. Van Werde K, Mondelaers D, Vanhoyland G, Nelis D and all, *Thermal decomposition of the ammonium zinc acetate citrate precursor for aqueous chemical solution deposition of ZnO*, J. Mat. Sci., 2002, **37**, 81-8.

21. Hardy A, Van Werde K, Vanhoyland G, Van Bael MK and all, *Study of the decomposition of an aqueous metal-chelate gel precursor for $(Bi,La)_4Ti_3O_{12}$ by means of TGA-FTIR, TGA-MS, and HT-DRIFT*, Thermochim. Acta, 2003.

22. Chu WF, Lehonard V, Erdmann H, Ilgenstein M, Sensors and actuators B, 1991, **4**, 321.

23. Niemann A, *Développement d'encres résistives pour applications à haute température de cuisson supérieure à 1000°C*, Thèse de l'université de Limoges, 1994.

24. Murakami Y, Tsuchiya S, Yahikozawa K, Takasu Y, *Preparation of ultrafine RuO_2 and IrO_2 particles by a sol-gel process*, Journal of materials science letters, 994, **13**, 1773-4.

25. Angus HC, Gainsbury PE, Electronic Components, 1968, 84.

26. Kuzel R, Broukal J, *Cadmium oxide thick film resistors*, IEEE transactions on components, hybrids, and manufacturing technology, 1981, **CHMT-4**, 239-44.

27. Prudenziati M, Tankiewicz S, Morten B, Piccinini S, Golonka L, *Piezoresistive effects in thick film piezoresistors: the effect of the conductive phase*, 20th international spring seminar on electronic technology - ISSE'97 - Poland, 1997.

28. Prudenziati M, Zanardi F, Morten B, Gualtieri AF, *Lead-free thick film resistors: an explorative investigation*, Journal of materials science: materials in electronics, 2002, **13**, 31-7.

Curriculum Vitae

Sonia MENOT (VIONNET)

born September 18th, 1975 in Pontarlier - France
French citizen

Education

2002-2005 **PhD Thesis**, Swiss Federal Institute of Technology (EPFL), Laboratoire de Production Microtechnique, Lausanne, Switzerlan
«Low firing temperature thick-film piezoresistive composites - Properties and conduction mechanism»

1999-2000 **Master Degree** in chemistry and interface physics, University of Franche-Comté, Besançon, France
«Mise au point d'un système de perméation électrochimique de l'hydrogene dans un matériau métallique»

1994-1999 **University Degree (Licence and Maîtrise)** in chemistry, University René Descartes Paris V, France
«Etude de la pollution atmosphérique d'origine automobile: étude d'un indice d'exposition aux oxydes d'azote et dosage des oxydes d'azote»

1992-1993 **Baccalaureat** type C, Pontarlier, France

Professionnal experience

2000-2002 **Chemical Engineer** at the Laboratoire de Production Microtechnique (LPM), EPFL, Lausanne, Switzerland *«Qualification of hybrid force sensors»*

In charge of the laboratory of chemistry of the LPM

Publications

S. Vionnet, T. Maeder, P. Ryser, *Firing, quenching and annealing studies on thick-film resistors*, Journal of the European Ceramic Society, 2004, **24**, 1889-1892.

S. Vionnet-Menot, C. Grimaldi, T. Maeder, S. Strässler, and P. Ryser, *Strain modulation of transport criticality in RuO_2-based thick-film resistors,* **Applied Physics Letters**, 2004, **85**, 5619-21.

S. Vionnet, C. Grimaldi, T. Maeder, P. Ryser, and S. Strässler, *Strain dependence of transport critical exponent in RuO_2-glass systems*", Ann. Phys., Leipzig, 2004, **13**, 99-100.

C. Jacq, S. Vionnet, T. Maeder, P. Ryser, *Integrated thick-film hybrid microelectronics on aluminium substrates*, Proceedings, European Microelectronics and Packaging Symposium, Prague, 2004, 267-271.

C. Grimaldi, S. Vionnet-Menot, T. Maeder, P. Ryser, *Effect of composition and microstructure on the transport and piezoresistive properties of thick-film resistors,* 2004, Proceeding IMAPS Poland, Wroclaw September.

S. Vionnet-Menot, C. Grimaldi, T. Maeder, S. Strässler, and P. Ryser, *Tunneling-percolation origin of nonuniversality: theory and experiments,* **Physical Review B**, 2005, **71**, 064201-1-12.

S. Vionnet-Menot, C. Grimaldi, T. Maeder, P. Ryser, and S. Strässler, *Study of electrical properties of piezoresistive pastes and determination of the electrical transport*, Electroceramics IX, Cherbourg, Journal of the European Ceramic Society, 2005, **25**, 2129-32.

C. Jacq, T. Maeder, S. Vionnet, P. Ryser, *Low-temperature thick-film dielectrics and resistors for metal substrates*, Electroceramics IX, Cherbourg, Journal of the European Ceramic Society, 2005, **25**, 2121-24.

C. Jacq, T. Maeder, S. Menot-Vionnet, H. Birol, I. Saglini, and P. Ryser, *Integrated thick-film hybrid microelectronics applied on different material substrates,* EMPC, Brugges, Belgium, 2005, in press.

S. Menot-Vionnet, T. Maeder, C. Grimaldi, C. Jacq, and P. Ryser, *Properties and stability of thick-film resistors with low processing temperatures - Effect of composition and processing parameters*, EMPC, Brugges, Belgium, 2005, in press.

C. Jacq, T. Maeder, S. Vionnet-Menot, C. Grimaldi, I. Saglini, P. Ryser and E. Carreno-Morelli, *Development of low-temperature thick-film materials for piezoresistive sensors,* Sintering 05, in press.